ELECTROMAGNETIC RESONANT BEHAVIOR OF A CONFOCAL SPHEROIDAL CAVITY SYSTEM IN THE MICROWAVE REGION

by

JOHN CRANKSHAW SIMONS, JR.

B.S. in Chemical Engineering, Drexel Institute of Technology (1942)

SUBMITTED IN PARTIAL FULFILLMENT OF THE REQUIREMENTS FOR THE DEGREE OF DOCTOR OF PHILOSPHY at the MASSACHUSETTS INSTITUTE OF TECHNOLOGY (1950)

Signature of Author..... Department of Physics, July 31, 1950

Certified by..... Thesis Supervisor

..... Chairman, Department Committee on Graduate Students

ABSTRACT

Useful in the experimental determination of surface impedance of conductors and superconductors is the microwave technique of introducing a test specimen of the subject material into a resonant cavity and then measuring the Q-value of the system. This technique has advantages over the method of constructing the entire cavity of the material to be tested when there is insufficient quantity of sample, or when surface preparation is a critical consideration. By analogy to the radiation fields of high-Q antennas and the high stored energy residing in the electromagnetic fields adjacent to such antennas at resonance, it is reasoned that a test specimen in the form of a high-Q radiator may have very high loss relative to that of the walls when placed inside a cavity. This high relative loss is conditioned on proper phase relation between radiated and reflected waves, or expressing it another way, on optimum interaction between cavity and specimen fields, in the nature of a resonance phenomenon.

To prove this proposition this thesis investigation was undertaken. The number of geometrical configurations one can analyze theoretically is small, owing to the mathematical complexities. It is not difficult to compute the case of two concentric spheres, and this has been done in Appendix B of this work. There it is shown that, for axially symmetric TM modes at least, there is a maximum in the ratio of loss in specimen to that in cavity walls for all modes higher than those designated by a zero value of the radial mode index p. The next step further is the consideration of the cavity contained between two confocal prolate spheroids. Such a cavity is of practical interest because

in the limit of unit eccentricity a prolate spheroid degenerates to a line segment and is a good approximation to a specimen in the form of a wire. In the other limit of zero eccentricity the outer spheroid becomes a sphere, which is a shape readily constructed. Mathematically the cavity is of interest because in prolate spheroidal coordinates the vector wave equation is separable, though only for axially symmetric solutions. Theoretical analysis of other useful geometries is not feasible since usable mathematical expressions of the solutions are not known.

The object of this thesis is to provide at least partial confirmation of the reasoning recommending the microwave technique mentioned earlier. This is accomplished by answering the specific question, "What is the optimum relation among the four parameters characterizing the microwave cavity contained between two confocal prolate spheroids, such that the ratio of surface loss in the inner spheroid to that in the outer spheroid is maximized?" The cavity is assumed filled with a non-conducting dielectric, bounded by metallic surfaces of good, but not necessarily infinite conductivity.

The problem is attacked first by application of general mathematical principles to the forms of the differential equations which arise, followed by numerical computation making use of the series representations and tables of spheroidal wave functions developed by Stratton, Morse, Chu, and Hutner.

The cavity system can be defined by specifying ℓ and p, which are indices identifying the axial and "radial" modes, and any two of three other parameters; these are ξ_1 and ξ_2, dimensionless variables related to the eccentricity and size of the inner and outer

spheroids, and c, the reduced or dimensionless frequency. Incidental to the determination of the final loss ratio data it has been necessary to compute the functions describing the field patterns, and to map the frequency behavior of the cavity. It is believed that this incidental information covers a much more complete range of variation of the parameters than has previously been published by any earlier workers.

From these data, the ratio of the losses in the two walls of the cavity has been computed for a similarly wide general range of the parameters. Specific cases have been worked out illustrating the frequency and loss behavior of a given cavity (external spheroid) as the inner spheroid is varied. It has been found that two different types of behavior are possible. For a given cavity the discriminant determining the type is a relation between frequency and the dimension ξ_1, characterizing the shape of the inner spheroid. For a specified value of the mode index ℓ it turns out that to each value of ξ_1 there corresponds a certain critical value of the reduced frequency. If the actual cavity frequency is less than this critical frequency, the first type of behavior exists, in which there is a resonant peak or maximum in the loss ratio function $q_\ell^1(\xi_1)$. If on the other hand the cavity frequency exceeds the critical frequency then one has the second type of behavior, in which the relative loss in the inner spheroid approaches infinity as it becomes more and more needle-like. The criteria necessary to distinguish between the two types are given.

The first type of behavior, characteristic of the lower modes, should be useful when absolute values of Q are to be measured and compared with computed values, as in the absolute measurement of conductivity of a material. The resonant frequency of the cavity experiences

a minimum close to the loss ratio maximum, so that by proper choice of the parameters the cavity will operate in a region where neither frequency nor loss ratio will be overly sensitive to dimensional discrepancies, such as may arise in machining or from thermal expansion.

The second type of behavior, associated with the higher modes, allows a choice of loss ratio high enough that the loss in the outer wall may be neglected. Thus it may find use in experiments measuring relative values of Q, as in research on superconductors where conductivity is to be measured at various temperatures.

Those modes for which $p = 0$ are exceptions to the above comments. For them the loss ratio can never be much greater than unity, and consequently they are of little interest.

The numerical results obtained for the frequency and loss ratio are compared with the field distributions, and the physical interpretation and significance of the behavior given. The method of computing the unloaded Q is given, and the general theory of resonant cavity behavior and the problem of cavity coupling are discussed, since these are all relevant to experimental measurement.

Also of interest is the relation between loss ratio and frequency for a thin inner spheroid as the outer cavity wall is varied. As the inner spheroid becomes thinner the resonance peak of the loss ratio becomes higher and sharper, in much the same fashion as the input admittance of a center-driven spheroidal antenna radiating into space. A connection is thus established between the behavior of a radiating antenna in space and the same resonant structure completely enclosed in a cavity.

TABLE OF CONTENTS

CHAPTER I

INTRODUCTION

1. Measurement of Impedance at Microwave Frequencies

Experimentally determined values of the surface impedance of conductors and superconductors in the microwave region have been useful in evaluating theories of the structure of matter.[1] One method [2] of measurement is to excise a cavity from a block of the conducting material, introduce the cavity as a resonant element in a microwave circuit and determine the losses by measuring the "Q" of the cavity. The cavity is chosen of a form which readily allows calculation of the surface impedance.

In certain instances, however, the construction of such a cavity may be inadvisable; there may be insufficient material or machining may be overly difficult. A possible solution to this problem is to construct a cavity from a material of high conductivity and introduce a test specimen of appropriate shape in the inside. The "Q" of the cavity-specimen combination may then be determined as before.[3]

---

(1) A. B. Pippard, G. E. H. Reuter, and E. H. Sondheimer, "The Conductivity of Metals at Microwave frequencies," Phys. Rev. 73, 920 (1948). Reuter and Sondheimer, "Theory of the Anomalous Skin Effect in Metals," Proc. Roy. Soc. A, 195, 336 (1948). R. G. Chambers, "Anomalous Skin Effect in Metals," Nature 165, 239 (Feb. 11, 1950).

(2) E. Maxwell, "Conductivity of Metallic Surfaces at Microwave Frequencies," J. App. Phys. 18, 629 (1947). W. B. Nowak, Ph.D. Thesis, M.I.T., 1949.

(3) This technique is similar to that of A.B. Pippard, "The Surface Impedance of Superconductors and Normal Metals at High Frequencies," Proc. Roy. Soc. A. 191, 370-415 (1947), although he employed the cavity as a frequency-sensitive transmission element rather than as a terminal impedance.

The desirable situation is, of course, that the major contribution to "Q" should be that of the test specimen. The question may be asked, "What is the optimum geometrical configuration of the cavity system such that the ratio of loss in the test specimen to that in the cavity wall is maximized?" A complete treatment of this question would be a considerable task. We can acquire some feeling for the problem, though, by the following line of thought.

The losses in a conducting wall of finite conductivity are related to the strength of the tangential magnetic field at the surface. Consequently, the losses will be higher near a region of high stored magnetic energy density. Thus, we are led to seek a configuration in which the bulk of the stored magnetic energy is in the vicinity of the sample, with much less near the cavity walls.

2. Comparison with Radiating Antennas

For the moment let us divert our attention to the radiation of freely oscillating antennas.(1) Antenna behavior is frequently described in terms of a "Q" also. In any resonant system, we can consider Q as a measure of the ratio of stored energy to the energy loss per oscillation. If a radiating antenna were completely enclosed by a conducting shell, the radiated energy would be nearly all reflected, and standing waves would result instead of the outgoing traveling waves. At first glance one might then say that here is the answer: A high-Q antenna oscillating freely or driven at resonance will have a great deal of stored energy in its vicinity, of which on the average half is magnetic energy. The radiated energy, in contrast, will be much lower;

---

(1) A reasonably clear presentation of antenna theory in terms of normal modes is given by J. Aharoni, "Antennae," Oxford, 1946.

the loss per cycle should be a measure of the average field at the walls of the enclosing shell. Thus the loss in the sample will be much greater than in the cavity walls.

The fallacy in this naive argument lies in the altered situation when the radiator is enclosed in a reflecting shell. There is no assurance that the interaction of radiated and reflected waves will not affect the energy density distribution. The energy density at a point varies as the square of the field strength there, but the field to be considered is the net field, the sum of the amplitudes of the radiated and reflected waves, taking proper consideration of their relative phases. This restriction against adding energy densities of superimposed waves is a familiar one in all wave phenomena.

While the foregoing reasoning is fallacious, it is not wholly without merit. It is not totally unreasonable to believe that perhaps a configuration can be found in which the radiated and reflected waves have appropriate phase relationships such that the desired situation is realized, namely greater surface losses in the radiator than in the cavity walls. This may well be associated with some sort of resonant phenomenon.

3. The Case of Two Concentric Spheres

The analytical complexities involved in the solution of Maxwell's equations necessarily restrict a theoretical treatment to the simplest geometries. As a starting place consider first the cavity included between two concentric spheres. For simplicity we assume the outer shell unbroken, thus neglecting the very practical consideration of coupling to an external analyzing circuit. The field solutions are,

of course, well known. The first thorough investigation was made by Mie.[1] Debye[2] has shown that for a sphere the radiation loss is exceptionally rapid, corresponding to a very low Q. Calculations have been carried out for varying radii of the two concentric spheres, and the results are given in Appendix B. The dependence of the loss ratio is given in Figure 26. It should be noted that the situation may be discussed completely in terms of only three parameters.

4. The Linear Antenna as a Resonant Structure

A resonant linear antenna is known to have a high Q, and one next wonders how this will turn out as a specimen shape. More generally, of course, we should expect that almost any high-Q resonant structure will tend to have desirable characteristics. We limit further consideration to a linear antenna, because this case is still capable of calculation while more general shapes, such as a horseshoe or hairpin[3] present almost insurmountable difficulties in analysis. In addition, the limit of eccentricity of a prolate spheroid is a long thin wire of mathematically zero thickness. This is the approximation we shall use for a linear antenna since in prolate spheroidal coordinates the wave equation is separable under certain conditions. From the practical viewpoint, small samples are quite likely to be furnished in the form of wires so that this case is still realistic.

---

(1) G. Mie, Ann. d. Physik 25, 377 (1908).

(2) P. Debye, Ann. d. Physik 30, 57 (1909).

(3) This is the type of element used by Pippard. It was not necessary for him to compute the theoretical Q of the system since he only measured relative values of impedance (rather than absolute) as a function of temperature.

5. Statement of the Problem

In view of the foregoing discussion it was decided to attempt to find an answer to the question asked in Section I, attacking the problem theoretically, and restricting its scope to a prolate spheroidal coordinate system which allows solution of Maxwell's equations by the method of separation of variables. The question may be restated, "What is the optimum relation among the four parameters characterizing a microwave cavity contained between two confocal prolate spheroids, such that the ratio of surface loss in the internal spheroid to that in the external spheroid is maximized?" The cavity will be assumed filled with a non-conducting dielectric, and bounded by metallic surfaces of good, but not necessarily infinite, conductivity. Consideration will also be given to the problem of coupling the cavity to external measuring equipment, and to the correlation of cavity behavior (in terms of normal modes) with experimental observations. The cavity configuration is shown in Figure 1, where coupling to an external system is indicated by a waveguide output.

6. Earlier Work

There seems to be very little work reported concerned specifically with the solution of the electromagnetic field problem inside a spheroidal cavity,[1] although the theory has certainly been known for a great while. No mention has been found of any previous investigation of the cavity contained between two confocal spheroids. For numerical work, the only method practical requires the separation of the vector

---

(1) M. Jouget, Rev. Gén. Élect. 51, 484 (1942); also Bull. Soc. Franç. Élect. 5, 52 (1945).

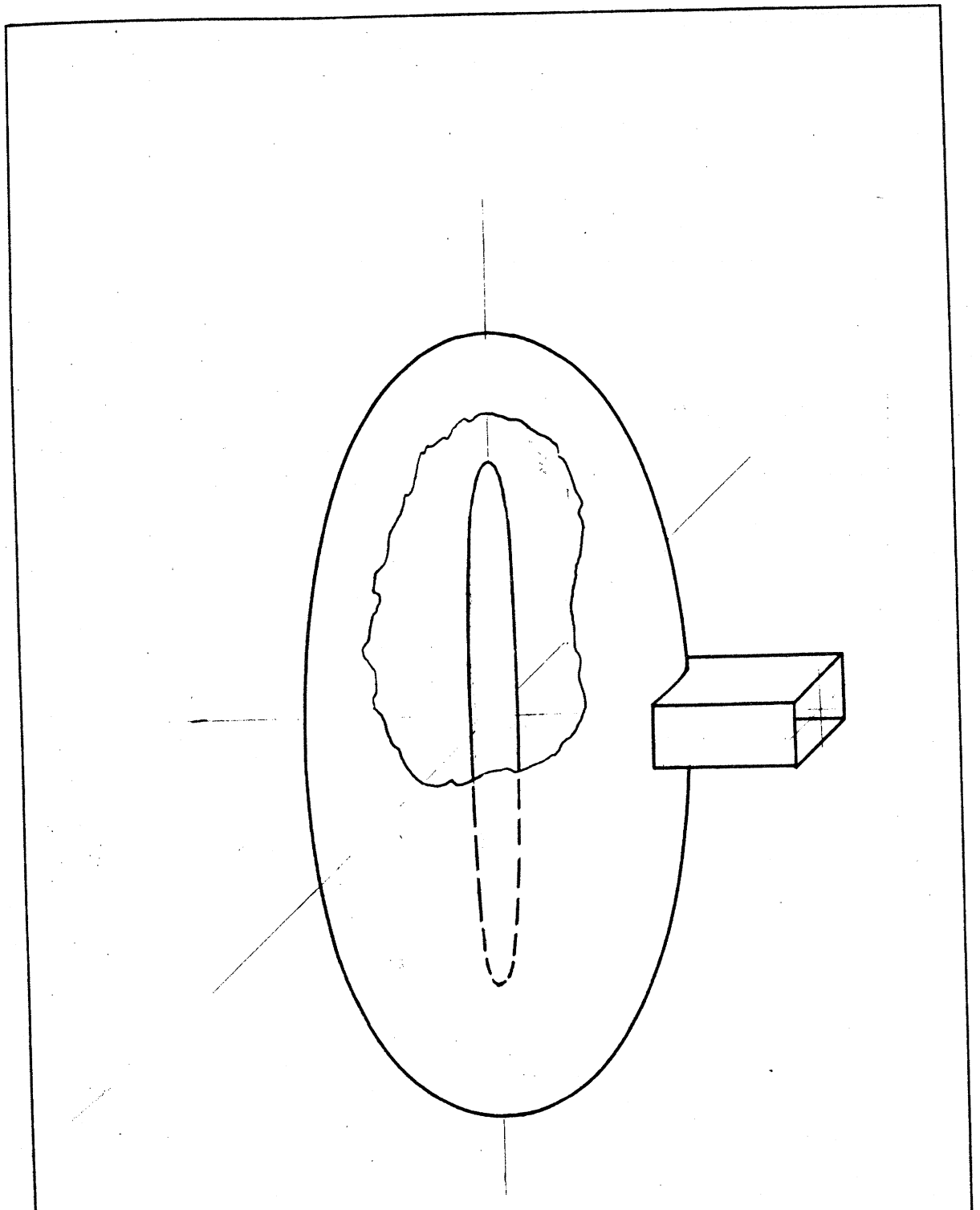

FIGURE 1

CONFOCAL SPHEROIDAL CAVITY SYSTEM

wave equation, reducing it to several ordinary scalar differential equations. This restricts the study, in the case of spheroidal coordinates, to axially symmetric solutions since only in this instance is the partial differential equation separable. In the extensive literature of the antenna, one finds that in this way have been studied the fields of a prolate spheroid by Abraham,[1] Page and Adams,[2] Chu and Stratton,[3] and Ryder.[4] The concern of these authors was mainly for the free and forced oscillations of spheroidal antennas, but much of their mathematical treatment of travelling wave fields can be carried over bodily into the analysis of standing wave fields. Actually, the theoretical mathematical foundations for spheroidal wave functions[5] have been known for many years, but it was not until the tables of Stratton, Morse, Chu, and Hutner[6] appeared that numerical computations of other than limiting cases could be readily made. The only published work employing these tables (to the author's knowledge) is that of Chu and Stratton.[7]

---

(1) M. Abraham, Ann. d. Physik 66, 435 (1898).

(2) L. Page and N. I. Adams, Phys. Rev. 53, 819 (1938).

(3) L. J. Chu and J. A. Stratton, J. App. Phys. 12, 241 (1941).

(4) R. M. Ryder, J. App. Phys. 13, 327 (1942).

(5) M. J. O. Strutt, "Lamésche-Mathieusche und verwandte Funktionen in Physik und Technik," J. Springer, Berlin, 1932.

(6) J. A. Stratton, P. M. Morse, L. J. Chu, and R. A. Hutner, "Elliptic Cylinder and Spheroidal Wave Functions," Technology Press, John Wiley, 1941.

(7) Chu and Stratton, J. App. Phys. 12, 241 (1941).

7. Outline of the Project

The initial attack of the problem as outlined in Section 5 must necessarily involve consideration of Maxwell's equations, and the separation of the vector wave equation in prolate spheroidal coordinates; this is the subject of Chapter II. Chapter III continues with a discussion of boundary conditions and the eigenvalue problem. In the event that the parameter relationship $c^2 = \alpha$ holds, a special case results in which the system of ordinary differential equations is greatly simplified. Chapter IV discusses this special case and the solutions obtained by elementary methods of integration. In Chapter V, the form of the differential equations is considered and from this the qualitative behavior of the general solutions is deduced.

As an intermediate step towards the final result, the actual field expressions must be found. Chapter VI deals with the series representation of the field expressions, following the scheme of Stratton, Morse, Chu and Hutner, and outlines a method of numerical computation. Near a central spheroid of high eccentricity the SMCH representations vary rapidly and are not readily interpolated, although certain points (for which standard functions involved are tabulated to great accuracy) may be satisfactorily computed. On the surface of the limiting spheroid the series expressions become indeterminate. Chapter VII treats other approximate expressions employed to represent the solutions in this region.

The main problem is not that of ascertaining the field distribution, but of finding the loss in the cavity walls, and this is the subject of Chapter VIII. Coupling the cavity system to external measuring equipment involves the theory of resonant cavity behavior,

which is reviewed in Chapter IX. In Chapter X is outlined the method of computing the surface conductivity from a measured value of the unloaded Q, with further remarks on the coupling problem. Finally, Chapter XI reviews the pertinent parameters and examines their physical significance. It discusses the frequency behavior of a cavity and its relation to the field distribution as the parameters necessary to describe the system are varied. The chapter then considers the cavity losses, and the ratio of the losses in the two walls and their correlation with the frequency behavior; it endeavors to interpret the numerical results in terms of the physical quantities concerned. Included in Chapter XI is a summary of the thesis investigation and recommendations for further work. The numerical computation of the various functions involved has been relegated to the several appendices, where the mathematical details are considered at greater length, and the computed data presented in tabular and graphic form.

CHAPTER II

EQUATIONS OF THE ELECTROMAGNETIC FIELD

1. Maxwell's Equations

In rationalized m.k.s. units, Maxwell's equations have the form

$$\text{(I)} \qquad \operatorname{curl} \mathbf{E}(\mathbf{r}, t) + \mu \frac{\partial}{\partial t} \mathbf{H}(\mathbf{r}, t) = 0 \tag{2.1}$$

$$\text{(II)} \qquad \operatorname{curl} \mathbf{H}(\mathbf{r}, t) - \epsilon \frac{\partial}{\partial t} \mathbf{E}(\mathbf{r}, t) = \mathbf{J}(\mathbf{r}, t) \tag{2.2}$$

in a homogeneous isotropic medium characterized by inductive capacities, ϵ and μ. If further Ohm's Law be assumed, i.e., $\mathbf{J} = \sigma \mathbf{E}$, and harmonic time dependence, $e^{-j\omega t}$, be introduced, Eqs. (2.1) and (2.2) become

$$\operatorname{curl} \mathbf{E} = j\omega\mu \mathbf{H} \tag{2.3}$$

$$\operatorname{curl} \mathbf{H} = (-j\omega\epsilon + \sigma)\mathbf{E} \tag{2.4}$$

Frequently included as part of Maxwell's equations are the two divergence equations,

$$\text{(III)} \qquad \operatorname{div} \mathbf{B} = 0 \tag{2.5}$$

$$\text{(IV)} \qquad \operatorname{div} \mathbf{D} = \rho \tag{2.6}$$

If one assumes the conservation of charge, however, these relations are not independent of (I) and (II).

In a right-handed orthogonal system of curvilinear co-ordinates (η, ξ, φ) characterized by metrical coefficients h_η, h_ξ, h_φ, the curl is, generally,

$$\text{curl } \mathbf{H}(\eta, \xi, \varphi; t) = \frac{1}{h_\eta h_\xi h_\varphi} \begin{vmatrix} h_\eta \mathbf{i}_\eta & h_\xi \mathbf{i}_\xi & h_\varphi \mathbf{i}_\varphi \\ \frac{\partial}{\partial \eta} & \frac{\partial}{\partial \xi} & \frac{\partial}{\partial \varphi} \\ h_\eta H_\eta & h_\xi H_\xi & h_\varphi H_\varphi \end{vmatrix} \tag{2.7}$$

Utilizing (2.7), the two vector equations (2.3) and (2.4) can be rewritten as six scalar equations relating the field components:

$$\begin{aligned}
H_\eta &= \frac{1}{j\omega\mu} \frac{1}{h_\xi h_\varphi} \left[\frac{\partial}{\partial \xi}(h_\varphi E_\varphi) - \frac{\partial}{\partial \varphi}(h_\xi E_\xi) \right] \\
H_\xi &= \frac{1}{j\omega\mu} \frac{1}{h_\varphi h_\eta} \left[\frac{\partial}{\partial \varphi}(h_\eta E_\eta) - \frac{\partial}{\partial \eta}(h_\varphi E_\varphi) \right] \\
H_\varphi &= \frac{1}{j\omega\mu} \frac{1}{h_\eta h_\xi} \left[\frac{\partial}{\partial \eta}(h_\xi E_\xi) - \frac{\partial}{\partial \xi}(h_\eta E_\eta) \right] \\
E_\eta &= -\frac{1}{(j\omega\epsilon - \sigma)} \frac{1}{h_\xi h_\varphi} \left[\frac{\partial}{\partial \xi}(h_\varphi H_\varphi) - \frac{\partial}{\partial \varphi}(h_\xi H_\xi) \right] \\
E_\xi &= -\frac{1}{(j\omega\epsilon - \sigma)} \frac{1}{h_\varphi h_\eta} \left[\frac{\partial}{\partial \varphi}(h_\eta H_\eta) - \frac{\partial}{\partial \eta}(h_\varphi H_\varphi) \right] \\
E_\varphi &= -\frac{1}{(j\omega\epsilon - \sigma)} \frac{1}{h_\eta h_\xi} \left[\frac{\partial}{\partial \eta}(h_\xi H_\xi) - \frac{\partial}{\partial \xi}(h_\eta H_\eta) \right]
\end{aligned} \tag{2.8}$$

2. Effects of Rotational Symmetry

If now the co-ordinate system has rotational or axial symmetry with respect, say, to the co-ordinate φ, then the metrical coefficients

will be independent of φ. If we consider only fields having the same axial symmetry as the co-ordinate system, then the field components will also be independent of φ, the "azimuthal" or "equatorial" co-ordinate. Then the six scalar curl equations may be broken up into two independent groups of three equations each, as has been shown by Stratton:(1)

$$\text{(A)} \quad \begin{cases} (j\omega\epsilon - \sigma) E_\eta = -\dfrac{1}{h_\xi h_\varphi} \dfrac{\partial}{\partial \xi}(h_\varphi H_\varphi) \\ (j\omega\epsilon - \sigma) E_\xi = \dfrac{1}{h_\varphi h_\eta} \dfrac{\partial}{\partial \eta}(h_\varphi H_\varphi) \\ j\omega\mu H_\varphi = \dfrac{1}{h_\eta h_\xi}\left[\dfrac{\partial}{\partial \eta}(h_\xi E_\xi) - \dfrac{\partial}{\partial \xi}(h_\eta E_\eta)\right] \end{cases} \tag{2.9}$$

$$\text{(B)} \quad \begin{cases} j\omega\mu H_\eta = \dfrac{1}{h_\xi h_\varphi} \dfrac{\partial}{\partial \xi}(h_\varphi E_\varphi) \\ j\omega\mu H_\xi = -\dfrac{1}{h_\varphi h_\eta} \dfrac{\partial}{\partial \eta}(h_\varphi E_\varphi) \\ (j\omega\epsilon - \sigma) E_\varphi = -\dfrac{1}{h_\eta h_\xi}\left[\dfrac{\partial}{\partial \eta}(h_\xi H_\xi) - \dfrac{\partial}{\partial \xi}(h_\eta H_\eta)\right] \end{cases} \tag{2.10}$$

In the same rotationally symmetric co-ordinate system, the divergence equations (III) and (IV) become

$$\text{(A)} \quad \frac{\partial}{\partial \eta}(h_\xi h_\varphi E_\eta) + \frac{\partial}{\partial \xi}(h_\varphi h_\eta E_\xi) = \frac{\rho}{\epsilon} \tag{2.11}$$

$$\text{(B)} \quad \frac{\partial}{\partial \eta}(h_\xi h_\varphi H_\eta) + \frac{\partial}{\partial \xi}(h_\varphi h_\eta H_\xi) = 0 \tag{2.12}$$

---

(1) J. A. Stratton, "Electromagnetic Theory," p. 422, McGraw-Hill, 1941

They are, however, not independent of the curl equations, and contribute no new information other than to confirm the independence of the two groups of equations.

The solutions of group (A), it turns out, are analogous to the transverse magnetic (TM) waves of systems having spherical geometry, the H_φ lines having the form of circles concentric with the axis and there being no component of magnetic field normal to the surfaces of rotation. Similarly, the solutions of group (B) are analogous to the transverse electric (TE) waves in the spherical case, there being no electric field component normal to the spheroidal or other surfaces of rotation. We shall interest ourselves only in the TM solutions, which in the limit of unity eccentricity of a prolate spheroidal system describe the behavior of an electric dipole or center fed linear antenna.

3. Integration of the Field Equations

The equations of group (A) are satisfied by a potential,

$$Q(\eta, \xi; t) = h_\varphi(\eta, \xi)\, H_\varphi(\eta, \xi; t) \tag{2.13}$$

so that

$$H_\varphi = \frac{1}{h_\varphi} Q$$

$$E_\eta = -\frac{1}{(j\omega\epsilon - \sigma)} \frac{1}{h_\xi h_\varphi} \frac{\partial Q}{\partial \xi} = \frac{j\omega\mu}{k^2} \frac{1}{h_\xi h_\varphi} \frac{\partial Q}{\partial \xi} \tag{2.14}$$

$$E_\xi = \frac{1}{(j\omega\epsilon - \sigma)} \frac{1}{h_\varphi h_\eta} \frac{\partial Q}{\partial \eta} = -\frac{j\omega\mu}{k^2} \frac{1}{h_\varphi h_\eta} \frac{\partial Q}{\partial \eta}$$

where we have set $k^2 = \omega^2\epsilon\mu + j\omega\mu\sigma$, and where Q must satisfy

$$\frac{\partial}{\partial \eta}\left(\frac{h_\xi}{h_\varphi h_\eta} \frac{\partial Q}{\partial \eta}\right) + \frac{\partial}{\partial \xi}\left(\frac{h_\eta}{h_\xi h_\varphi} \frac{\partial Q}{\partial \xi}\right) + k^2 \frac{h_\eta h_\xi}{h_\varphi} Q = 0 \tag{2.15}$$

Group (B) may be integrated in similar fashion. This treatment is originally due to Abraham.[1]

4. Separation of the Variables

Restricting the discussion to prolate spheroidal co-ordinates[2] from now on, one finds upon substituting the explicit expressions for the metrical coefficients[3] that Eq. (2.15) can be solved by the method of separation of variables. For let

$$Q(\eta, \xi, t) = A_0 Y(\eta) X(\xi) e^{-j\omega t} \tag{2.16}$$

where $Y(\eta)$ and $X(\xi)$ are dimensionless functions of the dimensionless variables η and ξ, and A_0 is a constant factor introducing the dimensions of current, or ampere-turns. Substituting in Eq. (2.15), one has

$$X(\xi)\frac{\partial}{\partial\eta}\left[\frac{h_\xi}{h_\varphi h_\eta}\frac{dY(\eta)}{d\eta}\right] + Y(\eta)\frac{\partial}{\partial\xi}\left[\frac{h_\eta}{h_\xi h_\varphi}\frac{dX(\xi)}{d\xi}\right] + k^2\frac{h_\eta h_\xi}{h_\varphi}Y(\eta)X(\xi) = 0 \tag{2.17}$$

which becomes, on replacing h_η, h_ξ, h_φ, by their explicit equivalents,

$$X(\xi)\frac{\partial}{\partial\eta}\left[\frac{1}{f(\xi^2-1)}\frac{dY(\eta)}{d\eta}\right] + Y(\eta)\frac{\partial}{\partial\xi}\left[\frac{1}{f(1-\eta^2)}\frac{dX(\xi)}{d\xi}\right] + \frac{k^2f^2(\xi^2-\eta^2)}{(\xi^2-1)(1-\eta^2)}Y(\eta)X(\xi) = 0 \tag{2.18}$$

or

$$\frac{(1-\eta^2)}{Y(\eta)}\frac{d^2Y(\eta)}{d\eta^2} + \frac{(\xi^2-1)}{X(\xi)}\frac{d^2X(\xi)}{d\xi^2} + k^2f^2(\xi^2-\eta^2) = 0 \tag{2.19}$$

---

(1) M. Abraham, Ann. d. Physik 66, 435 (1898).

(2) The prolate spheroidal co-ordinate system to be employed is defined in Appendix A, where the properties of the system are reviewed in detail.

(3) See Appendix A.

Here f is the semi-interfocal distance of the family of confocal prolate spheroids. Further manipulation gives

$$-\frac{(1-\eta^2)}{Y(\eta)}\frac{d^2Y(\eta)}{d\eta^2}+k^2f^2\eta^2=\frac{(\xi^2-1)}{X(\xi)}\frac{d^2X(\xi)}{d\xi^2}+k^2f^2\xi^2=\alpha \qquad (2.20)$$

where both sides have now been set equal to a separation constant, α, since each is a function of only one variable. Thus Eq. (2.15) reduces to the pair of ordinary differential equations,

$$(1-\eta^2)\frac{d^2Y(\eta)}{d\eta^2}-(c^2\eta^2-\alpha)\,Y(\eta)=0 \qquad (2.21)$$

$$(\xi^2-1)\frac{d^2X(\xi)}{d\xi^2}+(c^2\xi^2-\alpha)\,X(\xi)=0 \qquad (2.22)$$

where kf has been replaced by the dimensionless frequency variable, c. Eqs. (2.14) may now be written

$$H_\varphi=\frac{A_0}{f}\frac{1}{\sqrt{(1-\eta^2)(\xi^2-1)}}\,Y(\eta)\,X(\xi)\,e^{-j\omega t} \qquad (2.23)$$

$$E_\eta=\frac{j\omega\mu A_0}{c^2}\frac{1}{\sqrt{(\xi^2-\eta^2)(1-\eta^2)}}\,Y(\eta)\frac{dX(\xi)}{d\xi}\,e^{-j\omega t} \qquad (2.24)$$

$$E_\xi=-\frac{j\omega\mu A_0}{c^2}\frac{1}{\sqrt{(\xi^2-\eta^2)(\xi^2-1)}}\frac{dY(\eta)}{d\eta}\,X(\xi)\,e^{-j\omega t} \qquad (2.25)$$

5. Alternative Transformations

It will occasionally be convenient to make the transformations

$$S(\eta)=\frac{1}{\sqrt{1-\eta^2}}\,Y(\eta) \qquad (2.26)$$

$$R(\xi)=\frac{1}{\sqrt{\xi^2-1}}\,X(\xi) \qquad (2.27)$$

for then Eq. (2.23) reduces to

$$H_\varphi = \frac{A_o}{f} S(\eta) R(\xi) e^{-j\omega t} \tag{2.28}$$

and Eqs. (2.24) and (2.25) may be written

$$E_\eta = \frac{j\omega\mu A_o}{c^2} \frac{1}{\sqrt{\xi^2-\eta^2}} S(\eta) \frac{dX(\xi)}{d\xi} e^{-j\omega t} \tag{2.29}$$

$$E_\xi = -\frac{j\omega\mu A_o}{c^2} \frac{1}{\sqrt{\xi^2-\eta^2}} \frac{dY(\eta)}{d\eta} R(\xi) e^{-j\omega t} \tag{2.30}$$

The additional pair of transformations

$$V(\eta) = \frac{1}{1-\eta^2} Y(\eta) \tag{2.31}$$

$$U(\xi) = \frac{1}{\xi^2-1} X(\xi) \tag{2.32}$$

must also be considered. Their usefulness, as will be more apparent later, stems from the fact that the functions $V(\eta)$ and $U(\xi)$ satisfy the equations

$$(1-\eta^2)\frac{d^2V(\eta)}{d\eta^2} - 4\eta\frac{dV(\eta)}{d\eta} + (\alpha - 2 - c^2\eta^2)V(\eta) = 0 \tag{2.33}$$

$$(\xi^2-1)\frac{d^2U(\xi)}{d\xi^2} + 4\xi\frac{dU(\xi)}{d\xi} - (\alpha - 2 - c^2\xi^2)U(\xi) = 0 \tag{2.34}$$

Eq. (2.23) becomes

$$H_\varphi = \frac{A_o}{f}\sqrt{(1-\eta^2)(\xi^2-1)}\, V(\eta)U(\xi) e^{-j\omega t}$$

$$= \frac{A_o}{f^2} k_\varphi V(\eta) U(\xi) e^{-j\omega t} \tag{2.35}$$

Finally, the relations

$$S(\eta) = \sqrt{1-\eta^2}\ V(\eta) \tag{2.36}$$

$$R(\xi) = \sqrt{\xi^2-1}\ U(\xi) \tag{2.37}$$

will be set down for future reference.

6. Singularities

The singularities of the differential equations at $\eta = \pm 1$, $\xi = \pm 1$, are regular singular points. The points at infinity are irregular or essential singular points. It is well known that differential equations of this form (2 regular singularities and 1 irregular singularity) are very difficult to solve. Solution by series methods is not simple; they cannot be reduced to equations giving two-term recursion formulas for the coefficients of their series expansions. Characteristically, their development in series involves three-term recursion formulas. Further, their solutions cannot be expressed in the form of an integral of algebraic and exponential functions, as can the solutions of less complicated differential equations.

In this discussion, it is not relevant that this problem is concerned only with limited ranges of the variables, namely

$$+1 \geqslant \eta \geqslant -1\,, \qquad \infty > \xi \geqslant 1 \tag{2.38}$$

and that certain singularities of the differential equations fall outside these intervals. It may be recalled that the solution of differential equations relies heavily on the theory of analytic functions of a complex variable, and that solutions are characterized by the nature

and total number of singularities in the entire complex plane, rather than by those along the portions of the real axis to which a given problem is confined by certain boundary conditions.

CHAPTER III

BOUNDARY CONDITIONS AND EIGENVALUES

1. Boundary Conditions Owing to Symmetry Considerations

For any given cavity system the electromagnetic fields within and without the cavity will be described by solutions of Maxwell's equations satisfying certain conditions of continuity across the boundary walls. Regardless of the cavity shape or materials or boundary conditions due to discontinuities in the material properties of the system, by virtue of the symmetry of the co-ordinate system and its inherent geometric singularities certain additional boundary conditions must be satisfied by the solutions. We exclude from our concern the extremely singular behavior of the point at which $\xi = 1$, $\eta = \pm 1$.

First we require that all fields be finite along the z-axis, i.e.,

$$\left.\begin{aligned} H_\varphi(\eta,\xi,t)\Big|_{\eta=\pm1} &< \infty \qquad (3.1)\\ E_\xi(\eta,\xi,t)\Big|_{\eta=\pm1} &< \infty \qquad (3.2)\end{aligned}\right\} \text{ when } \xi > 1.$$

Further, the electric field must be continuous across the z-axis, or

$$E_\eta(\eta,\xi,t)\Big|_{\eta=\pm1} = 0 \qquad (3.3)$$

Now

$$H_\varphi(\eta,\xi,t) = \frac{A_o}{f} S(\eta) R(\xi) e^{-j\omega t} \qquad (3.4)$$

For H_φ finite at $\eta = \pm 1$, this requires

$$S(\eta)\Big|_{\eta=\pm1} < \infty \qquad (3.5)$$

or, $S(\eta)$ is an analytic function having no poles even at the limiting values of η. By Eq. (2.29),

$$E_\eta(\eta,\xi,t) = \frac{j\omega\mu A_0}{c^2}\frac{1}{\sqrt{\xi^2-\eta^2}}\,S(\eta)\frac{dX(\xi)}{d\xi}\,e^{-j\omega t} \tag{3.6}$$

so that for $E_\eta = 0$ at $\eta = \pm 1$, we require

$$S(1) = S(-1) = 0 \tag{3.7}$$

a stronger condition than (3.5). Since

$$Y(\eta) = \sqrt{1-\eta^2}\,S(\eta) \tag{3.8}$$

it must also be true that

$$Y(1) = Y(-1) = 0 \tag{3.9}$$

In view then of (2.31), $V(\eta)$ must remain finite at $\eta = \pm 1$. From Eq. (2.30),

$$E_\xi(\eta,\xi,t) = -\frac{j\omega\mu_0 A_0}{c^2}\frac{1}{\sqrt{\xi^2-\eta^2}}\frac{dY(\eta)}{d\eta}\,R(\xi)\,e^{-j\omega t} \tag{3.10}$$

we see that in order for E_ξ to be finite at $\eta = \pm 1$, it is necessary that

$$\left.\frac{dY(\eta)}{d\eta}\right|_{\eta=\pm 1} < \infty \tag{3.11}$$

Using (3.8) we can write

$$\frac{dY(\eta)}{d\eta} = \frac{d}{d\eta}\left[\sqrt{1-\eta^2}\,S(\eta)\right]$$

$$= \sqrt{1-\eta^2}\,\frac{dS(\eta)}{d\eta} - \frac{1}{\sqrt{1-\eta^2}}\,S(\eta) \tag{3.12}$$

For this last expression to remain finite at $\eta = \pm 1$, we must have

$$S(1) = S(-1) = 0 \tag{3.13}$$

as before, and in addition

$$\left.\frac{d S(\eta)}{d \eta}\right|_{\eta=\pm 1} < \infty \tag{3.14}$$

In consequence of (3.13) and (3.14), application of L'Hôpital's rule to (2.36) shows that $V(\eta)$ must vanish at $\eta = \pm 1$.

2. Eigenproperties and Symmetry of the "Angular" or η-Solutions

In the preceding chapter, it was shown that the fields could be obtained from a potential,

$$Q(\eta, \xi, t) = A_0 Y(\eta) X(\xi) e^{-j\omega t} \tag{3.15}$$

whose components satisfied the ordinary linear differential equations

$$(1-\eta^2)\frac{d^2Y}{d\eta^2} - (c^2\eta^2 - \alpha)Y = 0 \tag{3.16}$$

$$(\xi^2-1)\frac{d^2X}{d\xi^2} + (c^2\xi^2 - \alpha)X = 0 \tag{3.17}$$

Let us first consider these equations individually. If (3.16) be divided by $(1-\eta^2)$, there results

$$\frac{d^2Y}{d\eta^2} - \frac{c^2\eta^2}{1-\eta^2}Y + \frac{\alpha}{1-\eta^2}Y = 0 \tag{3.18}$$

which is self-adjoint.[1] If in addition there be imposed either

---

(1) Self adjoint differential equations are discussed in Courant-Hilbert, "Methoden der mathematischen Physik," Vol. I, p. 238, J. Springer, Berlin, 1931. Interscience Reproduction.

Dirichlet[1] or Neumann boundary conditions at the terminal points of a finite interval, the system constitutes a familiar Sturm-Liouville[2] characteristic value or eigenvalue problem.

For a specified value of the parameter, c, the boundary condition given by (3.9) defines a discrete but infinite set of solutions to the second-order equation (3.16) or (3.18), to each of which corresponds a unique value of α. Now if $Y_\ell(\eta)$ is such a solution of (3.16), corresponding to a certain α_ℓ, then $Y_\ell(-\eta)$ is also a solution since the coefficients are all even functions of η. Further, $Y_\ell(-\eta)$ will satisfy the boundary condition (3.9). The two solutions then are not independent but can differ only by a multiplicative constant:

$$Y_\ell(-\eta) = \epsilon\, Y_\ell(\eta) \tag{3.19}$$

One can replace η by $-\eta$ in this equation, giving

$$Y_\ell(\eta) = \epsilon\, Y_\ell(-\eta) \tag{3.20}$$

Simultaneous solution of (3.19) and (3.20) yields

$$\epsilon^2 = 1, \qquad \epsilon = \pm 1 \tag{3.21}$$

from which it may be concluded[3] that the solutions of (3.16) of interest to us must be either even or odd with respect to change of sign of η.

---

(1) See P. M. Morse and H. Feshbach, "Methods of Theoretical Physics," pp. 137ff., Technology Press, Cambridge, 1946. These are the only boundary conditions of interest to us, although certain others are also permissible.

(2) Courant-Hilbert, loc. cit., pp. 250ff.

(3) A similar treatment is given for an entirely different physical problem by L. I. Schiff, "Quantum Mechanics," p. 39, McGraw-Hill, 1949, in discussing a one-dimensional square-well potential problem. The same approach is also found in Abraham's paper.

The implied conditions of continuity of $Y_\ell(\eta)$ and its derivatives within the interval $1 \gg \eta \gg -1$ require that at $\eta = 0$, even solutions have zero slope and odd solutions have zero value. Obviously, $S_\ell(\eta)$ has the same symmetry as $Y_\ell(\eta)$.

Since we are dealing with a Sturm-Liouville problem, it is to be expected that the solutions satisfy the orthogonality relation,

$$\int_{-1}^{1} Y_\ell(\eta, c) Y_m(\eta, c) \frac{d\eta}{1-\eta^2} = 0, \qquad m \neq \ell \tag{3.22}$$

or its equivalent,

$$\int_{-1}^{1} S_\ell(\eta, c) S_m(\eta, c)\, d\eta = 0, \qquad m \neq \ell \tag{3.23}$$

3. The "Radial" Eigenvalue Problem

No boundary conditions have yet been stipulated for the $X(\xi)$ functions. These bring in for the first time the dimensions and material properties of the cavity system. As was the case with the equation in η, we have again a Sturm-Liouville problem in which to specify a set of unique solutions to Eq. (3.17) for a given value of the parameter, c, over a continuous bounded interval in ξ, we are required to prescribe boundary conditions at the limits of the interval, ξ_1 and ξ_2. In the simplest case, we consider the cavity, defined by $\xi_1 < \xi < \xi_2$, to be a perfect dielectric included between spheroidal bounding walls $\xi < \xi_1$ and $\xi_2 < \xi$ which are of infinite conductivity. Since the fields vanish in the walls, there must then be satisfied

$$E_\eta(\eta, \xi_1) = E_\eta(\eta, \xi_2) = 0 \tag{3.24}$$

or using (2.29),

$$\left.\frac{d X(\xi)}{d \xi}\right|_{\xi=\xi_1} = \left.\frac{d X(\xi)}{d \xi}\right|_{\xi=\xi_2} = 0 \tag{3.25}$$

Application of this boundary condition to (3.17) results in a discrete set of eigenfunctions $X_p(\xi)$ and corresponding eigenvalues α_p, all of which will be continuous functions of the frequency variable, c.

4. Eigenfrequencies of the Cavity

Keeping ξ_1 and ξ_2 constant, solution of the given cavity problem then requires simultaneous solution of the two sets:

$$\left\{ \alpha_\ell (c) \right\}, \quad \ell = 0,1,2,3,\ldots \tag{3.26}$$

$$\left\{ \alpha_p (c) \right\}, \quad p = 0,1,2,3,\ldots \tag{3.27}$$

since the same values of α and c are required in (3.16) and (3.17). This will result in a doubly infinite but discrete set of eigenvalues,

$$\left\{\alpha_{\ell p}\right\} = \left\{\alpha_\ell (c_{\ell p})\right\} = \left\{\alpha_p (c_{\ell p})\right\} \tag{3.28}$$

and a corresponding set of eigenfrequencies:[1]

$$c_{\ell p} \longleftrightarrow \alpha_{\ell p} \tag{3.29}$$

The indices ℓ and p will indicate the order of the modes. Thus for a cavity of specified dimensions, we have formally obtained the eigenfrequencies. An example of the graphical simultaneous solution of (3.26) and (3.27) is shown in Fig. 2 .

---

(1) The symbolism of (3.29) will be employed to describe a one-to-one correspondence between quantities having common indices.

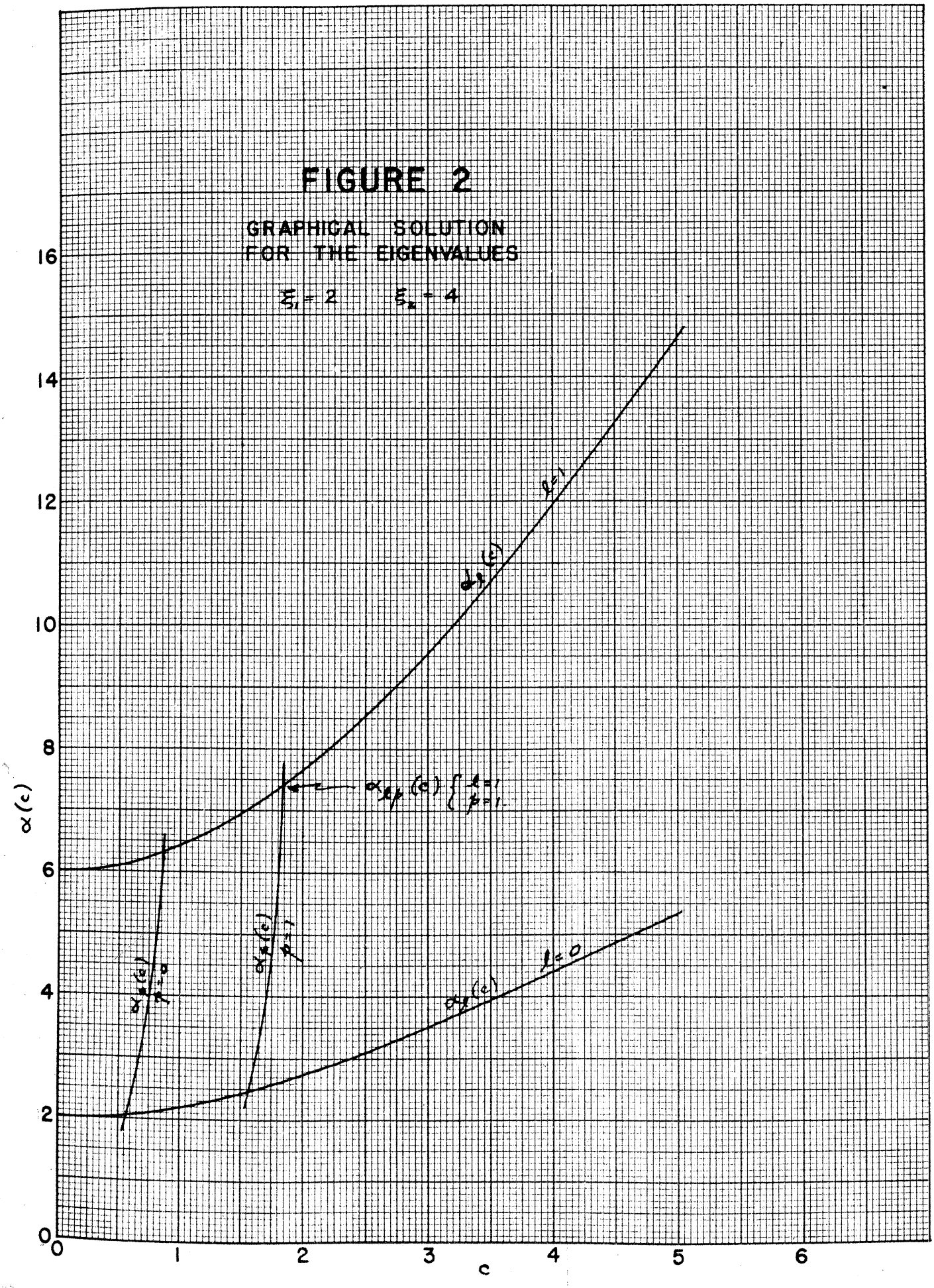
FIGURE 2
GRAPHICAL SOLUTION
FOR THE EIGENVALUES
$\xi_1 = 2$ $\xi_2 = 4$
$\alpha(c)$
c
0
2
4
6
8
10
12
14
16
1
3
5
$\alpha_{k,0}(c)$
$\alpha_{k,1}(c)$
$\alpha_{k,2}(c)$
$\alpha_{k,3}(c)$
$\alpha_{k,4}(c)$
$\alpha_{k,5}(c)$
$\alpha_{k,6}(c)$
$\alpha_{k,7}(c)$
$\alpha_{k,8}(c)$
$\alpha_{k,9}(c)$
$\alpha_{k,10}(c)$
$\alpha_{k,11}(c)$
$\alpha_{k,12}(c)$
$\alpha_{k,13}(c)$
$\alpha_{k,14}(c)$
$\alpha_{k,15}(c)$
$\alpha_{k,16}(c)$
$\alpha_{k,17}(c)$
$\alpha_{k,18}(c)$
$\alpha_{k,19}(c)$
$\alpha_{k,20}(c)$
$\alpha_{k,21}(c)$
$\alpha_{k,22}(c)$
$\alpha_{k,23}(c)$
$\alpha_{k,24}(c)$
$\alpha_{k,25}(c)$
$\alpha_{k,26}(c)$
$\alpha_{k,27}(c)$
$\alpha_{k,28}(c)$
$\alpha_{k,29}(c)$
$\alpha_{k,30}(c)$
$\alpha_{k,31}(c)$
$\alpha_{k,32}(c)$
$\alpha_{k,33}(c)$
$\alpha_{k,34}(c)$
$\alpha_{k,35}(c)$
$\alpha_{k,36}(c)$
$\alpha_{k,37}(c)$
$\alpha_{k,38}(c)$
$\alpha_{k,39}(c)$
$\alpha_{k,40}(c)$
$\alpha_{k,41}(c)$
$\alpha_{k,42}(c)$
$\alpha_{k,43}(c)$
$\alpha_{k,44}(c)$
$\alpha_{k,45}(c)$
$\alpha_{k,46}(c)$
$\alpha_{k,47}(c)$
$\alpha_{k,48}(c)$
$\alpha_{k,49}(c)$
$\alpha_{k,50}(c)$
$\alpha_{k,51}(c)$
$\alpha_{k,52}(c)$
$\alpha_{k,53}(c)$
$\alpha_{k,54}(c)$
$\alpha_{k,55}(c)$
$\alpha_{k,56}(c)$
$\alpha_{k,57}(c)$
$\alpha_{k,58}(c)$
$\alpha_{k,59}(c)$
$\alpha_{k,60}(c)$
$\alpha_{k,61}(c)$
$\alpha_{k,62}(c)$
$\alpha_{k,63}(c)$
$\alpha_{k,64}(c)$
$\alpha_{k,65}(c)$
$\alpha_{k,66}(c)$
$\alpha_{k,67}(c)$
$\alpha_{k,68}(c)$
$\alpha_{k,69}(c)$
$\alpha_{k,70}(c)$
$\alpha_{k,71}(c)$
$\alpha_{k,72}(c)$
$\alpha_{k,73}(c)$
$\alpha_{k,74}(c)$
$\alpha_{k,75}(c)$
$\alpha_{k,76}(c)$
$\alpha_{k,77}(c)$
$\alpha_{k,78}(c)$
$\alpha_{k,79}(c)$
$\alpha_{k,80}(c)$
$\alpha_{k,81}(c)$
$\alpha_{k,82}(c)$
$\alpha_{k,83}(c)$
$\alpha_{k,84}(c)$
$\alpha_{k,85}(c)$
$\alpha_{k,86}(c)$
$\alpha_{k,87}(c)$
$\alpha_{k,88}(c)$
$\alpha_{k,89}(c)$
$\alpha_{k,90}(c)$
$\alpha_{k,91}(c)$
$\alpha_{k,92}(c)$
$\alpha_{k,93}(c)$
$\alpha_{k,94}(c)$
$\alpha_{k,95}(c)$
$\alpha_{k,96}(c)$
$\alpha_{k,97}(c)$
$\alpha_{k,98}(c)$
$\alpha_{k,99}(c)$
$\alpha_{k,100}(c)$

However, one may further consider the eigenvalues and separation constants as continuous functions of the bounding co-ordinates, ξ_1 and ξ_2, or

$$c_{\ell p}(\xi_1, \xi_2) \longleftrightarrow \alpha_{\ell p}(\xi_1, \xi_2) \tag{3.30}$$

The eigenfunctions are likewise continuous functions of the bounding co-ordinates and so their dependence is completely given by

$$Y_\ell = Y_\ell(\eta, t; c) \tag{3.31}$$

$$X_p = X_p(\xi, t; c, \xi_1, \xi_2) \tag{3.32}$$

although we may omit the time in further discussion. The one-to-one correspondence expressed by (3.30) establishes a connection between (3.31) and (3.32) which is more clearly expressed by writing

$$Y_\ell = Y_\ell(\eta; c_{\ell p}) \tag{3.33}$$

$$X_{\ell p} = X_{\ell p}(\xi; c_{\ell p}, \xi_1, \xi_2) \tag{3.34}$$

to describe the functional dependence of a particular mode.

5. Alternate Approach to the Eigenvalue Problem

The method set down above for determining the eigenfrequencies is fundamentally correct, but in practice their computation is a difficult procedure, especially when one is interested in the effect of variation of all possible variables, as in this instance. We now proceed to outline an equivalent scheme of analysis which makes calculations less tedious and more direct. Since for the complete system, identical values of α and c are required simultaneously in (3.16) and (3.17), we consider first the "angular" equation (3.16), as its boundary conditions are inde-

pendent of ξ_1 and ξ_2, which is not the case for (3.17). That is, we can write (3.26) and (3.27) as

$$\{ \alpha_\ell(c) \} \tag{3.35}$$

$$\{ \alpha_p(c; \xi_1, \xi_2) \} \tag{3.36}$$

It is obviously much simpler to establish the set of functions (3.35) than the set (3.36). Further, the only points of the set (3.36) which interest us are those included in $\{ \alpha_{\ell p}(c_{\ell p}) \}$ which must also satisfy (3.35). A further attraction is that the set (3.35) is already available in tabulated form, and that the coefficients for series representations of solutions of (3.16) and (3.17) are also tabulated for values of α and c having the same relation. Consequently, the logical attack is to form the series representations of the solutions of (3.17) consistent with (3.35) and from these determine those pairs of values of ξ_1 and ξ_2 for which the boundary condition (3.25) is satisfied. This we shall do.

6. Independent Solutions of the Second-Order Equations

Now Eqs. (3.16) and (3.17) being ordinary second order linear differential equations, have each two independent solutions for specified values of c and α. The particular solutions desired are required to be analytic over the entire interval. Only one solution of (3.16) can vanish at $\eta = \pm 1$, so it is the particular solution desired; the second independent solution is non-vanishing at these points, and is sometimes singular. Thus, the specification of c and an index ℓ uniquely defines a solution $S_\ell(\eta, c)$ of (3.16) [which satisfies the boundary condition (3.9)] and a corresponding value of the separation constant α_ℓ.

The two independent solutions of (3.17) behave similarly. In this instance however, the pole at $\xi = 1$ is not always included in the interval of interest. Assuming the dependence of α upon c to be that of Eq. (3.35) we can use the notation

$$X_\ell^{(1)}(\xi, c) \; ; \quad X_\ell^{(2)}(\xi, c) \tag{3.37}$$

to denote the two independent solutions of (3.17); note that boundary conditions have not yet been imposed, and that the index is the same as for $Y_\ell(\eta, c)$. At $\xi = 1$ only one solution of (3.17) can be zero and we shall choose to specify this one as $X_\ell^{(1)}(\xi, c)$. The other independent solution,[1] which is non-vanishing at $\xi = 1$ and sometimes infinite there, we call $X_\ell^{(2)}(\xi, c)$. Then for a pair of boundary co-ordinates, ξ_1 and ξ_2, the particular solution of (3.17) desired is a linear combination of (3.37) which we shall write as

$$X_{\ell p}(\xi; c, \xi_1, \xi_2) = a_{\ell p}(c, \xi_1, \xi_2) X_\ell^{(1)}(\xi, c) + b_{\ell p}(c, \xi_1, \xi_2) X_\ell^{(2)}(\xi, c) \tag{3.38}$$

where the coefficients are recognized as functions of the frequency and geometry, and are determined by certain boundary conditions which $X_{\ell p}(\xi ; c, \xi_1, \xi_2)$ must satisfy at the walls. It should be realized that c, ξ_1, and ξ_2 are not all independent variables for a given mode of indices ℓ and p, but that specifying two of the three determines the third, in accordance with (3.30). If we assume the walls to be perfectly conducting and impose the boundary condition (3.25) we have

$$\frac{\partial}{\partial \xi} X_{\ell p}(\xi; c, \xi_1, \xi_2)\Big|_{\xi=\xi_1} = \frac{\partial}{\partial \xi} X_{\ell p}(\xi; c, \xi_1, \xi_2)\Big|_{\xi=\xi_2} = 0 \tag{3.39}$$

---

(1) The corresponding U and V solutions of the second kind are invariably infinite at the poles while those of the first kind are the ones which always remain finite there. This is the basis of discrimination employed by SMCH, p. 39, and is probably more generally applicable.

Applying this to (3.38) yields

$$X'_{\ell p}(\xi_1; c, \xi_1, \xi_2) = a_{\ell p}(c, \xi_1, \xi_2) \left.\frac{\partial X^{(1)}_\ell(\xi, c)}{\partial \xi}\right|_{\xi=\xi_1} + b_{\ell p}(c, \xi_1, \xi_2) \left.\frac{\partial X^{(2)}_\ell(\xi, c)}{\partial \xi}\right|_{\xi=\xi_1} \tag{3.40}$$

$$= a_{\ell p}(c, \xi_1, \xi_2)\, X^{(1)\prime}_\ell(\xi_1, c) + b_{\ell p}(c, \xi_1, \xi_2)\, X^{(2)\prime}_\ell(\xi_1, c) \tag{3.41}$$

where we have defined[1]

$$X'_{\ell p}(\xi_1; c, \xi_1, \xi_2) \triangleq \frac{\partial}{\partial \xi} X_{\ell p}(\xi; c, \xi_1, \xi_2)\Big|_{\xi=\xi_1} \tag{3.42}$$

$$X^{(i)\prime}_\ell(\xi_1, c) \triangleq \frac{\partial}{\partial \xi} X^{(i)}_\ell(\xi, c)\Big|_{\xi=\xi_1} \tag{3.43}$$

Then

$$X'_{\ell p}(\xi_1; c, \xi_1, \xi_2) = a_{\ell p}(c, \xi_1, \xi_2) X^{(1)\prime}_\ell(\xi_1, c) + b_{\ell p}(c, \xi_1, \xi_2) X^{(2)\prime}_\ell(\xi_1, c) = 0 \tag{3.44}$$

$$X'_{\ell p}(\xi_2; c, \xi_1, \xi_2) = a_{\ell p}(c, \xi_1, \xi_2) X^{(1)\prime}_\ell(\xi_2, c) + b_{\ell p}(c, \xi_1, \xi_2) X^{(2)\prime}_\ell(\xi_2, c) = 0 \tag{3.45}$$

Simultaneous solution gives

$$\frac{b_{\ell p}(c, \xi_1, \xi_2)}{a_{\ell p}(c, \xi_1, \xi_2)} = -\frac{X^{(1)\prime}_\ell(\xi_1, c)}{X^{(2)\prime}_\ell(\xi_1, c)} = -\frac{X^{(1)\prime}_\ell(\xi_2, c)}{X^{(2)\prime}_\ell(\xi_2, c)} \tag{3.46}$$

For given ξ_1 and ξ_2, this can then be regarded as an equation in c, a condition determining the eigenfrequencies, analogous to (3.30).

7. Auxiliary Functions

We can now define a function

$$\gamma_\ell(\xi, c) \triangleq -\frac{X^{(1)\prime}_\ell(\xi, c)}{X^{(2)\prime}_\ell(\xi, c)} = -\frac{\frac{\partial}{\partial \xi} X^{(1)}_\ell(\xi, c)}{\frac{\partial}{\partial \xi} X^{(2)}_\ell(\xi, c)} \tag{3.47}$$

---

(1) The symbol $\triangleq$ denotes "is equal to by definition," and is a convenience acquired from Prof. M. F. Gardner.

which is not an explicit function of the bounding co-ordinates, ξ_1 and ξ_2, and in terms of which the eigencondition may be written

$$\gamma_\ell^{\mu}(\xi_1, c) = \gamma_\ell^{\mu}(\xi_2, c) \tag{3.48}$$

where $\gamma_\ell^{\mu}(\xi_1, c) \triangleq \gamma_\ell^{\mu}(\xi, c)\big|_{\xi=\xi_1}$. We may consider $\gamma_\ell^{\mu}(\xi, c)$ as determining a geometrical surface whose interpretation in terms of contours of constant elevation may provide a better insight into the problem.

From (3.46) one sees that if (3.48) is satisfied then the ratio of the coefficients is fixed:

$$\frac{b_{\ell p}(c, \xi_1, \xi_2)}{a_{\ell p}(c, \xi_1, \xi_2)} = \gamma_\ell^{\mu}(\xi_1, c) = \gamma_\ell^{\mu}(\xi_2, c) \tag{3.49}$$

For convenience (and this is purely arbitrary) it is desirable to normalize by imposing the additional restriction

$$\left[a_{\ell p}(c, \xi_1, \xi_2)\right]^2 + \left[b_{\ell p}(c, \xi_1, \xi_2)\right]^2 = 1 \tag{3.50}$$

We may then define

$$\beta_{\ell p}(c, \xi_1, \xi_2) = \arccos a_{\ell p}(c, \xi_1, \xi_2) = \arcsin b_{\ell p}(c, \xi_1, \xi_2) \tag{3.51}$$

which is permissible since by (3.50)

$$\cos^2 \beta_{\ell p} + \sin^2 \beta_{\ell p} = 1 \tag{3.52}$$

It follows at once that

$$\beta_{\ell p}(c, \xi_1, \xi_2) = \arctan \gamma_\ell^{\mu}(\xi_1, c) = \arctan \gamma_\ell^{\mu}(\xi_2, c) \tag{3.53}$$

where $\beta_{\ell p}$ is assumed to have its principal value. From the preceding discussion, and in particular Eq. (3.46), it should be apparent that c, ξ_1, and ξ_2 are not independent variables, but that fixing two of the three

establishes a discrete set of values which the third may sssume, according to (3.30). Following the example set for $\gamma_\ell^{\mu}(\xi, c)$, Equation (3.47), we can define then the more general function

$$\beta_\ell(\xi, c) \triangleq \arctan \gamma_\ell^{\mu}(\xi, c) \tag{3.54}$$

which again is not an explicit function of ξ_1 and ξ_2. Its advantage over $\gamma_\ell^{\mu}(\xi, c)$ lies in the fact that the zeroes of the continuous analytic functions $X_\ell^{(\omega)'}(\xi, c)$ introduce poles in the functions γ_ℓ^{μ}. $\beta_\ell(\xi, c)$ on the other hand remains an analytic function over the entire range of the variables c and ξ. We choose now to define β_ℓ as a continuous function rather than restrict it to values between π and $-\pi$. Equivalent to (3.48) the eigencondition may now be written

$$\beta_\ell(\xi_1, c) = \beta_\ell(\xi_2, c) - p\pi \tag{3.55}$$

where $\beta_\ell(\xi_1, c) \triangleq \beta_\ell(\xi, c)\big|_{\xi=\xi_1}$, and where $p = 0, 1, 2, \ldots$.

This establishes the identity of the p th mode unambiguously and shows why we chose to define β_ℓ as a continuous function.

CHAPTER IV

THE SPECIAL CASE OF TRIGONOMETRIC SOLUTIONS

1. "Angular" Solutions when $c^2 = \alpha$.

In the particular case where $c^2 = \alpha$, Eqs. (2.21) and (2.22) reduce to

$$\frac{d^2 Y(\eta)}{d\eta^2} + c^2 Y(\eta) = 0 \qquad (4.1)$$

$$\frac{d^2 X(\xi)}{d\xi^2} + c^2 X(\xi) = 0 \qquad (4.2)$$

whose solutions are of course sines and cosines. It will be recalled that $Y_\ell(\eta)$ must be either an even or an odd function of η. We choose the particular solution of (4.1) to be

$$Y_\ell(\eta) = A \cos(c\eta) \qquad (4.3)$$

if ℓ is even, and

$$Y_\ell(\eta) = A \sin(c\eta) \qquad (4.4)$$

if ℓ is odd. The smallest positive value of c for which the boundary condition (3.9) is satisfied is $\pi/2$, employing (4.3). We may call this the mode for $\ell = 0$, and find then that we can set up the relation

$$c_{\ell p} = \frac{\pi}{2}(\ell + 1) \qquad (4.5)$$

not forgetting that it holds only when $c^2 = \alpha$. Owing to the continuous character of the functions, however, we can use this to define the ℓ th mode. $Y_\ell(\eta)$ is then a function with ℓ nodes, not counting the two at the ends of the interval $1 \geqslant \eta \geqslant -1$.

2. The "Radial" Solutions

We choose the first solution of (4.2) to be that which vanishes at $\xi = 1$, with positive slope. Such a solution is

$$X_\ell^{(1)} = B \sin[c(\xi-1)]$$

$$= B \sin\left[\tfrac{\pi}{2}(\ell+1)(\xi-1)\right] \tag{4.6}$$

The second solution we choose to be

$$X_\ell^{(2)} = -B \cos[c(\xi-1)] \tag{4.7}$$

This is not the only way in which two independent solutions could be specified. This choice is made because it conforms with those of the series representations to be discussed in Chapter VI.

The slopes are then

$$X_\ell^{(1)\prime} = Bc \cos[c(\xi-1)]$$

$$X_\ell^{(2)\prime} = Bc \sin[c(\xi-1)] \tag{4.8}$$

3. Values of the Auxiliary Functions

The function γ_ℓ defined by (3.47) has the value

$$\gamma_\ell(\xi_1, c) = \frac{-X_\ell^{(1)\prime}(\xi_1, c)}{X_\ell^{(2)\prime}(\xi_1, c)} = -\cot[c(\xi-1)] \tag{4.9}$$

The function β_ℓ is

$$\beta_\ell(\xi_1, c) = \arctan \gamma_\ell(\xi_1, c) = c(\xi_1 - 1) - \frac{\pi}{2}, \tag{4.10}$$

a linear function of ξ_1. Introducing into (3.55),

$$\beta_\ell(\xi_1, c) = \beta_\ell(\xi_2, c) - \frac{p\pi}{2} \tag{4.11}$$

the values given by (4.10) we obtain

$$c(\xi_1 - 1) - \frac{\pi}{2} = c(\xi_2 - 1) - \frac{\pi}{2} - p\pi \tag{4.12}$$

or

$$\xi_2 = \xi_1 + \frac{p\pi}{c} \tag{4.13}$$

which yields

$$\xi_2 = \xi_1 + \frac{2p}{\ell + 1} \tag{4.14}$$

upon making use of (4.5). The parameters p and ℓ, being integers characterizing the various modes, make the difference term in (4.14) a rational fraction.

The coefficients $a_{\ell p}$ and $b_{\ell p}$, given by (3.51), are found to be

$$\begin{aligned} a_{\ell p}(c, \xi_1, \xi_2) &= \cos\beta_\ell(\xi_1, c) = \cos\left[c(\xi_1 - 1) - \tfrac{\pi}{2}\right] = \sin\left[c(\xi_1 - 1)\right] \\ b_\ell(\xi_1, c) &= \sin\beta_\ell(\xi_1, c) = \sin\left[c(\xi_1 - 1) - \tfrac{\pi}{2}\right] = -\cos\left[c(\xi_1 - 1)\right] \end{aligned} \tag{4.15}$$

Since

$$X_{\ell p}(\xi; c, \xi_1, \xi_2) = a_{\ell p}(c, \xi_1, \xi_2) X_\ell^{(1)}(\xi, c) + b_{\ell p}(c, \xi_1, \xi_2) X_\ell^{(2)}(\xi, c) \tag{4.16}$$

then

$$X_\ell(\xi_1, c) = X_{\ell p}(\xi; c, \xi_1, \xi_2)\Big|_{\xi=\xi_1}$$

$$= a_{\ell p}(c, \xi_1, \xi_2) X_\ell^{(1)}(\xi_1, c) + b_{\ell p}(c, \xi_1, \xi_2) X_\ell^{(2)}(\xi_1, c)$$

$$= B\left\{ \sin^2[c(\xi_1 - 1)] + \cos^2[c(\xi_1 - 1)] \right\}$$

$$= B \qquad (4.17)$$

The function $X_{\ell p}$ has then the same value at both walls.

4. Expressions for the Fields

The fields become

$$H_\varphi = \frac{A_0}{f} \frac{1}{\sqrt{(\xi^2-1)(1-\eta^2)}} \cos(c\eta) \cos[c(\xi - \xi_1)] e^{-j\omega t}$$

$$E_\eta = -\frac{j\omega\mu_0 A_0}{c} \frac{1}{\sqrt{(\xi^2-\eta^2)(1-\eta^2)}} \cos(c\eta) \sin[c(\xi - \xi_1)] e^{-j\omega t}$$

$$E_\xi = \frac{j\omega\mu_0 A_0}{c} \frac{1}{\sqrt{(\xi^2-\eta^2)(\xi^2-1)}} \sin(c\eta) \cos[c(\xi - \xi_1)] e^{-j\omega t}$$

(4.18)

The condition that $c^2 = \alpha$ is in effect a type of resonance. This is the situation when a linear antenna in free space is said to be at "resonance".[1] It should not be confused with the normal or resonant modes of oscillation of a confocal spheroidal cavity. It is rather a

---

(1) See R. M. Ryder, J. App. Phys. 13, 329 (1942).

specific result given only by certain particular relations among the cavity parameters, namely (4.14), with the corresponding frequency as given by (4.5).

The foregoing relations are developed here for subsequent comparison with the corresponding functions when $c^2 \neq \alpha$, whose behavior will be discussed in Chapters VI and VII.

CHAPTER V

QUALITATIVE BEHAVIOR OF THE SOLUTIONS

1. Standard Form of the Equations

In an earlier chapter, it was shown that the fields could be obtained from a potential,

$$Q(\eta, \xi, t) = A_0 Y(\eta) X(\xi) e^{-j\omega t} \tag{5.1}$$

whose components satisfied the ordinary linear differential equations

$$(1-\eta^2)\frac{d^2Y(\eta)}{d\eta^2} - (c^2\eta^2 - \alpha) Y(\eta) = 0 \tag{5.2}$$

$$(\xi^2-1)\frac{d^2X(\xi)}{d\xi^2} + (c^2\xi^2 - \alpha) X(\xi) = 0 \tag{5.3}$$

These equations may be rewritten as

$$Y'' + \frac{\alpha - c^2\eta^2}{1-\eta^2} Y = 0 \tag{5.4}$$

$$X'' + \frac{c^2\xi^2 - \alpha}{\xi^2-1} X = 0 \tag{5.5}$$

which are of the form

$$u''(x) + f(x)\, u(x) = 0 \tag{5.6}$$

From the equations in this form, the qualitative behavior of the continuous solutions of (5.2) and (5.3) may be readily investigated. Theorems concerning this behavior are already well known.(1)

---

(1) See for example P. Frank and R. von Mises, "Die Differential- und Integralgleichungen der Mechanik und Physik," Rosenberg, New York, 1943.

2. Behavior of the "Angular" Solutions

It is apparent at once, for example, that if

$$f(\eta) = \frac{\alpha - c^2\eta^2}{1-\eta^2} \tag{5.7}$$

is positive then Y"/Y is negative. The curvature of the graph of $Y(\eta)$ as a function of η is concave toward the η axis and $Y(\eta)$ will be oscillatory in character; this will be the case whenever $|\eta| < \frac{\sqrt{\alpha}}{c}$. If on the other hand, $|\eta| > \frac{\sqrt{\alpha}}{c}$, then $f(\eta)$ is negative, and the curvature of $Y(\eta)$ is away from the η axis. We require $Y(\eta)$ to vanish at $\eta = \pm 1$, in accordance with the boundary condition (3.9).

When $\frac{\sqrt{\alpha}}{c} > 1$, $f(\eta)$ is positive for all values of $1 \geq \eta \geq -1$. $Y(\eta)$ will then have the general form of Figure 3A, which shows the mode for $\ell = 8$, following Ryder.[1] In the special instance of Chapter IV where $\frac{\sqrt{\alpha}}{c} = 1$, $f(\eta)$ is not dependent on η but is constant, and $Y(\eta)$ is then a true sinusoid, as shown in Figure 3B.

When $\frac{\sqrt{\alpha}}{c} < 1$, then $f(\eta)$ changes sign and $Y(\eta)$ has inflection points at $\eta = \pm \frac{\sqrt{\alpha}}{c}$. Except for the two nodes at the end of the interval, the nodes are all confined to the interval $\frac{\sqrt{\alpha}}{c} > \eta > -\frac{\sqrt{\alpha}}{c}$. The character of $Y(\eta)$ becomes radically different, as Figures 3C and D show for two different values of $\frac{\sqrt{\alpha}}{c}$.

The function $\frac{\sqrt{\alpha}}{c}$ is a monotonically decreasing function of c. Consequently, Figures 3A through D represent the behavior of $Y(\eta)$ as c continuously increases. Note how the loops and nodes move in toward the center of the interval. Obviously we must always have $\frac{\sqrt{\alpha}}{c} > 0$, in order to satisfy (3.9) at both ends of the interval simultaneously.

---

(1) R. M. Ryder, J. App. Phys. 13, 329 (1942).

FIGURE 3

$Y_\ell(\eta)$ vs. η
$\ell = 8$

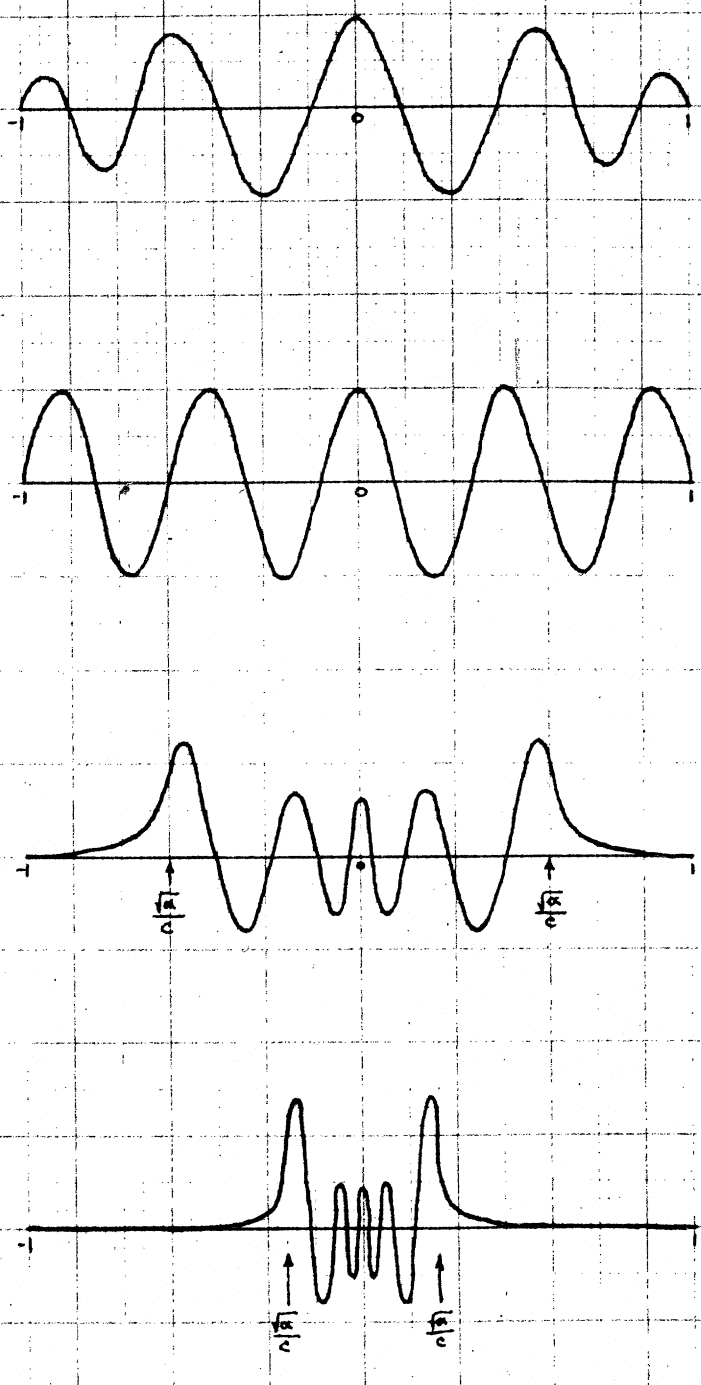

3. The "Radial" Solutions

In similar fashion we discuss

$$\mathcal{G}(\xi) = \frac{c^2\xi^2 - \alpha}{\xi^2 - 1} \tag{5.8}$$

Now if $\xi > \frac{\sqrt{\alpha}}{c}$, $\mathcal{G}(\xi)$ is positive and $X(\xi)$ will be an oscillatory function. For $\xi < \frac{\sqrt{\alpha}}{c}$, the curvature of $X(\xi)$ is away from the axis. Whenever $\frac{\sqrt{\alpha}}{c} \leqslant 1$, $X(\xi)$ will be oscillatory everywhere in the interval $\infty > \xi \geqslant 1$. If $\frac{\sqrt{\alpha}}{c} > 1$, $X(\xi)$ will have an inflection point at $\xi = \frac{\sqrt{\alpha}}{c}$. It should be noted that for a given $\frac{\sqrt{\alpha}}{c}$, an inflection point must occur in either $X(\xi)$ or $Y(\eta)$, but never in both. As before, if $\frac{\sqrt{\alpha}}{c} = 1$, then $X(\xi)$ is a true sinusoid.

On differentiating, we find

$$\mathcal{G}'(\xi) = \frac{2c^2\xi}{(\xi^2-1)^2}\left(\frac{\alpha}{c^2} - 1\right) \tag{5.9}$$

Therefore, $\mathcal{G}(\xi)$ is monotonically increasing or decreasing, according as $\frac{\sqrt{\alpha}}{c}$ is greater or less than unity. As ξ tends to infinity, $\mathcal{G}(\xi)$ reduces to c^2 and Eq. (5.5) becomes

$$X''(\xi) + c^2 X(\xi) = 0 \tag{5.10}$$

so that at large distances the solutions become sinusoids, regardless of the relationship between c^2 and α. As $\xi \to 1$, the two types of behavior become more pronounced. If $\frac{\sqrt{\alpha}}{c} < 1$, $\mathcal{G}(\xi)$ grows more and more positive; the oscillations of $X(\xi)$ become more frequent, and their amplitude smaller. But if $\frac{\sqrt{\alpha}}{c} > 1$, $\mathcal{G}(\xi)$ becomes less positive, goes through zero at $\xi = \frac{\sqrt{\alpha}}{c}$, and approaches $-\infty$ as $\xi \to 1$. Thus $X(\xi)$ oscillates less frequently with decreasing ξ; $X''(\xi)$ vanishes at $\xi = \frac{\sqrt{\alpha}}{c}$, and $X(\xi)$ goes to infinity as $\xi \to 1$.

FIGURE 4

$X_\beta^{(1)}(\xi)$, $X_\beta^{(2)}(\xi)$ vs. ξ

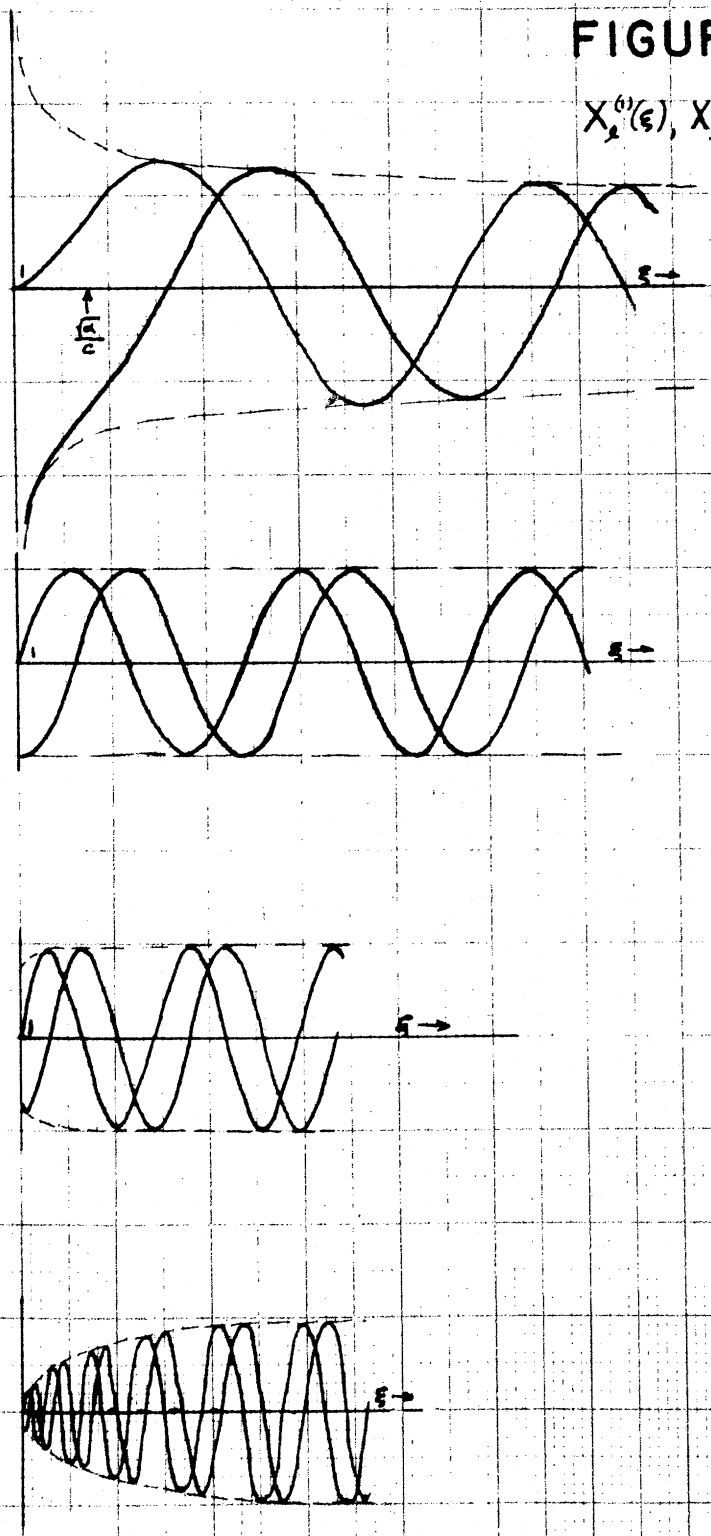

4. Independent Solutions of the "Radial" Equation

Eq. (5.5), being an ordinary second order differential equation, has two independent solutions. The particular solution desired in any given case is a linear combination of these two which satisfies the boundary condition (3.25) that $X'(\xi)$ vanish at ξ_1 and ξ_2, the ends of the subinterval $\infty > \xi_2 \gg \xi \gg \xi_1 \gg 1$. However, any solution must behave as outlined in the preceding paragraph. Figures 4A to D each show two independent solutions of (5.5) for values of $\frac{\sqrt{\alpha}}{c}$ corresponding to those of Figure 3. No attempt has been made to pick the particular solutions necessary for any chosen ξ_1 and ξ_2. Note that even if $\frac{\sqrt{\alpha}}{c} > 1$, the inflection point of $X(\xi)$ will not be included in the interval $\xi_2 \gg \xi \gg \xi_1$ if $\xi_1 > \frac{\sqrt{\alpha}}{c}$. In order to satisfy (3.25) it is necessary that $\xi_2 > \frac{\sqrt{\alpha}}{c}$, as should be apparent from the graphs. The envelope of $X(\xi)$,

$$\text{env } X(\xi) = \sqrt{[X^{(1)}(\xi)]^2 + [X^{(2)}(\xi)]^2} \tag{5.11}$$

is also shown.

5. Behavior near $\xi = 1$

The behavior near $\xi = 1$ will be of interest later on. Letting $\chi = \xi - 1$ and integrating (5.5) once we obtain

$$X'(\chi_0) = X'(\chi) + \int_{\chi_0}^{\chi} X(z)\, g(z)\, dz \tag{5.12}$$

At $\chi = 0$, $g(\chi)$ has a first order pole. In contrast, near $\chi = 0$, $X(\chi)$ varies slowly enough that we can replace it with an average value $\bar{X}$. Then

$$X'(\chi_0) = X'(\chi) + \bar{X} \int_{\chi_0}^{\chi} \frac{a}{z}\, dz$$

$$= X'(\chi) + \bar{X}\, a [\ln \chi - \ln \chi_0] \tag{5.13}$$

As $\chi_0 \to 0$, $\ln \chi_0 \to -\infty$ so that $X'(\chi_0)/a\bar{X} \to \infty$.

We can pick one solution which will vanish at the pole. In this case, $\bar{X}$ can no longer be considered constant but varies linearly. $X'(\chi)$ then is finite and slowly varying at the singularity. Any other solution must necessarily have infinite slope there. If $\sqrt{\alpha} > c$, the curvature is away from the axis and the second solution is infinite at the pole. However, if $\sqrt{\alpha} < c$, there is no inflection point and the second solution must remain finite owing to the oscillatory character of the solutions. These points will be apparent from Figure 4.

6. Field Patterns

The qualitative behavior of $Y(\eta)$ and $X(\xi)$ has been given by Figures 3 and 4. The corresponding behavior of $S(\eta)$ and $R(\xi)$ is easily deduced from the transformations (2.26) and (2.27). Then the field patterns may be readily inferred from the expressions (2.28), (2.29) and (2.30). Figure 5 indicates typical field pattern behavior and shows the modes described by various values of the ordering index ϕ. Solid lines denote the electric field, which lies in meridional planes. The magnetic field lines are circles concentric with the axis of rotation, and show as dots in the figure. Since these are standing waves, the electric and magnetic fields differ in time phase by 90°.

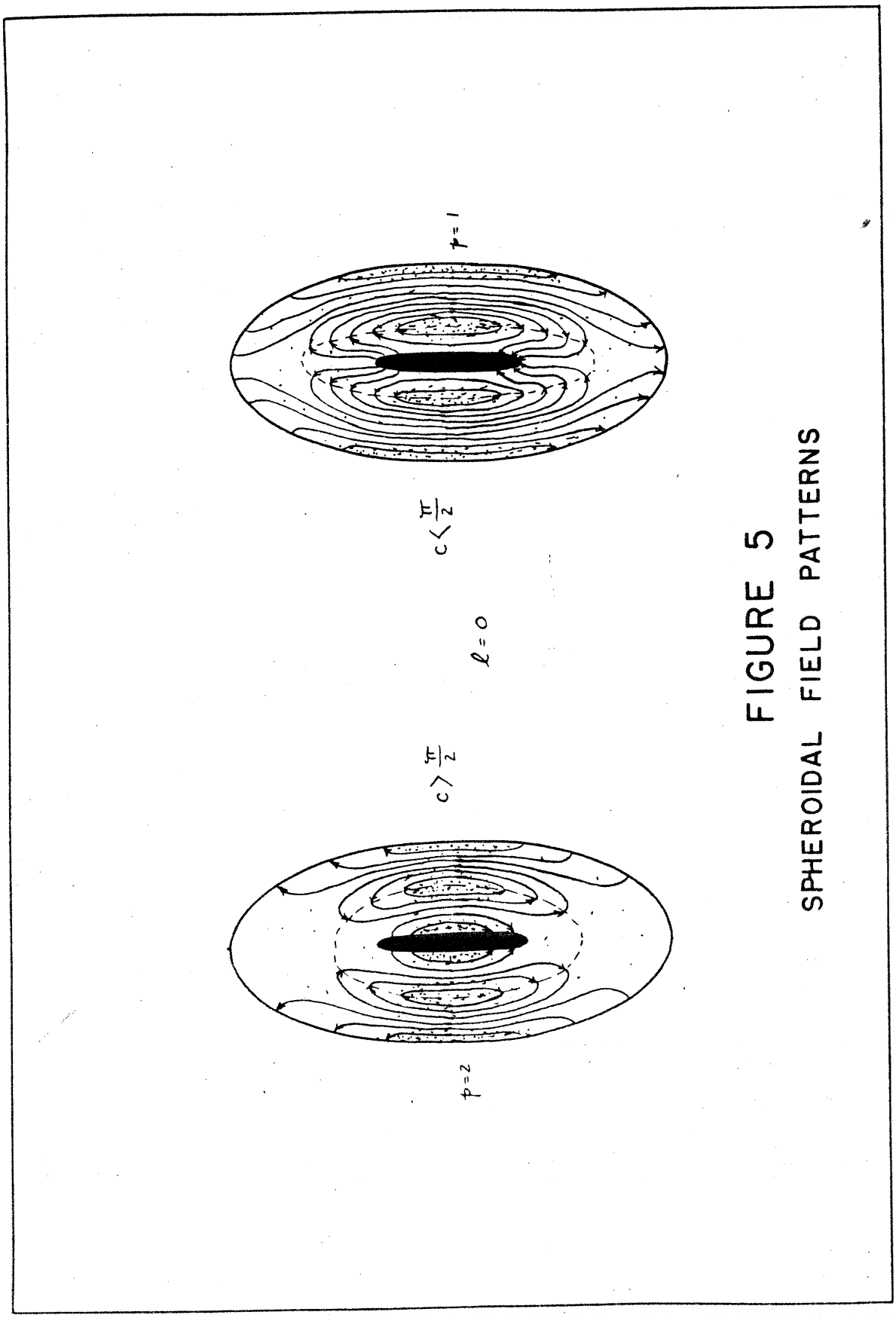

FIGURE 5

SPHEROIDAL FIELD PATTERNS

CHAPTER VI

SERIES REPRESENTATIONS OF THE SOLUTIONS

1. Reduction of the Differential Equations to Standard Form

An important part of this project is the solution of the pair of differential equations (2.21) and (2.22) of Chapter II:

$$(1-\eta^2)\frac{d^2Y(\eta)}{d\eta^2} - (c^2\eta^2-\alpha)\,Y(\eta) = 0 \tag{6.1}$$

$$(\xi^2-1)\frac{d^2X(\xi)}{d\xi^2} + (c^2\xi^2-\alpha)\,X(\xi) = 0 \tag{6.2}$$

Alternatively, one can use the pair of equations (2.33) and (2.34):

$$(1-\eta^2)\frac{d^2V(\eta)}{d\eta^2} - 4\eta\frac{dV(\eta)}{d\eta} + (\alpha-2-c^2\eta^2)\,V(\eta) = 0 \tag{6.3}$$

$$(\xi^2-1)\frac{d^2U(\xi)}{d\xi^2} + 4\xi\frac{dU(\xi)}{d\xi} - (\alpha-2-c^2\xi^2)\,U(\xi) = 0 \tag{6.4}$$

All four of these equations can be reduced to the standard form,

$$(1-z^2)\,W''(z) - 2(\sigma+1)z\,W'(z) + (\tau-c^2z^2)\,W(z) = 0 \tag{6.5}$$

It is known that the scalar wave equation is separable in spheroidal coordinates and that factors of the resulting Lamé product satisfy ordinary differential equations of the form of Eq. (6.5).

2. Earlier Investigations

Stratton, Morse, Chu and Hutner[1] have made a thorough investigation of series representations of the solutions of Eq. (6.5), initiat-

---

(1) J. A. Stratton, P. M. Morse, L. J. Chu, and R. A. Hutner, "Elliptic Cylinder and Spheroidal Wave Functions," Technology Press, John Wiley, 1941. This work will hereafter be referred to as SMCH, and the series representations developed therein will occasionally be referred to as SMCH functions. Reference is made therein to earlier papers on the same subject by the authors and associates at M.I.T.

ing as well a consolidation of earlier work by Mathieu,[1] Ince,[2] Humbert,[3] Strutt[4] and others, by publishing tables from which values of the solutions could be obtained. Since a sizeable number of computations in this thesis are based on the formulation of the solutions as presented by SMCH, it seems worthwhile to review their work briefly. The succeeding eight sections abstract the pertinent points of their development, in order to maintain the continuity and completeness of this paper.

3. Limiting Cases

If one passes to the limits $f \to 0$, $\xi \to \infty$, in such a way that $f\xi \to R$, then the eccentricity reduces to zero, $e = 1/\xi \to 0$, and the spheroid reduces to a sphere, of radius R. In this limit, (6.5) is replaced by

$$z^2 W''(z) + 2(a+1) z W'(z) + (c^2 z^2 - b) W(z) = 0 \qquad (6.6)$$

which is satisfied by

$$W(z) = (cz)^{-a-\frac{1}{2}} Z_{[b+(a+\frac{1}{2})^2]^{\frac{1}{2}}}(cz) \qquad (6.7)$$

where $Z_p(cz)$ is any Bessel function of order p and argument cz. For this reason, the spheroidal functions [solutions of Eq. (6.5)] will

---

(1) E. Mathieu, J. Math. (Liouville) (2) 13, 137 (1868).

(2) E. L. Ince, Proc. Edinburgh Math. Soc. 33, 2 (1914-15); Monthly Not. Roy. Astron. Soc. 75, 436 (1915); Phil. Mag. (7) 6, 547 (1928).

(3) P. Humbert, "Fonctions de Lamé et Fonctions de Mathieu," Fasciscule X du Mémorial des sciences mathématiques, Gauthier-Villars, Paris, 1926.

(4) M.J.O. Strutt, "Lamésche-Mathieusche und verwandte Funktionen in Physik und Technik," Julius Springer, Berlin, 1932. This is a very complete account of earlier investigations of elliptic and spheroidal wave functions, and includes an extensive bibliography.

be represented in the neighborhood of the essential singularity at infinity by expansions in Bessel functions.

If, on the other hand, one places c = 0, then (6.5) reduces to

$$(1-z^2)\,W''(z) - 2(a+1)\,z\,W'(z) + b\,W(z) = 0 \qquad (6.8)$$

This is essentially the Gegenbauer equation, a hypergeometric equation with three regular singularities. About the ordinary point, z = 0, the spheroidal functions will be expanded in terms of the solutions of Eq. (6.8), and consequently a brief discussion of the properties of these solutions, the Gegenbauer functions, is in order.

4. Gegenbauer Functions

The functions $T_n^a(z)$ and $\mathcal{T}_n^a(z)$ are defined for all values of a, n, and z by

$$T_n^a(z) = (z^2-1)^{-\frac{a}{2}}\, P_{n+a}^a(z) \qquad (6.9)$$

$$\mathcal{T}_n^a(z) = (z^2-1)^{-\frac{a}{2}}\, Q_{n+a}^a(z) \qquad (6.10)$$

where $P_{n+a}^a(z)$ and $Q_{n+a}^a(z)$ are the associated Legendre functions of the first and second kinds. In the literature, definitions of the Legendre functions differ with respect to phase, or location of the cut in the complex z-plane. To resolve these difficulties, we adhere to the definitions of Hobson.(1) The functions $T_n^a(z)$ and $\mathcal{T}_n^a(z)$ differ slightly from the original definitions of Gegenbauer. They satisfy the equation

$$(z^2-1)\,w''(z) + 2(a+1)\,z\,w'(z) - n(n+2a+1)\,w(z) = 0 \qquad (6.11)$$

---

(1) E. W. Hobson, "Spheroidal and Ellipsoidal Harmonics," pp. 188 and 195. Cambridge University Press, 1931.

which is likewise satisfied by each of the following six additional functions:

$$T^{a}_{-n-2a-1}, \qquad (z^2-1)^{-a} T^{-a}_{n+2a}, \qquad (z^2-1)^{-a} T^{-a}_{-n-1},$$
$$\mathcal{T}^{a}_{-n-2a-1}, \qquad (z^2-1)^{-a} \mathcal{T}^{-a}_{n+2a}, \qquad (z^2-1)^{-a} \mathcal{T}^{-a}_{-n-1}. \tag{6.12}$$

Since the second order equation (6.11) admits only two independent solutions, certain linear relations must exist between the eight functions above. These relations are known, and follow directly from the theory of the hypergeometric function.

5. Integer Values of the Parameters

Scalar spheroidal wave functions associated with a complete spheroidal surface must be periodic in the equatorial angle φ. In this case, the parameter a in (6.5) is a positive integer or zero and will be designated by the letter m. Since the Gegenbauer functions are solutions of a hypergeometric equation, they are expressible in terms of a hypergeometric series. When n as well as m is a positive integer, some of the series break off and are finite for all finite values of z. In this event, the various solutions fall into two classes; a set of integral functions, and a set characterized by singularities at $z = \pm 1$, as well as at infinity. Those solutions that are finite at the poles $z = \pm 1$ are termed functions of the first kind. Functions of the second kind are infinite at these points.

6. Representations in the Interval $1 \geq z \geq -1$

It was noted earlier that the solutions of Eq. (6.5) in the interval $1 \geq z \geq -1$ would be expanded in terms of the Gegenbauer functions. The standard function of the first kind is defined by Stratton as

$$V^{(1)}_{mn}(c,z) = \sum_{n=0,1}^{\infty\,\prime} d^{n}_{n}(c)\, T^{m}_{n}(z) \tag{6.13}$$

where the prime denotes that the summation starts from $n = 0$ and extends only over even values of n when ℓ is even, and starts from $n = 1$ extending only over odd values of n when ℓ is odd. The coefficients, $d_n^\ell(c)$, satisfy a three term recursion formula and are normalized such that each spheroidal function reduces to the corresponding spherical function as $c \to 0$. For given values of c and the parameter m, $V_{m\ell}^{(\omega)}(c,z)$ denotes a set of functions all of which remain finite at the poles, $z = \pm 1$. To each of these corresponds a specific separation constant, $b_\ell(c)$, characterized by the ordering index ℓ. Since the solutions desired in this interval must all be finite at $z = \pm 1$, the corresponding solutions of the second kind [the analogous expansions in $T_n^m(z)$] need not be considered in this interval. They will be found of interest in another connection, however.

7. Representations in the Interval $z \gg 1$

In the interval $z \gg 1$ the standard function of the first kind is chosen as

$$U_{m\ell}^{(1)}(c,z) = K_\ell (cz)^{-m} \sum_{n=0,1}^{\infty\,\prime} a_n^\ell(c)\, j_{n+m}(cz) \tag{6.14}$$

where K_ℓ is an appropriate normalization factor, and the function

$$j_{n+m}(cz) = \sqrt{\frac{\pi}{2cz}}\, J_{n+m+\frac{1}{2}}(cz) \tag{6.15}$$

is the spherical Bessel function, following Morse's definition.[1] When $(cz) \to \infty$,

$$j_{n+m}(cz) \longrightarrow \frac{i^{n-\ell}}{cz} \sin\left(cz - \frac{\ell+m}{2}\pi\right) \tag{6.16}$$

---

(1) P. M. Morse, "Vibration and Sound," p. 246, McGraw-Hill, 1936

The normalization is chosen so that as $(cz)\to\infty$,

$$(z^2-1)^{\frac{m}{2}}\, U^{(1)}_{m\ell}(c,z) \longrightarrow \frac{1}{cz}\sin\left(cz-\frac{\ell+m}{2}\pi\right) \tag{6.17}$$

This leads to

$$\mathcal{K}_\ell = \frac{c^m}{\sum_{n=0,1}^{\infty}{}' a^\ell_n(c)\, i^{n-\ell}} \tag{6.18}$$

The corresponding functions of the second kind over the interval are

$$U^{(2)}_{m\ell}(c,z) = \mathcal{K}_\ell\,(cz)^{-m} \sum_{n=0,1}^{\infty}{}' a^\ell_n(c)\, n_{n+m}(cz) \tag{6.19}$$

where now $n_{n+m}(cz)$ is a spherical Bessel function of the second kind (spherical Neumann function). As $(cz)\to\infty$,

$$(z^2-1)^{\frac{m}{2}}\, U^{(2)}_{m\ell}(c,z) \longrightarrow -\frac{1}{cz}\cos\left(cz-\frac{\ell+m}{2}\pi\right) \tag{6.20}$$

8. Relation of the Expansion Coefficients

$U^{(1)}_{m\ell}(c,z)$ and $U^{(2)}_{m\ell}(c,z)$ are solutions of (6.5) for the same set of separation constants, $\{b_\ell(c)\}$ corresponding to the functions $V^{(1)}_{m\ell}(c,z)$. By reason of the analytic continuation of the solutions, it turns out that $U^{(1)}_{m\ell}(c,z)$ is proportional to $V^{(1)}_{m\ell}(c,z)$. More remarkable, however, is the fact that only one set of expansion coefficients need be determined; this one finds upon comparing the coefficients of like powers of z in the several series expansions. The consequence is that

$$i^{\ell-n} d^\ell_n(c)\,\frac{(n+2m)!}{n!} = a^\ell_n(c) \tag{6.21}$$

One should also suspect that $U^{(2)}_{m\ell}(c,z)$ would be proportional to $V^{(2)}_{m\ell}(c,z)$, a function we declined to discuss earlier; this is the case and its usefulness will now be shown.

9. Alternate Representations

In the vicinity of $z = 1$, or for larger values of m (such as 3) the expression (6.19) for $U^{(2)}_{m\ell}(c,z)$ may converge too slowly or perhaps not at all. In this instance $U^{(2)}_{m\ell}(c,z)$ can be represented by the analytic continuation of the $V^{(2)}_{m\ell}(c,z)$ function with the appropriate proportionality factor. The formula is, for ℓ even,

$$U^{(2)}_{m\ell}(c,z) = \frac{2c^{m-1}\left(\frac{\ell+2m-1}{2}\right)!}{\left(\frac{\ell}{2}\right)!\left(m-\frac{3}{2}\right)!\, d^{\ell}_{-2m}\sum_{n=0}^{\infty}{}' d^{\ell}_{n}\frac{(n+2m)!}{n!}}\sum_{n=\text{even}=-\infty}^{\infty}{}' d^{\ell}_{n}\, \mathcal{J}^{m}_{n}(z) \qquad (6.22)$$

while for ℓ odd,

$$U^{(2)}_{m\ell}(c,z) = \frac{-2c^{m-2}\left(\frac{\ell+2m}{2}\right)!}{\left(\frac{\ell-1}{2}\right)!\left(m-\frac{5}{2}\right)!\, d^{\ell}_{1-2m}\sum_{n=1}^{\infty}{}' d^{\ell}_{n}\frac{(n+2m)!}{n!}}\sum_{n=\text{odd}=-\infty}^{\infty}{}' d^{\ell}_{n}\, \mathcal{J}^{m}_{n}(z) \qquad (6.23)$$

In these cases, the summation of $\mathcal{J}^{m}_{n}(z)$ extends from $-\infty$ to $+\infty$. The prime as before denotes only even or odd values of n, according as ℓ is even or odd.

10. Convergence

The convergence of these series representations has not been rigorously proved. This difficulty is due at least in part to the fact that the recursion formulas are of three terms rather than two. Over certain portions of the complex plane the convergence of the functions has been demonstrated by the use of their asymptotic representations. A limited discussion of the details of the arguments for convergence has been given by Chu and Stratton.[1] The correctness of the representations has been supported also by extensive numerical calculations. Nevertheless, more thorough investigation seems desirable.

---

(1) L. J. Chu and J. A. Stratton, "Elliptic and Spheroidal Wave Functions," J. Math. and Phys. 20, pp. 278ff (1941). Actually this paper is included in toto as the theory of SMCH; the convergence section begins on p. 20.

11. Application of the SMCH Functions

It now becomes necessary to apply to the problem at hand these representations of the solutions of differential equations arising from an attack on the scalar wave equation. Comparing Eqs. (6.1) and (6.2) with Eq. (6.5), one sees that they have the same form; they are identical if the parameter a, (or rather m, since it is an integer) has the value -1. This would be satisfactory save for the fact that the only available tables of the coefficients, $d_n^\ell(c)$, are those of Stratton, Morse, Chu, and Hutner, which are computed only for $m = 0$, 1, 2 and 3. However, the pair of equations (6.3) and (6.4) reduce to the standard form (6.5) for $m = 1$, so that we can now make use of the results of Stratton, et al. The spheroidal functions $U_{m\ell}(c,z)$ and $V_{m\ell}(c,z)$ defined in the previous sections may be carried over directly as solutions of (6.3) and (6.4) with no significant changes in notation, and will be used as basic solutions from which the other more appropriate functions $Y(\eta)$, $X(\xi)$, $S(\eta)$ and $R(\xi)$ can be derived by the transformations (2.31), (2.32), (2.36), and (2.37). Since $m = 1$ throughout the balance of the work, this will be henceforth understood, and the index will be deleted to simplify subsequent notation. In contrast to the Gegenbauer functions, the associated Legendre functions are well tabulated[1] and so the relations (6.9) and (6.10) will be reintroduced to make the expansions more usable. As only the first kind of function is of interest in the interval $1 > z > -1$, the superscript may be dropped from the function $V_{m\ell}^{(1)}(c,z)$.

---

(1) Mathematical Tables Project, National Bureau of Standards, "Tables of Associated Legendre Functions." Columbia University Press, 1945.

Recall that in accordance with the convention of Eq. (3.36) we have

$$U_{lp}(\xi;c,\xi_1,\xi_2) = a_{lp}(c,\xi_1,\xi_2)\,U_l^{(1)}(\xi,c) + b_{lp}(c,\xi_1,\xi_2)\,U_l^{(2)}(\xi,c) \qquad (6.24)$$

Introducing the foregoing modifications, the solutions now assume the following more useful forms.

12. The "Angular" Solutions

Valid in the region $1 \gtrsim \eta \gtrsim -1$, the solution of Eq. (6.3) is

$$V_l(\eta,c) = \frac{1}{\sqrt{1-\eta^2}} \sum_{n=0,1}^{\infty}{}' d_n^l(c)\, P_{n+1}^1(\eta) \qquad (6.25)$$

Correspondingly, one has

$$Y_l(\eta,c) = \sqrt{1-\eta^2} \sum_{n=0,1}^{\infty}{}' d_n^l(c)\, P_{n+1}^1(\eta) \qquad (6.26)$$

and

$$S_l(\eta,c) = \sum_{n=0,1}^{\infty}{}' d_n^l(c)\, P_{n+1}^1(\eta) \qquad (6.27)$$

These constitute the so-called angular solutions. They all vanish at $\eta = \pm 1$.

13. The "Radial" Solutions

In the region $\xi \gtrsim 1$, the function of the first kind which is the solution of Eq. (6.4) is

$$U_l^{(1)}(\xi,c) = \frac{1}{\xi \sum_{n=0,1}^{\infty}{}' a_n^l(c)\, i^{n-l}} \sum_{n=0,1}^{\infty}{}' a_n^l(c)\, j_{n+1}(c\xi) \qquad (6.28)$$

$$= \frac{2}{\xi\, \sigma_l(c)} \sum_{n=0,1}^{\infty}{}' a_n^l(c)\, j_{n+1}(c\xi) \qquad (6.29)$$

where we have defined

$$\sigma_l(c) \triangleq 2 \sum_{n=0,1}^{\infty}{}' a_n^l(c)\, i^{n-l} \qquad (6.30)$$

The function of the second kind is similarly

$$U_\ell^{(2)}(\xi,c) = \frac{2}{\xi\,\sigma_\ell(c)} \sum_{n=0,1}^{\infty}{}' a_n^\ell(c)\, n_{n+1}(c\xi) \tag{6.31}$$

The more appropriate "radial" functions, solutions of Eq. (6.2), are

$$X_\ell^{(1)}(\xi,c) = (\xi^2-1)\, U_\ell^{(1)}(\xi,c)$$

$$= 2\left(\frac{\xi^2-1}{\xi}\right)\frac{1}{\sigma_\ell(c)} \sum_{n=0,1}^{\infty}{}' a_n^\ell(c)\, j_{n+1}(c\xi) \tag{6.32}$$

and

$$X_\ell^{(2)}(\xi,c) = 2\left(\frac{\xi^2-1}{\xi}\right)\frac{1}{\sigma_\ell(c)} \sum_{n=0,1}^{\infty}{}' a_n^\ell(c)\, n_{n+1}(c\xi) \tag{6.33}$$

14. Alternate Forms for Computation

For computational purposes, it is convenient to define

$$J_\ell(\xi,c) \triangleq 2\left(\frac{\xi^2-1}{\xi}\right) \sum_{n=0,1}^{\infty}{}' a_n^\ell(c)\, j_{n+1}(c\xi) \tag{6.34}$$

$$K_\ell(\xi,c) \triangleq 2\left(\frac{\xi^2-1}{\xi}\right) \sum_{n=0,1}^{\infty}{}' a_n^\ell(c)\, n_{n+1}(c\xi) \tag{6.35}$$

for then Eqs. (6.32) and (6.33) become[1]

$$X_\ell^{(1)}(\xi,c) = \frac{1}{\sigma_\ell(c)}\, J_\ell(\xi,c) \tag{6.36}$$

$$X_\ell^{(2)}(\xi,c) = \frac{1}{\sigma_\ell(c)}\, K_\ell(\xi,c) \tag{6.37}$$

When expression (6.33) converges poorly, one can make use of (6.22) and (6.23), yielding[2] for ℓ even,

---

(1) This notation is not to be confused with the familiar Bessel functions, which are distinguished by a single argument.

(2) Recall that the summation now extends from $-\infty$ to ∞, although still over only even or odd values of n.

$$X_\ell^{(2)e}(\xi,c) = \sqrt{\xi^2-1}\,\frac{4\left(\frac{\ell+1}{2}\right)!}{\left(\frac{\ell}{2}\right)!\left(-\frac{1}{2}\right)!\,d_{-2}^{\ell}(c)\,\sigma_\ell(c)}\sum_{n=-\infty}^{\infty}{}' d_n^{\ell}(c)\,Q_{n+1}^{1}(\xi) \tag{6.38}$$

$$= \frac{\mu_\ell^{e}(c)}{\sigma_\ell(c)}\;K_\ell(\xi,c) \tag{6.39}$$

where[1] the notation is simplified by defining

$$\mu_\ell^{e}(c) \triangleq \frac{4\left(\frac{\ell+1}{2}\right)!}{\left(\frac{\ell}{2}\right)!\left(-\frac{1}{2}\right)!\,d_{-2}^{\ell}(c)} \tag{6.40}$$

$$K_\ell(\xi,c) \triangleq \sqrt{\xi^2-1}\sum_{n=-\infty}^{\infty}{}' d_n^{\ell}(c)\,Q_{n+1}^{1}(\xi) \tag{6.41}$$

Similarly, for ℓ odd,

$$X_\ell^{(2)o}(\xi,c) = \sqrt{\xi^2-1}\,\frac{-16\left(\frac{\ell+2}{2}\right)!}{c\left(\frac{\ell-1}{2}\right)!\left(-\frac{3}{2}\right)!\,d_{-1}^{\ell}(c)\,\sigma_\ell(c)}\sum_{n=-\infty}^{\infty}{}' d_n^{\ell}(c)\,Q_{n+1}^{1}(\xi) \tag{6.42}$$

$$= \frac{\mu_\ell^{o}(c)}{\sigma_\ell(c)}\;K_\ell(\xi,c) \tag{6.43}$$

where

$$\mu_\ell^{o}(c) \triangleq \frac{-16\left(\frac{\ell+2}{2}\right)!}{c\left(-\frac{3}{2}\right)!\left(\frac{\ell-1}{2}\right)!\,d_{-1}^{\ell}(c)} \tag{6.44}$$

It is apparent that

$$K_\ell(\xi,c) = \mu_\ell(c)\;K_\ell(\xi,c) \tag{6.45}$$

It will be remembered that Eq. (3.45) defined a function

$$\gamma_\ell^{(4)}(\xi,c) = -\frac{X_\ell^{(1)\prime}(\xi,c)}{X_\ell^{(2)\prime}(\xi,c)}. \tag{6.46}$$

---

(1) Here $Q_{n+1}^{1}(\xi)$ is the associated Legendre function of second kind. The factorial is used to denote the gamma function for non-integral as well as integral values of the argument so that $a! = \Gamma(a+1)$.

where the prime denoted differentiation with respect to ξ. In consequence of Eqs. (6.36) and (6.37) we can then write

$$\gamma_\ell'(\xi,c) = -\frac{J_\ell'(\xi,c)}{K_\ell'(\xi,c)} \tag{6.47}$$

We have now to place in a form suitable for computation,

$$\begin{aligned}
J_\ell'(\xi,c) &\triangleq \frac{\partial}{\partial\xi}\left[J_\ell(\xi,c)\right] \\
&= \frac{\partial}{\partial\xi}\left[2\left(\xi-\frac{1}{\xi}\right)\sum_{n=0,1}^{\infty}{}' a_n^\ell(c)\, J_{n+1}(c\xi)\right] \\
&= \frac{\partial}{\partial\xi}\left[2\left(\xi-\frac{1}{\xi}\right)\sum_{n=0,1}^{\infty}{}' a_n^\ell(c)\sqrt{\frac{\pi}{2c\xi}}\, J_{n+\frac{3}{2}}(c\xi)\right] \\
&= 2\sqrt{\frac{\pi}{2c}}\sum_{n=0,1}^{\infty}{}' a_n^\ell(c)\frac{\partial}{\partial\xi}\left[\left(\sqrt{\xi}-\frac{1}{\xi^{3/2}}\right)J_{n+\frac{3}{2}}(c\xi)\right] \\
&= 2\sqrt{\frac{\pi}{2c}}\sum_{n=0,1}^{\infty}{}' a_n^\ell(c)\left[\left(\frac{1}{2\sqrt{\xi}}+\frac{3}{2\xi^{5/2}}\right)J_{n+\frac{3}{2}}(c\xi)\right. \\
&\qquad \left. + c\left(\sqrt{\xi}-\frac{1}{\xi^{3/2}}\right)\frac{d}{d(c\xi)}J_{n+\frac{3}{2}}(c\xi)\right]
\end{aligned} \tag{6.48}$$

But[1]

$$\frac{d}{dz}\left[J_m(z)\right] = \frac{1}{2}\left[J_{m-1}(z) - J_{m+1}(z)\right] \tag{6.49}$$

---

(1) Morse and Feshbach, loc. cit., p. 344, Eq. (1.26).

so

$$J_\ell'(\xi,c) = \left(1+\frac{3}{\xi^2}\right)\sum_{n=0,1}^{\infty}{}' a_n^\ell(c)\sqrt{\frac{\pi}{2c\xi}}\, J_{n+3/2}(c\xi)$$
$$+ c\left(\xi-\frac{1}{\xi}\right)\sum_{n=0,1}^{\infty}{}' a_n^\ell(c)\sqrt{\frac{\pi}{2c\xi}}\left[J_{n+\frac{1}{2}}(c\xi) - J_{n+\frac{5}{2}}(c\xi)\right]$$
$$= \left(1+\frac{3}{\xi^2}\right)\sum_{n=0,1}^{\infty}{}' a_n^\ell(c)\, j_{n+1}(c\xi)$$
$$+ c\left(\xi-\frac{1}{\xi}\right)\sum_{n=0,1}^{\infty}{}' a_n^\ell(c)\left[j_n(c\xi) - j_{n+2}(c\xi)\right] \tag{6.50}$$

In similar fashion,

$$K_\ell'(\xi,c) = \left(1+\frac{3}{\xi^2}\right)\sum_{n=0,1}^{\infty}{}' a_n^\ell(c)\, n_{n+1}(c\xi)$$
$$+ c\left(\xi-\frac{1}{\xi}\right)\sum_{n=0,1}^{\infty}{}' a_n^\ell(c)\left[n_n(c\xi) - n_{n+2}(c\xi)\right] \tag{6.51}$$

We have also to place

$$\underline{K}_\ell(\xi,c) = \sqrt{\xi^2-1}\sum_{n=-\infty}^{\infty}{}' d_n^\ell(c)\, Q_{n+1}^1(\xi) \tag{6.52}$$

in a form suitable for computation. Now for

$$\begin{aligned} n &< -2m, \qquad \ell = \text{even} \\ n &< -2m+1, \qquad \ell = \text{odd} \end{aligned} \tag{6.53}$$

d_n^ℓ vanishes, but $Q_{n+1}^1(\xi)$ becomes infinite, so that we are faced with an indeterminate form. Returning momentarily to consideration of the more general SMCH functions, it happens that as the parameter $a \to m$, an integer, the quantity $\rho \to 0$. However, the quantity $\left(\frac{d_n^\ell}{\rho}\right)$ remains finite, and is available in tabular form. We then must make use of the

relation[1]

$$Q^m_{m-n}(\xi) = \frac{P^m_{n-m-1}(\xi)}{\rho} \tag{6.54}$$

which is valid for $|n|>2m$. Inserting $m=1$, this gives the summation (6.52) the form

$$K_\ell(\xi,c) = \sqrt{\xi^2-1}\left\{ \sum_{n=-2,-1}^{\infty}{}' d^\ell_n(c)\, Q^1_{n+1}(\xi) + \sum_{n=4,3}^{\infty}{}' \left(\frac{d^\ell_{-n}(c)}{\rho}\right) P^1_{n-2}(\xi)\right\} \tag{6.55}$$

This expression involves Q^1_0 and Q^1_{-1} which are not found tabulated. We make use then of the recurrence relation[2]

$$(n-m)\, U^m_n(x) = (2n-1)x\, U^m_{n-1}(x) - (n+m-1)\, U^m_{n-2}(x) \tag{6.56}$$

or

$$U^m_{n-2}(x) = \frac{2n-1}{n+m-1} x\, U^m_{n-1}(x) - \frac{n-m}{n+m-1} U^m_n(x) \tag{6.57}$$

which yields

$$Q^1_0(\xi) = \frac{3}{2}\xi\, Q^1_1(\xi) - \frac{1}{2} Q^1_2(\xi) \tag{6.58}$$

$$Q^1_{-1}(\xi) = \xi\, Q^1_0(\xi) = \frac{3}{2}\xi^2 Q^1_1(\xi) - \frac{1}{2}\xi\, Q^1_2(\xi) \tag{6.59}$$

---

(1) SMCH, p. 72, Eq. (1).

(2) Mathematical Tables Project, N.B.S., "Tables of Associated Legendre Functions," p. xvi, Eq. (8a), Columbia University Press, 1945.

which are now expressed in terms of tabulated functions. Alternatively, we can use[1]

$$Q_0(x) = \frac{1}{2} \ln\left(\frac{x+1}{x-1}\right) \tag{6.60}$$

and

$$Q_n^m(x) = (x^2-1)^{\frac{m}{2}} \frac{d^m}{dx^m} Q_n(x) \tag{6.61}$$

so that we have

$$\begin{aligned} Q_0^1(\xi) &= \frac{\sqrt{\xi^2-1}}{2} \frac{d}{d\xi}\left[\ln\left(\frac{\xi+1}{\xi-1}\right)\right] \\ &= -\frac{1}{\sqrt{\xi^2-1}} \end{aligned} \tag{6.62}$$

and

$$\begin{aligned} Q_{-1}^1(\xi) &= \xi\, Q_0^1(\xi) \\ &= -\frac{\xi}{\sqrt{\xi^2-1}} \end{aligned} \tag{6.63}$$

as explicit representations.

For ℓ even then,

$$\begin{aligned} K_\ell(\xi,c) = {} & \sqrt{\xi^2-1} \sum_{n=0}^{\infty}{}' d_n^\ell(c)\, Q_{n+1}^1(\xi) \\ & + \sqrt{\xi^2-1} \sum_{n=4}^{\infty}{}' \left(\frac{d_n^\ell(c)}{\rho}\right) P_{n-2}^1(\xi) \\ & - \xi\, d_{-2}^\ell(c) \end{aligned} \tag{6.64}$$

---

(1) Op. cit., p. xiv, Eq. (5b).

Further,

$$K_\ell'(\xi,c) \triangleq \frac{\partial}{\partial\xi} K_\ell(\xi,c)$$

$$= \sqrt{\xi^2-1}\left\{\begin{array}{l} \sum_{n=0}^{\infty}{}' d_n^\ell(c)\,\frac{d}{d\xi}\left[Q_{n+1}^1(\xi)\right] \\ + \sum_{n=4}^{\infty}{}'\left(\frac{d_{-n}^\ell(c)}{\rho}\right)\frac{d}{d\xi}\left[P_{n-2}^1(\xi)\right] \end{array}\right.$$

$$+ \frac{\xi}{\sqrt{\xi^2-1}}\left\{\begin{array}{l} \sum_{n=0}^{\infty}{}' d_n^\ell(c)\;\; Q_{n+1}^1(\xi) \\ + \sum_{n=4}^{\infty}{}'\left(\frac{d_{-n}^\ell(c)}{\rho}\right) P_{n-2}^1(\xi) \end{array}\right.$$

$$- d_{-2}^\ell(c)$$

(6.65)

Correspondingly, for ℓ odd,

$$K_\ell(\xi,c) = \sqrt{\xi^2-1}\sum_{n=1}^{\infty}{}' d_n^\ell(c)\; Q_{n+1}^1(\xi)$$

$$+ \sqrt{\xi^2-1}\sum_{n=3}^{\infty}{}'\left(\frac{d_{-n}^\ell(c)}{\rho}\right) P_{n-2}^1(\xi)$$

$$- d_{-1}^\ell(c)$$

(6.66)

and

$$\underline{K}_{\ell}'(\xi,c) = \sqrt{\xi^2-1}\left\{\sum_{n=1}^{\infty}{}' d_n^{\ell}(c)\,\frac{d}{d\xi}\left[Q_{n+1}^{1}(\xi)\right] + \sum_{n=3}^{\infty}{}'\left(\frac{d_{-n}^{\ell}(c)}{\rho}\right)\frac{d}{d\xi}\left[P_{n-2}^{1}(\xi)\right]\right.$$

$$+\frac{\xi}{\sqrt{\xi^2-1}}\left\{\sum_{n=1}^{\infty}{}' d_n^{\ell}(c)\,Q_{n+1}^{1}(\xi) + \sum_{n=3}^{\infty}{}'\left(\frac{d_{-n}^{\ell}(c)}{\rho}\right)P_{n-2}^{1}(\xi)\right. \tag{6.67}$$

These functions are now expressed entirely in terms of available tabulated functions.

CHAPTER VII

SOLUTIONS OF THE "RADIAL" EQUATION NEAR A SPHEROID OF HIGH ECCENTRICITY

1. Behavior of the Solutions near the Pole at $\xi = 1$

The series representations developed in Chapter VI are satisfactory for $J_\ell(\xi c)$, the function of the first kind, over the entire interval, $1 \leq \xi < \infty$. This function is the solution which always remains finite at the pole, $\xi = 1$, regardless of the value of c, and consequently may readily be expanded in a power series about this point.

If $c^2 < \alpha$ then there is a zero of $(c^2\xi^2 - \alpha)$ in the interval $1 < \xi < \infty$, in which case the function of the second kind, $K_\ell(\xi, c)$, is singular at the pole. If on the other hand $c^2 > \alpha$, there is no zero of $(c^2\xi^2 - \alpha)$ in the interval of interest, $K_\ell(\xi, c)$ is everywhere oscillatory, and the function remains finite at the pole. Points calculated according to SMCH are satisfactory in this instance for values of $\xi > 1$. At the pole, however, while the function remains finite, the series representation becomes of indeterminate form. Since the behavior of the function in the vicinity of the pole is of considerable interest, we resort to Langer's[1] method as a tool for further investigation.

2. Langer's Representations

An approximate solution of

$$U''(z) + \left[w^2(z) - \frac{n(n+1)}{z^2}\right] U(z) = 0 \qquad (7.1)$$

---

(1) R. E. Langer, "On the Connection Formulas and the Solutions of the Wave Equation," Phys. Rev. 51, 669 (1937).

where the lowest power of z appearing in $w^2(z)$ is z^p, $p>-2$, is given[1] by Langer as

$$U(z) \cong \frac{\left[\int_0^z w(x)\,dx\right]^{\frac{1}{2}}}{\sqrt{w(z)}}\; J_{\pm\frac{2n+1}{p+2}}\left[\int_0^z w(x)\,dx\right] \tag{7.2}$$

which is valid around the singular point at the origin. If the index of the Bessel function turns out to be an integer, the second independent solution will involve $N_{\frac{2n+1}{p+2}}$ instead of $J_{-\frac{2n+1}{p+2}}$.

3. Application of Langer's Solutions

The equation we are considering is (6.2),

$$X''(\xi) + \left(\frac{c^2\xi^2-\alpha}{\xi^2-1}\right)X(\xi) = 0 \tag{7.3}$$

If we transform the pole at $\xi = 1$ to the origin by letting

$$\xi = x + 1, \quad x = \xi - 1 \tag{7.4}$$

then (7.3) becomes

$$X''(x) + \frac{c^2-\alpha+2c^2x+c^2x^2}{2x+x^2}X(x) = 0 \tag{7.5}$$

The coefficient of the second term can be readily expanded in a Laurent series,

$$\frac{c^2-\alpha}{2x} + \left(c^2 - \frac{c^2-\alpha}{4}\right) + \frac{c^2-\alpha}{8}x - \frac{c^2-\alpha}{16}x^2 + \cdots \tag{7.6}$$

valid for $x^2 < 4$. For small enough values of the argument, we need

---

(1) This presentation of Langer's method follows Morse and Feshbach, "Methods of Theoretical Physics," p. 125, Technology Press, Cambridge, 1946.

consider no terms beyond the constants. Then in (7.1)

$$w(x) \cong \sqrt{\frac{c^2-\alpha}{2x} + \frac{3c^2+\alpha}{4}} \tag{7.7}$$

and the index n is zero--there is only a single order pole at the origin. If we define

$$v(x) \triangleq \int_0^x w(z)\, dz \tag{7.8}$$

then (7.2) becomes

$$X(x) \cong \left[\frac{v(x)}{w(x)}\right]^{\frac{1}{2}} J_1[v(x)] \tag{7.9}$$

Since the Bessel function is of integral order the second solution involves $N_1[v(x)]$. For appropriate values of c and x, these solutions have been computed and are tabulated in Appendix E, where the method is discussed in further detail. The derivatives dX/dx and the function γ_ℓ^m are also given.

4. Connections between the Two Sets of Solutions

To be of any value however, these solutions, termed $F_\ell(\xi, c)$ and $G_\ell(\xi, c)$, must be transformed to an equivalent basis with $J_\ell(\xi, c)$ and $K_\ell(\xi, c)$. At the pole both $F_\ell(\xi, c)$ and $J_\ell(\xi, c)$ vanish and consequently must be identical, except for a constant factor which is easily evaluated. One cannot, however, assume so readily that $G_\ell(\xi, c)$ and $K_\ell(\xi, c)$ are equivalent. The most general relation is

$$K_\ell(\xi, c) = f\, F_\ell(\xi, c) + g\, G_\ell(\xi, c) \tag{7.10}$$

Taking two sets of values of the functions and/or their derivatives suffices to determine the coefficients and establish the connection between the two sets of solutions.

These connections have been established. $F_\ell(\xi, c)$ and $G_\ell(\xi, c)$ have been computed for much smaller intervals than $J_\ell(\xi, c)$ and $K_\ell(\xi, c)$, so that the behavior of the function $\delta_\ell^M(\xi, c)$ is well known in the vicinity of $\xi = 1$. This has also made possible a better knowledge of $X_{\ell\rho}(\xi; c, \xi_1, \xi_2)$ in this region, allowing a better representation also of the loss ratio to be discussed later in Chapter X.

5. Failure of the Langer Representation

It has been found in certain cases [namely where $0 < (c^2 - \alpha) \ll c^2$] that the Langer approximation is not valid. For positive values of $\varkappa$ near the origin, the function $w(\varkappa)$ as given by (7.7) is then constant except for extremely small values of $\varkappa$, of the order of magnitude

$$\varkappa \approx \frac{c^2 - \alpha}{c^2} \tag{7.11}$$

or smaller. In this eventuality, we can extend the functions $J_\ell(\xi, c)$ and $K_\ell(\xi, c)$ inward toward the pole, employing the Wentzel-Kramers-Brillouin-Jefferys approximation and the known behavior of the functions at $\xi = 1.1$. This representation should be valid in to the region of (7.11), so that the behavior of J_ℓ and K_ℓ is known over practically the entire interval of interest.

J_ℓ of course is known in the balance of the interval as well, since its Taylor expansion exists at the pole. K_ℓ on the other hand has a logarithmic slope at the pole, and series representations here are unsatisfactory. From study of the differential equation however, we know qualitatively what the behavior of the solutions must be and can obtain enough information to allow satisfactory extrapolation of δ_ℓ^M and X, which are after all the functions of greater interest.

6. Qualitative Behavior of the Solutions

From Chapter V, we know that if $c^2 > \alpha$, both independent solutions of (7.3) must be everywhere oscillatory in the interval $1 \leqslant \xi < \infty$. Consequently, they never become infinite, and specifically must both be finite at the pole, $\xi = 1$. The first solution, J_ℓ, has been chosen as that which vanishes at the pole. Its expansion in Taylor series around this point shows that near the pole the function behaves almost linearly. In spite of the large values of $\nu(\lambda)$ due to its singularity, the value of the function is so small that the curvature here is nearly zero. Thus there are no rapid oscillations of J_ℓ in this region.

In the vicinity of $\xi = 1.1$, J_ℓ and K_ℓ have a relation similar to that of sine and cosine. As we extrapolate inward toward the pole, we know the behavior of J_ℓ. K_ℓ will follow the cosine pattern but with gradually increasing curvature, eventually having infinite slope at $\xi = 1$, but not necessarily zero value. Now we can make use of a theorem[1] from the theory of differential equations which tells us that the zeroes of J_ℓ and K_ℓ must alternate along the ξ axis. Since K_ℓ already has one zero between the pole and the next consecutive zero of J_ℓ, it may not have another, and therefore, does not return to the axis except possibly at the pole. There can then be one and only one maximum of K_ℓ in this region, or correspondingly a zero of K_ℓ', which implies a pole of γ_ℓ' at this point. More important, we are assured there are no additional poles of γ_ℓ' between this point and its zero at $\xi = 1$.

---

(1) L. Bieberbach, "Theorie der Differentialgleichungen," p. 156, Dover, 1944.

7. Application of the WKBJ Method

If n = 0 in (7.1) and if $w^2(z)$ is a slowly varying positive function then an approximate solution of (7.1) is given by[1]

$$U(z) \cong \frac{1}{\sqrt{w(z)}} \exp\left[\pm i \int_{z_0}^{z} w(\chi)\, d\chi\right] \tag{7.12}$$

generally termed the WKBJ approximation. The exponentials may be combined to form the sine and cosine. Some similarity will be observed with the Langer solutions mentioned previously. Using (7.8) we can write the solution of (7.5) as

$$X(\chi) \cong \frac{1}{\sqrt{w(\chi)}} \left\{ \begin{matrix} \sin \\ \cos \end{matrix} \left[v(\chi) - v(\chi_0)\right] \right\} \tag{7.13}$$

Linear combinations of these two solutions are necessary to join the two solutions already established by SMCH representations. For those cases where Langer's solutions have failed, the WKBJ solutions have been computed, the connection coefficients determined, and the functions J_ℓ and K_ℓ found in a region as close to the pole as possible. The data and details will be found in Appendix E.

---

(1) Morse and Feshbach, loc. cit., p. 122.

CHAPTER VIII

LOSS IN THE WALLS OF A TOTALLY ENCLOSED CAVITY

1. Skin Effect

The preceding calculations of the natural frequencies of oscillation and of the field patterns have assumed the boundaries to be perfectly conducting, i.e., lossless. The actual situation for boundaries of finite conductivity is that the fields do penetrate slightly, and because of this there is energy dissipation in the surface layers, which is frequently referred to as the skin effect.

The exact treatment of the electromagnetic field problem in the vicinity of the boundary between a perfect dielectric and a good conductor is quite complicated.(1) The law of refraction is not Snell's law in the usual sense, although Snell's law is satisfied in a purely formal way if one admits complex angles of refraction and a complex index of refraction, which leads to a very different physical interpretation.

2. General Approach to the Refraction Problem

Assuming for convenience a plane boundary, the general approach is to assume a general solution of the wave equation of the form

$$e^{j(\mathbf{k}\cdot\mathbf{r} - \omega t)} \tag{8.1}$$

---

(1) Refraction phenomena have been extensively investigated. The ensuing discussion, in justification of certain approximations, has been drawn mainly from J. A. Stratton, "Electromagnetic Theory," Chap. IX, McGraw-Hill, 1941; J. C. Slater and N. H. Frank, "Electromagnetism," Chaps. X, XI, McGraw-Hill, 1947, and especially J. C. Slater, "Microwave Transmission," Chap. II, McGraw-Hill, 1942.

where $\mathbf{r}$ is as usual the radius vector but now the propagation vector $\mathbf{k}$, instead of being real, is complex,

$$\mathbf{k} = \mathbf{k}_r + j\mathbf{k}_i \tag{8.2}$$

and the real and imaginary components need not have the same direction in space. This means that the surfaces of constant phase, or the wave fronts, are not in general parallel to the surfaces of constant amplitude. One can readily show that in a conducting medium

$$k^2 = \mathbf{k}\cdot\mathbf{k} = \omega^2\epsilon\mu + j\omega\mu\sigma \tag{8.3}$$

Since

$$\mathbf{k}\cdot\mathbf{k} = k_r^2 - k_i^2 + 2j\mathbf{k}_r\cdot\mathbf{k}_i \tag{8.4}$$

it follows at once that

$$k_r^2 - k_i^2 = \omega^2\epsilon\mu \tag{8.5}$$

$$2\,\mathbf{k}_r\cdot\mathbf{k}_i = \omega\mu\sigma \tag{8.6}$$

The incidence of an electromagnetic disturbance upon the plane boundary from the dielectric region results in an attenuated wave in the metallic absorbing medium, whose surfaces of constant amplitude are parallel to the bounding surface, i.e., $\mathbf{k}_i$ is normal to the surface. Looking back at Maxwell's equations, one may observe that the first term on the right hand side of (8.3) comes from the displacement current, the second from the conduction current. In metallic conductors it turns out that the

displacement current is negligible compared to the conduction current, that is,

$$\frac{\omega \epsilon}{\sigma} \ll 1 \tag{8.7}$$

at frequencies lower than those in the ultraviolet region. The consequence from Eqs. (8.5) and (8.6) is that $\mathbf{k}_r$ is almost exactly equal in magnitude to $\mathbf{k}_i$, and the angle between the two extremely small; the magnitudes of $\mathbf{k}_r$ and $\mathbf{k}_i$ are approximately $\sqrt{\sigma\mu\omega/2}$. Thus regardless of the disturbance in the dielectric, within the conductor one has effectively a plane wave directed into the conductor, the wave normal being almost exactly along the normal to the surface. The field in the conductor is not strictly transverse, a small TE wave being necessary to satisfy boundary conditions.

Within the conductor one finds that the relation between the field components is

$$\mathbf{E} = - \frac{\mathbf{k} \times \mathbf{H}}{j\sigma \left(1 - j\frac{\omega \epsilon}{\sigma}\right)} \tag{8.8}$$

with $\mathbf{k}$ still the complex propagation factor. Assuming (8.7) holds, we can simplify matters by considering $\mathbf{k}_r$ and $\mathbf{k}_i$ parallel to each other and to $\mathbf{n}_o$, the unit normal directed into the conductor. In this case (8.8) becomes

$$\mathbf{E} = \frac{-|\mathbf{k}|(\mathbf{n}_o \times \mathbf{H})}{j\sigma} \tag{8.9}$$

which may also be written

$$\mathbf{E} = Z(\mathbf{H} \times \mathbf{n}_o) \tag{8.10}$$

Here Z is the wave impedance in the conductor,

$$Z = \frac{|k|}{j\sigma} = \frac{1}{j\sigma}\sqrt{j\omega\mu\sigma}$$

$$= (1-j)\sqrt{\frac{\omega\mu}{2\sigma}}$$

$$= (1-j)\sqrt{\frac{\mu}{\epsilon}}\sqrt{\frac{\omega\epsilon}{2\sigma}} \qquad (8.11)$$

showing that the ratio of $\mathbf{E}$ to $\mathbf{H}$ is much smaller than in empty space, in view of (8.7).

3. Approximation to the Field Distribution

A very satisfactory solution to our problem is now apparent, one which is quite usually applied in such cases. The tangential component of magnetic field in the dielectric just outside the conductor will ordinarily be large and is readily computed for a perfect conductor. It may reasonably be assumed that it will change but slightly if the wall conductivity be finite rather than infinite. Because of the continuity conditions at the boundary, the tangential component of magnetic field just inside the conductor will equal that just outside. The principal result of having walls of finite conductivity will be a small tangential electric field inside the metal, which will be given by (8.10) and which by continuity equals a corresponding tangential component of electric field just outside the surface. Such a procedure allows us to describe with entirely satisfactory accuracy the tangential component of electric field at the surface of a good, though not perfect, conductor. While the transverse magnetic wave predominates, the small TE component which spoils the transversality may be considered a correction term taking account of the finiteness of the conductivity.

4. Condition on Validity of Approximations

Inside the conductor the fields are attenuated by a factor of 1/e in a distance defined by

$$\delta \triangleq \sqrt{\frac{2}{\omega \mu \sigma}} \tag{8.12}$$

generally referred to as the skin depth. Stratton, discussing currents within cylinders[1] develops the conditions for which the preceding treatment is valid for more general surface contours. He states that one may assume for conductors of arbitrary cross section that the field and current distributions near the surface differ negligibly from those near the surface of an infinite plane provided the radius of curvature is very much greater than the skin depth. For our problem, this condition is well satisfied in the microwave region until one begins to approach $\xi \to 1$ for the inner spheroid, i.e., the mathematical limiting case of a wire of negligible thickness.

5. Power Loss

Of more interest to us, however, is the rate of energy loss in the walls. The time average value of Poynting's vector is

$$\overline{S}^t = \frac{1}{2} \mathrm{Re} \left(E \times H^* \right) \tag{8.13}$$

---

(1) Stratton, loc. cit., p. 536.

Making use of (8.10) and (8.11) we have

$$\overline{S}^t = \frac{1}{2} \mathcal{R}e \left\{ Z (H \times n_o \times H^*) \right\}$$

$$= \frac{1}{2} \mathcal{R}e \left\{ Z (H \cdot H^*) \, n_o \right\}$$

$$= n_o \sqrt{\frac{\omega \mu}{8 \sigma}} \; |H|^2 \tag{8.14}$$

The normal component of $\overline{S}^t$, evaluated at the surface, will then be the time average power loss per unit area of the cavity surface. The total power loss for a single cavity wall resulting from finite conductivity of the walls is then given for our purposes by

$$W_1 = \sqrt{\frac{\omega \mu_1}{8 \sigma_1}} \oint_{S_1} |H_t|^2 \, da \tag{8.15}$$

where H_t denotes the magnitude of the tangential field at the surface, and the parameters have the values for the conductor. The subscript 1 identifies the particular wall considered.

In prolate spheroidal co-ordinates, the element of surface area[1] for a spheroidal surface $\xi = \xi_1$, a constant, is

$$da = h_\varphi h_\eta \, d\varphi \, d\eta \tag{8.16}$$
$$= f^2 \sqrt{(\xi_1^2 - 1)(\xi_1^2 - \eta^2)} \, d\varphi \, d\eta$$

so that

$$W_1 = \sqrt{\frac{\omega \mu_1}{8 \sigma_1}} \int_0^{2\pi} \int_{-1}^{1} \sqrt{(\xi_1^2 - 1)(\xi_1^2 - \eta^2)} \, f^2 \, |H_t(\eta, \xi_1, \varphi; t)|^2 \, d\eta \, d\varphi \tag{8.17}$$

---

(1) See Appendix A.

Since we are considering only axially symmetric TM waves, H_t has no φ dependence, and is identical with H_φ. For a particular mode of a given closed resonant cavity we have

$$H_\varphi(\eta, \xi_1, t; c_{\ell p}) = \frac{A_0}{f} S_\ell(\eta, c_{\ell p}) R_{\ell p}(\xi_1, c_{\ell p}) e^{-j\omega t} \tag{8.18}$$

for free oscillations (no losses), where ω is related to $c_{\ell p}$ by $\omega = c_{\ell p}/f\sqrt{\epsilon_0\mu_0}$. Assuming as before that the magnetic field at any point of the surface of the conducting wall differs negligibly from its value were the conductivity infinite, the power loss can be written

$$W_1 = \sqrt{\frac{\omega\mu_1}{2\sigma_1}}\, 2\pi A_0^2 \int_{-1}^{1} \sqrt{(\xi_1^2-1)(\xi_1^2-\eta^2)}\; S_\ell^2(\eta, c_{\ell p})\, R_{\ell p}^2(\xi_1, c_{\ell p})\, d\eta$$

$$= \sqrt{\frac{\omega\mu_1}{2\sigma_1}}\, 2\pi A_0^2 \sqrt{\xi_1^2-1}\; R_{\ell p}^2(\xi_1, c_{\ell p}) \int_{-1}^{1} \sqrt{\xi_1^2-\eta^2}\; S_\ell^2(\eta, c_{\ell p})\, d\eta \tag{8.19}$$

provided only the one mode is excited. Since $X_{\ell p}(\xi_1, c_{\ell p}) = \sqrt{\xi_1^2-1}\, R_{\ell p}(\xi_1, c_{\ell p})$, an alternate form of (8.19) is

$$W_1 = \sqrt{\frac{\omega\mu_1}{2\sigma_1}}\, 2\pi A_0^2 X_{\ell p}^2(\xi_1, c_{\ell p}) \left[\frac{1}{\sqrt{\xi_1^2-1}} \int_{-1}^{1} \sqrt{\xi_1^2-\eta^2}\; S_\ell^2(\eta, c_{\ell p})\, d\eta\right] \tag{8.20}$$

For computation purposes, it proves to be convenient to define the quantity in brackets,

$$\mathcal{Q}_\ell(\xi_1, c) \triangleq \frac{1}{\sqrt{\xi_1^2-1}} \int_{-1}^{1} \sqrt{\xi_1^2-\eta^2}\; S_\ell^2(\eta, c)\, d\eta \tag{8.21}$$

As $\xi_1 \to \infty$, this function approaches a limit

$$\mathcal{Q}_\ell(\xi_1, c) \longrightarrow 2 \sum_{n=0,1}^{\infty}{}' \frac{[d_n^\ell(c)]^2 (n+1)(n+2)}{(2n+3)} \triangleq N_\ell(c) \tag{8.22}$$

Since as $\xi_1 \to \infty$,

$$X_{\ell f}(\xi_1, c_{\ell f}) = X_{\ell f}(\xi, c_{\ell f})\Big|_{\xi=\xi_1} \longrightarrow \pm\frac{1}{c} \qquad (8.23)$$

we can define a new function

$$\Psi_\ell(\xi_1, c) \triangleq \frac{c^2}{N_\theta(c)}\, X^2_{\ell f}(\xi_1, c_{\ell f})\, \Omega_\ell(\xi_1, c_{\ell f}) \qquad (8.24)$$

which approaches unity for large values of ξ_1 . Then (8.20) can be written

$$W_1 = \sqrt{\frac{\omega\mu_1}{8\sigma_1}}\,\frac{2\pi A_0^2}{c^2}\, N_\theta(c)\, \Psi_\ell(\xi_1, c) \qquad (8.25)$$

As $\xi_1 \to 1$, the functions Ω_ℓ and Ψ_ℓ may become infinite or have infinite slope so we shall make use also of

$$\Omega_\ell(\xi_1, c) \triangleq \sqrt{\xi_1^2 - 1}\;\; \Omega_\ell(\xi_1, c)$$
$$= \int_{-1}^{1} \sqrt{\xi_1^2 - \eta^2}\; S_\ell^2(\eta, c)\, d\eta \qquad (8.26)$$

and

$$\Phi_\ell(\xi_1, c) \triangleq \sqrt{\xi_1^2 - 1}\;\; \Psi_\ell(\xi_1, c) \qquad (8.27)$$

which remain regular near $\xi_1 = 1$, and are more readily interpolated there.

These auxiliary functions are especially useful and convenient in the computation of loss ratios, in Appendix F.

CHAPTER IX

GENERAL THEORY OF RESONANT CAVITY BEHAVIOR

1. Determination of Cavity Behavior

Up to this point, attention has been directed upon the behavior of the closed and isolated cavity with investigation in terms of the normal modes of free oscillation. For any actual experiments, however, it is necessary to introduce some coupling with the external surroundings in order to measure the properties of the cavity. The usual method of accomplishing this will be to provide a wave guide input lead to the cavity. A variable frequency oscillator will excite the system and from measurements of standing waves set up in the wave guide (or by other means) the unloaded Q of the cavity may be computed and thence the surface impedance of the material investigation. However, the computation of the unloaded Q and of the surface impedance from the measured quantities requires first an analysis of cavity behavior.

2. Orthogonal Function Development

Interpretation of the behavior of microwave circuits and resonant cavities has been notably facilitated by the application of orthogonal function theory. Contributions to the general theory of resonant cavities by development in orthogonal functions have been made by several workers,(1) mostly associated with the Radiation Laboratory

---

(1) One of the earlier general discussions of the oscillations of cavity resonators is that of E. U. Condon, "Principles of Microwave Radio," Rev. Mod. Phys. 14, 341 (1942). Bethe, Schwinger, and Feshbach were prominent in the field during the war. A bibliography of pre-war literature has been given by R. I. Sarbacher and W. A. Edson, "Hyper and Ultrahigh Frequency Engineering," p. 618, John Wiley, 1943.

at M.I.T. The unified approach of Slater[1] has introduced a correlation of the various points of view and consequently we shall follow his treatment closely. Rather than repeat his detailed development, we shall, in this chapter, outline briefly from his review article the points pertinent to this investigation, in order to preserve continuity and to insure uniformity with the previous discussion, since there are minor changes in notation.

Slater sets up inside a hollow cavity of arbitrary shape two orthogonal families of solenoidal functions, called the $\mathbf{E}_a$'s and $\mathbf{H}_a$'s, and one family of irrotational functions, the $\mathbf{F}_a$'s. The solenoidal functions satisfy the relations

$$k_a \mathbf{E}_a = \text{curl } \mathbf{H}_a$$

$$k_a \mathbf{H}_a = \text{curl } \mathbf{E}_a \qquad (9.1)$$

or

$$\text{curl curl } \mathbf{E}_a = k_a^2 \mathbf{E}_a$$

$$\text{curl curl } \mathbf{H}_a = k_a^2 \mathbf{H}_a \qquad (9.2)$$

The bounding surface is divided into two parts: over one part (denoted by S) one has short circuited boundary conditions, corresponding to a perfect conductor, while over the other (denoted by S') the boundary conditions are open circuited corresponding to a perfect insulator. The functions $\mathbf{E}_a$ and $\mathbf{H}_a$ are required to satisfy on S,

$$n \times \mathbf{E}_a = 0$$

$$n \cdot \mathbf{H}_a = 0 \qquad (9.3)$$

---

(1) J. C. Slater, "Microwave Electronics," Rev. Mod. Phys. 18, 441 (1946).

and on S',

$$n \times \mathbf{H}_a = 0$$

$$n \cdot \mathbf{E}_a = 0 \tag{9.4}$$

It can then be shown that the $\mathbf{E}_a$'s are orthogonal, likewise the $\mathbf{H}_a$'s, and normalization is demanded such that the relations

$$\int_v \mathbf{E}_a \cdot \mathbf{E}_b = \delta_{ab}$$

$$\int_v \mathbf{H}_a \cdot \mathbf{H}_b = \delta_{ab} \tag{9.5}$$

are satisfied. Note however, than an $\mathbf{E}_a$ is not orthogonal to an $\mathbf{H}_a$, but on the contrary one of the $\mathbf{E}_a$'s can be expanded in series in the $\mathbf{H}_a$'s or vice versa.

The $\mathbf{F}_a$'s, having zero curl, can be written

$$k_a \mathbf{F}_a = \text{grad } \psi_a \tag{9.6}$$

The scalar ψ_a is required to satisfy

$$\nabla^2 \psi_a + k_a^2 \psi_a = 0 \tag{9.7}$$

As boundary conditions, on both S and S', are assumed

$$\psi_a = 0$$

$$n \times \mathbf{F}_a = 0 \tag{9.8}$$

These functions are also orthonormal,

$$\int_v \mathbf{F}_a \cdot \mathbf{F}_b \, dv = 0$$

$$\int_v \psi_a \psi_b \, dv = 0 \tag{9.9}$$

It can also be proved that

$$\int_V \mathbf{F}_a \cdot \mathbf{E}_b \, dv = \int_V \mathbf{F}_a \cdot \mathbf{H}_b \, dv = 0 \tag{9.10}$$

3. Expansion of an Arbitrary Function in Series

It seems intuitively reasonable to suppose that the $\mathbf{E}_a$'s and $\mathbf{F}_a$'s, or the $\mathbf{H}_a$'s and the $\mathbf{F}_a$'s, form complete sets of functions, so that any arbitrary vector function of position within V, satisfying not very stringent conditions of continuity, could be expanded in a series in the functions. As has been mentioned, an $\mathbf{E}_a$ and an $\mathbf{H}_b$ are not orthogonal to each other and consequently we do not need both the $\mathbf{E}_a$'s and the $\mathbf{H}_a$'s for any given expansion; either the $\mathbf{E}_a$'s or the $\mathbf{H}_a$'s are chosen in any given case, according to convenience. Another point to be made clear is that the characteristic numbers k_a for the solenoidal functions are not the same as those for the irrotational functions, κ_a.

The expansion of an arbitrary vector function, say $\mathbf{A}$, in terms of the $\mathbf{E}_a$'s and $\mathbf{F}_a$'s, follows readily from the orthogonality and normalization conditions. If

$$\mathbf{A} = \mathbf{A}_1 + \mathbf{A}_2 \tag{9.11}$$

where $\mathbf{A}_1$ is the solenoidal part of $\mathbf{A}$, $\mathbf{A}_2$ the irrotational part, then $\mathbf{A}_1$ can be expanded in series in the $\mathbf{E}_a$'s (or $\mathbf{H}_a$'s) and $\mathbf{A}_2$ in the $\mathbf{F}_a$'s,

$$\mathbf{A} = \sum_a e_a \mathbf{E}_a + \sum_a f_a \mathbf{F}_a \tag{9.12}$$

Taking the scalar product of A with E_b, and integrating over V, all terms vanish except

$$e_b = \int_V A \cdot E_b \, dv \tag{9.13}$$

The other coefficients are obtained in like fashion so that (9.12) has the form

$$A = \sum_a \left(E_a \int_V A \cdot E_a \, dv + F_a \int_V A \cdot F_a \, dv \right) \tag{9.14}$$

The object of establishing these sets of vector functions is to make possible the expansion of the electric and magnetic fields, and related quantities, inside a hollow cavity. Then, by means of Maxwell's equations, relations will be found between the expansion coefficients. We choose to expand these quantities in the following manner:

$$E = \sum_a \left(E_a \int_v E \cdot E_a \, dv + F_a \int E \cdot F_a \, dv \right) \tag{9.15}$$

$$H = \sum_a H_a \int_v H \cdot H_a \, dv \tag{9.16}$$

$$J = \sum_a \left(E_a \int_v J \cdot E_a \, dv + F_a \int_v J \cdot F_a \, dv \right) \tag{9.17}$$

But,

$$\text{curl } E = \sum_a H_a \left(k_a \int_v E \cdot E_a \, dv + \oint_S (n \times E) \cdot H_a \, da \right) \tag{9.18}$$

Here, in addition to the sum of terms involving volume integrals which one obtains by taking the curl of equation (9.15), must also be introduced a sum of terms involving surface integrals. These integrals will be zero

if $\mathbf{E}$ is normal to the surface S, but cases will be treated where $\mathbf{E}$ has a tangential component over S, so that the surface integrals do not vanish. Similarly, we have

$$\text{curl } \mathbf{H} = \sum_a E_a \left(k_a \int_V \mathbf{H} \cdot \mathbf{H}_a \, dv + \oint_{S'} (\mathbf{n} \times \mathbf{H}) \cdot \mathbf{E}_a \, da \right) \tag{9.19}$$

4. Interpretation of the Surface Integrals

The significance of the surface integrals is not difficult to interpret. In eq. (9.19), the quantity $-(\mathbf{n} \times \mathbf{H})$ is the tangential component of surface current associated with the discontinuity in the tangential component of $\mathbf{H}$ at the surface, so that the surface integrals give us the contribution of surface currents. Similarly, the quantity $-(\mathbf{n} \times \mathbf{E})$, in the surface integrals of (9.18), would have to be interpreted as a surface density of fictitious magnetic current, which appears at a surface of discontinuity of the tangential component of $\mathbf{E}$. Thus the surface integrals are required to reduce the fields to zero outside the cavity.(1)

5. Differential Equations of the Coefficients

These series may now be substituted in Maxwell's equations, Eqs. (2.1) and (2.2). Equating coefficients of like functions, the

---

(1) The situation is analogous to that arising in Green's solution for a bounded region in potential theory, where Green's distribution of surface charge and double layer over the surface is necessary for the potential to have its desired values within the volume, but zero everywhere outside; cf. J. C. Slater and N. H. Frank, "Introduction to Theoretical Physics," p. 222, McGraw-Hill, 1933, or by the same authors, "Electromagnetism," p. 39, McGraw-Hill, 1947.

differential equations satisfied by the various series coefficients are found to be

$$k_a \int_v E \cdot E_a \, dv + \mu_0 \frac{d}{dt} \int_v H \cdot H_a \, dv = - \oint_S (n \times E) \cdot H_a \, da \tag{9.20}$$

$$k_a \int_v H \cdot H_a \, dv - \epsilon_0 \frac{d}{dt} \int_v E \cdot E_a \, dv = \int_v J \cdot E_a \, dv - \oint_{S'} (n \times H) \cdot E_a \, da \tag{9.21}$$

$$- \epsilon_0 \frac{d}{dt} \int_v E \cdot F_a \, dv = \int_v J \cdot F_a \, dv \tag{9.22}$$

As is expected, Eqs. (2.5) and (2.6) yield nothing further if the equation of continuity is assumed.

Following the conventional derivation of the wave equation, (9.20) and (9.21) may be combined to yield separate equations for $\int_v E \cdot E_a \, dv$ and $\int_v H \cdot H_a \, dv$,

$$\epsilon_0 \mu_0 \frac{d^2}{dt^2} \int_v E \cdot E_a \, dv + k_a^2 \int_v E \cdot E_a \, dv = -\mu_0 \frac{d}{dt} \left(\int_v J \cdot E_a \, dv - \oint_{S'} (n \times H) \cdot E_a \, da \right) - k_a \oint_S (n \times E) \cdot H_a \, da \tag{9.23}$$

$$\epsilon_0 \mu_0 \frac{d^2}{dt^2} \int_v H \cdot H_a \, dv + k_a^2 \int H \cdot H_a \, dv = k_a \left(\int_v J \cdot E_a \, dv - \oint_{S'} (n \times H) \cdot E_a \, da \right) - \epsilon_0 \frac{d}{dt} \oint_S (n \times E) \cdot H_a \, da \tag{9.24}$$

These two equations show that $\int_v E \cdot E_a \, dv$ and $\int_v H \cdot H_a \, dv$ which are functions only of time, are determined by the type of differential equations encountered in elementary problems of simple harmonic motion. The terms on the right hand sides assume the role of the external driving forces, so that we may expect to get solutions of (9.23) and (9.24) showing the properties of forced oscillations and resonance.

These two equations, or Eqs. (9.20) and (9.21), determine the solenoidal part of $\mathbf{E}$, and $\mathbf{H}$. It is this part of the field which shows properties of wave propagation, and with which we shall be concerned. On the other hand, the irrotational part of $\mathbf{E}$ is derivable from a scalar potential which can be shown to satisfy Poisson's equation; this part of the problem becomes identical with the electrostatic problem of finding the field of a known distribution of charge. Here the charge distribution, and hence the field, varies with time, but the effect of retardation does not enter.

Up to this point, the presentation of Slater's treatment has been completely general. For our problem however, we have assumed a cavity filled with a perfect dielectric and hence within the cavity the conductivity is zero and the current density $\mathbf{J}$ vanishes. Eq. (9.22) then becomes

$$-\epsilon_0 \frac{d}{dt} \int_v \mathbf{E} \cdot \mathbf{F}_a \, dv = 0 \tag{9.25}$$

so that the irrotational part of $\mathbf{E}$ is independent of time, merely the electrostatic field of a fixed distribution of charge, subject to the condition of zero potential on the boundary. This field is superposed on the time varying field without affecting it; its tangential component is zero on the boundary surface. Consequently, there is no contribution to loss in the walls, and we omit any further consideration of it.

6. Free Oscillations of the Cavity

We have assumed now that within the cavity $\mathbf{J} = 0$. Let us further assume that the surface S is a perfect conductor, so that over S the tangential component of $\mathbf{E}$ is zero, and that the surface S' is a

perfect insulator or open circuit so that over S' the tangential component of H is zero. The integrals on the right-hand sides of (9.23) and (9.24) would then be zero and the equations would have solutions

$$\int_v E \cdot E_a \, dv = \text{constant} \times e^{-j\omega_a t} \tag{9.26}$$

with

$$\omega_a^2 \epsilon_0 \mu_0 = k_a^2 \tag{9.27}$$

with similar solutions for $\int_v H \cdot H_a \, dv$. These then are the free oscillations of the cavity; the ω_a's are the angular frequencies of the resonant modes. The general solution of the problem of free oscillations would be a superposition of the various normal modes, each oscillating with arbitrary amplitude at its resonant frequency. From (9.20) and (9.21) the relation between the coefficients for the normal modes is found to be

$$\frac{\int_v E \cdot E_a \, dv}{\int_v H \cdot H_a \, dv} = j\sqrt{\frac{\mu_0}{\epsilon_0}} = j Z_0 \tag{9.28}$$

where Z_0 is the wave impedance of free space. If the entire boundary surface is conducting, i.e., there is no surface S', then the resonant frequencies above are to be identified with those calculated in Chapter VI, for the particular case of a cavity comprised of two confocal spheroids.

7. Damped Oscillations

In order to discuss the case of damped oscillations, we appropriate from circuit theory the notion of Q as a description of the rate of damping of an oscillatory system. We may use the definition

$$Q = \frac{2\pi \times \text{total energy}}{\text{decrease of energy per period}} \tag{9.29}$$

where the period concerned is $2\pi/\omega_o$, as determined from the angular frequency which would exist if the damping were absent. An equivalent definition is more convenient; an oscillation whose angular frequency is determined by

$$j\left(\frac{\omega}{\omega_o} - \frac{\omega_o}{\omega}\right) - \frac{1}{Q} = 0 \tag{9.30}$$

will be referred to as having a given Q. Note that while the undamped natural frequency, ω_o , is real, ω will in general be complex. Eq. (9.30) is a quadratic for the frequency whose solution is

$$\omega = -j\frac{\omega_o}{2Q} \pm \omega_o\left[1 - (1/2Q)^2\right]^{\frac{1}{2}} \tag{9.31}$$

so that the absolute value of ω is equal to ω_o . In the expected applications, Q is large enough that the distinction between ω_o and the damped angular frequency, $\omega_o\left[1-(1/2Q)^2\right]^{\frac{1}{2}}$, may be neglected. That is, ω_o and the real part of ω are negligibly different to first order. In many cases, we shall find that the angular frequency is very nearly equal to one of the resonant frequencies, ω_a , of (9.27); this will be the situation if the motion differs from the free oscillation by only a small perturbation. Then we may let

$$\omega_o = \omega_a + \Delta\omega_a \tag{9.32}$$

where $\Delta\omega_a$ is a small quantity. In such a case (9.30) may be rewritten in several forms, correct to the first order of small quantities:

$$\begin{aligned} \omega &= \omega_a + \Delta\omega_a - j\frac{\omega_a}{2Q} \\ j\left(\frac{\omega}{\omega_a} - \frac{\omega_a}{\omega}\right) - \frac{1}{Q} - 2j\frac{\Delta\omega_a}{\omega_a} &= 0 \\ \omega^2 - \omega_a^2 &= -j\frac{\omega_a^2}{Q} + 2\omega_a\Delta\omega_a \end{aligned} \tag{9.33}$$

8. Perturbations Leading to Damping

Perturbations of the problem of free oscillations of a cavity evidence themselves as terms on the right hand sides of (9.23) and (9.24). We shall consider only two types of perturbations showing how they are introduced as terms on the right hand side, and later, how they lead to damping and displacement of the resonant frequency.

First, the walls of the cavity, instead of being perfect conductors, may have only finite conductivity, resulting in resistive losses. In this case, the tangential component of E over the surface S will not vanish, and the integral $\oint_S (n \times E) \cdot H_a \, da$ will be different from zero. Second, the cavity may have certain windows, or wave guide outputs, which allow the escape of energy, with consequent decrease of the total energy. In this instance, the tangential component of H over the surface S' will not be zero and the integral $\oint_{S'} (n \times H) \cdot E_a \, da$ will not vanish. In order to have damped oscillations the various integrals must be proportional to the amplitude $\int_v E \cdot E_a \, dv$ of the field component, and must oscillate with the same period, since the equations are linear. Assuming a solution varying as $e^{-j\omega t}$, where ω is in general complex, (9.23) becomes

$$\frac{1}{Q} + 2j \frac{\Delta\omega_a}{\omega_a} = J \frac{1}{\omega_a \sqrt{\epsilon_0 \mu_0}} \frac{\oint_S (n \times E) \cdot H_a \, da}{\int_v E \cdot E_a \, dv}$$

$$- \frac{1}{\epsilon_0 \omega_a} \frac{\oint_{S'} (n \times H) \cdot E_a \, da}{\int_v E \cdot E_a \, dv} + \frac{1}{\epsilon_0 \omega_a} \frac{\int_v J \cdot E_a \, dv}{\int_v E \cdot E_a \, dv} \qquad (9.34)$$

where we have used (9.27) and (9.33). For our problem, the last term vanishes since $J = 0$.

We now proceed to consider the perturbations in detail.

9. Losses in the Cavity Walls

First, we give attention to the losses in the cavity resulting from the finite conductivity of the walls. In Chapter VIII we found that there is a small tangential component of E over the surface S, when the conductivity is finite, and showed that it is given by Eq. (8.10). From that equation, we have at once

$$n \times E = (1-j)\sqrt{\frac{\mu_0 \omega}{2\sigma}}\, H = (1-j)\frac{\delta \mu_0 \omega}{2} H \tag{9.35}$$

at the surface, where we have introduced the skin depth δ from (8.12). Consequently,

$$\oint_S (n \times E) \cdot H_a \, da = (1-j)\frac{\delta \mu_0 \omega}{2} \oint_S H \cdot H_a \, da \tag{9.36}$$

If the oscillation is taking place with almost the frequency of the a th resonant mode, Eq. (9.26), then the field is but a slight perturbation of this mode, and we may assume that to a first approximation the field distribution will be that of the a th mode as well. Based on this assumption, the ratio between $\int_V E \cdot E_a dv$ and $\int_V H \cdot H_a dv$ given by (9.28), which strictly holds only for the free oscillation, will also be a good approximation for damped oscillations. Using this, we then approximately have

$$H = H_a \int_V H \cdot H_a dv \cong -j\sqrt{\frac{\epsilon_0}{\mu_0}}\, H_a \int_V E \cdot E_a \, dv \tag{9.37}$$

so that (9.36) becomes

$$\oint_S (n \times E) \cdot H_a \, da = -(1+j)\frac{\delta \omega \sqrt{\epsilon_0 \mu_0}}{2} \oint_S H_a^2 da \int_V E \cdot E_a \, dv \tag{9.38}$$

Introducing this result into (9.34) yields

$$\frac{1}{Q} + 2j\left(\frac{\Delta \omega_a}{\omega_a}\right) = (1-j)\frac{\delta}{2} \oint_S H_a^2 \, da \tag{9.39}$$

We see from this that the surface losses in the walls result in a shift of frequency as well as a contribution to Q. The value of Q given by (9.39) is generally called the unloaded Q; it will be denoted by Q_α. This subscript is not to be confused with the α th mode; there should also be added a second subscript α to designate the αth mode, but this will be omitted unless it is necessary for clarity.

It is well to emphasize the limitations of the approximations made here. We have assumed that the field distribution is approximately that of a particular resonant mode, stipulating that the frequency is very close to the resonant frequency of the same mode. We may not assume, however, that if we have a number of modes coexisting, the losses are simply a sum of the losses in the various modes. The integral of the square of the tangential H over the surface of the cavity, which occurs in (9.38), has no orthogonality property, and there is no way of disentangling the effects of the various modes. The losses, being a quadratic rather than a linear function of the amplitudes, have no principle of superposibility, and the presence of one mode can affect the losses experienced by another mode oscillating in the same cavity with the same frequency. Detailed study of the situation would be necessary to find the behavior in any particular case.

10. Coupling to an External System

Secondly, we consider the effect of coupling the cavity to an outside system by an output lead, which will be assumed to take the form of a wave guide or coaxial line. The volume in which we are solving Maxwell's equations now includes not merely the cavity but part of the output lead out to the surface S', which is now a cross section of the

output line. The normal resonant mode corresponds to an open circuit at S', that is, an infinite standing wave ratio in the output line with a standing wave maximum at S'. Now we wish to substitute other boundary conditions at S' and find their effect on the oscillations of the cavity. The general case is one in which there are arbitrary impressed voltages or currents (E or H fields) across S'. In such a case, power can flow in as well as out through the guide, so that we may have forced oscillation of the cavity as well as damped oscillation. Damping due to energy loss through a window[1] into outside space is then a special case in which the impedance across S' has a definite stated value, resulting in a contribution to Q and a frequency shift.

We shall not present a detailed analysis of the coupling problem, but outline the method briefly and state specific forms of the general result which are of direct interest to the problem. First, the normal modes of the system must, within the wave guide, be expressible as an expansion in terms of the normal modes of the guide[2] itself. Recalling the characteristics of wave guides, as we proceed along the guide away from the cavity, the propagated guide modes will vary periodically with position. The higher modes on the contrary are attenuated exponentially along the guide and soon become negligible. If the surface S'

---

(1) A somewhat different approach from that following has been given by H. A. Bethe and J. Schwinger, Report NDRC-14-117, March 4, 1943.

(2) J. C. Slater, "Microwave Electronics," Rev. Mod. Phys. 18, pp. 460-466 (1946).

is chosen far enough from the cavity the expansion has non-vanishing terms only for the propagated modes. If the frequency is such that only the dominant guide mode is propagated, the expansion simplifies to a single term.

Over the surface S' the transverse component of the cavity function H_a is zero. The impressed tangential magnetic field over S' may be expanded in series in the normal modes of the guide. Utilizing the orthonormal properties of the guide functions, the integral $\oint_{S'} (n \times H) \cdot E_a \, da$ is readily computed in terms of the two sets of expansion coefficients. Assuming $\int_V E \cdot E_a \, dv$ varies as $e^{-j\omega t}$, and introducing the loss in cavity walls from (9.38) and (9.39), we find from (9.23) that

$$\int_V E \cdot E_a \, dv = \frac{\frac{1}{\epsilon_0 \omega_a} \oint_{S'} (n \times H) \cdot E_a \, da}{j\left(\frac{\omega}{\omega_a} - \frac{\omega_a}{\omega}\right) + \frac{1}{Q_a} + 2j\left(\frac{\Delta \omega_a}{\omega_a}\right)} \tag{9.40}$$

where $\Delta \omega_a$ is the frequency shift due to the wall loss. Restricting ourselves now to a region of wave-lengths where the guide can propagate only in its dominant mode, the situation is easily interpreted with the aid of the impedance concept, yielding the relation

$$\frac{Z_{11}}{Z_{01}} = \sum_a \frac{1/Q_{ext,a1}}{j\left(\frac{\omega}{\omega_a} - \frac{\omega_a}{\omega}\right) + \frac{1}{Q_a} + 2j\left(\frac{\Delta \omega_a}{\omega_a}\right)} \tag{9.41}$$

Here Z_{11} is the impedance looking into the cavity, and Z_{01} the characteristic impedance of the wave guide in the dominant mode. The summation is over the normal modes of the cavity. The quantity $Q_{ext,a1}$ is termed the external Q of the a th mode of the cavity and the 1st mode of the

guide and is a measure of the coupling of the a th cavity mode to the output, through the 1st guide mode. If the external Q is large, there is very small coupling. The situation is considerably more complicated if there are several output leads or if more than one mode is propagated in the input guide. If we let

$$\omega_a' = \omega_a + \Delta\omega_a \tag{9.42}$$

then to first order,

$$\left(\frac{\omega}{\omega_a} - \frac{\omega_a}{\omega}\right) + 2\left(\frac{\Delta\omega_a}{\omega_a}\right) = \left(\frac{\omega}{\omega_a'} - \frac{\omega_a'}{\omega}\right) \tag{9.43}$$

We see that Eq. (9.41) is a sum of resonant terms, the impedance becoming very large when the frequency equals the corrected resonant frequency of any one of the modes. The resonance term becomes purely resistive at resonance just like the input impedance of a parallel resonant circuit with finite loss, in ordinary circuit theory. At frequencies near ω_a', the term in this frequency is much greater than the others and varies rapidly with frequency while the other terms are small and slowly varying. It is often convenient to lump these other terms together, using the notation Z_{a1}/Z_{o1} to represent them so that instead of (9.41), we have

$$\frac{Z_{11}}{Z_{o1}} = \frac{1/Q_{ext,a1}}{j\left(\frac{\omega}{\omega_a} - \frac{\omega_a'}{\omega}\right) + \frac{1}{Q_a}} + \frac{Z_{a1}}{Z_{o1}} \tag{9.44}$$

where we have introduced the corrected resonant frequency, ω_a', from (9.42) to take account of the frequency shift arising from wall losses given by (9.39). The only instance in which we may not expect this formula to be accurate is that in which two resonant modes are close

enough together that the two adjacent resonant peaks overlap. In such a case, more sophisticated methods are necessary to obtain valid approximations to the input impedance. Eq. (9.44) should be accurate enough for ordinary purposes, however, in any frequency region where the resonances are well separated.

11. Determination of the Cavity Parameters

The input impedance looking into a cavity, as given by (9.44), can not be measured directly. However, a measure of the resonant behavior can be found by measurement of the standing wave ratio and position of standing wave minimum looking into the cavity, as a function of frequency. By analysis of the resonance curves, one can find the values of the three parameters Q_{ext} , Q_a , and ω_a characterizing each resonance of a cavity. The determination of these parameters from experimental measurements of input impedance based on the form of impedance predicted theoretically has been well proven in practice. It should be noted that this is not the only method of obtaining the cavity parameters experimentally. One other way frequently employed is to allow power to flow into a cavity through one lead, out through another, and measure the transmission as a function of frequency.

12. Perturbation of Boundaries

Another result of resonant cavity theory will prove useful in the following chapters. This is the change of frequency of a resonant cavity when the boundaries are perturbed, say by pushing a small section of the wall in or out. The perturbed frequency ω of a perfectly con-

ducting totally enclosed cavity, in a mode whose normal resonant frequency is ω_a, is given by the relation

$$\omega^2 = \omega_a^2 \left[1 + \int_{V'} (H_a^2 - E_a^2)\, dv \right] \qquad (9.45)$$

where the integral is over V', the volume removed from the volume of the resonant cavity by the inward perturbation of the surface. If the deformation is outward the sign of the volume element is reversed and the functions H_a and E_a are the analytic continuation of those within the cavity. This formula is strictly correct only for an infinitesimal distortion of the boundary surface. Its validity is based on the fact that while the frequency shift is an effect of first order, the variation in H_a and E_a is of second or higher order.

CHAPTER X

APPLICATION TO THE DETERMINATION OF SURFACE CONDUCTIVITY

1. Computation of the Conductivity

We have mentioned in Section 11 of the preceding chapter how the parameters Q_{ext} , Q_a , and ω_a can be determined from experimental data. Knowing Q_a, one could find the skin depth δ from (9.39), by the relation

$$\frac{1}{Q_a} = \frac{\delta}{2} \oint_S H_a^2 \, da \tag{10.1}$$

provided the surface integral could be evaluated. Direct computation of the conductivity, σ, of the wall material would then be enabled by (8.12).

2. General Considerations of Coupled Cavity Behavior

The functions involved in the surface integral of (10.1) are solutions of (9.2) satisfying (9.3) and (9.4) where the volume concerned is that enclosed by a prolate spheroidal cavity containing a confocal conducting prolate spheroid and including a wave guide output out to a certain cross section in the guide termed S'. The surface integral is taken over S, the entire bounding surface save S'. If the cavity and wave guide are loosely coupled through a rather small iris, with the guide propagating only in the dominant mode, the system will be sharply tuned and the cavity will draw appreciable power only at frequencies very near the resonances of the isolated cavity.

There arises an ambiguity, however, as to the precise resonant frequency of the cavity, since the resonant frequency and Q of the isolated cavity are modified by the coupling. The set of resonant frequencies,

the ω_a's of Chapter IX, depends on the choice[1] of the reference plane S' in the wave guide output. For most purposes it is convenient to regard the resonant frequency of the over-all cavity and coupling circuit as the frequency at which a minimum standing-wave ratio is seen on the input transmission line looking toward the cavity.[2] We shall adhere to this definition. It is also convenient to choose as a reference plane the location of a minimum on the input line when the cavity is detuned, for then the term Z_{a1}/Z_{o1} in (9.44) is zero; this of course is possible only for tunable cavities.

The system behavior may also be expressed in terms of equivalent circuits. The resonant modes of the cavity may be described by an infinite number of parallel resonant circuits. Figure 6A shows just such a representation of equation (9.41). The external Q's are to be interpreted as the values of the respective mutual inductances coupling the various cavity modes to the wave guide. The terminals correspond to the reference plane in the guide, and R_o, C_o and L_o represent the effect of the coupling. In the vicinity of a resonance, that is, a pole of $\frac{Z_{11}}{Z_{o1}}(\omega)$, the reactance reflected in the primary loop is negligible for the off-resonance modes, and the circuit can be reduced to that of Figure 6B, or Figure 6C corresponding to (9.44). Insertion of the proper length of wave guide, i.e., translation of the reference plane, so that Z_{a1}/Z_{o1} vanishes, results in the circuit of Figure 6D.

---

(1) This dependence is clearly shown by Figs. 12 and 15 in Slater's review article.

(2) T. Moreno, "Microwave Transmission Design Data," p. 233, McGraw-Hill, 1948.

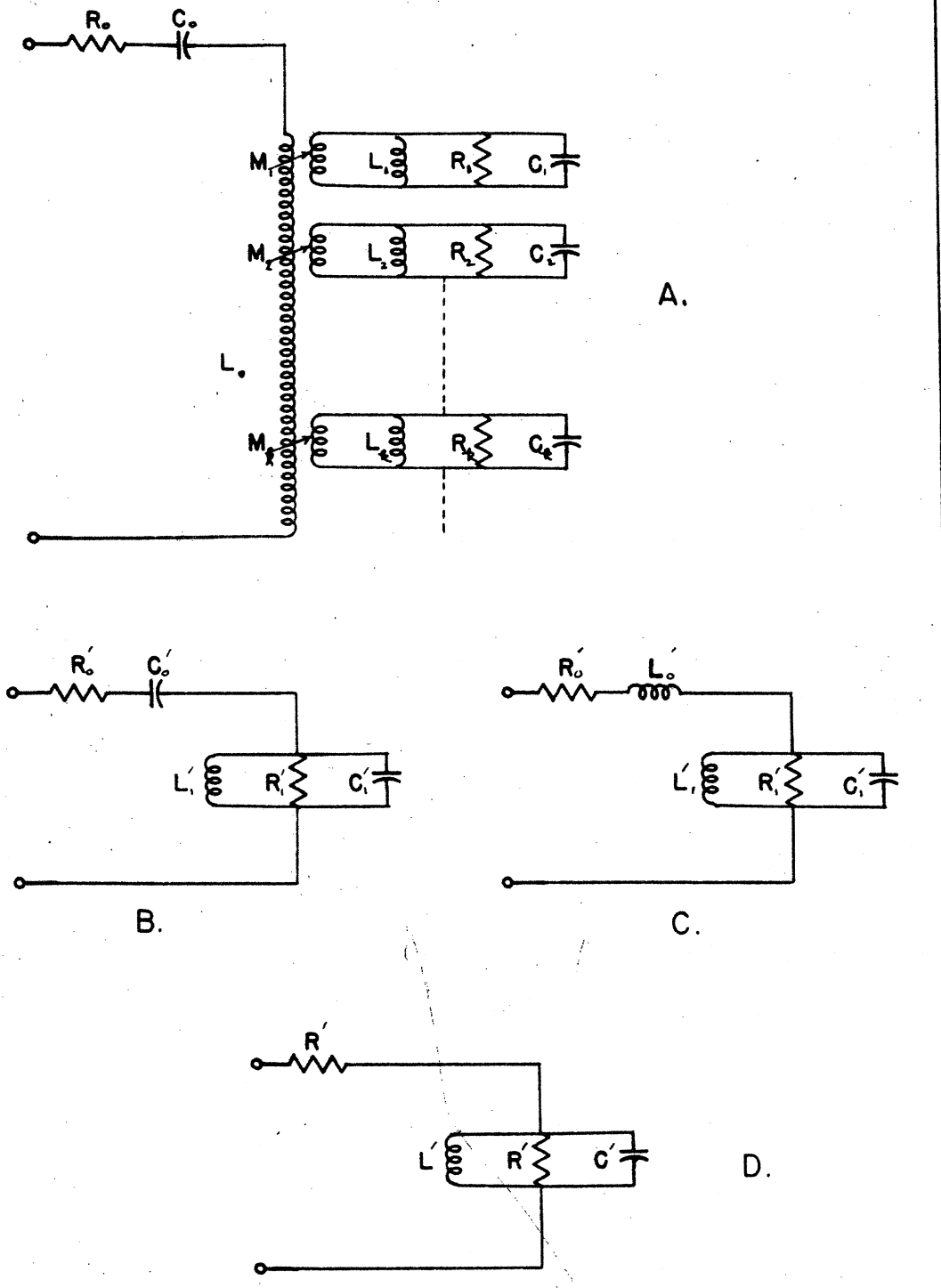

FIGURE 6

EQUIVALENT CIRCUIT REPRESENTATIONS

3. Treatment of Cavity Coupling Systems

Although we have the form of the equivalent circuit, determination of the coupling parameters still faces us. The exact treatment of cavity-coupling is extremely difficult and is possible only by an actual solution of the field problem. This unfortunately has been accomplished in only a few special cases. One of these is the case of a cavity coupled to a coaxial line by a small loop[1] or probe. According to Beringer[2] the details of the problem of iris-coupled waveguides have not been solved. For small irises, i.e., whose characteristic dimensions are small compared to a wave length, Bethe[3] has given a treatment which appears satisfactory theoretically but whose actual application to this problem seems to impose formidable calculation. Quite recently Slater[4] has given a very thorough-going discussion of the cavity-coupling problem.

If an iris is used, the nature of the coupling will depend on both the cavity mode and the shape of the iris. There will be magnetic coupling through a round hole if the magnetic field at the surface of the guide has a component parallel to the magnetic field at the adjoining surface of the cavity. There will be electric coupling if both cavity and guide have components of electric field normal to the common surface between them. If a narrow slot is used instead of a round hole, the electric coupling will be very small, and there will be appreciable

---

(1) This case is solved by J. C. Slater, "Forced Oscillations and Cavity Resonators," RL Report No. 188.

(2) R. Beringer, in "Principles of Microwave Circuits," p. 219, Vol. 8, MIT Rad. Lab. Series, McGraw-Hill, 1948.

(3) H. A. Bethe, "Theory of Diffraction by Small Holes," Phys. Rev. 66, 163-182 (1944).

(4) J. C. Slater, "Microwave Electronics," pp. 143-160, D. VanNostrand, 1950.

magnetic coupling only if the tangential magnetic field in both guide and cavity have components parallel to the slot.

None of the foregoing complications appear particularly troublesome, however, from the practical standpoint. If the coupling loop or iris has dimensions much smaller than a wavelength, the distortion of the cavity fields will be small, except of course, in the immediate region of coupling. As long as the coupling is loose enough the stored energy residing in the external coupling circuit will be an inappreciable fraction of the total stored energy, so that the resonant frequencies will be displaced but slightly from those of the isolated cavity. Likewise, the unloaded Q's calculated from the field equations will not differ greatly from those observed from the cavity-coupling system.(1) The deviations will be least for loop or probe coupling. These cases are also more susceptible to calculation than iris coupling.

The preceding discussion has dealt with cavity-coupling systems in general. The disturbance introduced by coupling to a confocal spheroidal cavity should be no worse so that we can reasonably approximate the ω_α's of Chapter IX by those computed for the isolated cavity according to Chapter VI. These results are presented in Appendix C.

4. Determination of the Normalization Factor

The H_α's required in (10.1) for the calculation of Q_α will have the same form as those for the isolated cavity but are subject to the normalization condition (9.5). If the normalization factor could be

---

(1) R. Beringer, in "Technique of Microwave Measurements," p. 292, MIT Radiation Laboratory Series, Vol. 11, McGraw-Hill, 1947.

readily found, the surface integral may be evaluated at once using (8.20). We can find this normalization factor by making use of the frequency shift due to perturbation of the boundary walls.

Equation (9.45) can be written

$$\frac{\omega^2}{\omega_a^2} - 1 = \int_{V'} (H_a^2 - E_a^2)\, dv \tag{10.2}$$

Now we let $H_a = NH$, where H is an unnormalized solution. From (2.3) and (9.1),

$$\text{curl } E = j\omega\mu_0 H$$

$$\text{curl } E_a = k_a H_a \tag{10.3}$$

we see that

$$\frac{E_a}{E} = \frac{k_a H_a}{j\omega\mu_0 H} = \frac{k_a N}{j\omega\mu_0} = \frac{1}{j}\sqrt{\frac{\epsilon_0}{\mu_0}}\, N = \frac{N}{Z_0} \tag{10.4}$$

where we have let $Z_0 = j\sqrt{\mu_0/\epsilon_0}$. Equation (10.2) then becomes

$$\frac{\omega^2}{\omega_a^2} - 1 = N^2 \int_{V'} \left[H^2 - \left(\frac{E}{Z_0}\right)^2\right] dv \tag{10.5}$$

where it will be recalled that the volume element is positive for an inward deformation of the cavity. Let us apply (10.5) to the case where we hold the inner spheroid, ξ_1, constant, and ask for the frequency shift for an infinitesimal increase in the "radial" dimension ξ_2 of the outer spheroid. In this case (10.5) is

$$\frac{\omega^2}{\omega_a^2} - 1 = -N^2 \int_{\xi_2}^{\xi_2 + \Delta\xi_2} \oint_{\xi = \text{const.}} \left[H^2 - \left(\frac{E}{Z_0}\right)^2\right] h_\xi\, da\, d\xi \tag{10.6}$$

For the small variation in ξ_2 to be considered, N^2, H^2, and E^2 may be considered essentially constant. H is tangential to the surface and E normal. Strictly speaking, the skin effect will introduce a small tangential electric field and also alter H, but these will be second order effects and may here be disregarded. Partial differentiation of (10.6) with respect to ξ_2, keeping ξ_1 constant, yields

$$\frac{2\omega}{\omega_a^2}\frac{\partial\omega}{\partial\xi_2}\bigg|_{\xi_1=\text{const.}} = -N^2\oint_{\xi_2=\text{const.}}\left[H^2-\left(\frac{E}{Z_0}\right)^2\right]h_\xi\,da \tag{10.7}$$

Since $\omega = c/f\sqrt{\epsilon_0\mu_0}$, where c is the dimensionless frequency variable of Chapter VI, we have

$$\frac{2\omega}{\omega_a^2}\frac{\partial\omega}{\partial\xi_2}\bigg|_{\xi_1=\text{const.}} = \frac{2}{c}\frac{\partial c}{\partial\xi_2}\bigg|_{\xi_1=\text{const.}} \tag{10.8}$$

Curves showing the variation of c with ξ_2 for constant ξ_1 are given in Appendix C, Figures 46 to 50. We have now to evaluate the surface integral in (10.7).

5. Evaluation of the Surface Integral

Using (2.28) and (2.30), we have

$$\oint_{\xi_2=\text{const.}} \left[H^2-\left(\frac{E}{Z_0}\right)^2\right] h_\xi \, da = f^3 \int_0^{2\pi} d\varphi \int_{-1}^{1} \left[H^2-\left(\frac{E}{Z_0}\right)^2\right](\xi_2^2-\eta^2)\, d\eta$$

$$= 2\pi f^3 \int_{-1}^{1} \left\{ \frac{A_0^2}{f^2} R^2(\xi_2) S^2(\eta) - \frac{\omega^2\mu^2 A_0^2}{k^4 f^4 Z_0^2} \frac{R^2(\xi_2)}{(\xi_2^2-\eta^2)} \left[\frac{dY(\eta)}{d\eta}\right]^2 \right\} (\xi_2^2-\eta^2)\, d\eta$$

$$= 2\pi f A_0^2 R^2(\xi_2) \int_{-1}^{1} \left\{ S^2(\eta)(\xi_2^2-\eta^2) - \frac{1}{c^2}\left[\frac{dY(\eta)}{d\eta}\right]^2 \right\} d\eta$$

$$= 2\pi f A_0^2 R^2(\xi_2) \left\{ \xi_2^2 \int_{-1}^{1} S^2(\eta)\, d\eta - \int_{-1}^{1} \eta^2 S^2(\eta)\, d\eta - \frac{1}{c^2}\int_{-1}^{1} \left[\sqrt{1-\eta^2}\, S'(\eta) - \frac{\eta}{\sqrt{1-\eta^2}} S(\eta)\right]^2 d\eta \right\}$$

$$= 2\pi f A_0^2 R^2(\xi_2) \left\{ \xi_2^2 \left(\int_{-1}^{1} S^2(\eta)\, d\eta\right) - \left(\int_{-1}^{1} \eta^2 S^2(\eta)\, d\eta + \frac{1}{c^2}\int_{-1}^{1} \left[\sqrt{1-\eta^2}\, S'(\eta) - \frac{\eta}{\sqrt{1-\eta^2}} S(\eta)\right]^2 d\eta \right) \right\} \tag{10.9}$$

Since $S(\eta)$ is given by a series of associated Legendre polynomials, (6.27), the integrals may be readily evaluated by taking advantage of the orthogonal properties of these functions. The evaluation is discussed in further detail in Appendix F.

Using (10.7) and (10.8) the normalization factor is given formally by

$$N^2 = \frac{-\frac{z}{c}\frac{\partial c}{\partial \xi_2}\Big|_{\xi_1 = \text{const.}}}{\oint_{\xi_2 = \text{const.}} \left[H^2 - \left(\frac{E}{z_0}\right)^2\right] h_\xi \, da} \tag{10.10}$$

and (10.1) becomes

$$\frac{1}{Q_a} = \frac{\delta}{2} N^2 \oint H^2 \, da$$

$$= \frac{N^2}{2}\left\{\delta_1 \oint_{\xi_1} H^2 \, da + \delta_2 \oint_{\xi_2} H^2 \, da\right\} \tag{10.11}$$

where the contributions of the inner and outer surfaces are considered separately. Making use of (8.20) and (8.21) we can write then

$$\frac{1}{Q_a} = \frac{N^2}{2}\left(\frac{4}{\omega\mu_0}\right)(W_1 + W_2)$$

$$= \frac{N^2 2\pi A_0^2}{2\mu_0}\left[\delta_1\mu_1 \odot(\xi_1) X^2(\xi_1) + \delta_2\mu_2 \odot(\xi_2) X^2(\xi_2)\right] \tag{10.12}$$

The functions X and $\odot$ have already been described in Chapters V and VIII, and are tabulated in Appendix F. The amplitude factor A_0^2 is cancelled by a similar term in the denominator of N^2.

This shows how the unloaded Q may be computed and predicted if the cavity dimensions and the electrical characteristics of the walls are known. Conversely it shows how one can compute δ_1, the skin depth of the sample, from a value of Q obtained experimentally. The computation in an actual case is straightforward and can be accomplished in a short time using the data given in the appendices. The value of the

conductivity σ_1 can be obtained at once from

$$\delta_1 = \sqrt{\frac{2}{\omega \mu_1 \sigma_1}} \tag{10.13}$$

where the permeability μ_1 has the value within the conductor.

CHAPTER XI

EFFECT OF PARAMETERS ON CAVITY BEHAVIOR

1. Physical Significance of the Parameters

The system of spheroidal coordinates η, ξ, and φ is discussed in detail in Appendix A. For a general discussion it is sufficient to recall that the "angular" coordinate, η, varies from -1 to +1, analogous to the variation of $\cos\vartheta$ in spherical coordinates. The "radial" coordinate ξ, varies from 1 to ∞ and measures position outward from the line joining the two foci. This line corresponds to $\xi = 1$. A given value of ξ characterizes an ellipsoid of revolution, or spheroid, confocal with the degenerate spheroid at $\xi = 1$. For large values of ξ, the spheroidal surfaces approach spherical ones, with ξ the radius measured in units of the semi-interfocal distance. Smaller and smaller values of ξ indicate spheroids growing more and more eccentric or needle-like. The coordinate φ measures azimuth about the axis of revolution and varies from 0 to 2π.

Now in Chapter II it was found that for axially symmetric TM solutions of Maxwell's equations, the only non-vanishing field components are given by

$$H_\varphi = \frac{A_0}{f} \frac{1}{\sqrt{(1-\eta^2)(\xi^2-1)}} Y(\eta) X(\xi) e^{-j\omega t} \tag{11.1}$$

$$E_\eta = \frac{j\omega\mu_0 A_0}{c^2} \frac{1}{\sqrt{(\xi^2-\eta^2)(1-\eta^2)}} Y(\eta) \frac{dX(\xi)}{d\xi} e^{-j\omega t} \tag{11.2}$$

$$E_\xi = -\frac{j\omega\mu_0 A_0}{c^2} \frac{1}{\sqrt{(\xi^2-\eta^2)(\xi^2-1)}} \frac{dY(\eta)}{d\eta} X(\xi) e^{-j\omega t} \tag{11.3}$$

where $2f$ is the interfocal distance and the functions $Y(\eta)$ and $X(\xi)$ satisfy

$$Y''(\eta) + \frac{\alpha - c^2\eta^2}{1-\eta^2} Y(\eta) = 0 \qquad (11.4)$$

$$X''(\xi) + \frac{c^2\xi^2 - \alpha}{\xi^2 - 1} X(\xi) = 0 \qquad (11.5)$$

subject to certain boundary conditions discussed in Chapter III. The parameter c is the dimensionless frequency variable kf, and in non-dissipative media is given by $\omega f\sqrt{\epsilon.\mu.}$. The parameter α enters the problem as the separation constant introduced in the reduction of the partial differential equation (2.19) to the set (11.4) and (11.5). Imposition of the boundary conditions restricts the values which c and α may assume to certain pairs (eigenvalues) simultaneously satisfying (11.4) and (11.5). Now (11.5) can be written

$$X''(\xi) + \left(c^2 + \frac{c^2 - \alpha}{\xi^2 - 1}\right) X(\xi) = 0 \qquad (11.6)$$

so that for large values of ξ the solutions of (11.6) behave like $\sin(c\xi)$. Thus c is physically the limiting value of the propagation constant $2\pi/\lambda$, where λ is the wavelength, measured in units of ξ, for wave fronts parallel to surfaces of constant ξ. As ξ grows large, E_ξ falls off more rapidly than E_η and H_φ and consequently the field at large distances from the origin is transverse, as we should expect it to be.

In similar fashion we can write (11.4) in the form

$$Y''(\eta) + \left(\alpha + \frac{(\alpha - c^2)\eta^2}{1-\eta^2}\right) Y(\eta) = 0 \qquad (11.7)$$

Near the equatorial plane, η approaches zero and $Y(\eta)$ approaches the limiting form $\sin(\sqrt{\alpha}\,\eta)$. Physically this means that $2\pi/\sqrt{\alpha}$ is the limiting value of the wavelength in the η direction, at the equatorial plane of the spheroid, measured in units of η.

2. Field Patterns and Mode Indices

For a given cavity, i.e., for specified ξ_1 and ξ_2, an infinite number of discrete resonant frequencies c_{lp} are possible. To each of these corresponds a definite field pattern which can be classified by integral mode indices l and p. The index l takes on values 0, 1, 2, 3,.... and gives the number of nodes of H in the η direction, excluding those at $\eta = \pm 1$. The index p likewise may have the values 0, 1, 2, 3,.... and it designates the number of nodes of H in the ξ direction. Patterns of several of the lowest modes are shown in cross section in Figure 7. Solid lines denote the electric field, which lies in meridional planes. The magnetic field lines are circles concentric with the axis of rotation, and show as dots in the figure. Since these are standing waves, the electric and magnetic fields differ in time phase by 90°. The dashed ellipses represent spheroidal surfaces on which E_η is zero. These surfaces could be made conducting without disturbing the field pattern, and therefore, represent other possible boundaries which yield the same field distribution.

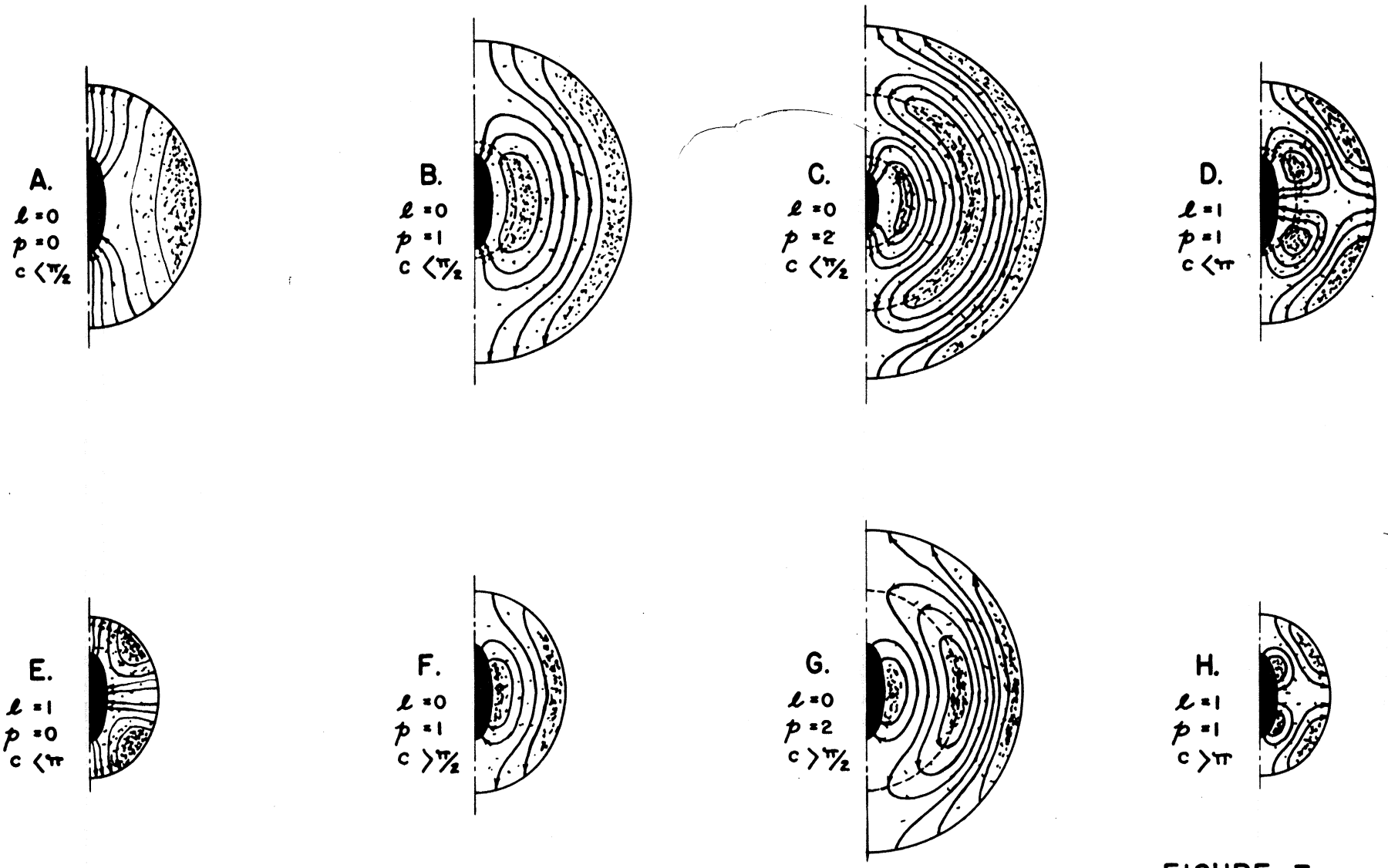

FIGURE 7
SPHEROIDAL FIELD PATTERNS

It is important to note that a spheroidal cavity system of rotational symmetry is completely defined by specifying four parameters. These are ℓ and p, the indices identifying the axial and radial modes, and any two of ξ_1, ξ_2 and c, the bounding coordinates and the reduced frequency, respectively.

3. Dependence of Field Components and Field Distribution on Frequency

A considerable part of this work has been spent in consideration of the function $X(\xi)$, owing to its importance in the field components, given by expressions (11.1) to (11.3). The character of this function varies markedly with the reduced frequency c. In discussing this character an essential parameter is $\sqrt{\alpha}/c$ which can be considered a function of c for a specified value of ℓ. Now $\sqrt{\alpha}/c$ can never be negative; when it is less than one then possible solutions of (11.5) have the forms shown qualitatively in Figure 8A. Recall that $X(\xi)$ must have zero slope at the boundaries ξ_1 and ξ_2. Also shown in this figure is the function $X(\xi_1)$ which consists of $X(\xi)$ evaluated at the points of zero slope. This implies normalization of all the $X(\xi)$ solutions to unit amplitude for large values of ξ. When $\sqrt{\alpha}/c$ equals unity, then the $X(\xi)$ solutions are pure sinusoids, as Figure 8B shows; $X(\xi_1)$ is now a constant. The character changes when $\sqrt{\alpha}/c$ exceeds unity, as Figure 8C shows. The point where $\xi = \sqrt{\alpha}/c$ is a critical one; here the curvature is zero. For larger values of ξ the solutions are still oscillatory but for smaller values become concave away from the ξ axis. When $\xi = \sqrt{\alpha}/c$, $X(\xi_1)$ attains a maximum as is better shown by the quantitative curves of Figure 9. In Figure 9, $X(\xi_1)$ is plotted for several values of c, for the $\ell=1$ mode; for this mode $(\ell+1)\pi/2 = \pi$. The maxima at $\sqrt{\alpha}/c$ are clearly marked.

FIGURE 8

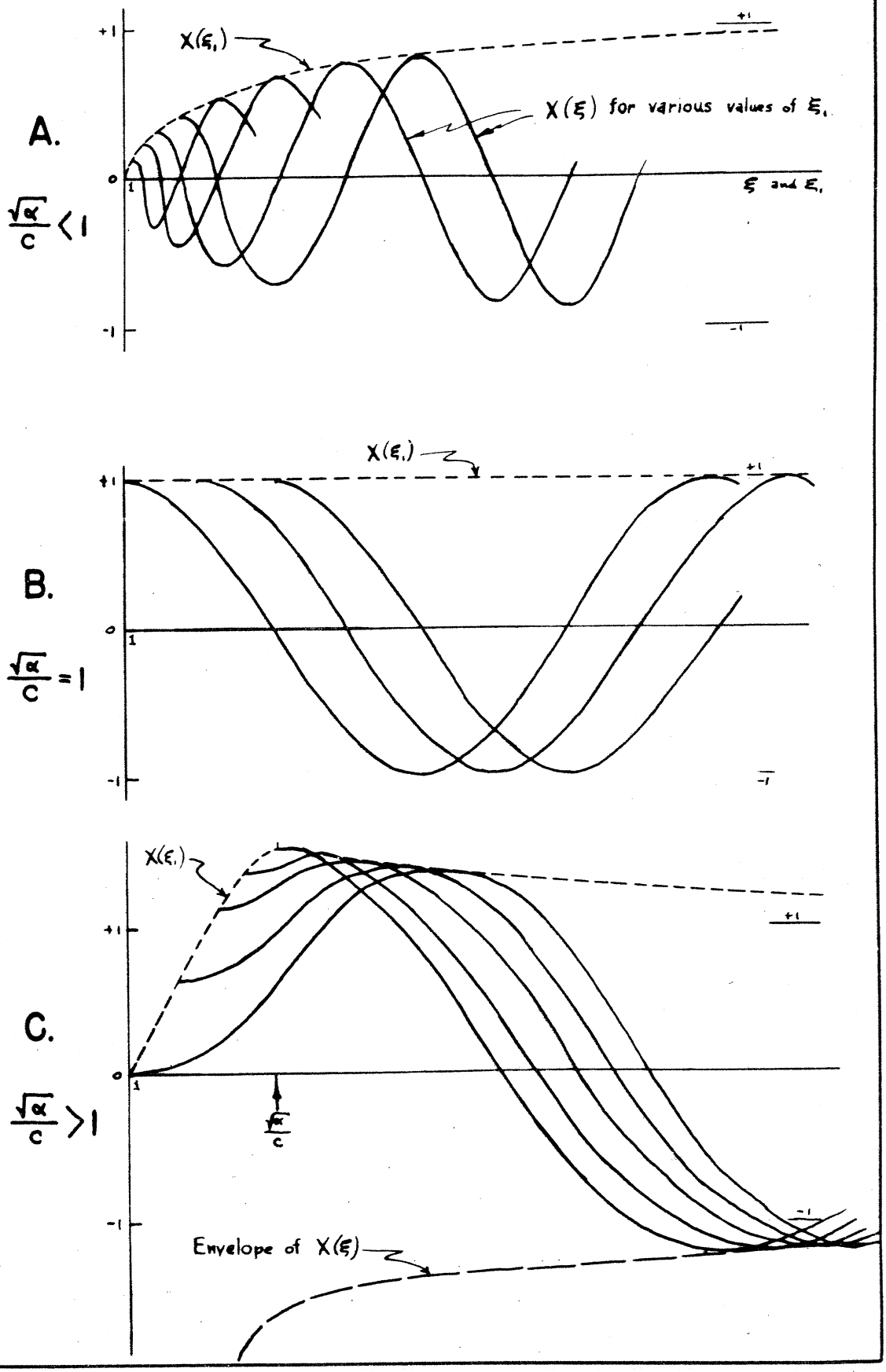
A.
$\frac{\sqrt{\alpha}}{c} < 1$
$X(\xi_1)$
$X(\xi)$ for various values of ξ_1
+1
0
1
-1
ξ and ξ_1
B.
$\frac{\sqrt{\alpha}}{c} = 1$
$X(\xi_1)$
C.
$\frac{\sqrt{\alpha}}{c} > 1$
$X(\xi_1)$
$\frac{\sqrt{\alpha}}{c}$
Envelope of $X(\xi)$

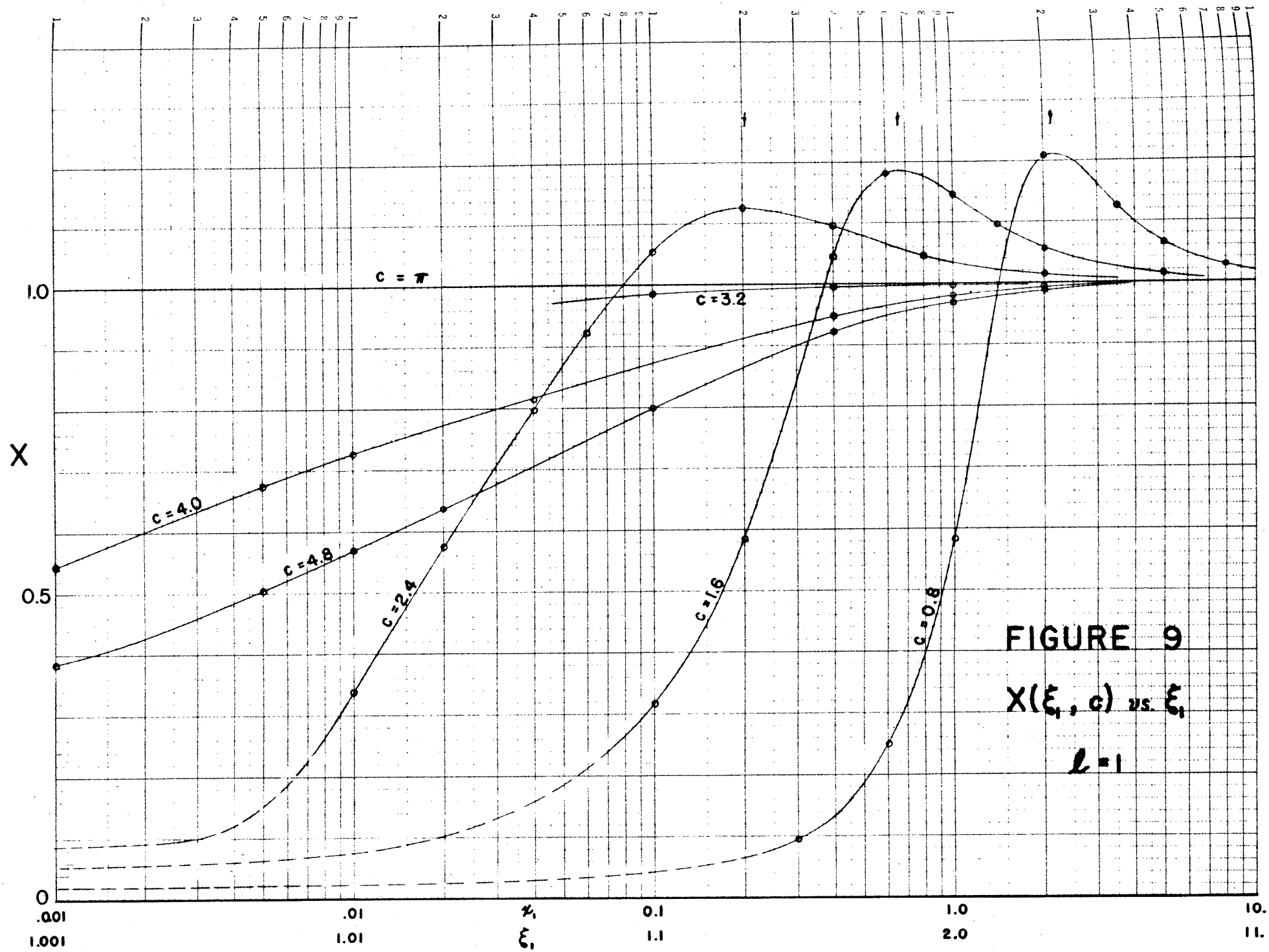

FIGURE 9

$X(\xi_1, c)$ vs. ξ_1

$\ell = 1$

The frequency c at which $\sqrt{\alpha}/c$ is unity has already been given as $(\ell+1)\pi/2$. For $\sqrt{\alpha}/c > 1$, it is necessary that $c < (\ell+1)\pi/2$. In this situation it may be seen from Figure 8C that for a given cavity the value of $X(\xi)$ at the boundary ξ_1, will not be a maximum if $\xi_1 < \sqrt{\alpha}/c$, even though $X'(\xi_1)$ is zero. Consequently, neither electric nor magnetic fields tend to have their maximum values close to the inner spheroid. See for example Figures 7A, 7B, and 7C.

On the other hand, if $\xi_1 > \sqrt{\alpha}/c$, and this will always be true when $\sqrt{\alpha}/c < 1$, then $X(\xi)$ has a maximum at ξ_1 and the innermost bands of high magnetic flux density move in adjacent to the inner boundary as can be seen from Figures 7F and 7G. With increasing frequency, both electric and magnetic fields tend to move in closer to the equatorial plane.

4. Variation of Frequency with Cavity Parameters

By the methods of Chapters VI and VII the resonant frequencies of a closed spheroidal cavity system have been computed for a wide range of variation of the parameters c, ξ_1, and ξ_2 and for several of the lowest axially symmetric TM modes. The results of these computations are presented in Figures 37 to 50, Appendix C. These figures give a thorough graphical presentation of the results so that, given the dimensions of a spheroidal cavity, the resonant frequencies can be obtained almost at once upon consulting the appropriate graphs.

A more practical way of evaluating the results and determining their physical significance is to study their application to a specific case. Suppose we have a spheroidal cavity of given eccentricity, that is, ξ_2 is specified. Then suppose we place in this cavity a smaller

confocal spheroid, and observe the behavior of the resonant frequency of a particular mode as ξ_1 varies from 1 to ξ_2. Figure 10 shows just this for the mode for which $\ell = 1$ and $p = 1$, for several values of ξ_2. Figures 11 and 12 give similar information for the modes for which $p = 2$, 3 and 0. Also plotted in the figures is the parameter $\sqrt{\alpha}/c$ as a function of c, that is, the locus of points at which $\xi_1 = \sqrt{\alpha}/c$. To interpret these curves we may use to advantage the formula of Chapter IX describing the shift in frequency arising from an infinitesimal perturbation of the boundaries,

$$\frac{\omega^2}{\omega_a^2} - 1 = \int_{V'} \left(H_a^2 - E_a^2\right) dv \qquad (11.8)$$

where the integral is over V', the volume removed from the resonant cavity by the inward perturbation of the surface, and H_a and E_a are vector functions of position proportional to the field vectors. As was pointed out in Chapter X, a more useful form for our purposes is

$$\left.\frac{\partial c}{\partial \xi_1}\right|_{\xi_2 = \text{const.}} = \frac{c}{2} N^2(c, \xi_1, \xi_2) \oint_{\xi_1} \left[H^2 - \left(\frac{E}{Z_0}\right)^2\right] h_\xi \, da$$

$$= \frac{c}{2} N^2 2\pi f^3 \int_{-1}^{1} \left[H^2 - \left(\frac{E}{Z_0}\right)^2\right] (\xi_1^2 - \eta^2) \, d\eta$$

$$= \frac{c}{2} N^2 2\pi f A_0^2 R^2(\xi_1) \int_{-1}^{1} \left\{ S^2(\eta)(\xi_1^2 - \eta^2) - \frac{1}{c^2}\left[\frac{dY(\eta)}{d\eta}\right]^2 \right\} d\eta$$

$$= \frac{c}{2} N^2 2\pi f A_0^2 \frac{X^2(\xi_1)}{(\xi_1^2 - 1)} \int_{-1}^{1} \left\{ \xi_1^2 \left[S^2(\eta)\right] - \left[\eta^2 S^2(\eta) + \frac{1}{c^2}\left(\frac{dY(\eta)}{d\eta}\right)^2\right] \right\} d\eta$$

(11.9)

This expression for the slope of the frequency has three major factors. These are the integral, the factor $X^2(\xi_1)/(\xi_1^2-1)$ and the normalization factor N^2. The N^2 factor is necessary because expression (11.8) requires that $\int_V H_a^2 dv$ over the cavity volume be unity, which is to say that the total energy is made the same for any cavity. As mentioned in Chapter X, H_a and H are related by $H_a = NH$; the normalization of H employed throughout the balance of this work has been one more convenient for other purposes.

Along the line where $\xi_1 = \sqrt{\alpha}/c$ the integral vanishes, as can be readily demonstrated by integration by parts. Consequently, the slope must be zero, or there is a minimum in each of the frequency curves along this line. This is borne out precisely by Figures 10 to 12. Physically, this means that for a value of ξ_1 along this line, equal maximum electrical and magnetic energies are contained in a spheroidal shell of infinitesimal thickness $\delta\xi$. Note that constant $\delta\xi$ is not quite the same as uniform thickness, so it is not correct to say that the electric and magnetic surface energy densities averaged over the inner surface are equal. As ξ_1 grows larger and the inner spheroid approaches a sphere, then this last statement becomes more nearly correct.

The factors N^2 and $X^2(\xi_1)/(\xi_1^2-1)$ are always positive. In Figures 10 to 12, in the area above and to the right of $\xi_1 = \sqrt{\alpha}/c$, the integral is always positive, so that here the slope must always be positive. Conversely, in the remaining area the integral is negative, and the slope must also be negative. In the vicinity of the dividing line, the predominant effect is due to the variation of the integral.

From inspection of (11.9) it is apparent that the integral has the form $A\xi_1^2 - B$ where A and B are positive functions of c . As can be seen from Figure 9, $X^2(\xi_1)$ is very nearly a constant for all but the smallest values of ξ_1 , when c is greater than $(\ell+1)\pi/2$. It is not surprising then that the product

$$\frac{X^2(\xi_1)}{(\xi_1^2-1)} \int_{-1}^{1} \left[\xi_1^2 S^2(\eta) - \left(\eta^2 S^2(\eta) + \frac{1}{c^2}[Y'(\eta)]^2 \right) \right] d\eta \qquad (11.10)$$

is practically constant for the larger values of ξ_1 . The normalization factor N^2 increases with ξ_1 however, so that the slope grows more and more positive. This is mainly a volume effect, the frequency increasing as the resonating volume grows smaller and smaller.

With c still greater than $(\ell+1)\pi/2$, as we now consider ξ_1 approaching unity we find that N^2 is almost constant. The product (11.10), constant for larger values of ξ_1 , suddenly begins to grow without limit and the slope becomes infinite at $\xi_1 = 1$. This effect can be attributed to the factor (ξ_1^2-1) in the denominator which tends to zero more rapidly than does $X^2(\xi_1)$, and is evidenced by the rather sharp break in the frequency curve, such as in the curve for $\xi_2 = 2.5$ in Figure 11. While the fields grow without limit as $\xi \to 1$ [due to the factor $(\xi_1^2-1)^{-1}$] , the normalization factor is practically unchanged, since the volume occupied by these high fields is so small that the contribution to the total energy is a small part of the total. In this region of high field intensities, however, it is to be expected that the reaction to a small perturbing influence (as a minute change in ξ_1) will be much enlarged, and the frequency shift considerable.

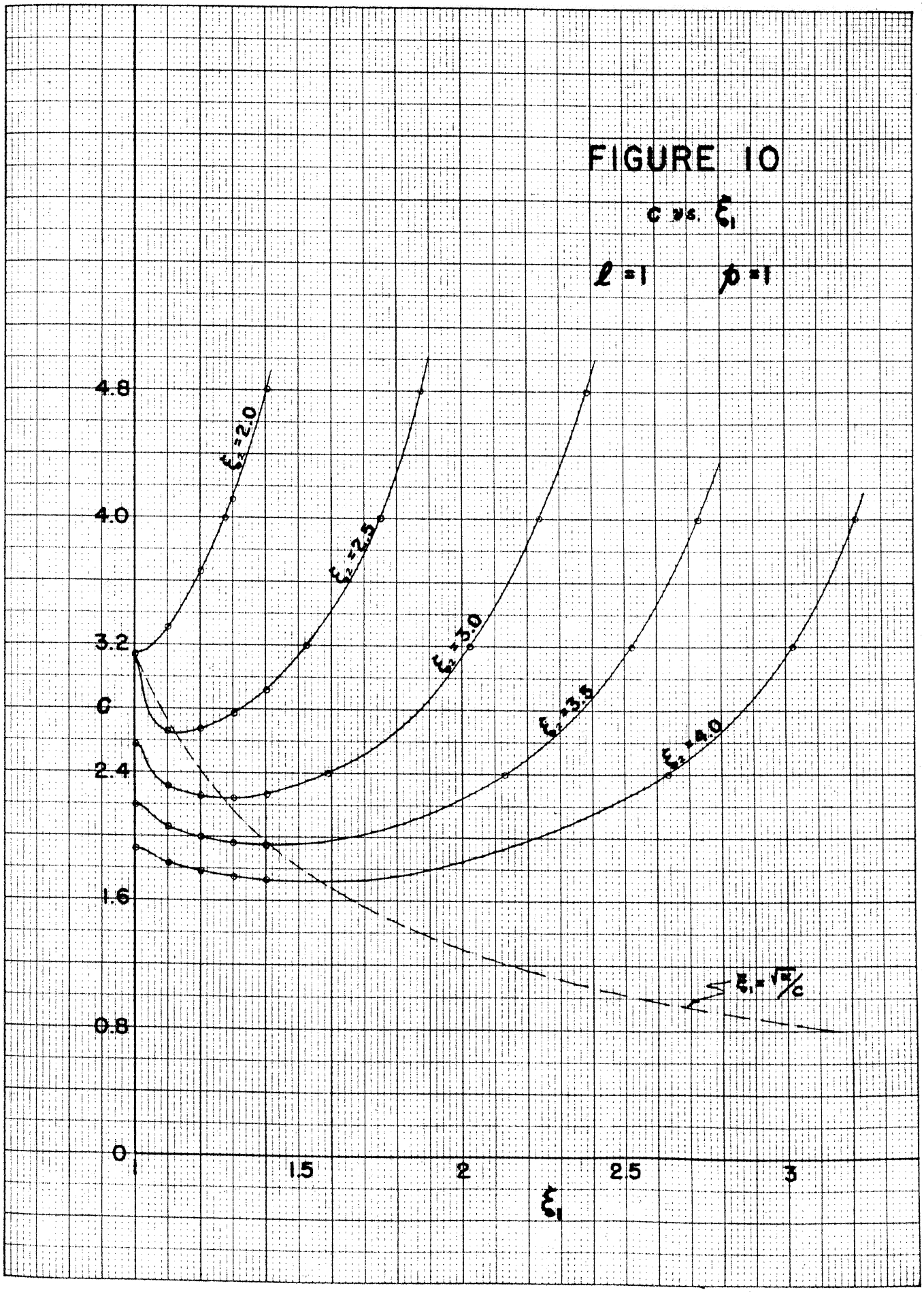
FIGURE 10
c vs. ξ_1
$\ell = 1$ $p = 1$
4.8
4.0
3.2
2.4
1.6
0.8
0
c
1
1.5
2
2.5
3
ξ_1
$\xi_2 = 2.0$
$\xi_2 = 2.5$
$\xi_2 = 3.0$
$\xi_2 = 3.5$
$\xi_2 = 4.0$
$\xi_1 = \sqrt{\pi}/c$

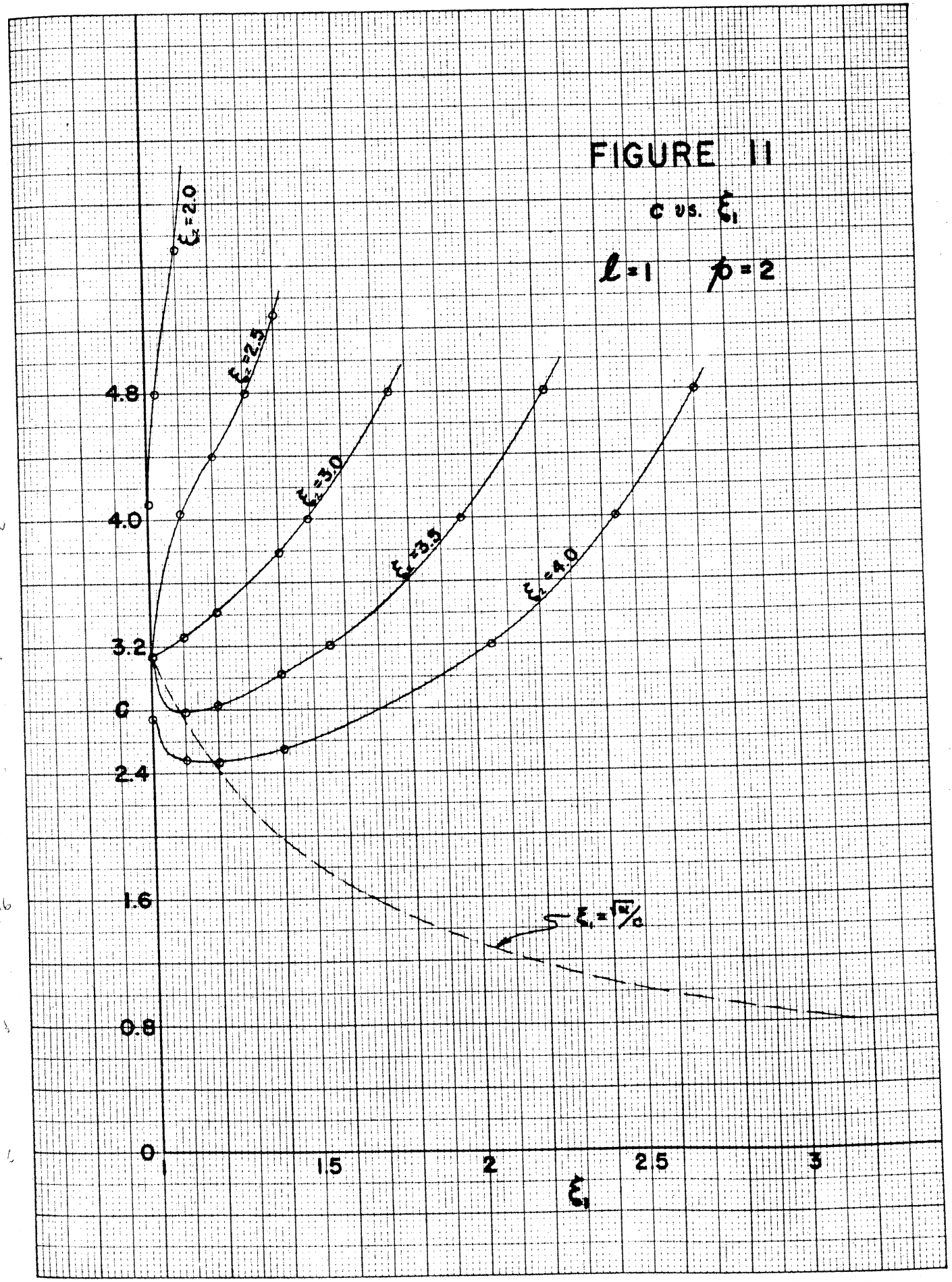
FIGURE 11
c vs. ξ1
ℓ=1 p=2
ξ2=2.0
ξ2=2.5
ξ2=3.0
ξ2=3.5
ξ2=4.0
ξ1=√n/c
4.8
4.0
3.2
c
2.4
1.6
0.8
0
1
1.5
2
2.5
3
ξ1

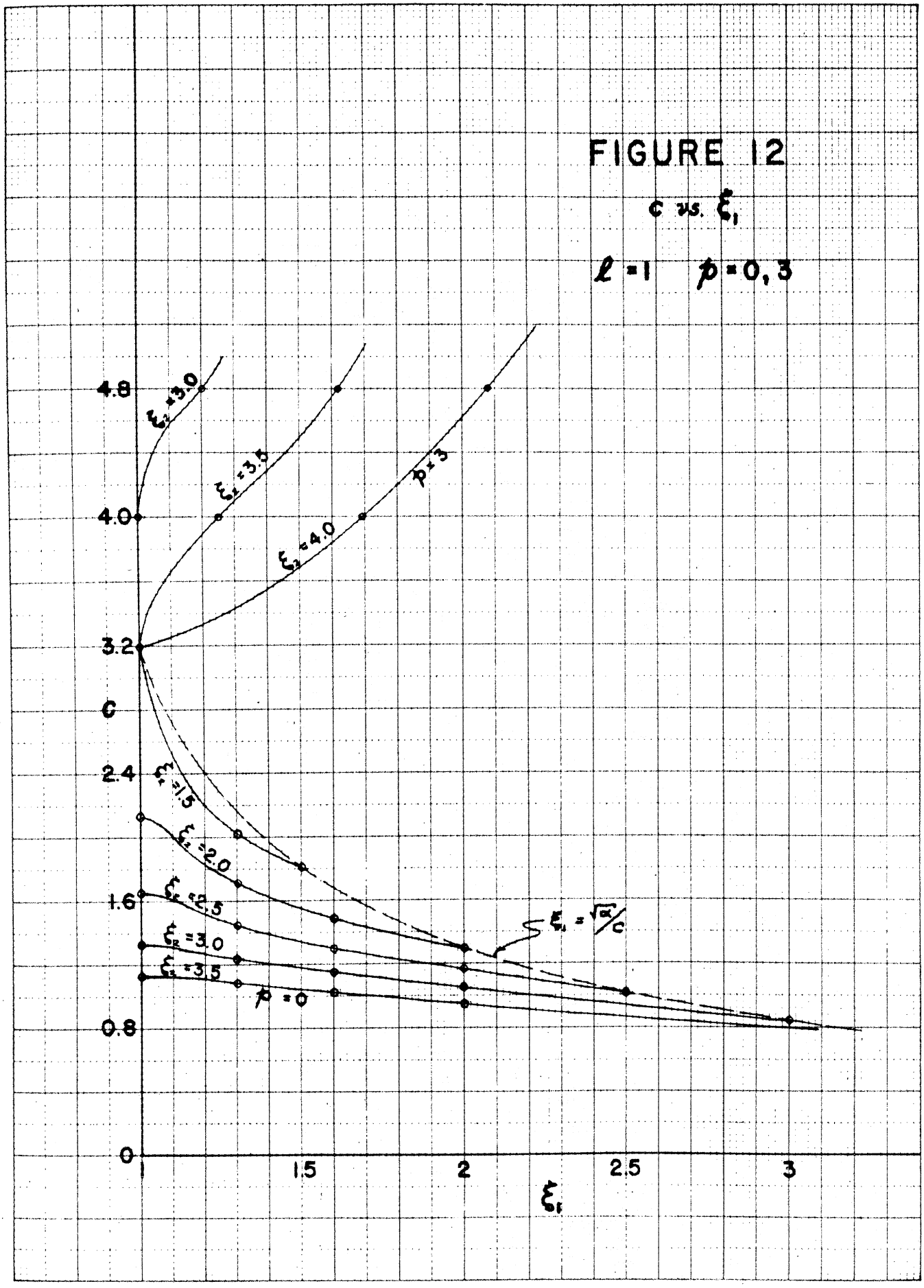
FIGURE 12
c vs. ξ_1
$\ell = 1$ $p = 0, 3$
4.8
4.0
3.2
2.4
1.6
0.8
0
c
1
1.5
2
2.5
3
ξ_1
$\xi_2 = 3.0$
$\xi_2 = 3.5$
$\xi_2 = 4.0$
$p = 3$
$\xi_2 = 1.5$
$\xi_2 = 2.0$
$\xi_2 = 2.5$
$\xi_2 = 3.0$
$\xi_2 = 3.5$
$p = 0$
$\xi_1 = \sqrt{\alpha}/c$

Let us look now at the area to the left of the line $\xi_1 = \sqrt{\alpha}/c$, the area of negative frequency slope. Directly on the line we recall that the slope is zero, because the integral is zero. To the left the slope slowly grows more negative as the integral increases in value. In this region the field is predominantly electric as is confirmed by Figures 7B and 7D. For smaller values of ξ_1 the slope changes more rapidly, as the field intensities increase under the effect of the $(\xi_1^2-1)^{-1}$ factor. For values of ξ_1 very close to unity the fields fall again as $X^2(\xi_1)$ drops to zero, and at $\xi_1 = 1$ the slope is zero.

5. Behavior of the Loss Ratio

The more important object of this investigation is to determine the optimum relation among the parameters c, ξ_1, and ξ_2 so that for a given cavity mode the ratio of the contributions to Q of the inner and outer surfaces will be as high as possible. Expressed another way, we wish to maximize the function

$$\frac{W_1(\xi_1, c)}{W_2(\xi_2, c)} = \frac{\delta_1 \mu_1 \Psi_\ell(\xi_1, c)}{\delta_2 \mu_2 \Psi_\ell(\xi_2, c)} \qquad (11.11)$$

where W_1 and W_2 are the losses in the inner and outer spheroidal walls, respectively. Here δ is the skin depth $\sqrt{2/\mu\omega\sigma}$, determined by the electrical characteristics of the conducting wall material. The function Ψ_ℓ is proportional to $\oint_S H^2 \, da$, where the surface integral is taken over one of the bounding surfaces; it is defined by (8.24) and depends only on the field configuration. Consequently it is simpler to discuss the effect of cavity geometry in terms

of the function defined by

$$g_\ell^{\flat}(\xi_1, \xi_2, c) \triangleq \frac{\Psi_\ell(\xi_1, c)}{\Psi_\ell(\xi_2, c)} \tag{11.12}$$

which is independent of material properties. Upon specification of the wall materials, the actual loss ratio is given directly by

$$\frac{W_1}{W_2} = \frac{\delta_1 \mu_1}{\delta_2 \mu_2} g_\ell^{\flat}(\xi_1, \xi_2, c) \tag{11.13}$$

Throughout this work the term loss ratio will refer to $g_\ell^{\flat}$, but it is apparent that it differs from W_1/W_2 only by a constant factor $\delta_1\mu_1/\delta_2\mu_2$. Using (11.13) the expression for Q given by (10.12) may be written

$$\frac{1}{Q_a} = \frac{1}{Q_2}\left[1 + \frac{\delta_1 \mu_1}{\delta_2 \mu_2} g_\ell^{\flat}(\xi_1, \xi_2, c)\right] \tag{11.14}$$

where $1/Q_2$ is the contribution of the outer wall; this shows clearly the relation of $g_\ell^{\flat}$ to Q_a.

Values of $\Psi_\ell(\xi_1, c)$ have been computed for the same wide range of parameters as have the eigenfrequencies, and the details and results of computation are presented in Appendix F. For given reduced frequency c, corresponding values of ξ_1 and ξ_2 are known from the eigenfrequency computations of Appendix C; employing this knowledge corresponding values of $\Psi_\ell(\xi_1, c)$ and $\Psi_\ell(\xi_2, c)$ have been read off plots and from these values of $g_\ell^{\flat}$ have been computed. Curves have been plotted of $g_\ell^{\flat}$ versus ξ_1 for given c, and these are given in

Appendix F, Figures 56 to 65. Note that for a specified mode, fixing two of the parameters ξ_1, ξ_2, and c automatically determines the third. The loss ratio can be obtained at once by consulting the appropriate graphs.

From a study of these curves we find two kinds of behavior. For any given cavity, the behavior depends on the frequency c when ξ_1 is unity. For any mode in which this frequency exceeds $(\ell+1)\pi/2$, then q_ℓ^p becomes infinite as $\xi_1 \to 1$. If on the other hand this frequency is less than $(\ell+1)\pi/2$, then q_ℓ^p exhibits a maximum very close to the point where $\xi_1 = \sqrt{\alpha}/c$, and falls to zero at $\xi_1 = 1$. In either case, q_ℓ^p approaches unity as ξ_1 approaches ξ_2.

These points are borne out by the data of Appendix F but are more readily seen from Figure 13 which shows how q_ℓ^p varies with ξ_1 for several values of ξ_2 in the mode $\ell = 1$, $p = 1$. The results given by these curves cannot be considered highly quantitative due to instances of questionable accuracy in interpolation between points at coarse intervals, but they do show all the trends and are reasonably accurate for many purposes. From Figure 13 the peaks of q_ℓ^p for constant ξ_2 are seen to be quite flat for large values of ξ_2. As ξ_2 decreases, the peaks move closer to $\xi_1 = 1$, increasing in sharpness and amplitude, and finally becoming infinite when $\xi_2 = 1 + \frac{2p}{\ell+1}$.

Figure 14 shows the analogous behavior of the $\ell = 1$, $p = 0$ mode. While Figure 13 is typical of all higher modes, Figure 14 is markedly different. Here the maximum is very flat, never much greater than one, and occurs for a value of ξ_1 very close to ξ_2. The peak amplitude of q_ℓ^p tends to increase with decreasing ξ_2.

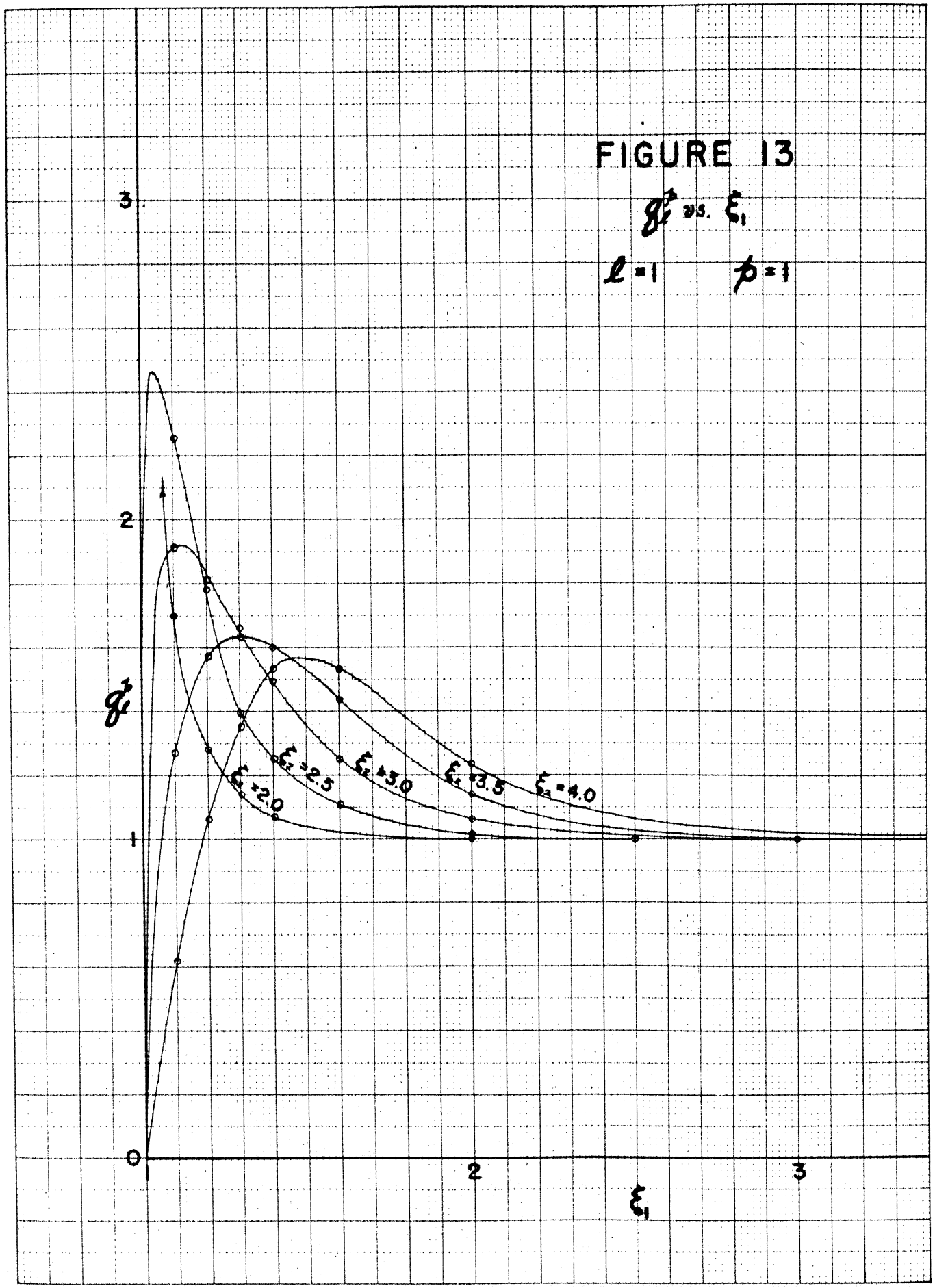
FIGURE 13
g_1^2 vs. ξ_1
$\ell = 1$ $p = 1$
3
2
1
0
g_1^2
ξ_1
1
2
3
$\xi_2 = 2.0$
$\xi_2 = 2.5$
$\xi_2 = 3.0$
$\xi_2 = 3.5$
$\xi_2 = 4.0$

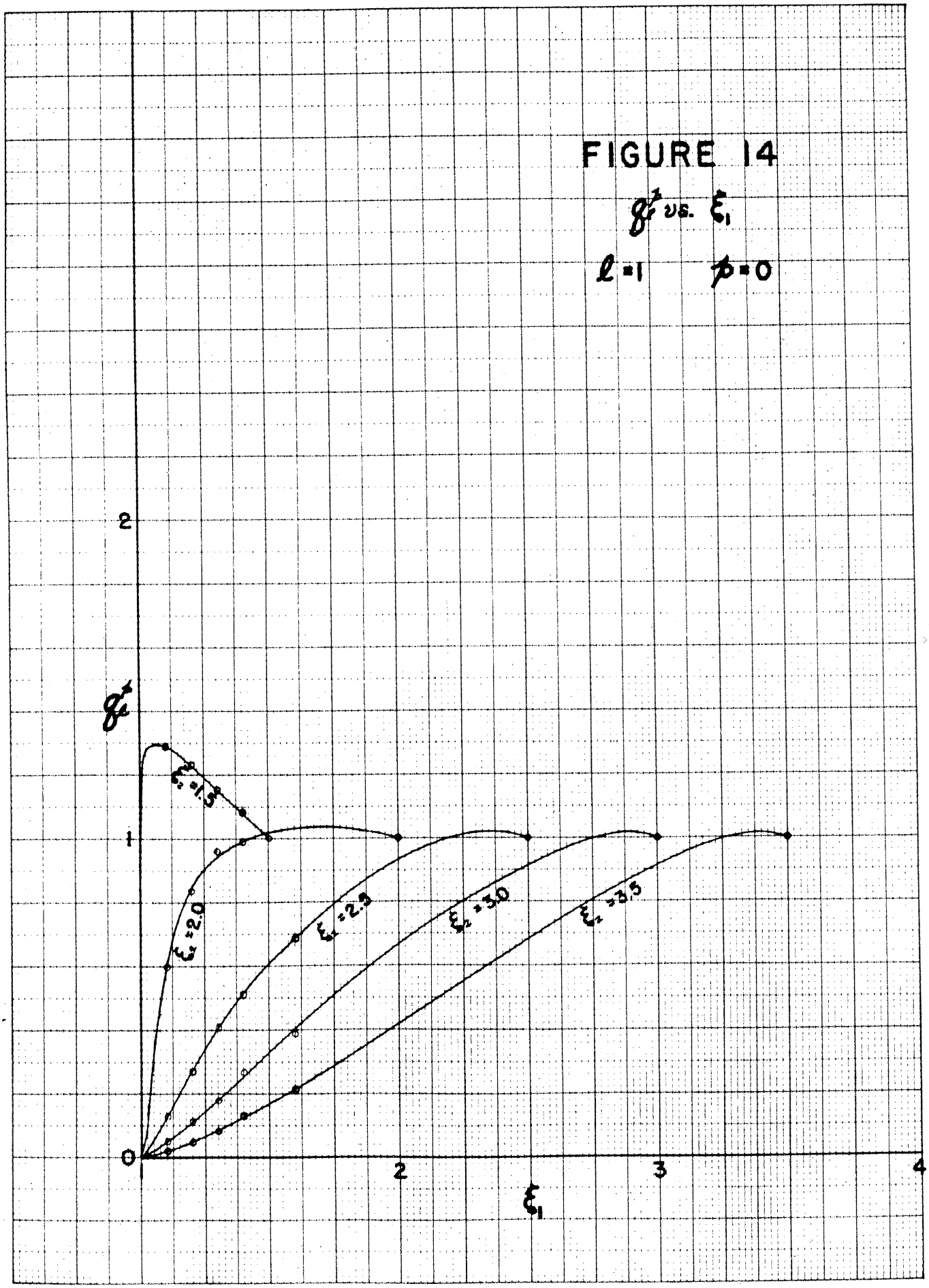

6. Correlation of Loss Ratio and Frequency Behavior

The behavior of the loss ratio is closely connected with that of the frequency. For large values of ξ_2 the peak in g_ℓ^p occurs at practically the same value of ξ_1 as does the minimum in frequency. This is so because at this minimum (on the line where $\xi_1 = \sqrt{\alpha}/c$) the function $X(\xi_1)$ of Figure 9 is a maximum, and in this region $X(\xi_1)$ is the controlling factor. As smaller values of ξ_2 are considered, the peak in g_ℓ^p shifts to the left of the frequency minimum. This can be attributed to the higher field intensities due to the factor $(\xi_1^2-1)^{-\frac{1}{2}}$. The frequency curve is not similarly shifted because it depends on a surface integral of the difference between magnetic and electric field intensities, while for the loss the integral is only over the magnetic field. For the group of curves of Figure 13, as ξ_1 approaches unity the inner surface finds itself in a region of strong electric field but reduced magnetic field, both of which eventually vanish since $X^2(\xi_1)/\sqrt{\xi_1^2-1}$ goes to zero at $\xi_1 = 1$. Consequently the loss falls to zero, while the slope of the frequency goes sharply negative and then returns to zero.

If on the other hand ξ_2 is less than $1 + 2p/(\ell+1)$ then g_ℓ^p blows up at $\xi_1 = 1$. This corresponds to the situation where the frequency c exceeds $(\ell+1)\pi/2$ and always has positive slope. Here the inner spheroid is in a strong magnetic field. $X(\xi_1)$ has a maximum at ξ_1, and the factor $(\xi_1^2 - 1)^{-\frac{1}{2}}$ intensifies it so that the expressions for both loss and frequency slope grow without limit. This says that the power loss in the inner spheroid becomes infinite. In any actual physical case, of course, infinities have no place and the fact

is that for values of ξ_1 extremely close to unity, our treatment is no longer valid. As pointed out in Section 4 of Chapter VIII we have assumed throughout this work that the field and current distributions at any point near a curved boundary surface are the same as if the surface were plane. This greatly simplifies the problem of calculating the losses in the conductor and is a valid assumption as long as the radius of curvature greatly exceeds the skin depth. In our case this is true except for values of ξ_1 very close to 1. For a skin depth of 10^{-5} inches and an interfocal distance of one inch, our treatment should be satisfactory for values of $(\xi_1 - 1)$ greater than 10^{-7}, corresponding to a wire whose diameter at the center is about .0004". For smaller values of $(\xi_1 - 1)$, the surface curvature is so great that the current layers just beneath the surface interfere with one another, and our approximation must be replaced by a more rigorous analysis.

7. Solution to the Problem

In Chapter I we stated as the object of this investigation the determination of the optimum relation among the four parameters characterizing the microwave cavity contained between two confocal prolate spheroids, such that the ratio of surface loss in the internal spheroid to that in the external spheroid is maximized. The system is completely specified by the mode indices ℓ and p and any two of the parameters ξ_1, ξ_2, and c. The investigation has been restricted to consideration of the axially symmetric modes since only then can the method of separation of variables be used successfully to attack the wave equation in the prolate spheroidal coordinate system.

In this chapter we have found that two types of behavior are possible. In the first, generally associated with the lower modes, the loss ratio g_e^{ϕ} is zero when the inner "radial" parameter ξ_1 is unity; in this instance the inner spheroid is an infinitely thin wire. As we keep ξ_2 constant and increase ξ_1, g_e^{ϕ} rises to a maximum and then falls off to unity as $\xi_1 \to \xi_2$. The reduced resonant frequency c passes through a minimum near the value of ξ_1 for which g_e^{ϕ} is a maximum. This type of behavior is useful when absolute values of Q are to be measured and compared with computed values, as in the absolute measurement of conductivity of a sample. By choosing cavity parameters ξ_1 and ξ_2 and a mode such that operation is close to both the frequency minimum and the loss ratio maximum, then these last two quantities will not be too sensitive to dimensional discrepancies as might arise in machining or from thermal expansion.

In the second type of behavior, which accompanies the modes of higher frequency, the loss ratio is theoretically infinite when $\xi_1 = 1$. In an actual case this will not be so; one of our basic assumptions regarding the field behavior at a conducting boundary is no longer valid. The loss ratio however may still be very high, of the order of several hundred. As ξ_1 increases, g_e^{ϕ} falls rapidly and reaches unity when $\xi_1 = \xi_2$; there is no intermediate inflection and maximum. Cavity behavior of this type should find application in the accurate determination of relative values of Q, as for instance at different temperatures. The loss ratio can be chosen high enough that the loss in the outer wall may be neglected, as may be seen from (11.14). Compensation for dimensional changes due to thermal expansion will probably be necessary.

The above discussion does not apply to those modes for which $p = 0$. These are modes which have no node of H in the ξ direction and for them the function g_ℓ^p is almost always less than one. A maximum occurs for ξ_1 very close to ξ_2 but it is never much greater than one. This behavior seems to be of little value for the purposes outlined.

8. Another Viewpoint

An alternate way of examining the results provides a desirable connection with antenna theory. Suppose that instead of considering the outer spheroid fixed, we assume the inner spheroid given, and observe the behavior as we adjust the size of the outer cavity. In Figure 15 for the $\ell = 1$, $p = 1$ mode is plotted the loss ratio g_ℓ^p as a function of reduced frequency c , as the outer spheroid is varied and the inner spheroid kept fixed; several inner spheroids are shown. This figure is now to be compared with one given by Slater,(1) which he has adapted from the work of Chu and Stratton,(2) referred to earlier. He gives the input admittance of a center-driven spheroidal antenna as a function of ratio of antenna length to wave length, for various values of the ratio of length of antenna to maximum diameter. His curves show marked resonance peaks when the antenna length is just less than a half wave length. For thinner antennas the peaks are much sharper. The resonant length is considerably smaller than a half wave length for very thick antennas.

---

(1) J. C. Slater, "Microwave Transmission," pp. 219-232, McGraw-Hill, 1942. See especially Figure 58, p. 231.

(2) L. J. Chu and J. A. Stratton, J. App. Phys. 12, 241 (1941).

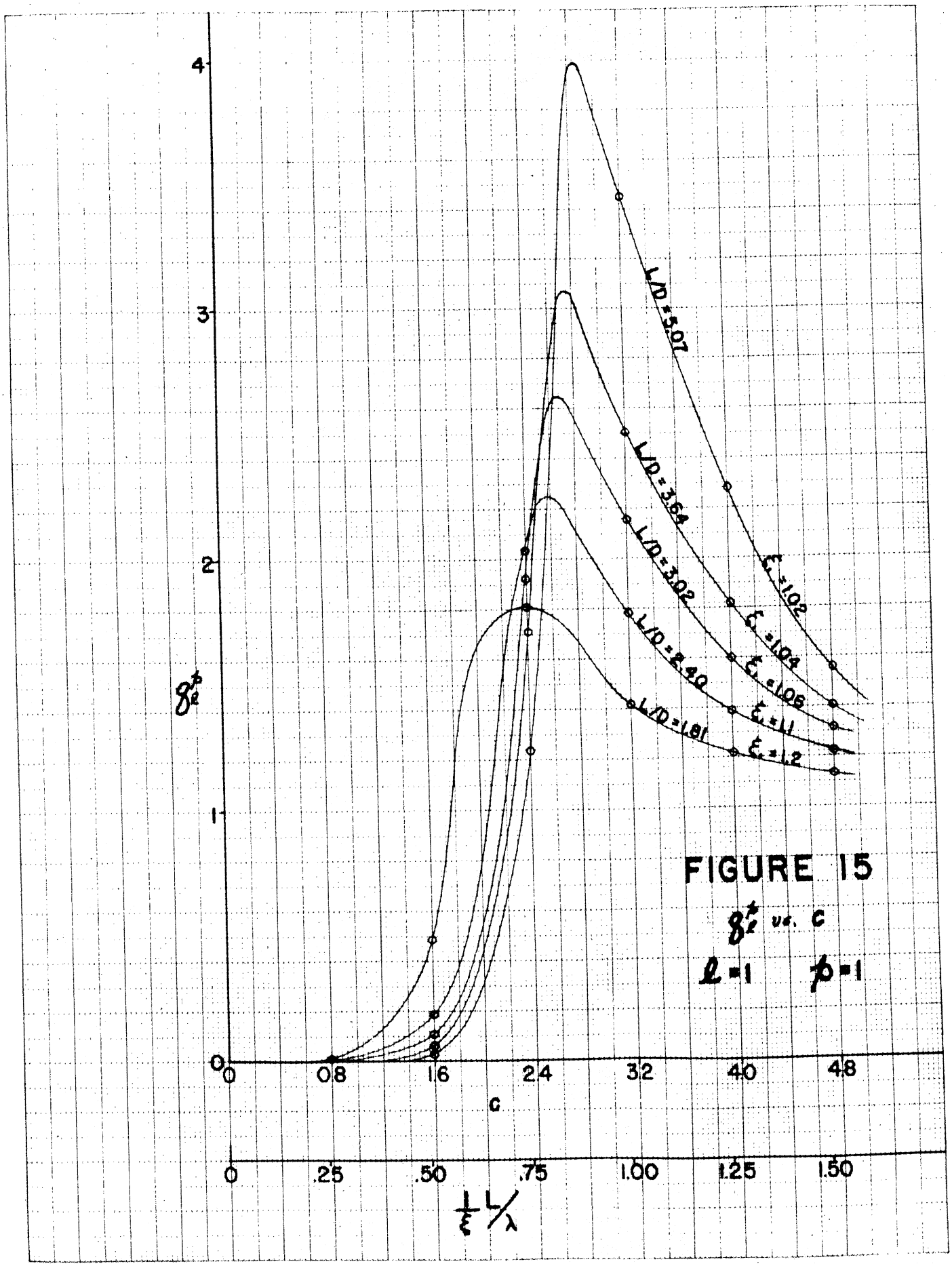

FIGURE 15

g_2^+ vs. c

$\ell = 1$ $p = 1$

In our case the loss ratio q_e' plotted as ordinate is not an input admittance, but there is a considerable analogy between the two. As abscissa we have plotted the parameter $c = \frac{2\pi f}{\lambda}$, so that wavelength is measured in units of the interfocal distance rather than actual length, but for thin spheroids the distinction is negligible. From Figure 15 we see that as $\xi_1 \longrightarrow 1$, which means that the inner spheroid becomes thinner, the peak of the loss ratio becomes higher and sharper, and moves nearer to the point where the antenna length is an integral number of half wave lengths. Peak values may be obtained easily from a curve such as the envelope in Figure 65 in Appendix F.

It is known that a thin antenna has a high Q value, and a thick antenna a relatively small Q value. As we have just found that the loss ratio peaks are higher and sharper for thin antennas than thick ones, this gives support to the hypothesis advanced in Chapter I that a high-Q radiator might be expected to have a very high loss relative to that of the walls when placed inside a cavity, on the theory that there will be high energy storage in the fields close to such a resonator. We see further that in order to get the maximum loss ratio the proper outer cavity must be chosen. It seems likely that the exact shape of the outer cavity is not too important, but that the system could be tuned by a short-circuiting tuning plunger in a wave guide output or a similar device. For thick spheroids curves similar to Figure 15 may be found in Appendix F, Figures 66 to 68.

9. Summary

In order to answer the problem outlined in the introduction, theoretical calculations have been made of the field patterns and frequency behavior of a closed confocal prolate spheroidal cavity system

for axially symmetric modes. It is believed that the data presented on this fundamental problem cover a much more complete range of variation of the parameters than has previously been published by any earlier workers. This has been made possible by the use of the Stratton-Morse-Chu-Hutner series representation of the solutions of the ordinary differential equations resulting from separation of Maxwell's equations. Use of these representations has been greatly facilitated by tables of spherical Bessel functions and associated Legendre functions which have become available quite recently. Near spheroids of high eccentricity use has also been made of the Langer and WKBJ approximations, and of the work of Yost, Wheeler, and Breit.

From these data, the ratio of the losses in the two walls of the cavity has been computed for a similarly wide general range of the parameters. Specific cases have been worked out illustrating the frequency and loss behavior of a given cavity (external spheroid) as the inner spheroid is varied. One finds that two different types of behavior are possible. For a given cavity the discriminant determining the type is a relation between frequency and the parameter ξ_1 characterizing the shape of the inner spheroid. For a specified value of the mode index ℓ it turns out that to each value of ξ_1 corresponds a certain value of reduced frequency c. If the cavity frequency is less than this frequency, the first type of behavior exists, in which there is a maximum in the loss ratio function q_ℓ^p. If on the other hand the cavity frequency exceeds this certain critical frequency then one has the second type of behavior, in which the loss ratio becomes infinite as $\xi_1 \to 1$. The criteria necessary to distinguish between the two types have been given.

The first type, characteristic of the lower modes, has possible application in the measurement of absolute conductivity of a metallic specimen. The second type of behavior, associated with the higher modes, may find use in experiments measuring relative values of Q, as in research on superconductors where conductivity is to be measured at various temperatures.

One can also examine the relation between loss ratio and frequency of a thin inner spheroid as the outer cavity wall is varied. As the inner spheroid becomes thinner the peak of the loss ratio becomes higher and sharper, in much the same fashion as the input admittance of a center-driven spheroidal antenna radiating into space. Thus a connection is made between the behavior of a radiating antenna in space and the same resonant structure completely enclosed in a cavity.

10. Recommendations for Further Work

The computations presented in this investigation cover a wide general range of variation of the parameters. Since for each point in the frequency scale a disproportionate amount of labor is involved in computation, the intervals are much coarser than is desirable. Treating this work as a survey one can now choose new arguments for computation which are more likely to yield a higher return of information for the labor invested. The region of greatest interest is that for which the frequency c is near the critical value $(\ell+1)\,\pi/2$, for values of ξ_1 close to unity. More work is indicated in this direction at finer intervals of c. Attention should also be given to the more fundamental problem of finding numerical solutions to the differential equation for

$\chi(\xi)$ when ξ is very close to one; neither the Langer nor WKBJ approximations are satisfactory in this area and the data of Yost, Wheeler, and Breit are useful only when c is less than $(\ell+1)\pi/2$. Effort should be directed finally of course toward more accurate determination of the loss function g_ℓ^c for small values of $(\xi_1 - 1)$, and values of c near the critical. Experimental investigation and confirmation is, of course, extremely desirable.

The viewpoint of Section 8 of this chapter is of considerable interest, offering as it does a connection between antenna theory and resonant cavity theory. There are numerous possibilities here for both theoretical and experimental investigation. The experimental attack seems most promising since the separability of the wave equation is not a restriction on possible geometries. Using the groundwork laid by this thesis however, further computation of the spheroidal case along the lines proposed just above should be relatively easy, although the tedium of computation can hardly be further reduced. A paper treating the connection of spheroidal cavity behavior to antenna theory is planned.

Hansen[1] has mentioned that of all shapes of hollow cavities operating in the lowest mode, a long prolate spheroid is most likely to have the highest Q. His arguments have been based on results for more simple geometries and a logical extrapolation thereof based on known behavior of the fields in consequence of a boundary deformation, but he made no exact calculations. The numerical results obtained here should be readily applicable to the obtaining of a more exact answer to Hansen's proposal (at least so far as prolate spheroids are concerned) and the author hopes to develop this possibility at a later date.

---

(1) W. W. Hansen, J. App. Phys. 9, 654 (1938).

APPENDIX A

COORDINATE SYSTEM DETAILS

1. Definition of a Prolate Spheroidal Coordinate System

A right-handed orthogonal system of prolate spheroidal coordinates μ, ψ, φ is defined [1] in terms of the cartesian system x, y, z, by

$$\begin{aligned} x &= f \sinh\mu \sin\psi \cos\varphi \\ y &= f \sinh\mu \sin\psi \sin\varphi \\ z &= f \cosh\mu \cos\psi \end{aligned} \tag{A.1}$$

where $0 \leq \mu \leq \infty, \quad 0 \leq \psi \leq \pi, \quad 0 \leq \varphi \leq 2\pi.$

The family of confocal spheroids can be generated by revolving around the z-axis the family of confocal ellipses whose foci are located on the z-axis at $\pm f$. Orthogonal to the spheroidal surfaces is the family of confocal hyperboloids (of two sheets) of revolution generated similarly by the hyperbolas confocal with the ellipses. The family of spheroids (μ = const.) is given by

$$\frac{z^2}{f^2\cosh^2\mu} + \frac{x^2+y^2}{f^2\sinh^2\mu} = 1 \tag{A.2}$$

while the family of hyperboloids (ψ = const.) is given by

$$\frac{z^2}{f^2\cos^2\psi} - \frac{x^2+y^2}{f^2\sin^2\psi} = 1 \tag{A.3}$$

---

(1) See, for example, H. Margenau and G. M. Murphy, "The Mathematics of Physics and Chemistry", p. 175, D. Van Nostrand, 1943.

It is convenient to introduce the transformations

$$\begin{aligned} \xi &= \cosh \mu \\ \eta &= \cos \psi \\ \varphi &= \varphi \end{aligned} \tag{A.4}$$

The relations given by (A.1) then become [1]

$$\begin{aligned} x &= f\sqrt{1-\eta^2}\,\sqrt{\xi^2-1}\,\cos\varphi \\ y &= f\sqrt{1-\eta^2}\,\sqrt{\xi^2-1}\,\sin\varphi \\ z &= f\eta\xi \end{aligned} \tag{A.5}$$

where $1 \leqslant \xi \leqslant \infty$, $1 \geqslant \eta \geqslant -1$, $0 \leqslant \varphi \leqslant 2\pi$. Figure 16 describes the system graphically. It is important to point out here that as ψ increases from 0 to π, $\cos\psi$, and consequently η, decreases from 1 to -1. Thus $d\eta$ goes as $-d\psi$, or in other words the unit vectors ι_ψ and ι_η are colinear but antiparallel. This means that for a right-handed system we must take either of the triplets (μ, ψ, φ) or (η, ξ, φ) but not (ξ, η, φ). The importance of this distinction appears in vector differentiation. In physical problems much of the significance is lost, since on successive differentiation one finds that the resulting wave equation is the same regardless of whether (η, ξ, φ) or (ξ, η, φ) is used.

2. Relation to Other Systems

The relation to the cylindrical system ρ, φ, z is

$$\begin{aligned} \rho &= f\sqrt{1-\eta^2}\,\sqrt{\xi^2-1} \\ \varphi &= \varphi \\ z &= f\eta\xi \end{aligned} \tag{A.6}$$

---

(1) See L. J. Chu and J. A. Stratton, "Forced Oscillations of a Prolate Spheroid", J. App. Phys. 12, 242 (1941).

and to the spherical system r, ϑ, φ,

$$\begin{aligned} r &= f\sqrt{\eta^2+\xi^2-1} \\ \cos\vartheta &= \frac{\eta\xi}{\sqrt{\eta^2+\xi^2-1}} \\ \varphi &= \varphi \end{aligned} \tag{A.7}$$

As $\xi \longrightarrow \infty$, the spheroid goes over to a sphere such that

$$r \longrightarrow f\xi, \quad \cos\vartheta \longrightarrow \eta \tag{A.8}$$

Therefore ξ is often called the radial, and η the angular variable. If i_η, i_ξ and i_φ are unit vectors in the direction of η, ξ, φ respectively, then

$$\nabla\eta = i_\eta/h_\eta, \quad \nabla\xi = i_\xi/h_\xi, \quad \nabla\varphi = i_\varphi/h_\varphi \tag{A.9}$$

and the metrical coefficients are

$$\begin{aligned} h_\eta &= f\left(\frac{\xi^2-\eta^2}{1-\eta^2}\right)^{\frac{1}{2}} \\ h_\xi &= f\left(\frac{\xi^2-\eta^2}{\xi^2-1}\right)^{\frac{1}{2}} \\ h_\varphi &= f\left[(\xi^2-1)(1-\eta^2)\right]^{\frac{1}{2}} \end{aligned} \tag{A.10}$$

The differential volume element has the form

$$\begin{aligned} d\upsilon &= h_\eta h_\xi h_\varphi \, d\eta \, d\xi \, d\varphi \\ &= f^3(\xi^2-\eta^2)\, d\eta \, d\xi \, d\varphi \end{aligned} \tag{A.11}$$

Similarly the element of surface area on a spheroidal surface (ξ = const.) is

$$\begin{aligned} da &= h_\eta h_\varphi \, d\eta \, d\varphi \\ &= f^2\sqrt{(\xi^2-\eta^2)(\xi^2-1)}\, d\eta \, d\varphi \end{aligned} \tag{A.12}$$

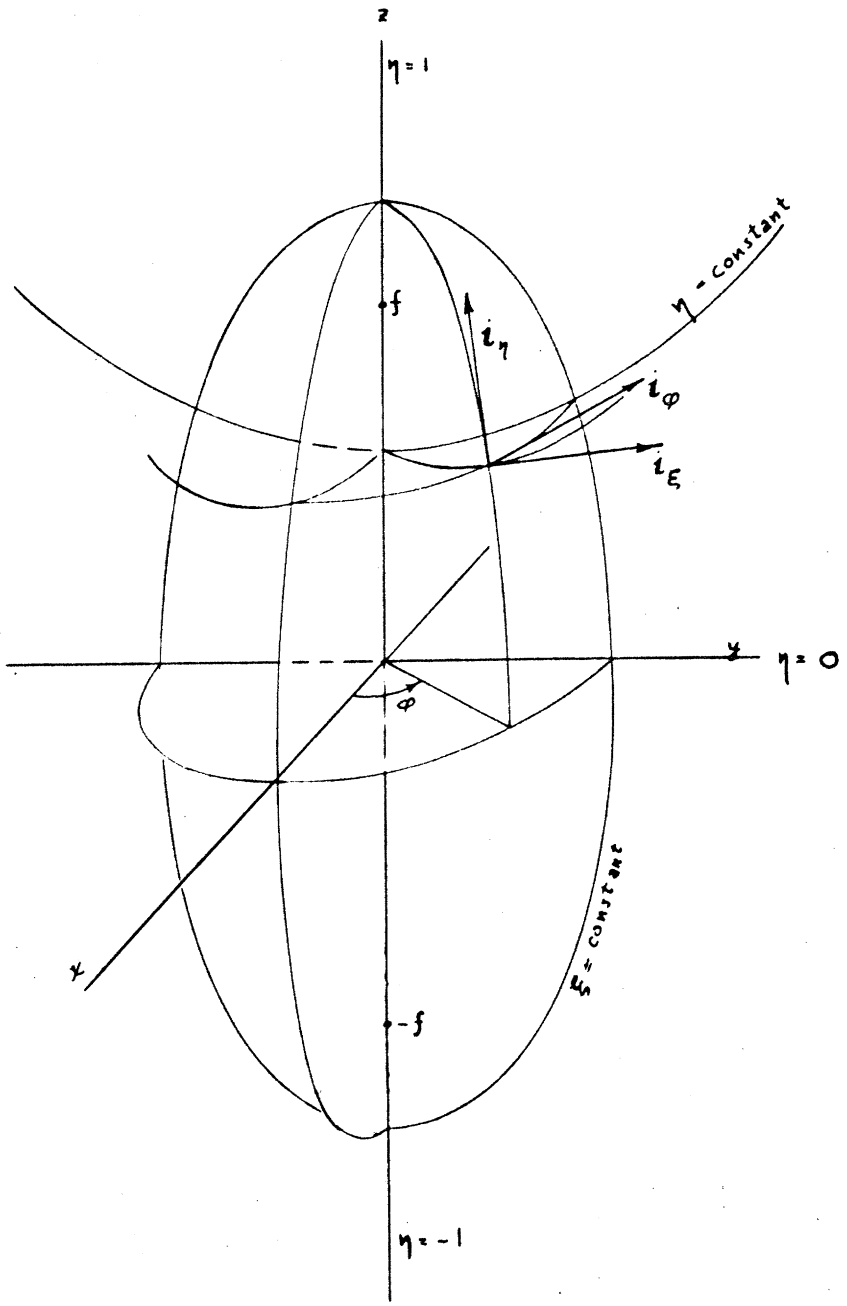

FIGURE 16

PROLATE SPHEROIDAL COORDINATE SYSTEM

APPENDIX B

THE SPHERICAL CASE

1. Field Relations and Boundary Conditions

Within the cavity contained between two concentric conducting spheres, Maxwell's equations[1] reduce to

$$E_r = -n(n+1)\,P_n(\cos\vartheta)\,\frac{z_n(kr)}{kr}\,e^{-j\omega t}$$

$$E_\vartheta = -\frac{\partial}{\partial\vartheta}P_n(\cos\vartheta)\,\frac{1}{kr}\left[kr\,z_n(kr)\right]'e^{-j\omega t} \qquad (B.1)$$

$$H_\varphi = \frac{k}{j\omega\mu}\,\frac{\partial}{\partial\vartheta}P_n(\cos\vartheta)\,z_n(kr)$$

$$E_\varphi = H_r = H_\vartheta = 0$$

for TM waves symmetrical about the polar axis. Here spherical coordinates have been employed and the prime denotes differentiation with respect to the argument kr. The function $z_n(kr)$ is a linear combination of the spherical Bessel functions $j_n(kr)$ and $n_n(kr)$ necessary to satisfy the boundary condition that E_ϑ vanish at the walls, r_1 and r_2 ($r_1 < r_2$). For convenience let $x = kr$, and define

$$z_n(x) \triangleq a\,j_n(x) + b\,n_n(x) \qquad (B.2)$$

Since we must have

$$\left[x_1\,z_n(x_1)\right]' = \left[x_2\,z_n(x_2)\right]' = 0 \qquad (B.3)$$

---

(1) See J. A. Stratton, "Electromagnetic Theory," p. 557, McGraw-Hill, 1941.

we can write

$$\frac{b}{a} = -\frac{[x_1 j_n(x_1)]'}{[x_1 n_n(x_1)]'} = -\frac{[x_2 j_n(x_2)]'}{[x_2 n_n(x_2)]'} \tag{B.4}$$

If we define

$$\gamma_n'(x) \triangleq -\frac{[x j_n(x)]'}{[x n_n(x)]'} \tag{B.5}$$

then the boundary condition becomes

$$\gamma_n'(x_1) = \gamma_n'(x_2) \tag{B.6}$$

Letting

$$\beta_n(x) \triangleq \arctan \gamma_n'(x) \tag{B.7}$$

we can define

$$a_n(x) \triangleq \cos\beta_n(x), \qquad b_n(x) \triangleq \sin\beta_n(x) \tag{B.8}$$

which implies normalization of (B.2) such that

$$[a_n(x)]^2 + [b_n(x)]^2 = 1. \tag{B.9}$$

The function defined by

$$y_n(x) \triangleq x\, z_n(x) \tag{B.10}$$

is analogous to the function $X(\xi)$ employed at great length in the spheroidal treatment. It satisfies the differential equation

$$x^2 y_n''(x) + [x^2 - n(n+1)]\, y_n(x) = 0 \tag{B.11}$$

which corresponds to Eq. (5.3). The boundary condition (B.3) becomes

$$\left.\frac{d y_n(x)}{dx}\right|_{x=x_1} = \left.\frac{d y_n(x)}{dx}\right|_{x=x_2} = 0 \qquad \text{(B.12)}$$

Following the qualitative arguments of Chapter V, one can show that $y_n(x_1)$ will be a maximum when $x = \sqrt{n(n+1)}$, that is, at the inflection point of (B.11). A distinction from the spheroidal case is that here there is always an inflection of $y_n(x)$ within the range of x considered, regardless of frequency.

Upon differentiating expression (B.5) and making use of (B.11), one finds that when $x = \sqrt{n(n+1)}$ there is a minimum of $\gamma_n^m(x)$, and therefore of $\beta_n(x)$.

2. Losses due to Finite Wall Conductivity

The loss in a single wall is given by

$$W_{1_n}(r_1) = \frac{\omega \mu_1 \delta_1}{4} \oint_{S_1} |H_t|^2 \, da$$

$$= \frac{2\pi \omega \mu_1 \delta_1}{4} \int_0^\pi |H_\varphi|^2 r_1^2 \sin\vartheta \, d\vartheta$$

$$= \frac{2\pi \omega \mu_1 \delta_1}{4} \frac{k^2}{\omega^2 \mu_0^2} \left[r_1 Z_n(kr_1)\right]^2 \int_0^\pi \left[P_n^1(\cos\vartheta)\right]^2 \sin\vartheta \, d\vartheta$$

$$= \frac{2\pi \omega \mu_1 \delta_1}{4} \frac{1}{\omega^2 \mu_0^2} \left[kr_1 Z_n(kr_1)\right]^2 \frac{2n(n+1)}{(2n+1)}$$

$$= \pi \delta_1 \frac{\mu_1}{\mu_0} \frac{n(n+1)}{(2n+1)} \frac{1}{\omega \mu_0} \left[x_1 Z_n(x_1)\right]^2 \qquad \text{(B.13)}$$

where in the last line we have let $\chi_1 = kr_1$. For a given mode the ratio of the losses in the two walls will be

$$\frac{W_1(r_1)}{W_2(r_2)} = \frac{\delta_1 \mu_1}{\delta_2 \mu_2} \frac{[\chi_1 Z_n(\chi_1)]^2}{[\chi_2 Z_n(\chi_2)]^2}$$

$$= \frac{\delta_1 \mu_1}{\delta_2 \mu_2} g_n^p(\chi_1) \qquad (B.14)$$

where we have defined

$$g_n^p(\chi_1) \triangleq \frac{[\chi_1 Z_n(\chi_1)]^2}{[\chi_2 Z_n(\chi_2)]^2} \qquad (B.15)$$

in consistency with the spheroidal case.

3. Numerical Computations

For $n = 1, 2$ and for representative values of $\chi = kr$ the numerical values of $2[\chi j_n(\chi)]'$, $2[\chi n_n(\chi)]'$, γ_n' , β_n , $Z_n(\chi_1)$, and $\chi_1 Z_n(\chi_1)$ have been computed. The results are tabulated in Tables 1 and 2. In Figures 17 and 18, $\beta_n(\chi)$ vs χ has been plotted and corresponding values of χ_2 have been read off. The function $\chi_1 Z_n(\chi_1)$ is plotted in Figure 19 from which corresponding values for χ_2 have been read off. From these the value of g_n^p has been computed; Figures 20 to 26 show the results graphically.

4. Discussion of the Results

For axially symmetric modes, a concentric spherical cavity system is defined uniquely by three parameters. These are the mode indices n and p, and any one of the three parameters kr_1, kr_2 or r_1/r_2. The spheroidal case, in contrast, requires four parameters and thus introduces one more degree of freedom or complexity. The mode for $n = 1$ corresponds generally to the axial spheroidal mode identified by $l = 0$; likewise the mode $n = 2$ corresponds to $l = 1$. The p indices describing the radial modes are the same for both spherical and spheroidal cases. Since this appendix constitutes a minor portion of the work, the accuracy of the graphs is not as high as for the spheroidal functions, being included mainly for comparison with the results obtained in the spheroidal case.

As predicted, the graphs of $\beta_n(\chi)$ given in Figures 17 and 18 exhibit minima when $\chi = \sqrt{n(n+1)}$; the minima in Figures 20 and 21 follow directly from these. Likewise Figure 19 shows maxima for $\chi_1 z_n(\chi_1)$ or $y_n(\chi_1)$ at $\chi_1 = \sqrt{n(n+1)}$.

Figures 22 and 23 may be compared to Figure 15. They show the relation between loss ratio and reduced frequency χ_1 as the inner sphere is held fixed and the radius of the outer sphere varied. It is to be noted that for all p modes higher than zero order, the resonance peaks are quite broad and flat in contrast to the sharp peaks for long, thin spheroids; the maxima occur precisely at $\chi_1 = \sqrt{n(n+1)}$. There is no maximum for the $p = 0$ mode.

Other methods of presenting the data are used in Figures 24 to 26 which employ r_1/r_2 as argument. The frequency behavior shown by Figure 25 may be compared with Figures 10, 11, and 12 in Chapter XI.

The curves for $p=0$ are similar to those in the spheroidal case, and for the higher modes the minima again occur at values corresponding to $kr_1 = \sqrt{n(n+1)}$. This follows from the minima of β_n but it can also be shown directly that $\oint_{r_1} [H^2 - (E/Z_0)^2]\, da$ vanishes when kr_1 has the values $\sqrt{n(n+1)}$ or zero, so that the perturbation formula (11.9) yields zero for the slope of the frequency curve at these points. The loss ratio curves plotted in Figure 26 are analogous to those in Figures 13 and 14. A comment is in order on the special behavior of the mode for which $p=0$. The plots of ν_2 <u>versus</u> ν_1 in Figures 20 and 21 show a discontinuity in slope at $\nu_1 = \sqrt{n(n+1)}$. For dimensionless frequencies ν_1 of this value and above, the inner and outer spheres coincide (spacing reduces to zero), so that the mode becomes degenerate. The corresponding phenomenon will be noticed in the spheroidal cases to be discussed in Appendix C.

Typical field patterns are shown in Figure 27, which confirm qualitatively the numerical data. One sees that if the reduced frequency kr_1 is less than $\sqrt{n(n+1)}$, the magnetic field stands off from the inner sphere, so that its loss relative to that in the outer wall will be quite small. If the frequency is above the critical value, then a region of strong magnetic field moves in adjacent to the inner sphere and the losses in the two walls will be roughly the same. In the figure, solid lines denote the electric field, which for TM waves lies in meridional planes. The magnetic field lines are circles concentric with the axis of rotation, and show as dots in the figure.

TABLE I

x	$z[x, j_1(x)]'$	$z[x, n_1(x)]'$	δ'	β	$z_1(x)$	$x\, z_1(x)$	x
0	0	∞	0-	0-	0	0	0
0.1	.133061	199.007	-.(3)166855	-.(3)166855	.100499	.0100499	0.1
0.2	.264538	49.0299	-.(2)539544	-.(2)539539	.203948	.0407896	0.2
0.4	.516412	11.6182	-.0444485	-.0444193	.429934	.171974	0.4
0.6	.743501	4.81667	-.154360	-.153151	.683940	.410364	0.6
0.8	.934741	2.57719	-.362698	-.347942	.911921	.729537	0.8
1.0	1.080605	1.68295	-.642090	-.570794	.999996	.999996	1.0
1.2	1.173509	1.33196	-.881039	-.722240	.938878	1.12665	1.2
1.4	1.208149	124129	-.973301	-.771869	.824729	1.15462	1.4
1.6	1.181731	1.28506	-.919592	-.743535	.715999	1.14560	1.6
2.0	.947800	1.53352	-.618055	-.555590	.554700	1.10940	2.0
2.4	.501896	1.78163	-.281706	-.274597	.450212	1.08051	2.4
3.0	-.409114	1.85407	.220657	.217177	.351123	1.05337	3.0
4.0	-1.743829	.847181	2.06075	1.11901	.257662	1.03065	4.0
5.0	-1.727669	.928199	-1.86131	-1.07779	.203954	1.01977	5.0
10.	-1.244976	1.55256	.801886	.670890	.100499	1.00499	10.
20.	1.862134	-.722830	2.57617	1.200527	.0500625	1.00125	20.

$\sqrt{n(n+1)} = 1.414$ $\qquad n = 1$

143

TABLE 2

$2[x J_2(x)]'$	$2[x N_2(x)]'$	δ''	β	$z_2(x)$	$x z_2(x)$	x
0	∞	0-	0-	0	0	0
.0159239	1499.90	-.(4)106166	-.(4)106166	.0066709	.0013334	0.2
.0627884	187.311	-.(3)335209	-.(3)335209	.0266936	.0106774	0.4
.236975	23.1195	-.0102500	-.0102496	.108128	.0865024	0.8
.482635	6.60750	-.0730435	-.0729140	.251569	.301883	1.2
.741489	2.71031	-.273581	-.267046	.444854	.711766	1.6
.947800	1.53352	-.618055	-.553590	.554700	1.10940	2.0
1.040868	1.25967	-.826302	-.690574	.509974	1.22394	2.4
.976978	1.34674	-.725439	-.627596	.429311	1.20207	2.8
.738639	1.55456	-.475143	-.443565	.363137	1.16204	3.2
.176248	1.803909	.0977034	.0973943	.275862	1.10345	4.0
1.266541	1.373616	.922048	.744864	.223006	1.07043	4.8
1.86418	-.441136	-4.22586	-1.338432	.174004	1.04402	6.0
.982550	-1.687494	.582254	.527269	.128027	1.02422	8.0
1.257569	1.516133	-.829458	-.692447	.101533	1.01533	10
-.531407	-1.920316	-.276729	-.269973	.050185	1.00377	20

$\sqrt{n(n+1)} = 2.450$ $\quad n = 2$

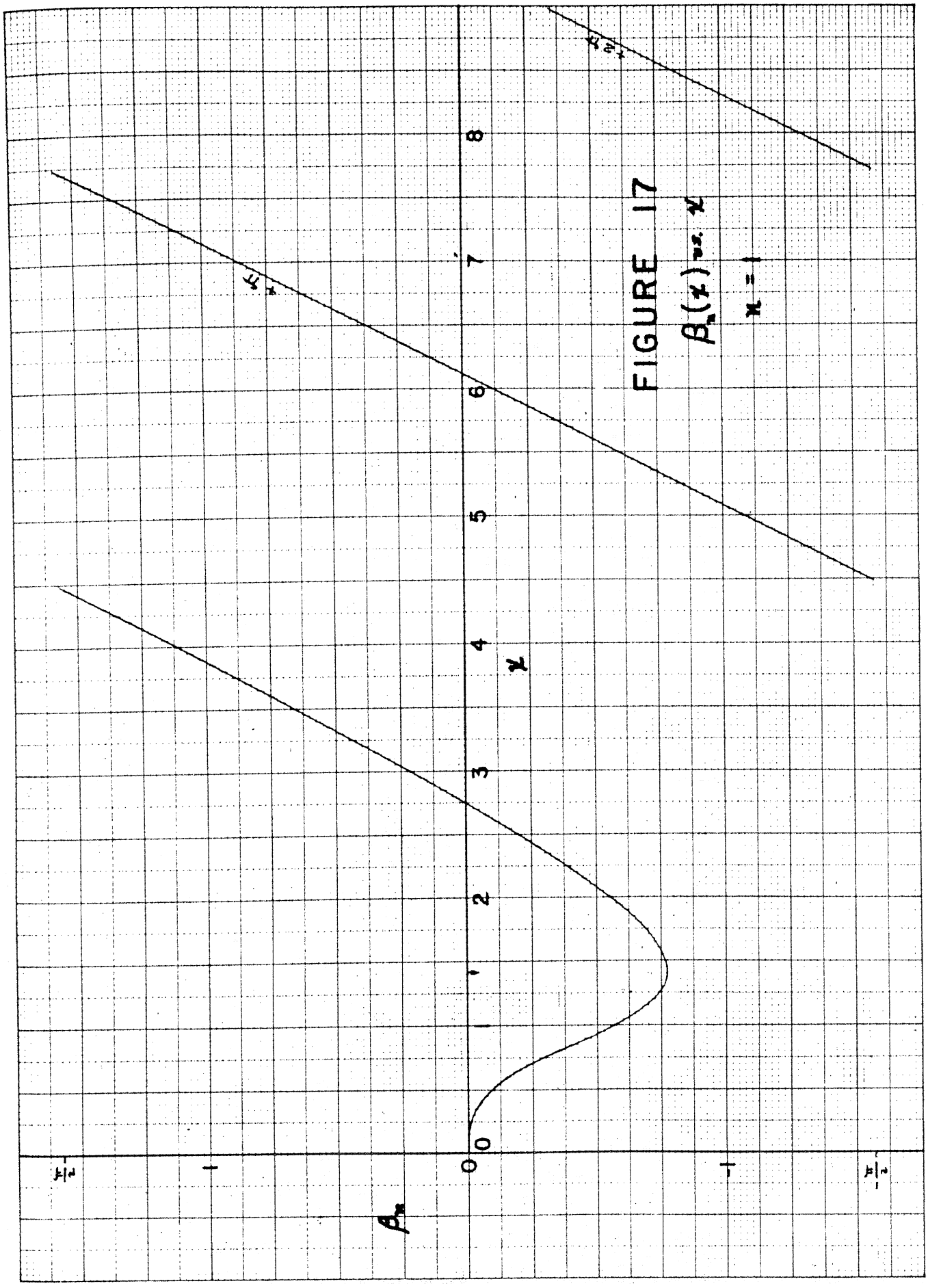

FIGURE 17

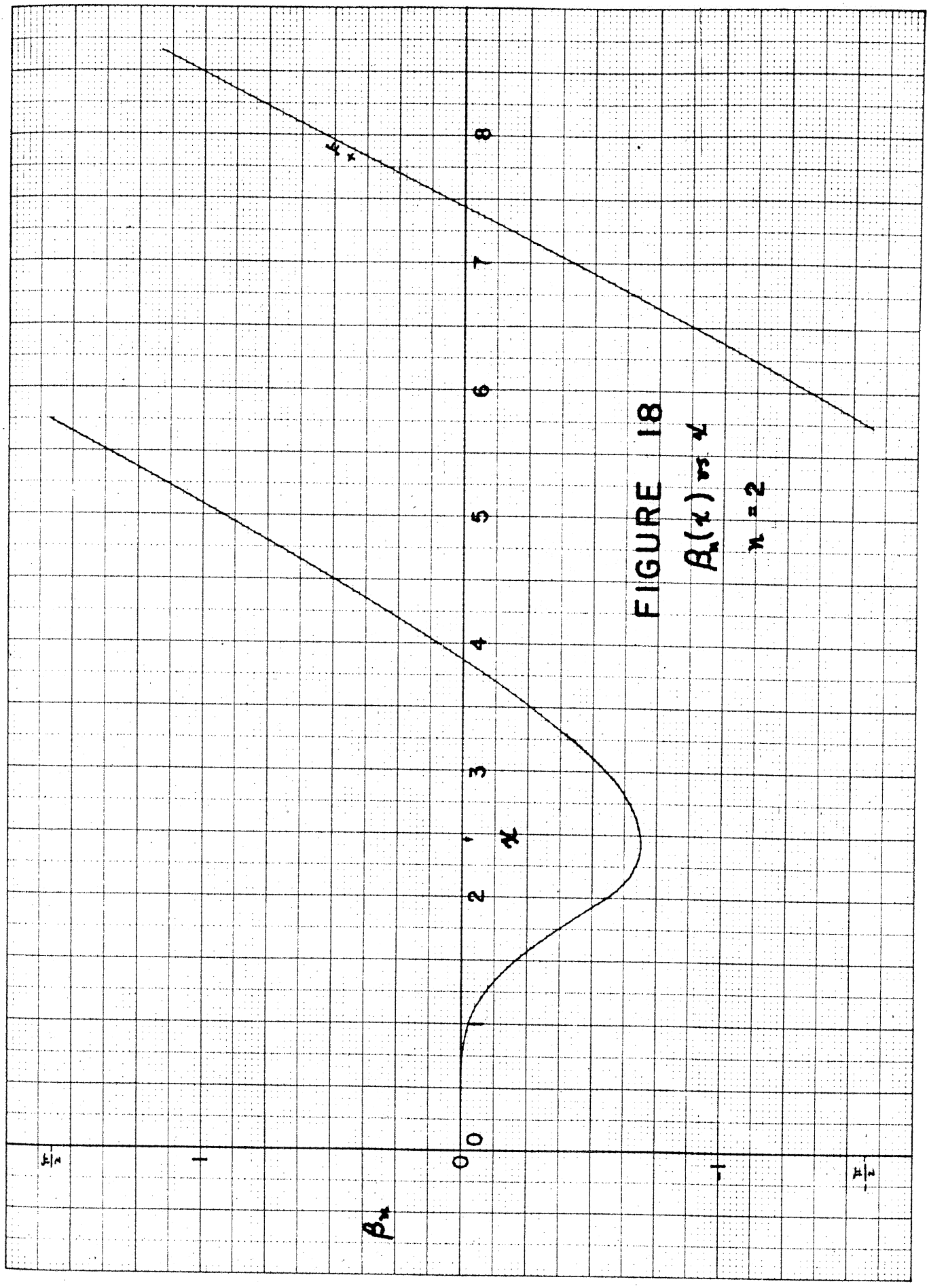

FIGURE 18
$\beta_x(x)$ vs x
$n = 2$

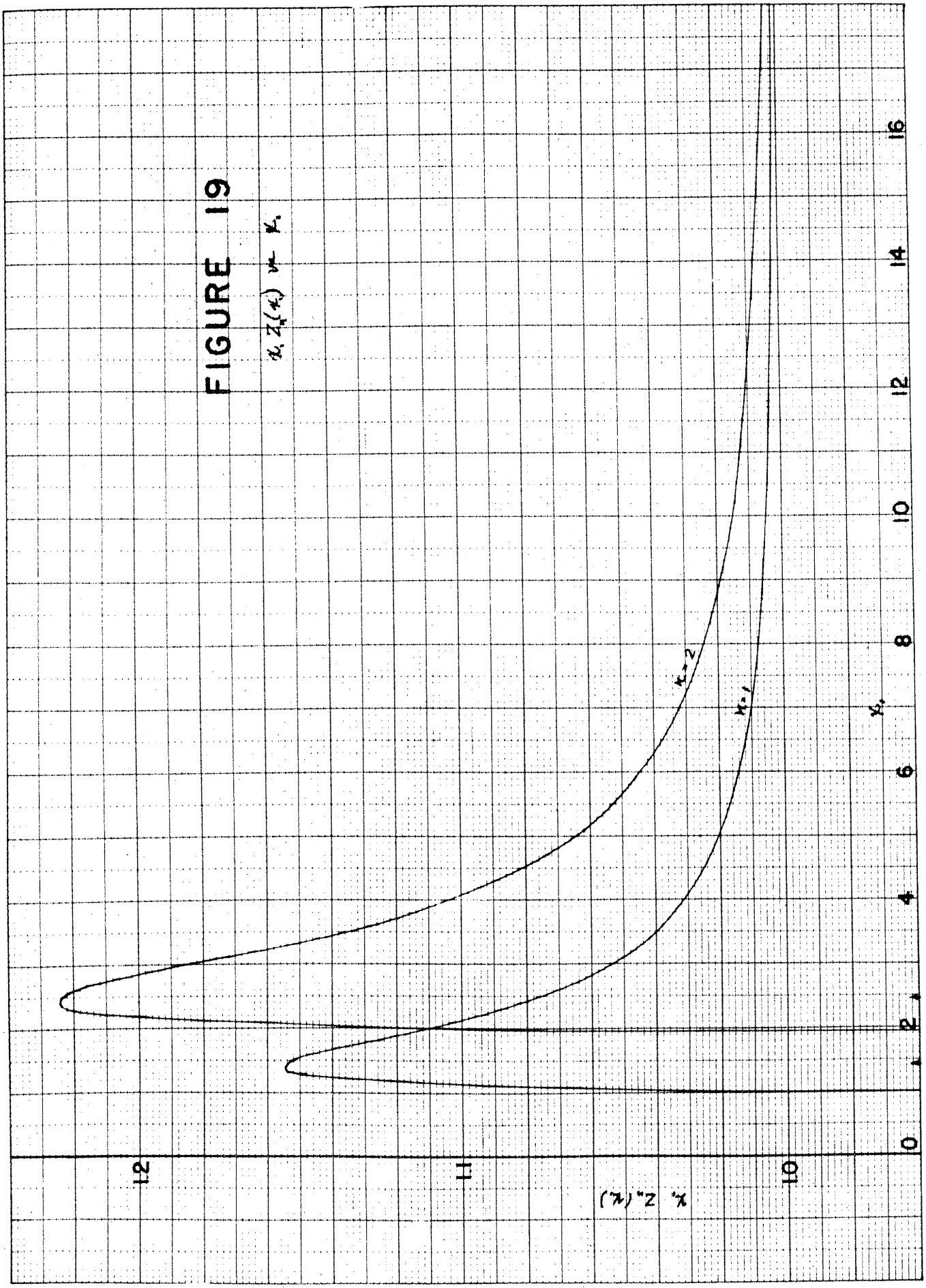

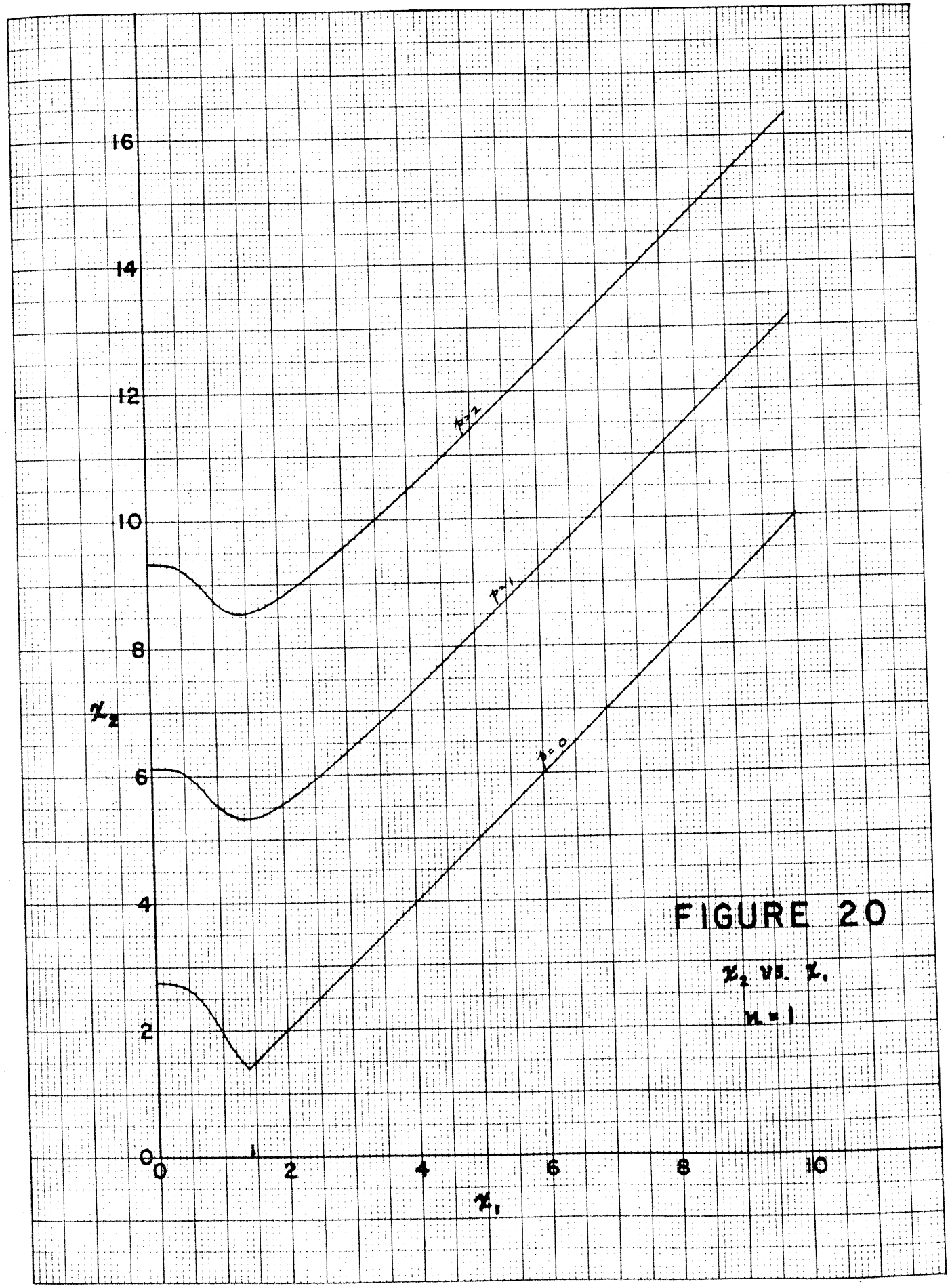

FIGURE 20

χ_2 vs. χ_1

$\kappa_1 = 1$

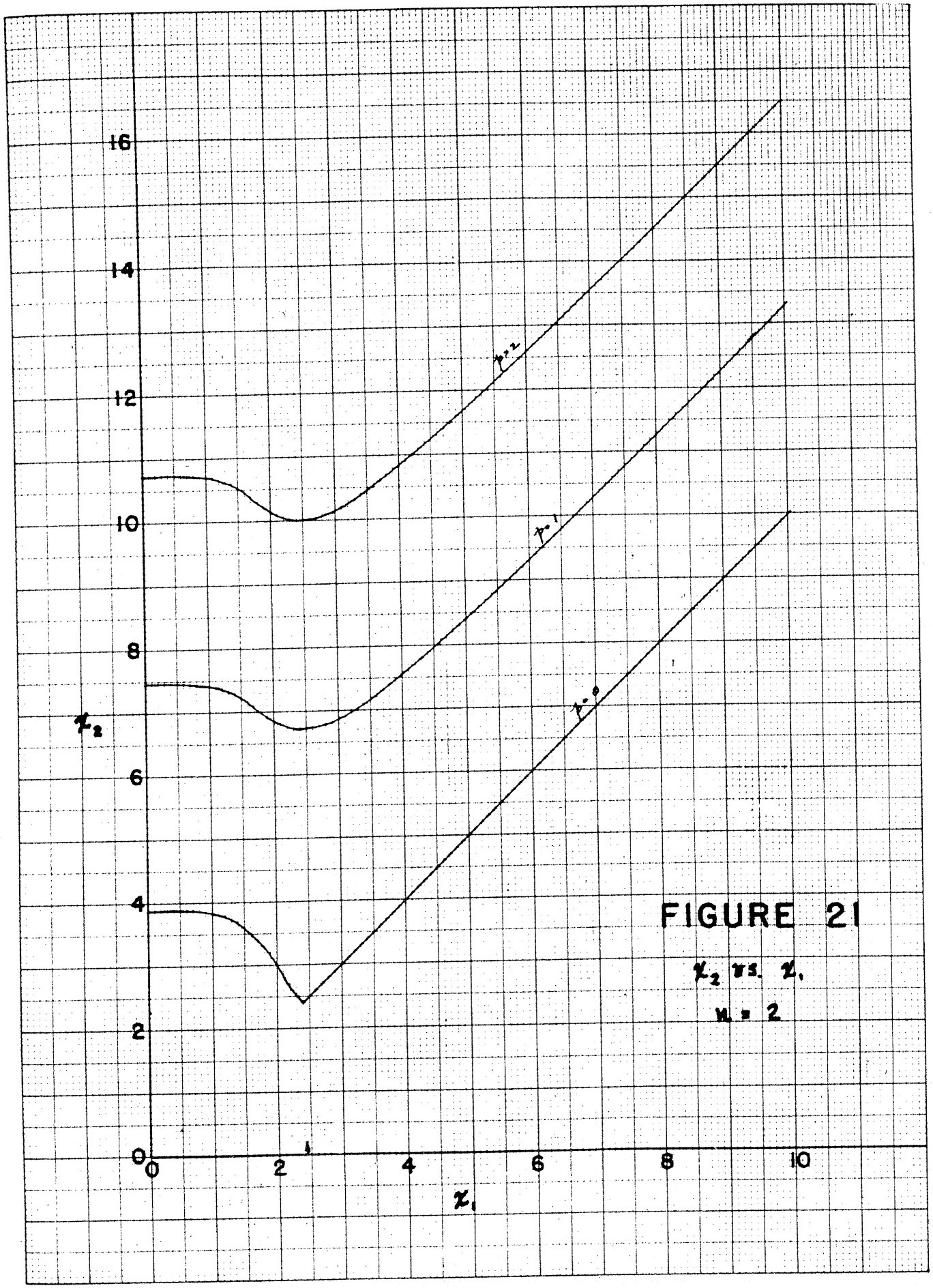

FIGURE 21

χ_2 vs. χ_1

$n = 2$

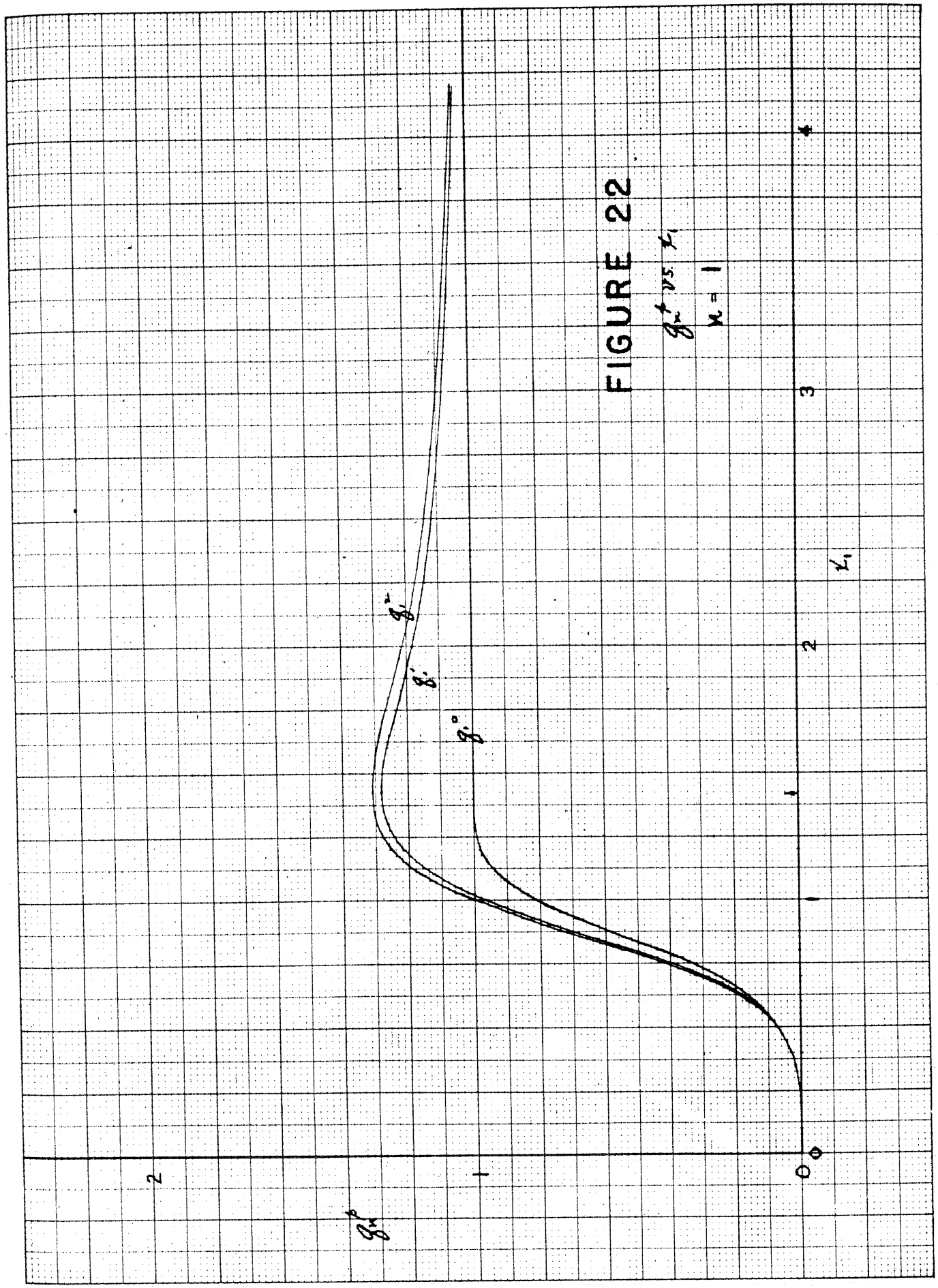
FIGURE 22
g^{ϕ} vs. χ_1
$\kappa = 1$
g^{ϕ}
χ_1
0
1
2
3
4
g^{2}
g^{1}
g^{0}

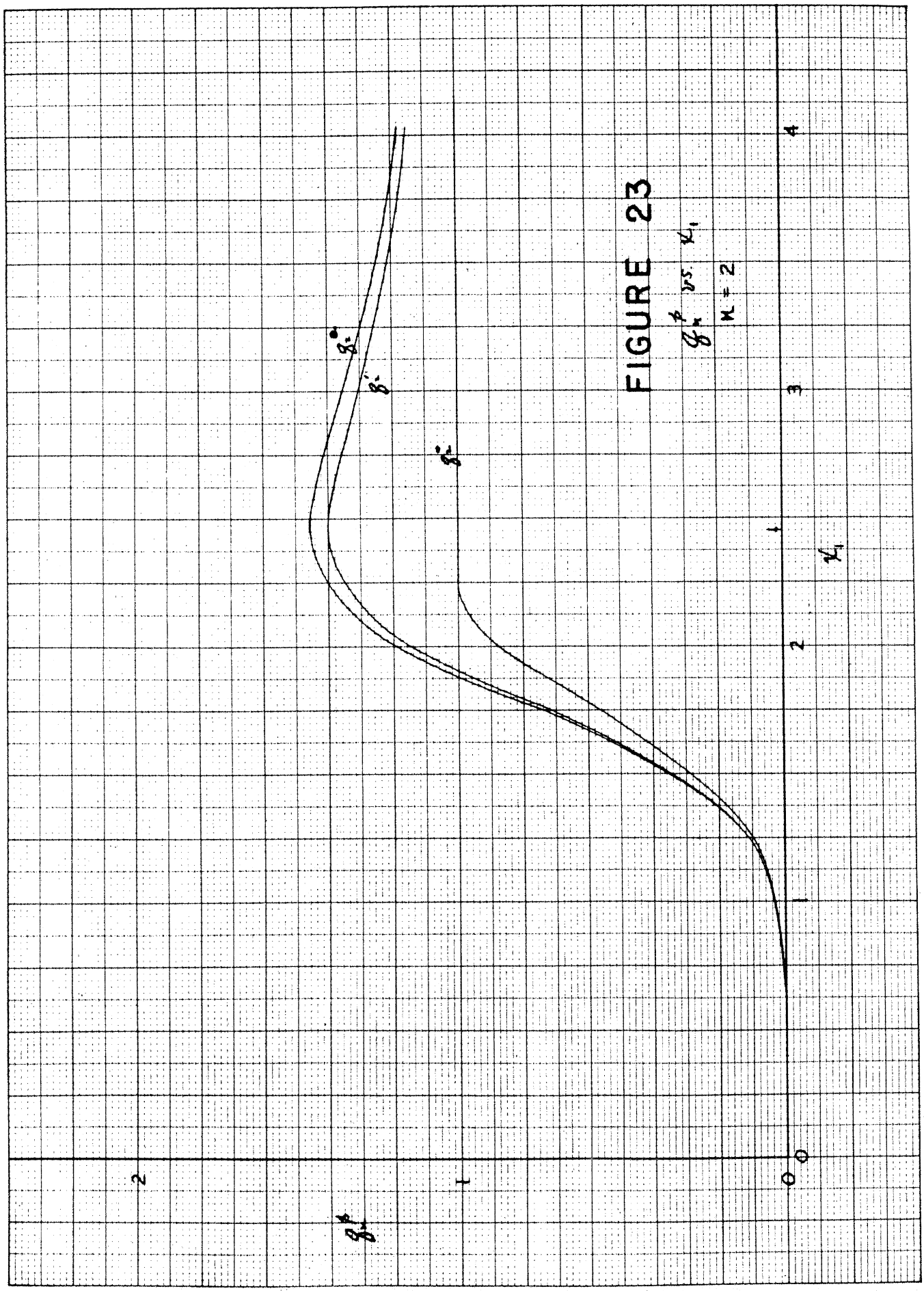

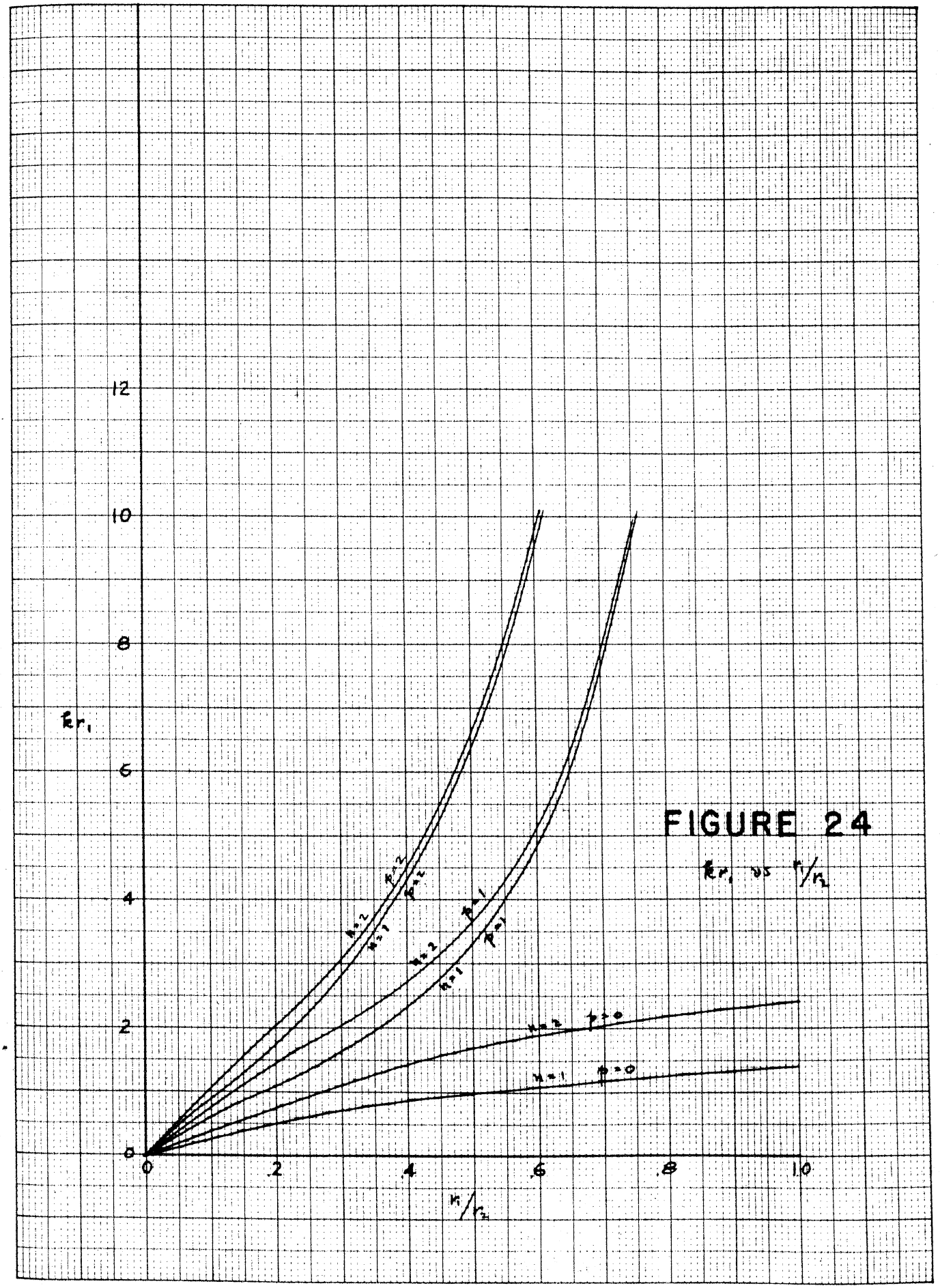

FIGURE 24

kr_1 vs r_1/r_2

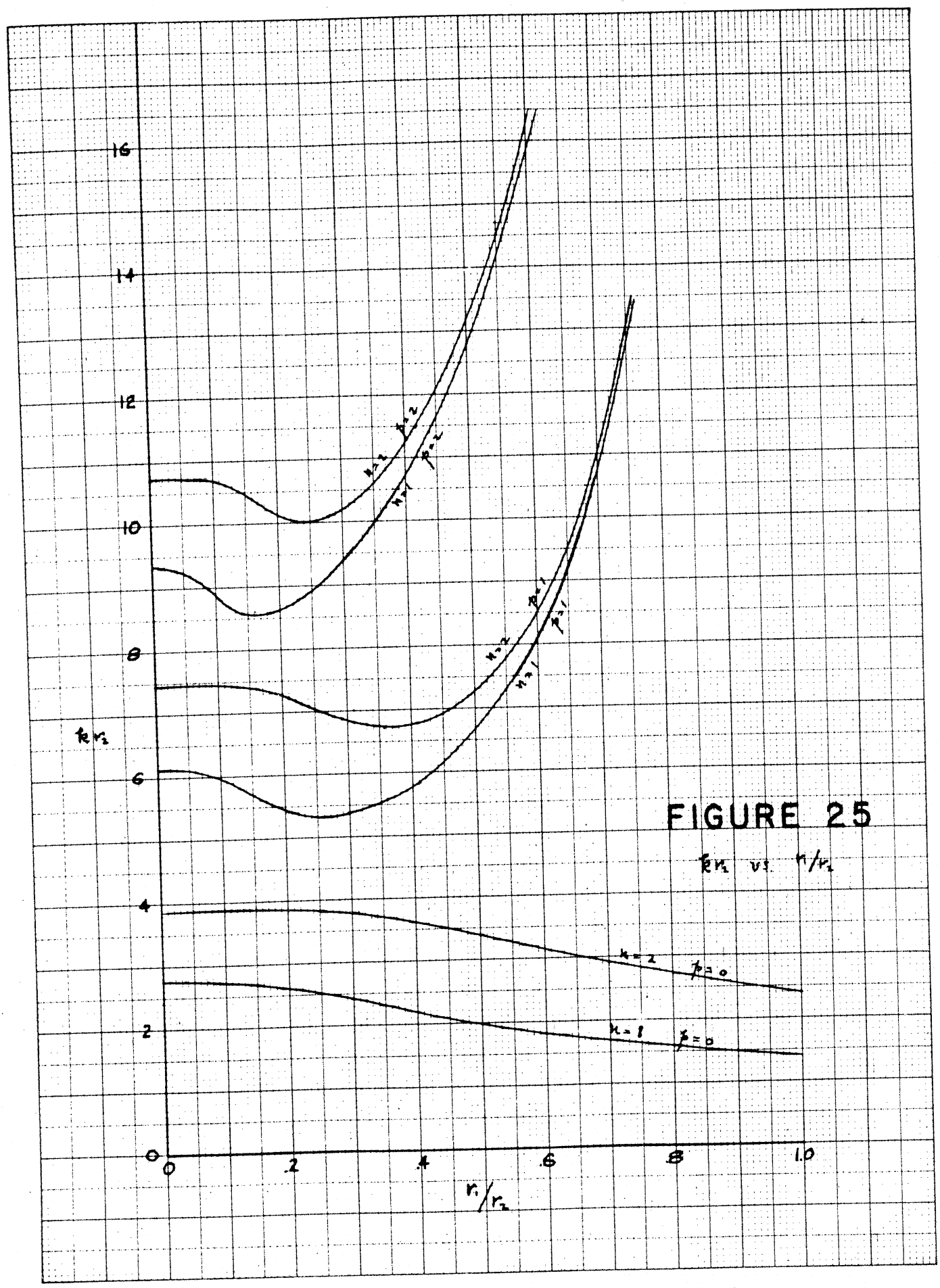

FIGURE 25

kr_2 vs. r_1/r_2

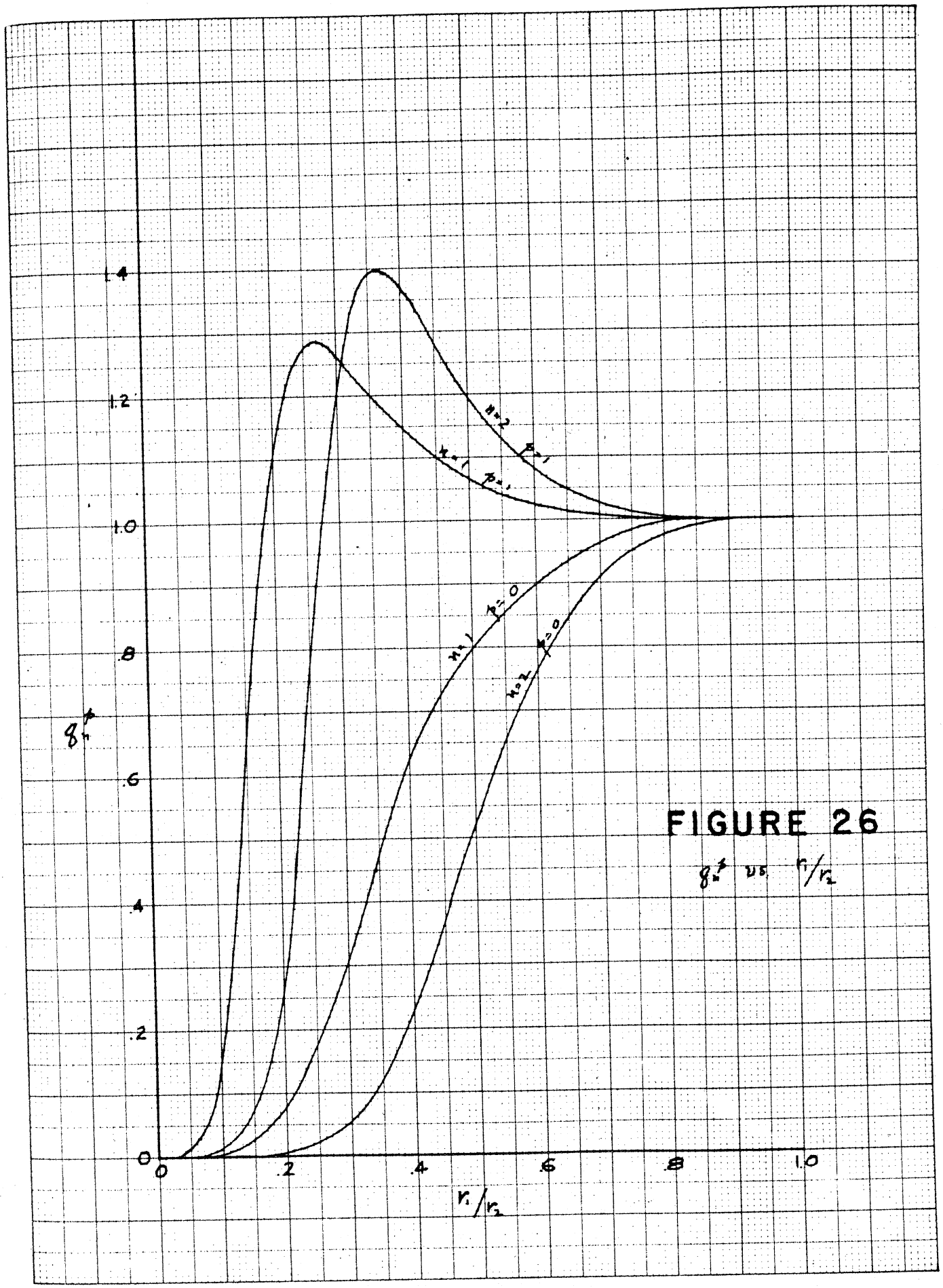

FIGURE 26

q_1^* vs r_1/r_2

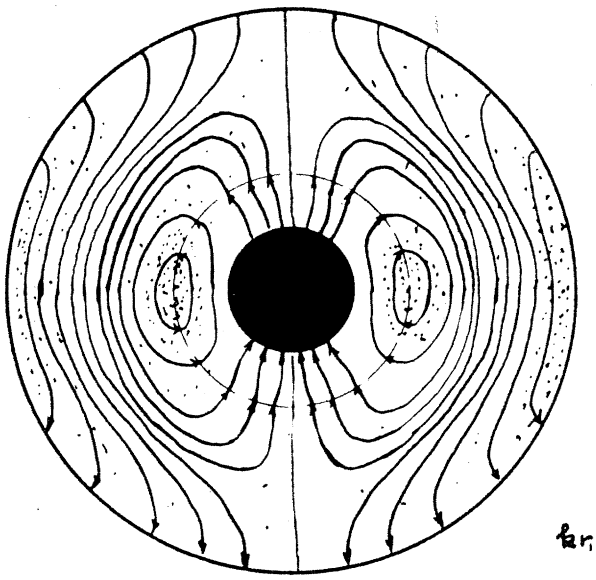

$p = 1$

$kr_1 < 1.4 = \sqrt{n(n+1)}$

$n = 1$

$kr_1 > 1.4$

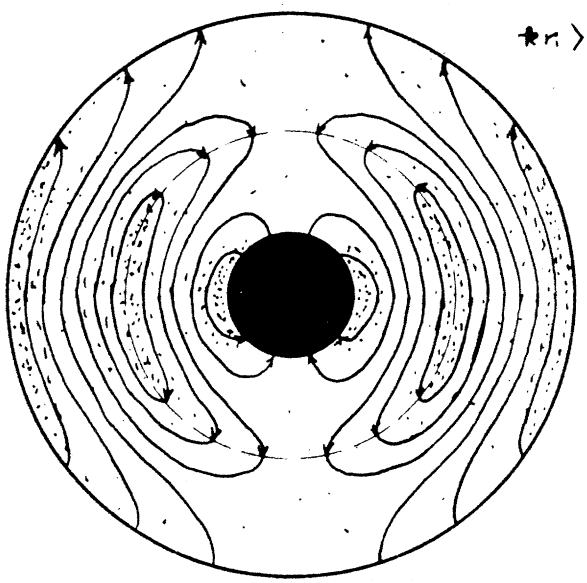

$p = 2$

FIGURE 27
SPHERICAL FIELD PATTERNS

APPENDIX C

EIGENFREQUENCIES AND EIGENFUNCTIONS

1. Method of Computation

Following the SMCH series representations outlined in Chapter VI representative numerical values have been computed for J_ℓ, K_ℓ, J'_ℓ, K'_ℓ, γ_ℓ, β_ℓ, and χ_ℓ. For $\ell = 0$, the results are given in Tables 3 to 5, while Tables 6 to 11 give the results for $\ell = 1$. Equations (6.34) and (6.35) were used to compute J_ℓ and K_ℓ, and Eqs. (6.50) and (6.51) for J'_ℓ and K'_ℓ. For values of ξ close to 1, expressions (6.35) and (6.51) converge poorly or not at all and it has been necessary to compute $\mathbb{K}_\ell$ and $\mathbb{K}'_\ell$, using (6.64), (6.65), (6.66) and (6.67), and then converting to K_ℓ and K'_ℓ by the factor $\mu_\ell(c)$. Where this procedure has been employed the value of K_ℓ is starred (*) in the tables. The values of $d^\ell_n(c)$ and $\left(\frac{d^\ell_{-n}(c)}{\rho}\right)$ required were taken from SMCH, pages 95-98; these are given to five significant figures, but the fifth figure is considered doubtful (SMCH, p. 76). Values of $a^\ell_n(c)$ required were calculated from (6.21). As mentioned in Chapter VI, Section 11, we use the SMCH coefficients for $m = 1$, and for the same ℓ as defined by Section 1 of Chapter IV. To obtain convergence to the maximum accuracy of the tabulated coefficients, it was found necessary to extend the tables of coefficients in every case. The additional coefficients, and the method of computing them, are given in Appendix D.

For values of ξ close to 1, it has been found necessary to use the representations involving the associated Legendre functions. The best tabulation available, and the one used, is that computed by the

Mathematical Tables Project, National Bureau of Standards, "Tables of Associated Legendre Functions," Columbia University Press, 1945. This volume gives values of $P_n^m(x)$, $Q_n^m(x)$ and their derivatives for values of x of 1.1, 1.2, 1.3.... to considerably more significant figures than required by us. However, in this region the functions are changing rapidly, and interpolation is highly unsatisfactory. Therefore, values of ξ for which computations were to be made were chosen so that the Legendre functions would be found tabulated for the exact argument required without the necessity of interpolation. Appendix E describes methods of evaluating the functions at finer intervals of ξ, where necessary.

The spherical Bessel and Neumann functions required were obtained from volumes I and II of Mathematical Tables Project, N.B.S., "Tables of Spherical Bessel Functions," Columbia University Press, 1947. Again, the functions are tabulated to much greater accuracy than we require. They are tabulated at quite close intervals so that interpolation is feasible, although this was rarely necessary.

2. Precision of the Results

The resulting values of J_ℓ, K_ℓ, J_ℓ' and K_ℓ' have been given to five significant figures, but in view of the precision of the SMCH coefficients an error of 5 units in the last figure is not unlikely. In some instances, the calculations involve a small difference of two large numbers and in this case correspondingly fewer significant figures are shown. W_ℓ has been computed using (6.47) and its precision follows from that of J_ℓ' and K_ℓ'.

β_ℓ is given by arc tan γ_ℓ' . It will be recalled from Chapter III, Section 7, that β_ℓ is defined as a continuous function. However Eq. (3.54) does not yield a value of β_ℓ uniquely but only within an integral multiple of π radians. The function γ_ℓ' is zero when $\xi = 1$ for all values of c except $(\ell+1)\pi/2$, when γ_ℓ' is infinite. This discontinuous behavior is inconvenient when stipulating a consistent datum for β_ℓ , so we adopt the following convention. For the smallest value of ξ greater than one (but not equal!) for which $\gamma_\ell' = 0$, we arbitrarily set $\beta_\ell = 0$. This results in a consistent and continuous behavior of β_ℓ with variations in c for all values of $\xi > 1$, and the discontinuity can be circumvented by a limiting process as $\xi \to 1$.

β_ℓ has been computed using "Table of Arc Tan x," Mathematical Tables Project, N.B.S., Works Project Administration, 1942, and is generally given to five decimal places although the final figure is questionable. The principal[1] value of β_ℓ is tabulated, together with the appropriate multiple of π to make β_ℓ a continuous function. The relation between β_ℓ and ξ , for various values of c and ℓ , is shown in Figures 28 to 36. Whenever $c < (\ell+1)\pi/2$, there is a minimum of β_ℓ . This minimum can be shown to occur when $\xi = \sqrt{\alpha}/c$, by differentiating expression (3.47) for γ_ℓ' and noting from (5.5) that $\sqrt{\alpha}/c$ is an inflection point; consequently, the second derivatives and γ_ℓ' vanish there.

---

(1) W. L. Hart, "Plane Trigonometry," p. 155, D. C. Heath, 1933.

3. Computation of X_ℓ

The function X_ℓ is defined by

$$X_\ell(\xi_1, c) \triangleq \sigma_\ell(c)\ X_{\ell p}(\xi_1;\ c, \xi_1, \xi_2)$$

$$= a_{\ell p}(c, \xi_1, \xi_2)\, J_\ell(\xi_1, c) + b_{\ell p}(c, \xi_1, \xi_2)\, K_\ell(\xi_1, c) \qquad (C.1)$$

in view of (3.38), (6.36) and (6.37). The coefficients $a_{\ell p}$ and $b_{\ell p}$ are cosines and sines of β_ℓ defined by (3.51); they have been computed using "Tables of Circular and Hyperbolic Sines and Cosines," 2nd Ed., The Computation Laboratory, N. B. S., U. S. Government Printing Office, 1949. Then X_ℓ has been computed, using (C.1); the values of this function find use in Appendix F, when losses are considered.

4. Solution of the Eigenvalue Problem

Using Equation (3.55),

$$\beta_\ell(\xi_1, c) = \beta_\ell(\xi_2, c) - p\pi \qquad (C.2)$$

we can find the eigenfrequencies of a confocal spheroidal cavity system. That is to say, for a given dimensionless frequency c, any two values of ξ whose corresponding β_ℓ values differ by an integral multiple of π radians constitute a solution to the eigenvalue problem. Looking at Figure 31 for instance, if $\xi_1 = 2.4$, then $\beta_\ell = -0.4600$; any intersection of the β_ℓ vs ξ curve with the horizontal line extended from $\beta_\ell = -0.4600$ represents a ξ_2 for which the boundary conditions are satisfied. Graphs of β_ℓ vs ξ, identical with Figures 28 to 36, but to as large a scale as possible consistent with the interval between

computed points, have been plotted. From these large scale plots corresponding values of ξ_1 and ξ_2 have been read off. The results are given graphically in Figures 37 to 45. There is an inaccuracy inherent in drawing the curves of β_ℓ between computed points, and a further source of error in reading off the points. The probable error in ξ_2 is estimated to be $\pm$ 0.008. For values of ξ near 1, the values of β_ℓ computed in Appendix E for closer intervals of ξ have been used in plotting Figures 28 to 36. It will be noted that for values of $c < (\ell+1)\pi/2$ the mode for $p=0$ behaves similarly to the spherical case, becoming degenerate (inner and outer spheroids coinciding, $\xi_1 = \xi_2$) when ξ_1 exceeds $\sqrt{\alpha}/c$. For $c > (\ell+1)\pi/2$ the mode does not exist for any values of ξ_1 .

5. Interpolation Methods

The graphs presented so far have each been for a particular frequency c . In order to interpolate for frequencies between those chosen for computation it is necessary to employ other ways of presenting the data. One such way is to plot c vs ξ_2 for specific values of ξ_1 as has been done in Figures 46 to 50, based on Figures 37 to 45. These give a very good idea of the trends, but the frequency intervals are quite large. Consequently, many possible curves can be drawn through the plotted points, and there is something to be desired in the way of accuracy. The obstacle is the formidable amount of work involved in the computations, for a single frequency. An envelope of these curves can be drawn through the points defined by the curves of constant ξ_1 and the values of c corresponding to $\sqrt{\alpha}/c = \xi_1$. On the basis of the results given, one may now make a judicious choice of frequencies which are likely to yield the most useful information, as a preliminary to an even more ambitious program than has been attempted here.

TABLE 3

cξ	J	K	J′	K′	δ	β	ξ
.96	.42272	−6.9125*	2.2401	5.0266	−.44564	−.41922	1.2
1.12	.89162	−6.1611*	2.4373	2.9083	−.83804	−.69751	1.4
1.28	1.3928	−5.6595*	2.5622	2.2321	−1.1479	−.85414	1.6
1.44	1.9114	−5.2355*	2.6104	2.0628	−1.2654	−.90204	1.8
1.6	2.4317	−4.8189*	2.5797	2.1336	−1.2091	−.87976	2.0
1.92	3.4146	−3.8903*	2.2835	2.5546	−.89386	−.72941	2.4
2.4	4.5218	−2.1303	1.3135	3.2755	−.40101	−.38137	3.0
3.2	4.6642	1.3768	−1.1080	3.4484	.32132	.31090	4.0
4.8	−1.139	4.6294	−3.5805	−.90743	−3.9458	−1.32260 π^+	6.0
7.2	−2.4743	−4.0258	3.1788	−1.9430	1.6344	1.02171	9.0
9.6	4.5613	1.1768	−.93694	3.6190	.25890	.25333 $2\pi^+$	12.
16.0	4.4319	1.5600	−1.2451	3.5331	.35220	.33863 $4\pi^+$	20.

$\sigma = 3.7534$

$\mu = 7.0544$

$\alpha = 2.12616$

$\frac{\sqrt{\alpha}}{c} = 1.825$

$l = 0$

$c = 0.8$

TABLE 4

cE	J	K	J′	K′	γ	β	E
1.76	.31472	−1.9006*	3.1145	44690	−6.9692	−1.42828	1.1
1.92	.62027	−1.8292*	2.9828	.97149	−3.0703	−1.25593	1.2
2.24	1.1733	−1.5408*	2.5002	1.8816	−1.3288	−.92565	1.4
2.56	1.6036	−1.0908*	1.7659	2.5779	−.68504	−.60061	1.6
3.2	1.9401	.08950*	−.13927	3.1170	.044681	.04465	2.0
3.84	1.5010	1.2345	−1.9788	2.4099	.82112	.68748	2.4
4.8	−.15455	1.9383	−3.1068	−.24653	−12.602	$-1.49161^{\pi+}$	3.0
6.4	−1.9333	.21513	.34407	−3.0963	.11112	.11067	4.0
9.6	1.9173	.33158	−.53061	3.0690	.17290	$.17120^{2\pi+}$	6.0
12.8	−1.8944	−.44486	.71189	−3.0318	.23481	$.23063^{3\pi+}$	8.0
16.0	1.8649	.55583	−.88943	2.9844	.29803	$.28965^{4\pi+}$	10.0

$\sigma = 3.1139$

$\mu = -0.093432$

$\alpha = 2.48399$

$\frac{\sqrt{\alpha}}{c} = 0.988$

$l = 0$

$c = 1.6$

TABLE 5

cξ	J	K	J′	K′	γ	β	ξ
2.64	.30990	-.73181*	2.8270	.50847	-5.5600	-1.39284	1.1
2.88	.56181	-.62543*	2.1961	1.5183	-1.4464	-.96588	1.2
3.12	.74670	-.44198*	1.4929	2.0982	-.71153	-.61842	1.3
3.36	.85928	-.21491*	.75633	2.4022	-.31485	-.30503	1.4
3.84	.86597	.27458*	-.65947	2.3617	.27923	.27230	1.6
4.8	.19791	.90959	-2.3295	.54437	4.2792	1.34123	2.0
5.76	-.67590	.65560	-1.6604	-1.6837	-.98615	$-.77843_{\pi^+}$	2.4
7.2	-.71279	.62773	1.5423	-1.7655	.87358	.71803	3.0
9.6	.95537	.02932	-.06768	2.3285	.02907	$.02906_{2\pi^+}$	4.0
14.4	.15975	-.94659	2.2873	.38490	-5.9426	$-1.40408_{4\pi^+}$	6.0

$\sigma = 2.3117$ $\qquad$ $l = 0$

$\mu = -1.5748$ $\qquad$ $c = 2.4$

$\alpha = 3.02128$

$\frac{\sqrt{\alpha}}{c} = 0.724$

TABLE 6

cE	J	K	J′	K′	γ	β	E
0.8	0	$-\infty$	.95940	$+\infty$	0-	0-	1.0
1.04	0.41683	-62.414*	1.8412	118.44	-.01555	-.01554	1.3
1.28	1.1139	-40.199*	2.8148	45.902	-.06132	-.06125	1.6
1.60	2.5024	-28.246*	4.1132	19.223	-.21398	-.21080	2.0
1.92	4.3795	-22.567*	5.2247	10.544	-.49551	-.46005	2.4
2.40	7.8426	-17.573	6.1304	7.2113	-0.85011	-.70456	3.0
3.60	15.332	-5.1954	2.3561	9.9168	-0.23758	-.23326	4.5
4.80	11.928	9.5882	-7.0031	8.1437	0.86000	.71024	6.0
7.20	-14.237	3.8134	-.27918	-10.791	-.25872	$-.25317^{\pi+}$	9.0
9.60	6.5804	-12.985	10.050	5.1370	-1.9564	$-1.0983^{2\pi+}$	12.0
16.0	6.5026	-12.859	10.288	5.1519	-1.9970	$-1.1065^{4\pi+}$	20.0

$\sigma = 11.464$

$\mu = 168.27$

$\alpha = 6.27270$

$\frac{\sqrt{\alpha}}{c} = 3.135$

$l = 1$

$c = 0.8$

TABLE 7

cE	J	K	J′	K′	γ^m	β	E
1.6	0	$-\infty$	3.1621	$+\infty$	0-	0-	1.0
1.76	.35117	-13.371*	3.8532	31.289	-.12315	-.12253	1.1
1.92	.76861	-11.113*	4.4832	16.508	-.27159	-.26519	1.2
2.24	1.7707	-8.8827*	5.4671	7.8763	-.69413	-.60677	1.4
2.56	2.9221	-7.5466*	5.9525	6.0187	-.98900	-.77986	1.6
3.20	5.2100	-5.0146	5.0521	7.1352	-.70805	-.61611	2.0
3.84	6.6348	-1.7610	1.7231	8.9640	-.19223	-1.8991	2.4
4.8	5.5609	3.5746	-5.3471	7.8037	.68520	.60072	3.0
6.4	-2.9468	5.7254	-8.5841	-4.5340	-1.8933	-1.08486^{π^+}	4.0
8.0	-5.7847	-2.6610	4.1476	-8.8979	.46613	.43619	5.0
9.6	2.5351	-5.8005	9.0371	3.9800	-2.2706	$-1.1559^{2\pi^+}$	6.0
14.4	-5.7387	-2.5631	4.0630	-9.0778	.44757	$.42083^{3\pi^+}$	9.0

$\sigma = 10.001$

$\mu = 17.837$

$\alpha = 7.07193$

$\frac{\sqrt{\alpha}}{c} = 1.663$

$l = 1$

$c = 1.6$

TABLE 8

cE	J	K	J′	K′	γ	β	E
2.4	0	$-\infty$	5.1868	$+\infty$	0−	0−	1.0
2.64	.54716	-4.1762*	5.7042	4.4619	-1.1496	-.85489	1.1
2.88	1.1298	-3.7533*	5.8913	3.9158	-1.5050	-.98417	1.2
3.12	1.7136	-3.3487*	5.7249	4.2983	-1.3319	-.92678	1.3
3.36	2.2629	-2.8803*	5.2032	5.1040	-1.0194	-.79502	1.4
3.84	3.1223	-1.6857*	3.1936	6.7747	-.47140	-.44051	1.6
4.32	3.4780	-.22711	0.25606	7.6131	-.03363	-.03362	1.8
5.76	.96473	3.2645	-7.5002	2.1378	3.5084	1.2931	2.4
7.2	-3.0079	1.5234	-3.5251	-7.0370	-.50094	-.16440 (π^+)	3.0
9.6	1.0289	-3.1881	7.5344	2.4455	-3.0810	-1.25695 ($2\pi^+$)	4.0
14.4	-3.1299	-1.1540	2.7553	-7.4626	.36921	.35368 ($3\pi^+$)	6.0

$\sigma = 7.9805$

$\mu = 3.3118$

$\alpha = 8.34293$

$\frac{\sqrt{\alpha}}{c} = 1.205$

$l = 1$

$c = 2.4$

TABLE 9

cE	J	K	J'	K'	γ	β	E
3.2	0		6.0130	$-\infty$	0+	$-\pi^+$	1.0
3.52	.58762	-1.7061*	5.6396	1.8222	-.30950	-1.2583	1.1
3.84	1.1090	-1.4329*	4.6995	3.5687	-1.3169	-.92132	1.2
4.16	1.5118	-1.0068*	3.2894	4.8818	-.67381	-.59293	1.3
4.48	1.7560	-.4746*	1.5534	.56691	-.27401	-.26774	1.4
5.12	1.6911	.67798	-2.1737	5.4513	.39875	.37943	1.6
6.40	-.17621	1.8161	-.58331	-.56182	-10.382	-1.4748^{π^+}	2.0
7.68	-1.7928	.34540	-1.1099	-5.7501	-.19302	-.19067	2.4
9.6	.29534	-1.8026	5.7767	.94549	-6.1097	$-1.4086^{2\pi^+}$	3.0
12.8	-.40615	1.7816	-5.7053	-1.3003	-4.3877	$-1.3467^{3\pi^+}$	4.0
16.0	.51294	-1.7540	5.6157	1.6420	-3.4200	$-1.2863^{4\pi^+}$	5.0
19.2	-.61670	1.7204	-5.5073	-1.9740	-2.7899	$-1.2266^{5\pi^+}$	6.0

$\sigma = 5.8494$

$\mu = -0.14489$

$\alpha = 10.00169$

$\frac{\sqrt{\alpha}}{c} = 0.988$

$l = 1$

$c = 3.2$

TABLE 10

cE	J	K	J′	K′	γ^M	β	E
4.0	0	−.74697	5.5692	−∞	0+.	$-\pi^+$	1.0
4.4	.48947	−.7079*	4.1201	2.0793	−1.9815	−1.1034	1.1
4.8	.80863	−.4033*	2.2110	3.7629	−.58757	−.53123	1.2
5.2	.92664	.0052*	.15146	4.2469	−.035663	−.03565	1.3
5.6	.84457	.4147*	−1.7395	3.8050	.45716	.42879	1.4
6.4	.23002	.92945	−3.9745	1.0452	3.8027	1.3136	1.6
7.2	−.55129	.79413	−3.3636	−2.2914	−1.4679	$-.97277^{\pi^+}$	1.8
8.0	−.96466	.12354	−.53721	−4.0098	−.13398	−.13318	2.0
9.6	−.045982	−.97820	4.0128	−.20068	19.996	$-1.5208^{2\pi^+}$	2.4
12.0	.66414	.72631	−2.9466	2.7018	1.0906	.82870	3.0
16.0	.16044	−.99456	3.8541	.64497	−5.9757	$-1.4050^{4\pi^+}$	4.0

$\sigma = 3.9672$

$\mu = -1.4429$

$\alpha = 11.94872$

$\frac{\sqrt{\alpha}}{c} = 0.864$

$l = 1$

$c = 4.0$

TABLE II

cE	J	K	J′	K′	γ	β	E
4.8	0	−.30681	4.4062	$-\infty$	0+	$-\pi+$	1.0
5.28	.33608	−.25609*	2.2763	2.1877	−1.0405	−.80524	1.1
5.76	.45538	.01308*	.14853	2.9005	−.05121	−.05116	1.2
6.24	.38026	.28135*	−1.5494	2.3199	.66785	.58882	1.3
6.72	.16998	.45313	−2.5190	1.039	2.428	.4793	1.4
7.68	−.33297	.36877	−2.0003	−1.7438	−.61471	$-.85380^{\pi+}$	1.6
8.64	−.49249	−.11308	.53048	−2.5651	.20680	.20393	1.8
9.6	−.16399	−.48152	2.4471	−.85304	2.8687	1.2357	2.0
12.0	.42105	.29638	−1.4669	2.0982	.69911	$.61013^{2\pi+}$	2.5
14.4	−.51706	.03012	−.15242	−2.5407	−.05999	$-.05992^{3\pi+}$	3.0
19.2	−.058794	.51741	−2.5156	−.28410	−8.8547	$1.4583^{4\pi+}$	4.0

$\sigma = 2.5156$

$\mu = -2.1295$

$\alpha = 14.08774$

$\frac{\sqrt{\alpha}}{c} = 0.783$

$l = 1$

$c = 4.8$

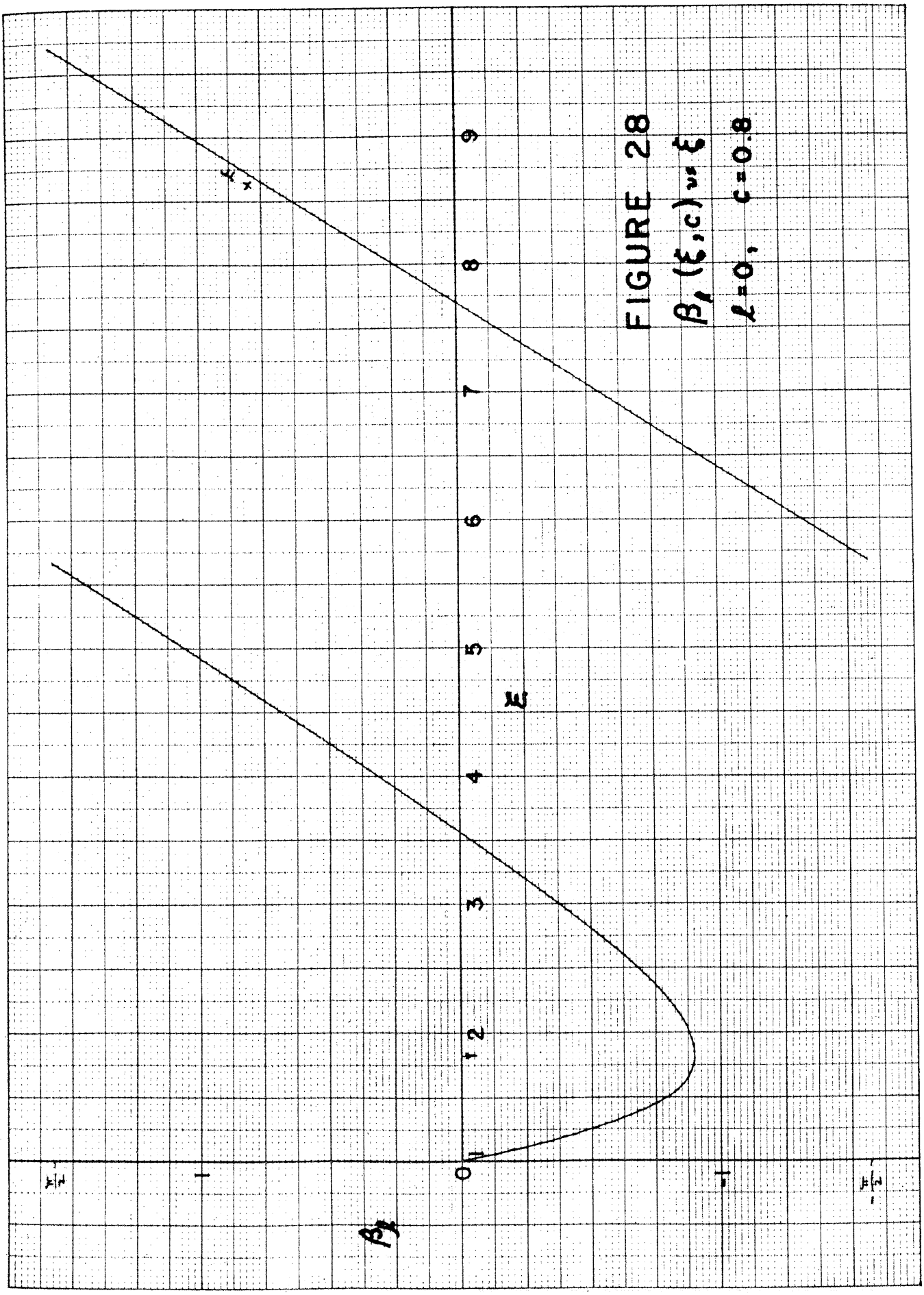

FIGURE 28
$\beta_\mu(\xi,c)$ vs ξ
$\mu=0$, $c=0.8$

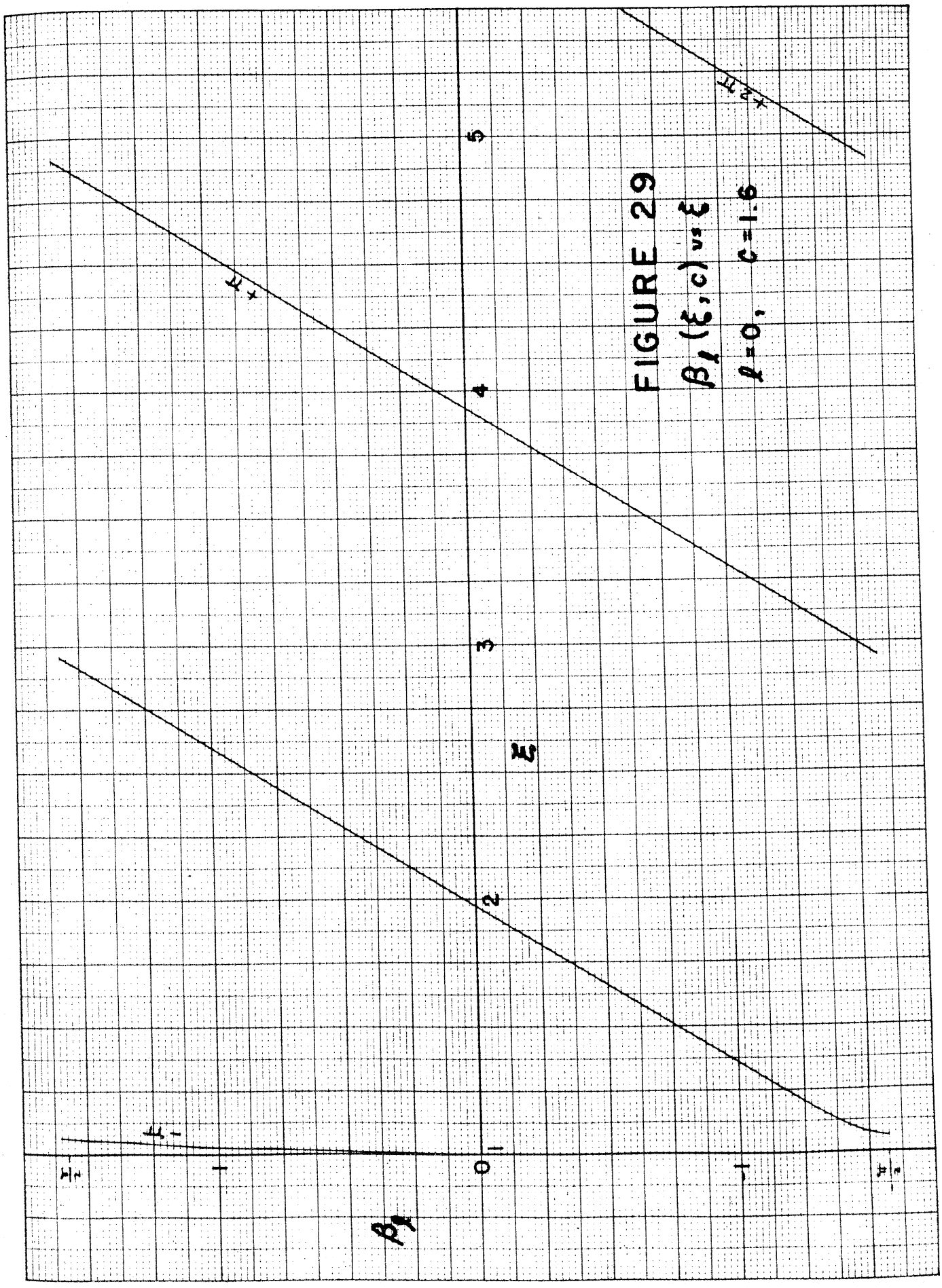

FIGURE 29
$\beta_\ell(\xi,c)$ vs ξ
$\ell=0$, $c=1.6$

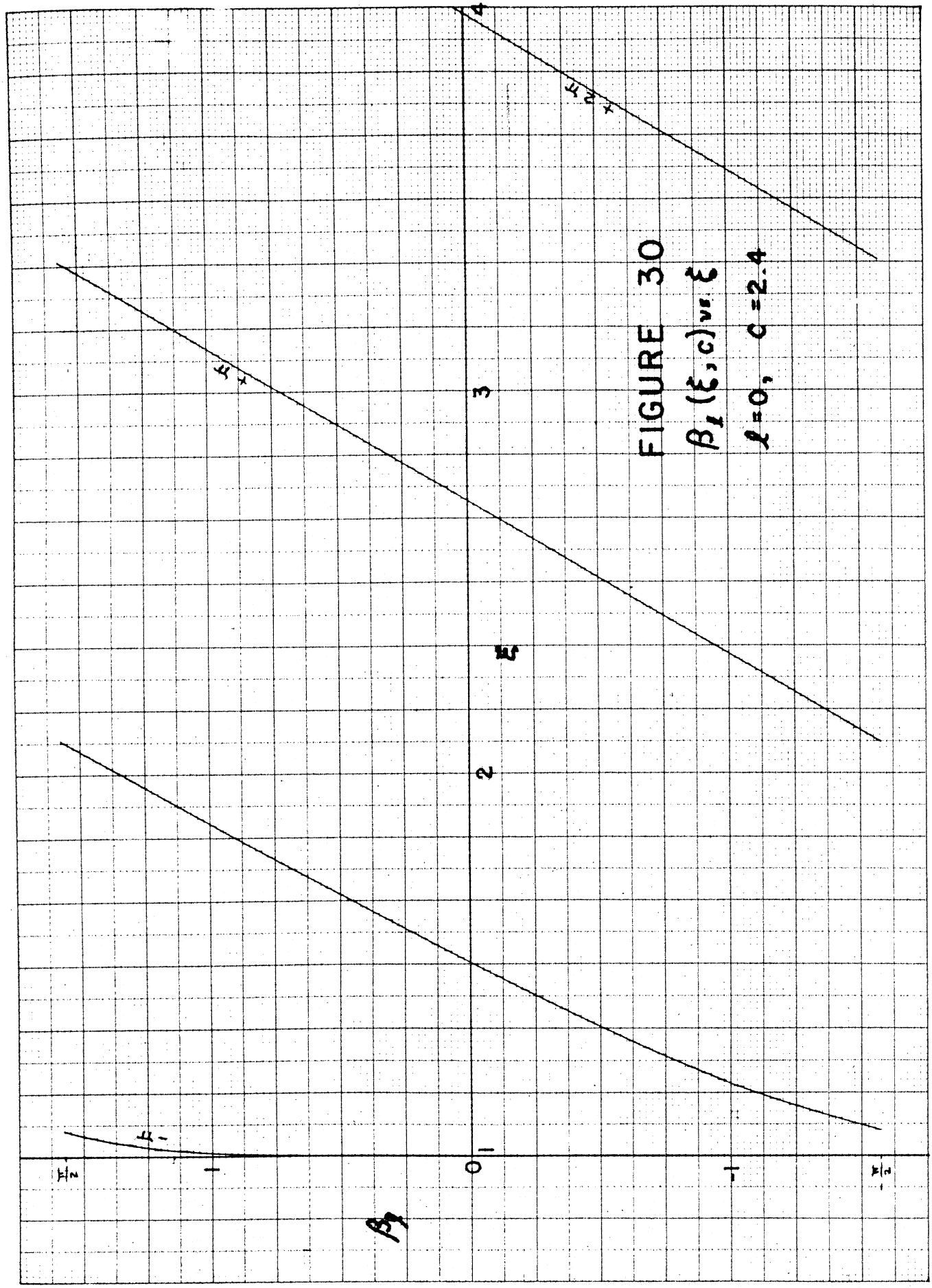
FIGURE 30
$\beta_1(\xi;c)$ vs ξ
$\ell=0$, $c=2.4$
β_1
ξ
$\pi/2$
$-\pi/2$
4
3
2
1
0
-1

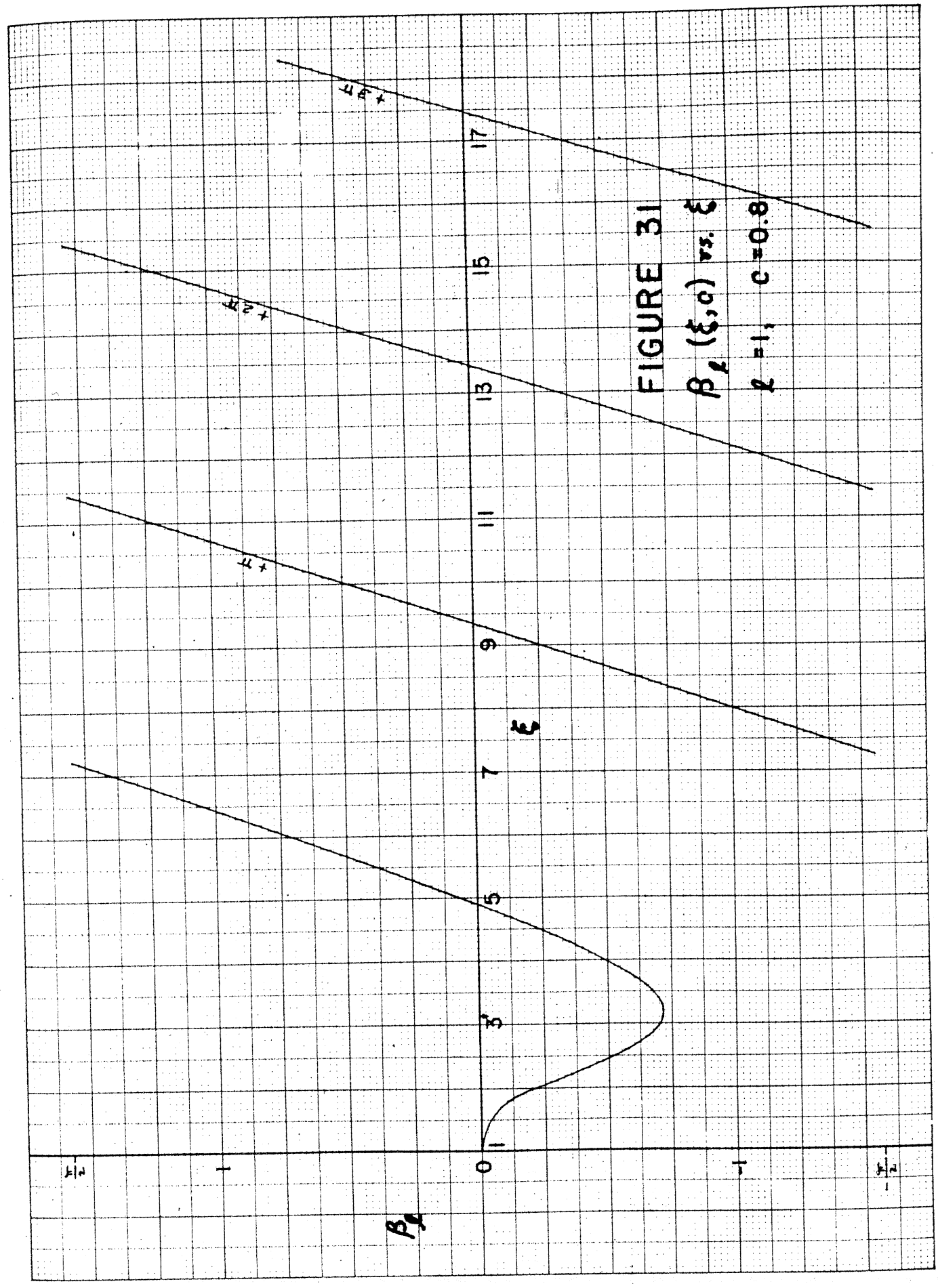
FIGURE 31
$\beta_\ell(\xi,c)$ vs. ξ
$\ell = 1$, $c = 0.8$
β_ℓ
ξ
0
1
3
5
7
9
11
13
15
17
$\pi/2$
π
2π
4π

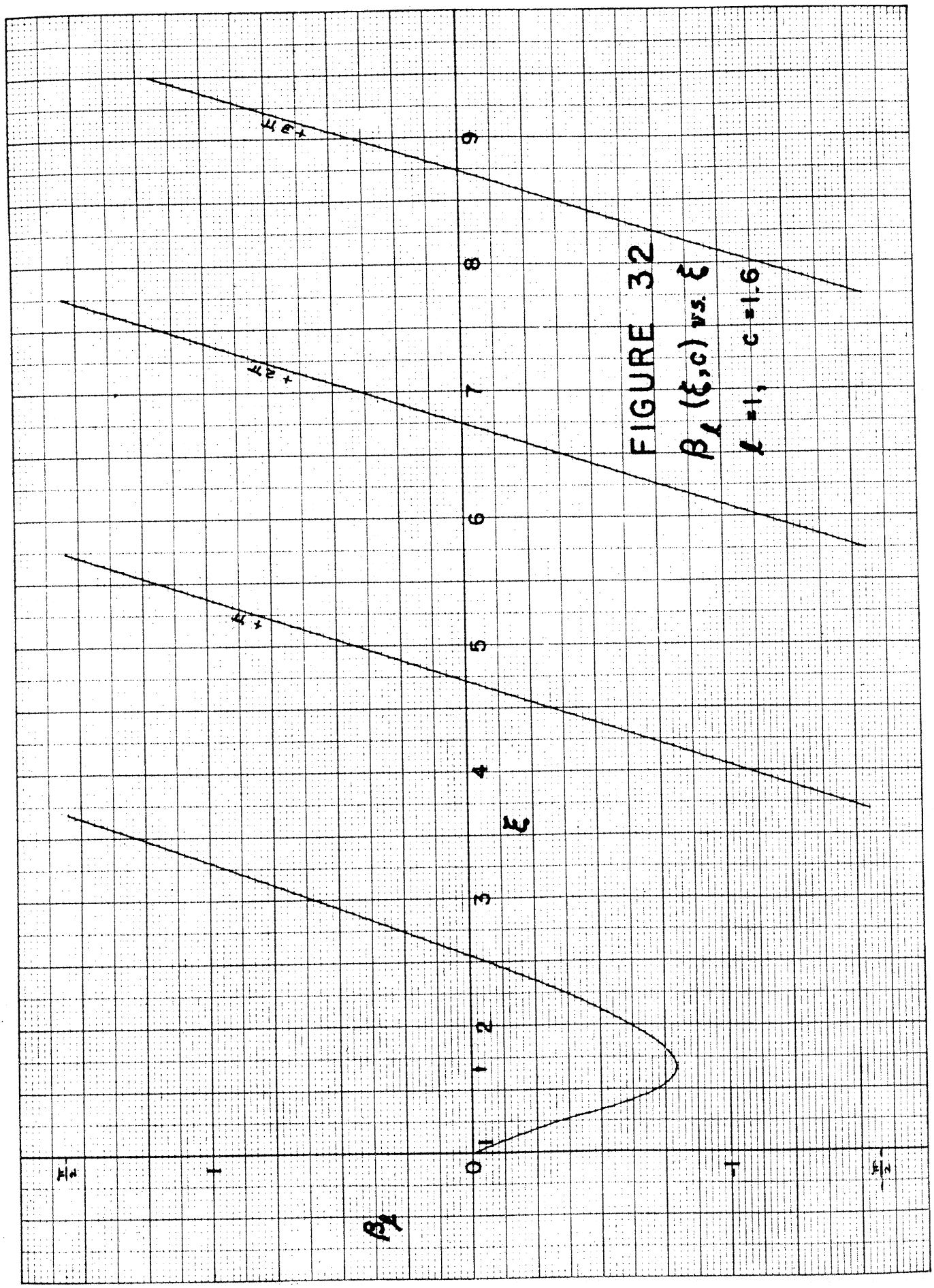

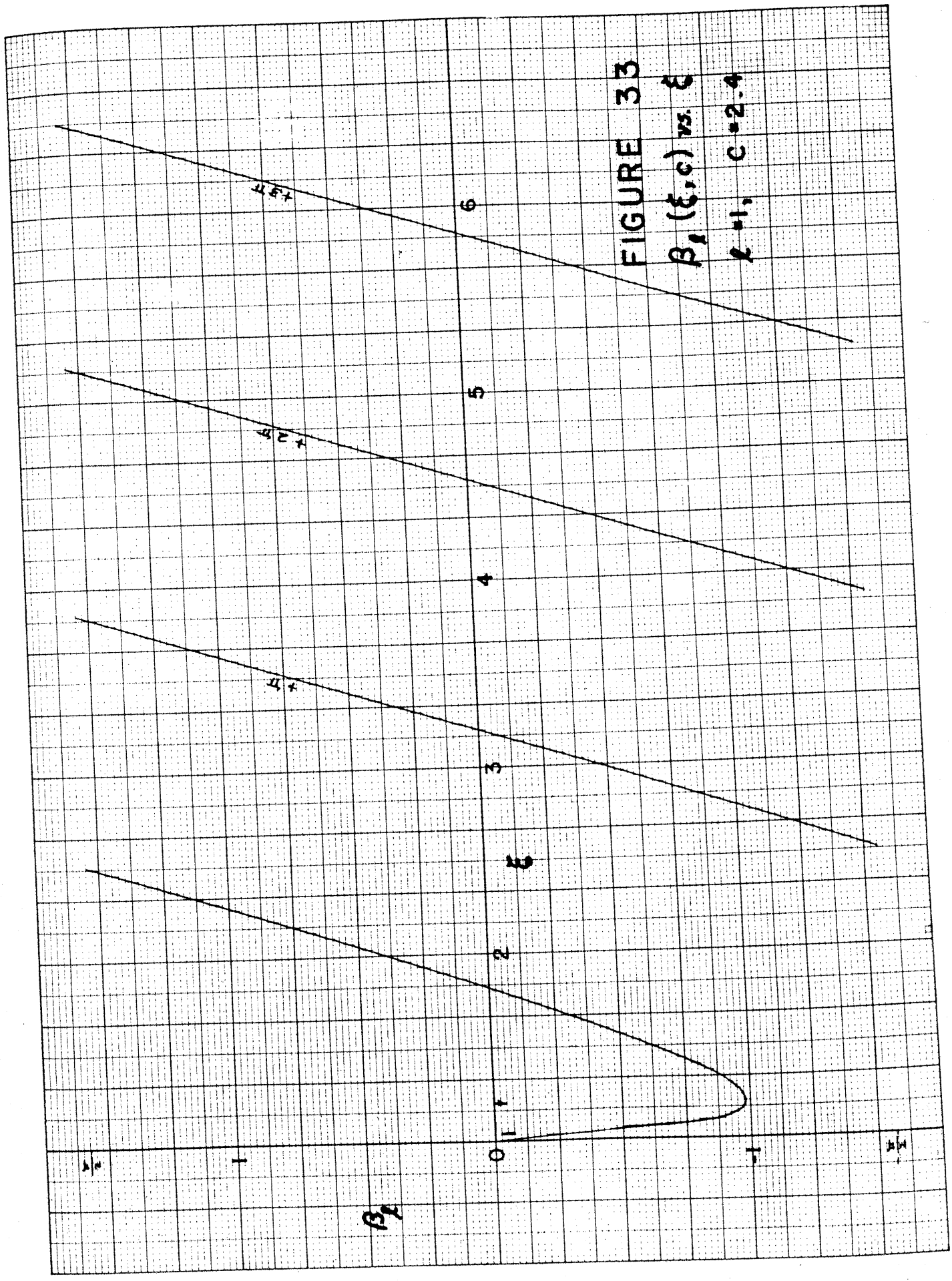

FIGURE 33
$\beta_\mu(\xi,c)$ vs. ξ
$\mu=1$, $c=2.4$

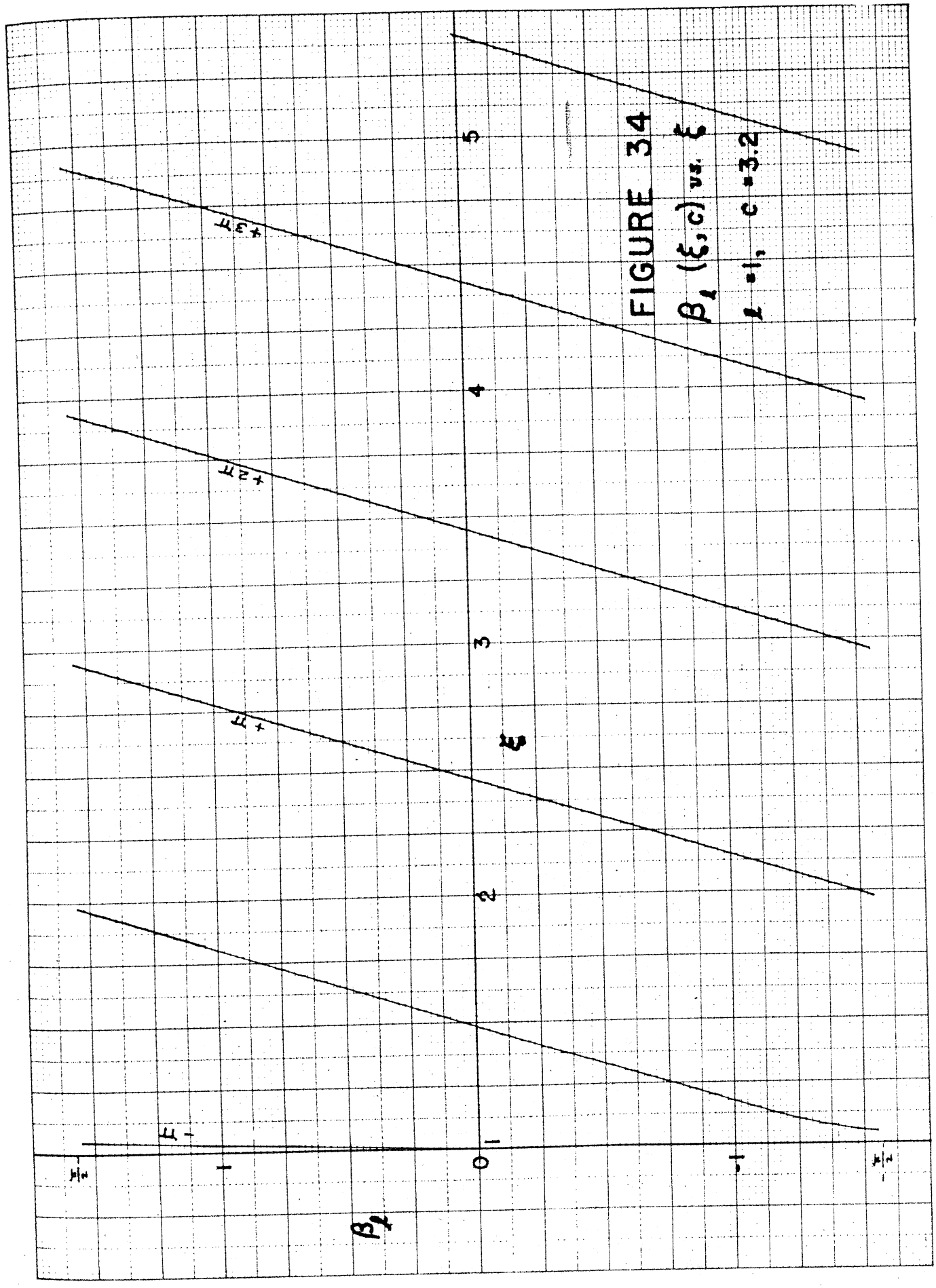
FIGURE 34
$\beta_1(\xi, c)$ vs. ξ
$\mu = 1$, $c = 3.2$
β_1
ξ
μ
$+3\pi$
$+2\pi$
$+\pi$
$-\pi$
-2π
-3π
0
1
2
3
4
5
-1
-2

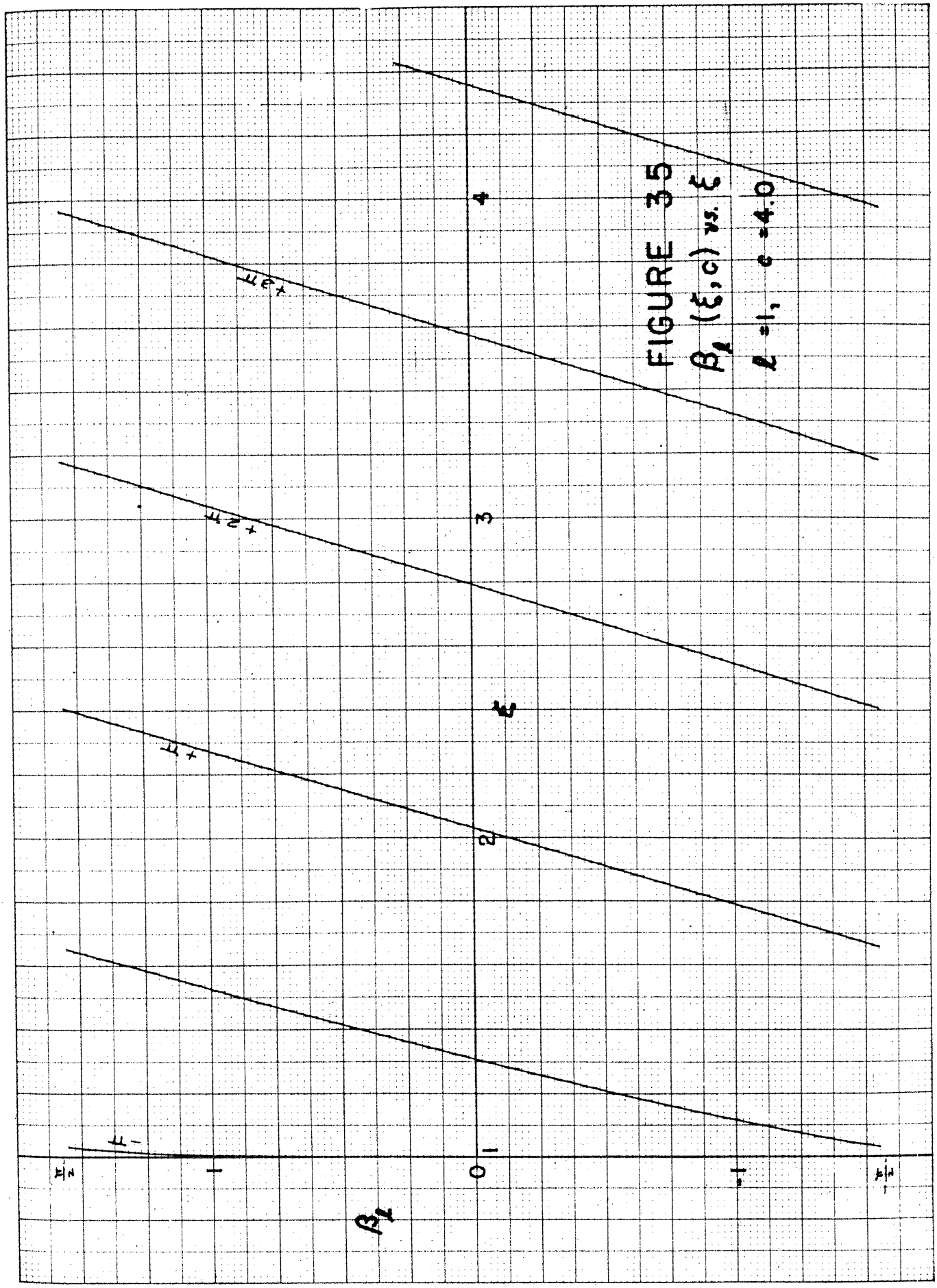
FIGURE 3.5
$\beta_1(\xi,\sigma)$ vs. ξ
$\alpha = 1$, $\epsilon = 4.0$
β_1
ξ
$\pi/4$
$-\pi/4$
-1
0
1
2
3
4
$-\pi$
$+\pi$
$+2\pi$
$+3\pi$

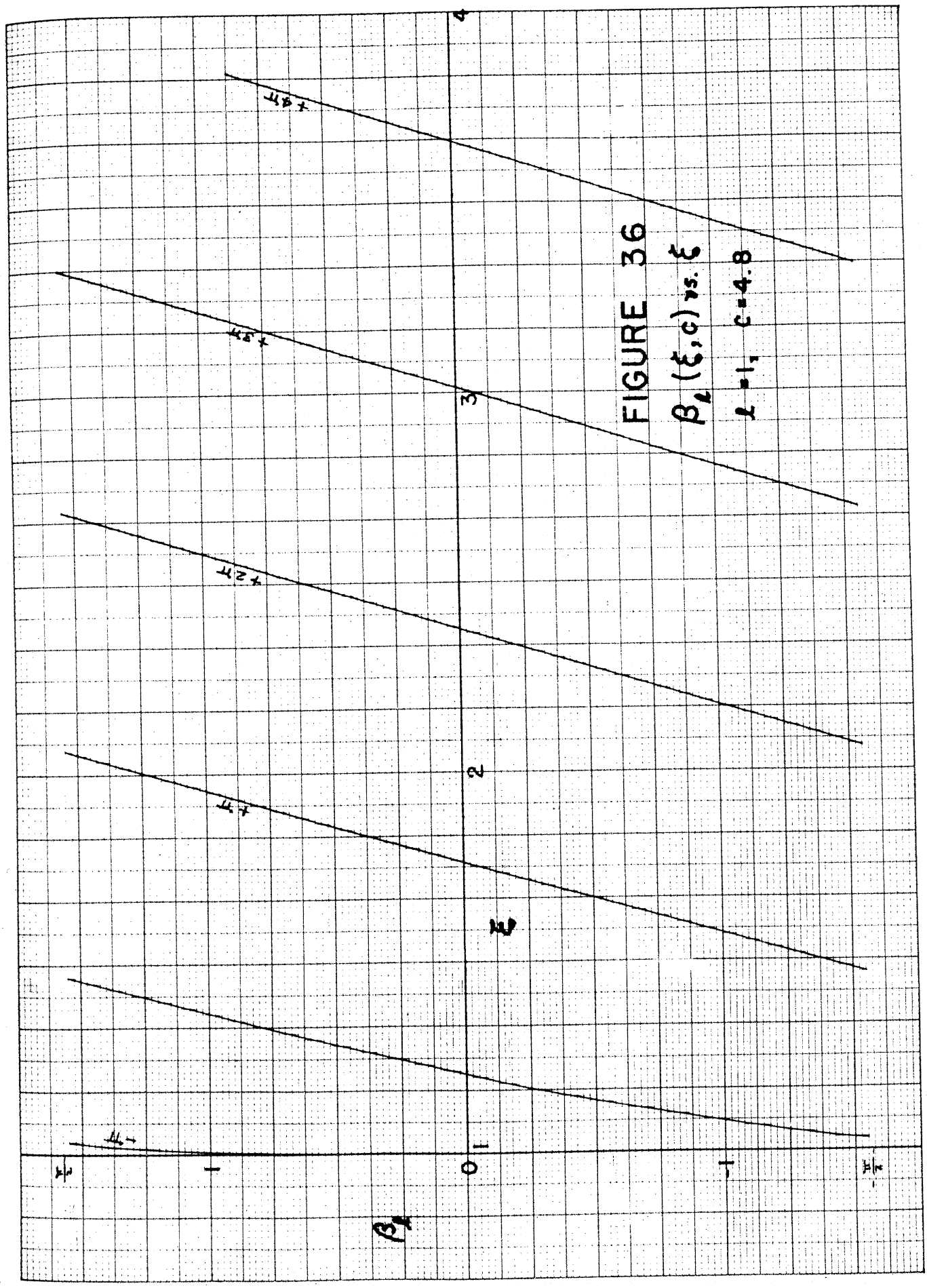
FIGURE 36
$\beta_2(\xi,c)$ vs. ξ
$L=1$, $c=4.8$
β_2
ξ
4
3
2
1
0
-1
$\pi/4$
$\pi/2$
$3\pi/4$
π
$5\pi/4$
$3\pi/2$
$7\pi/4$
2π

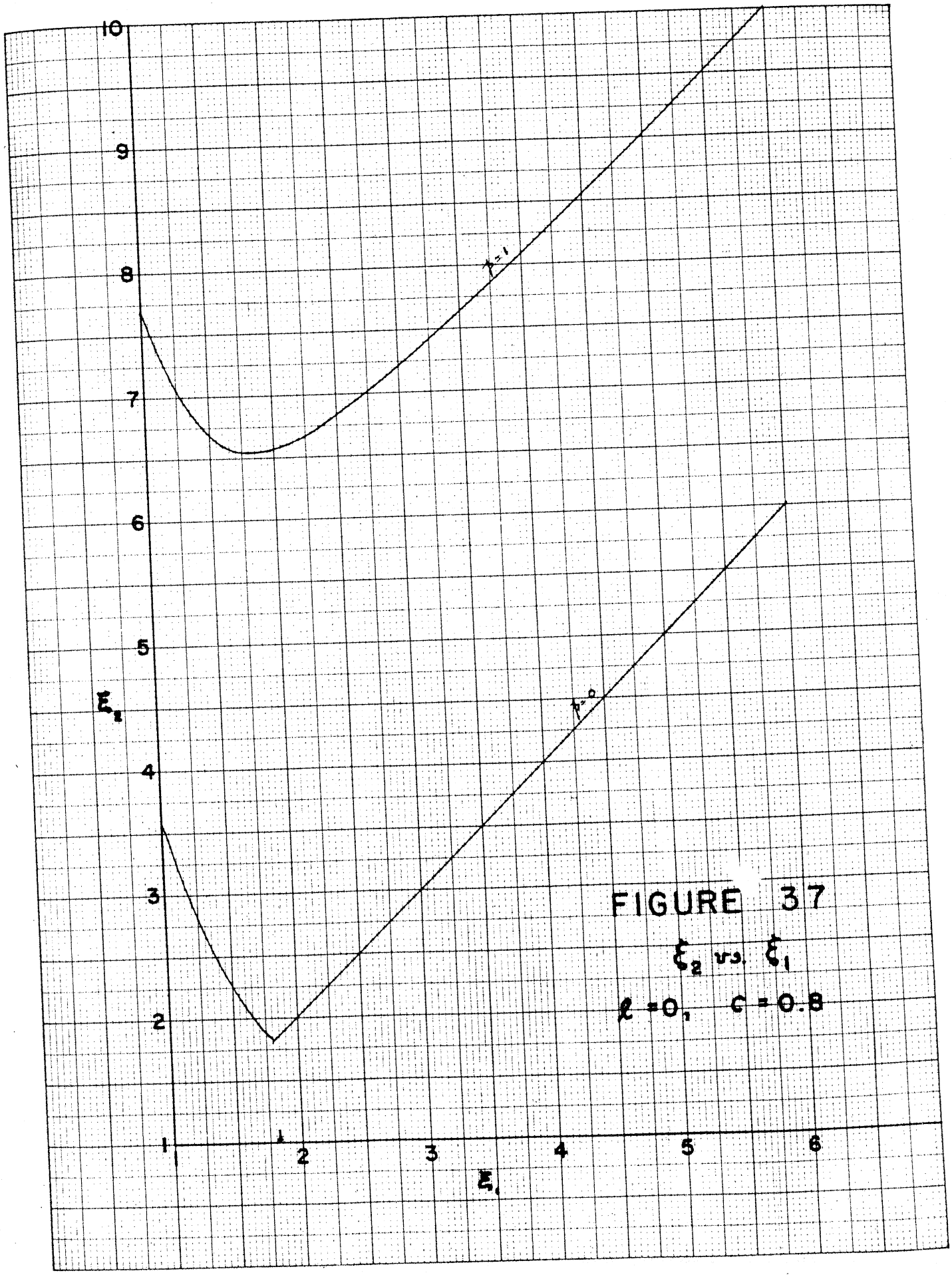

FIGURE 37

ξ_2 vs. ξ_1

$\ell = 0$, $c = 0.8$

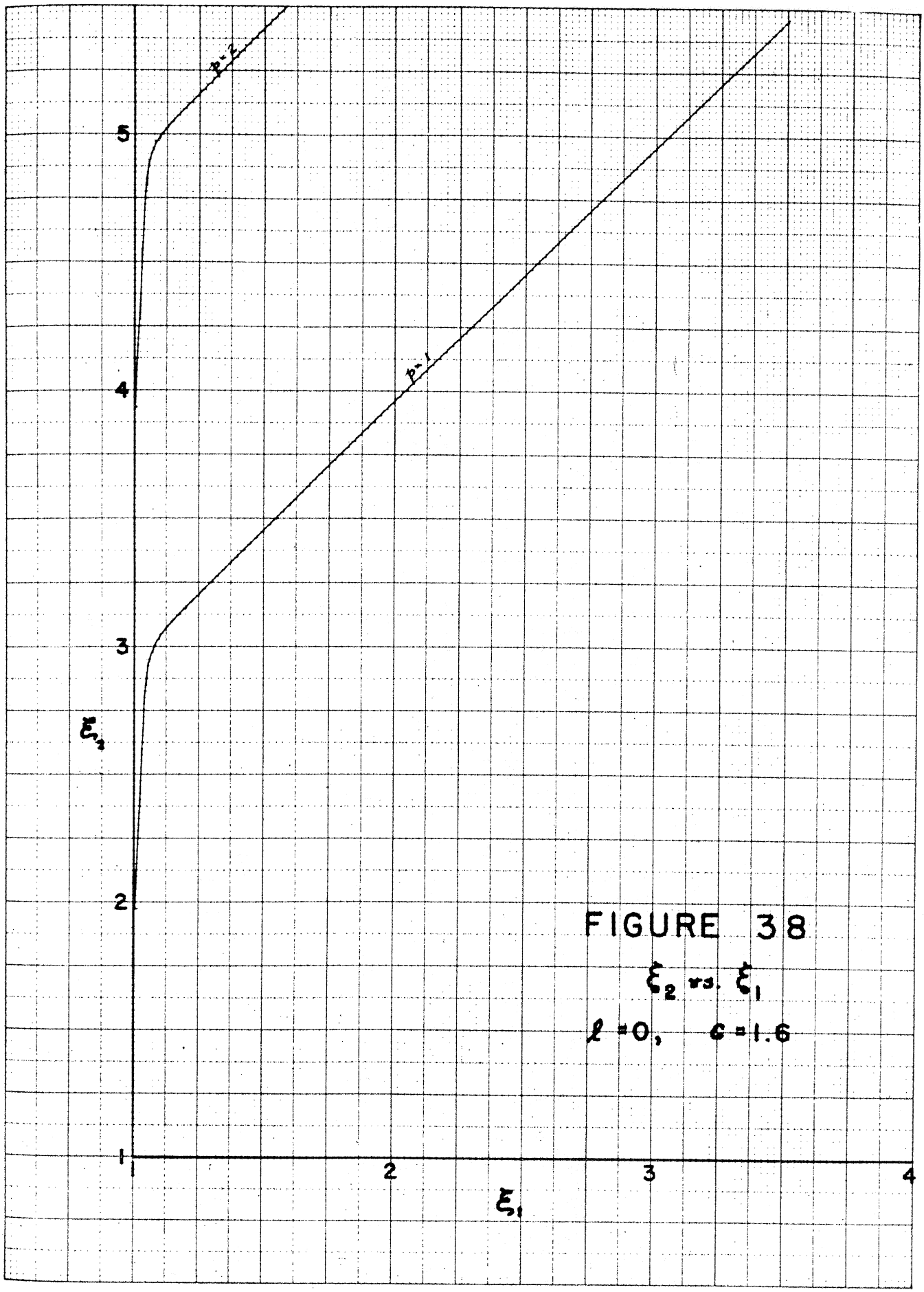

FIGURE 38

ξ_2 vs. ξ_1

$\ell = 0, \quad c = 1.6$

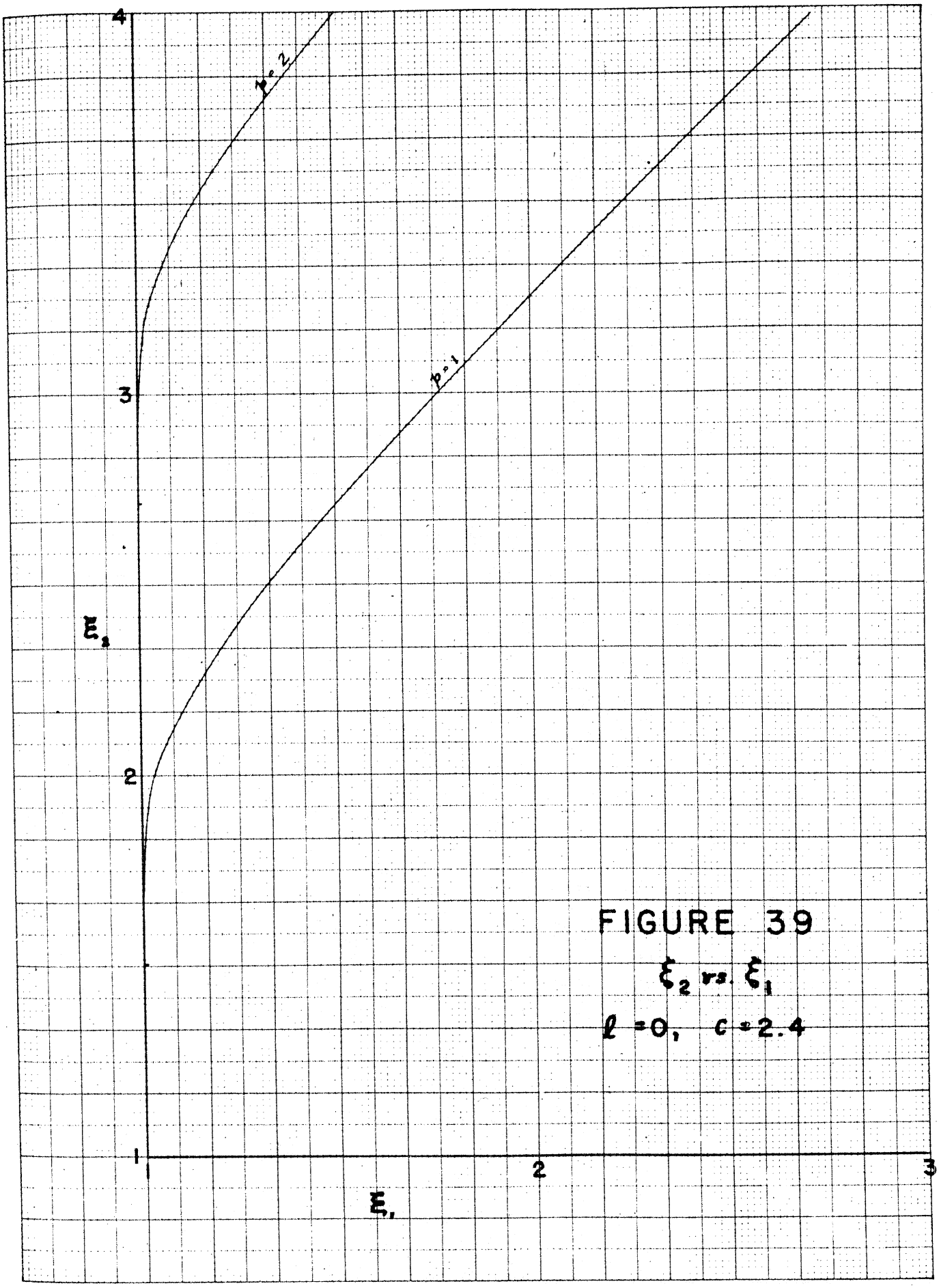

FIGURE 39

ξ_2 vs. ξ_1

$\ell = 0, \quad c = 2.4$

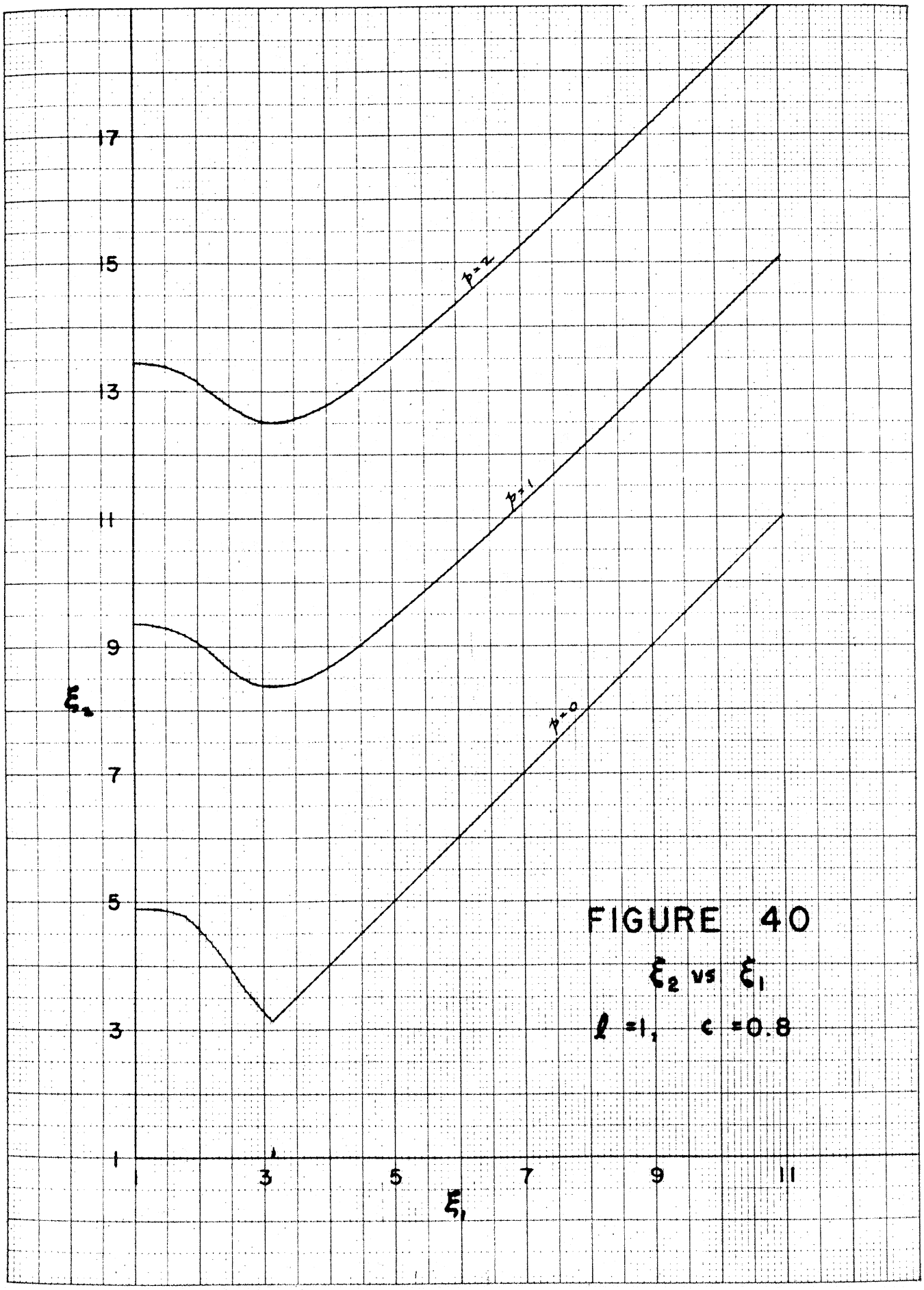

FIGURE 40

ξ_2 vs ξ_1

$\ell = 1, \quad c = 0.8$

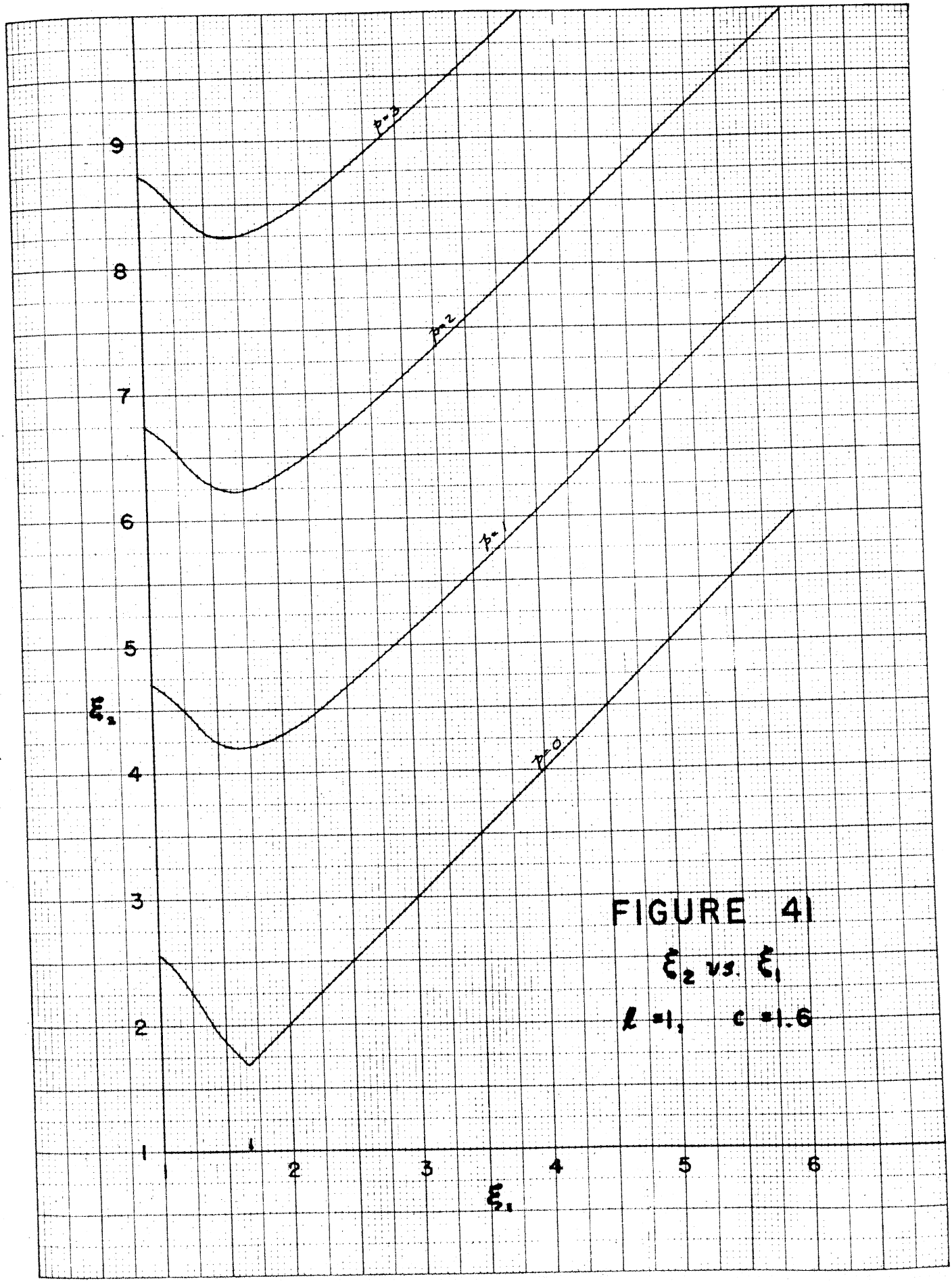

FIGURE 41

ξ_2 vs. ξ_1

$\ell = 1, \quad c = 1.6$

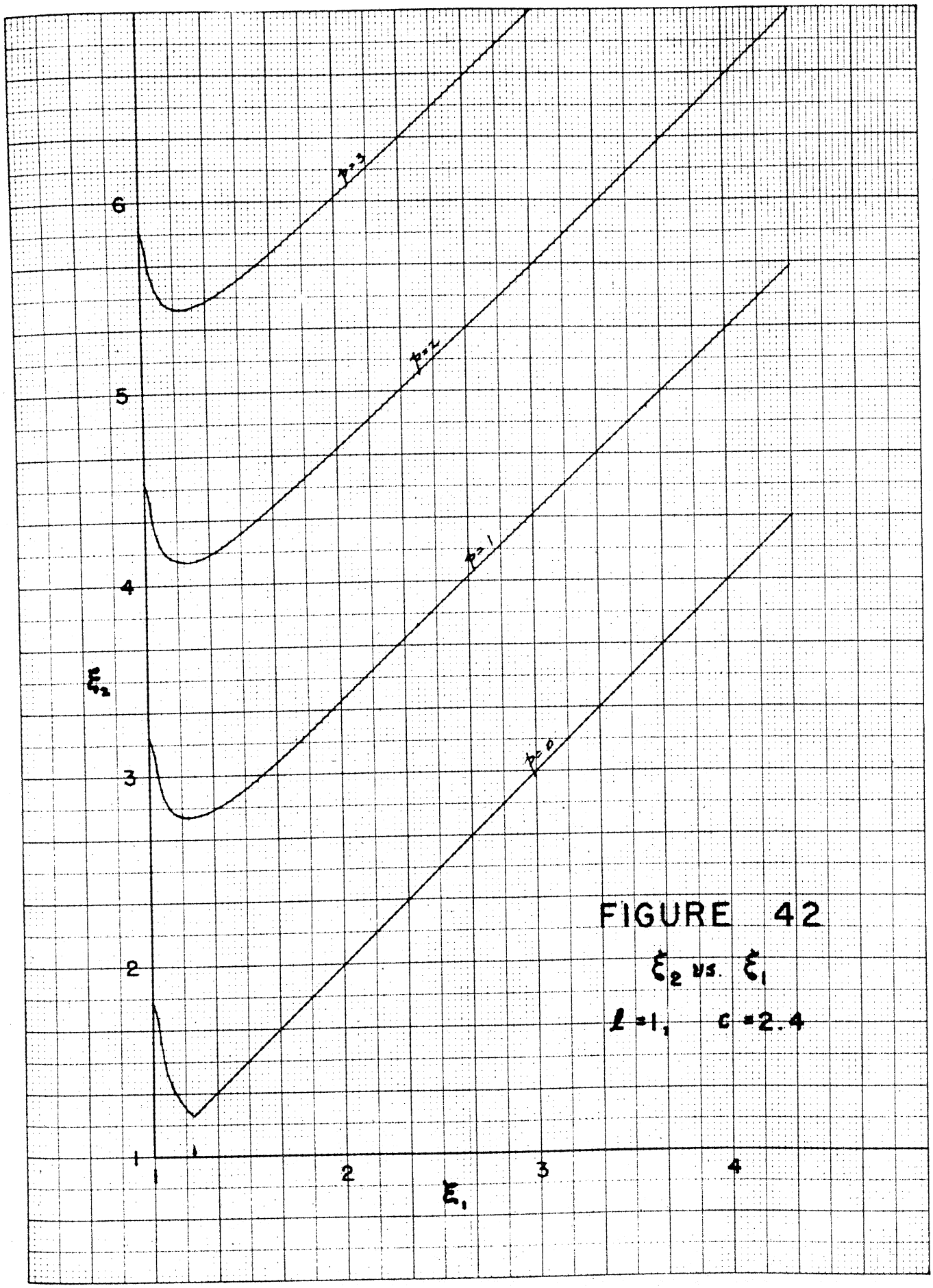

FIGURE 42

ξ_2 vs. ξ_1

$l = 1,\quad c = 2.4$

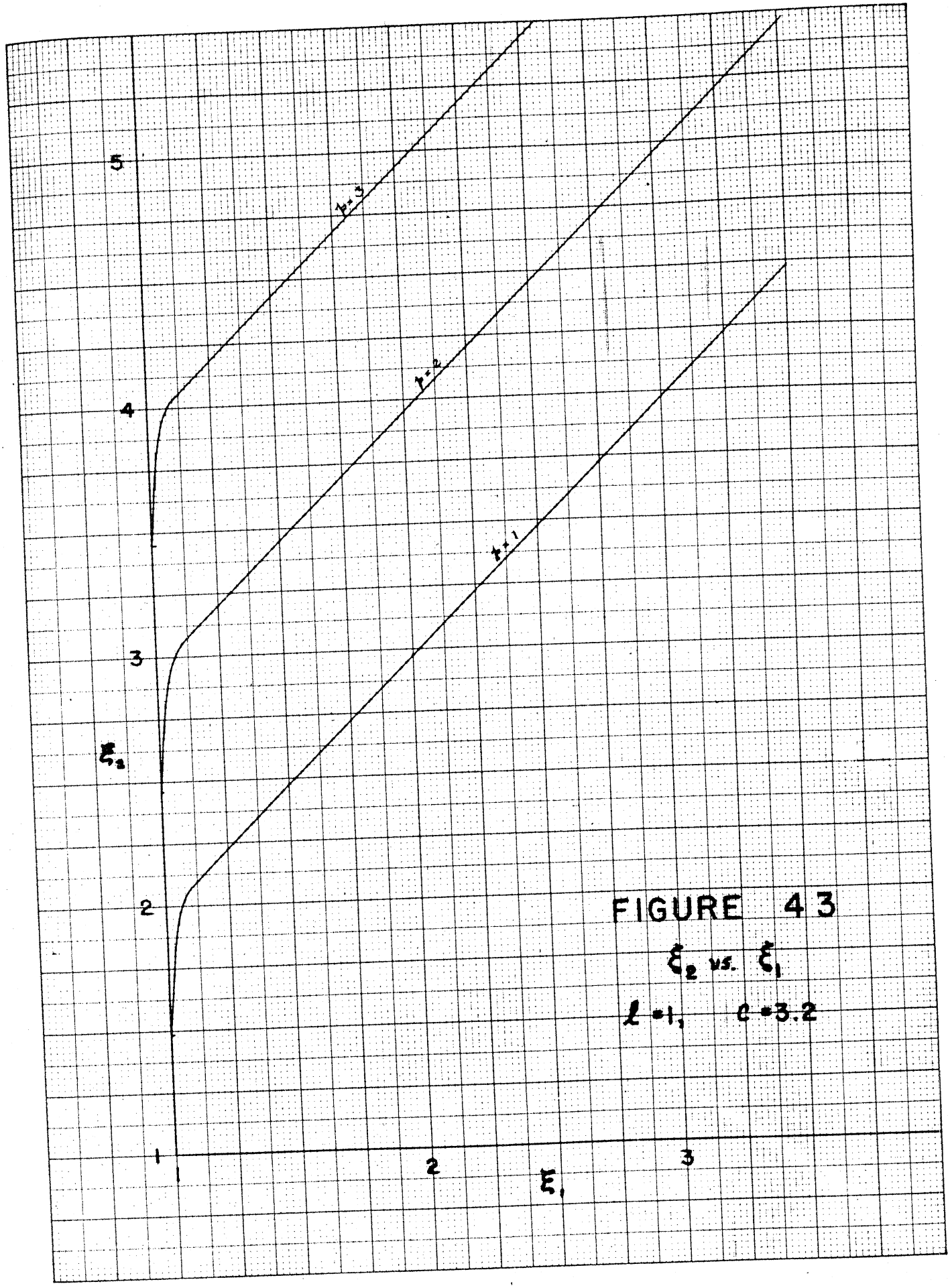

FIGURE 43

ξ_2 vs. ξ_1

$\ell = 1, \quad c = 3.2$

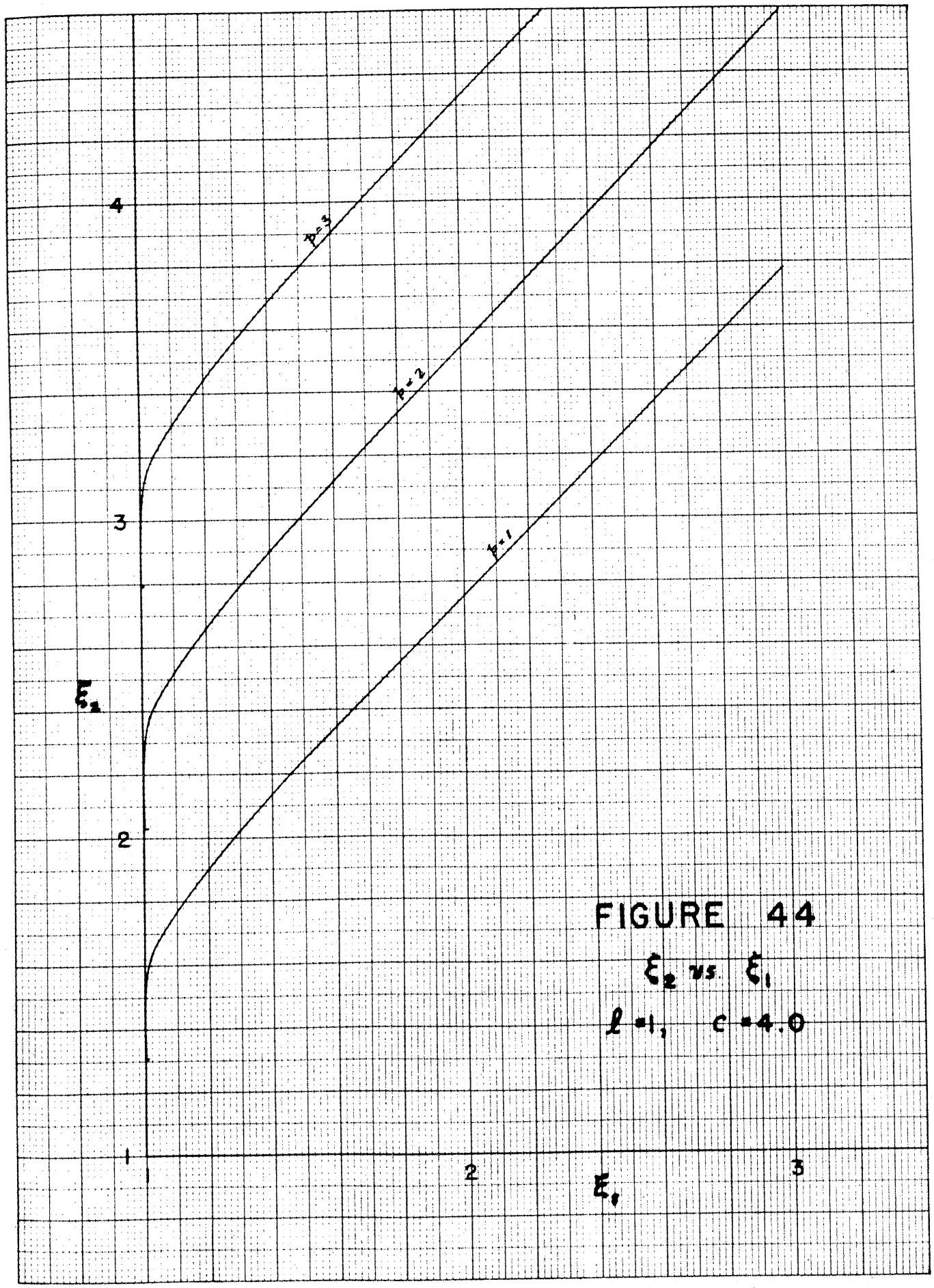

FIGURE 44

ξ_2 vs. ξ_1

$\ell = 1, \quad c = 4.0$

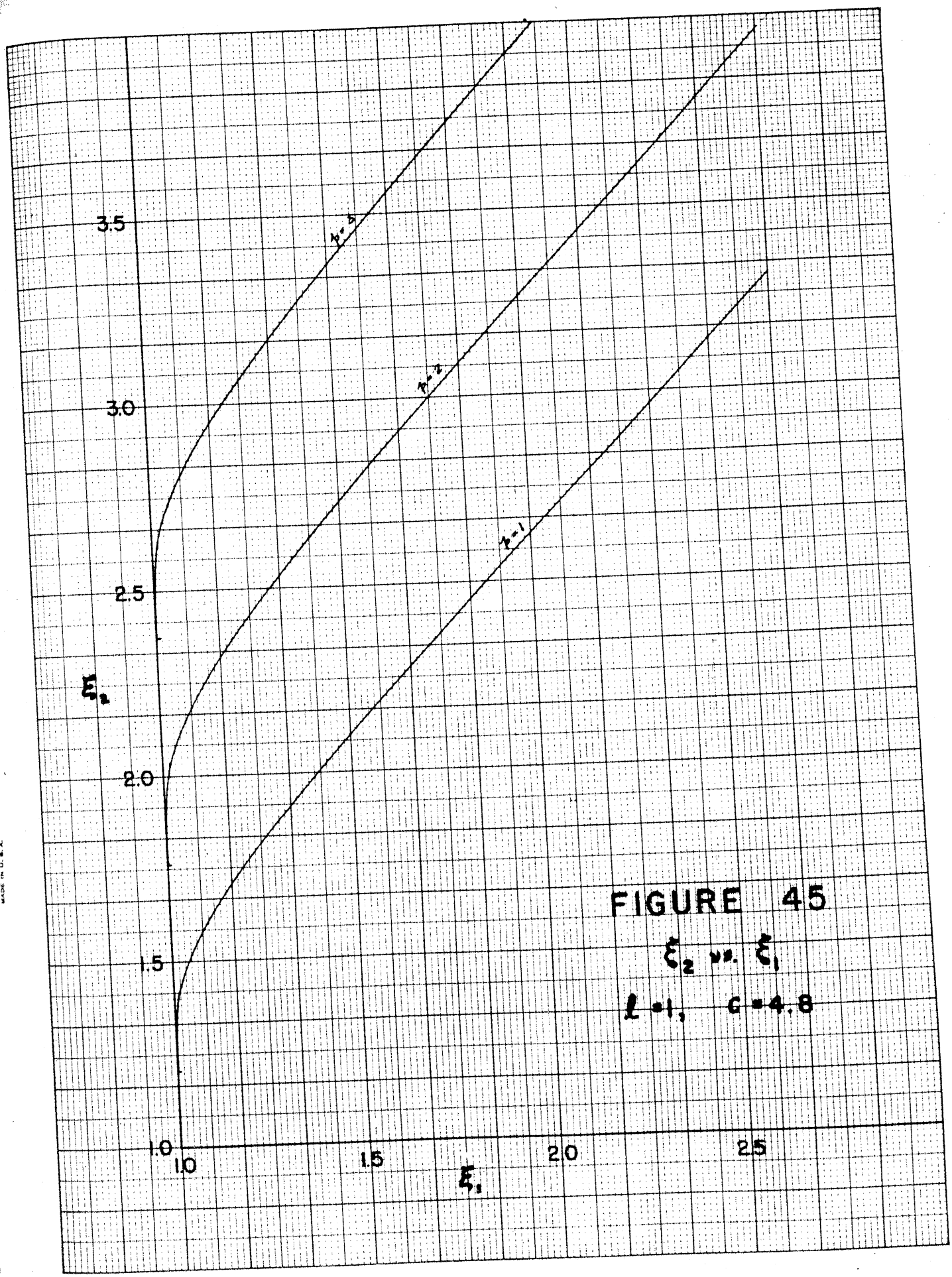

FIGURE 45

ξ_2 vs. ξ_1

$\ell = 1, \quad c = 4.8$

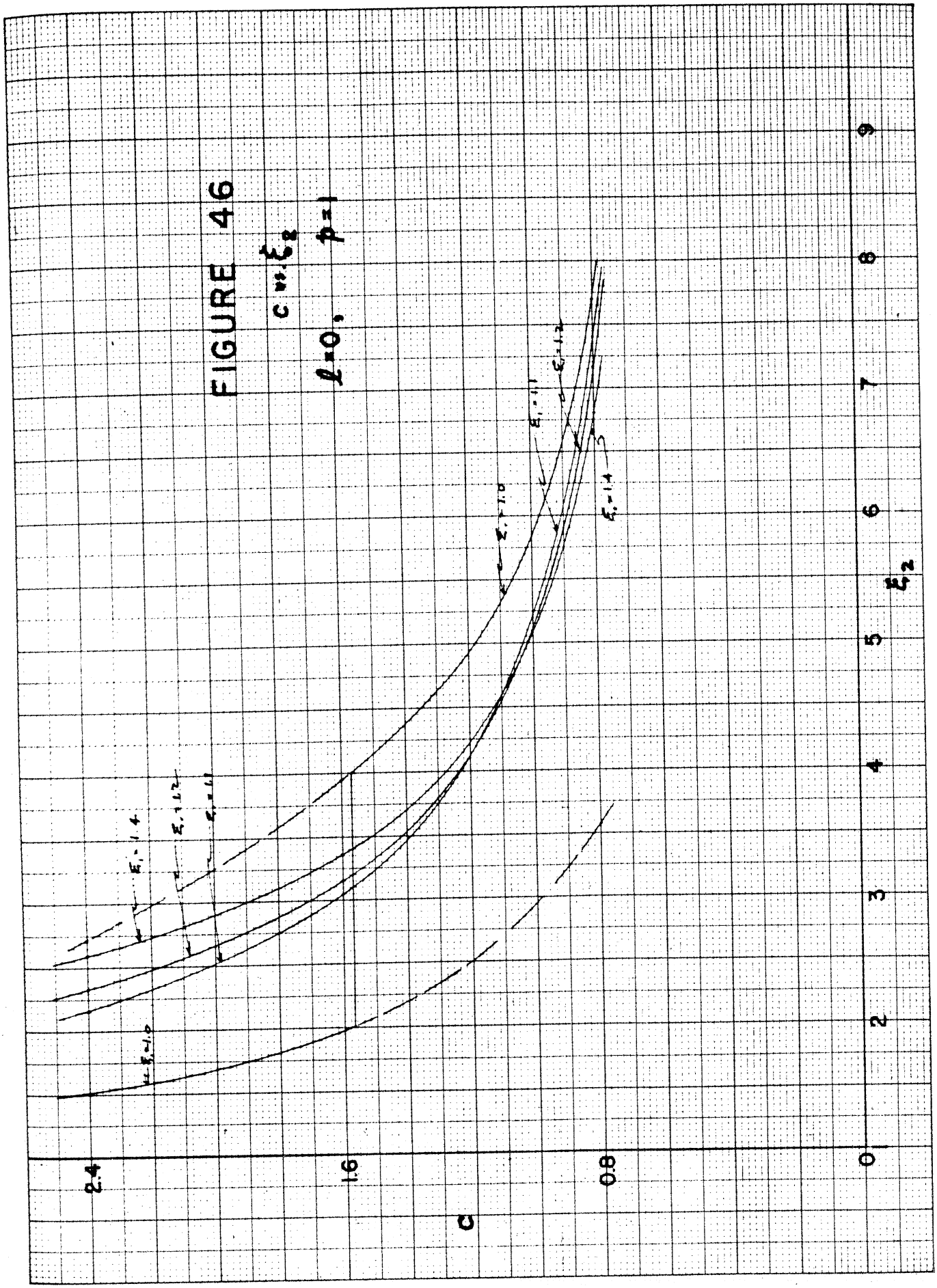
FIGURE 46
c vs. ξ_2
$\ell = 0$, $p = 1$
c
2.4
1.6
0.8
0
2
3
4
5
6
7
8
9
ξ_2
$\xi_1 = 1.4$
$\xi_1 = 1.2$
$\xi_1 = 1.1$
$\xi_1 = 1.0$
$\xi_1 = 1.1$
$\xi_1 = 1.2$
$\xi_1 = 1.4$
$\xi_1 = 1.0$

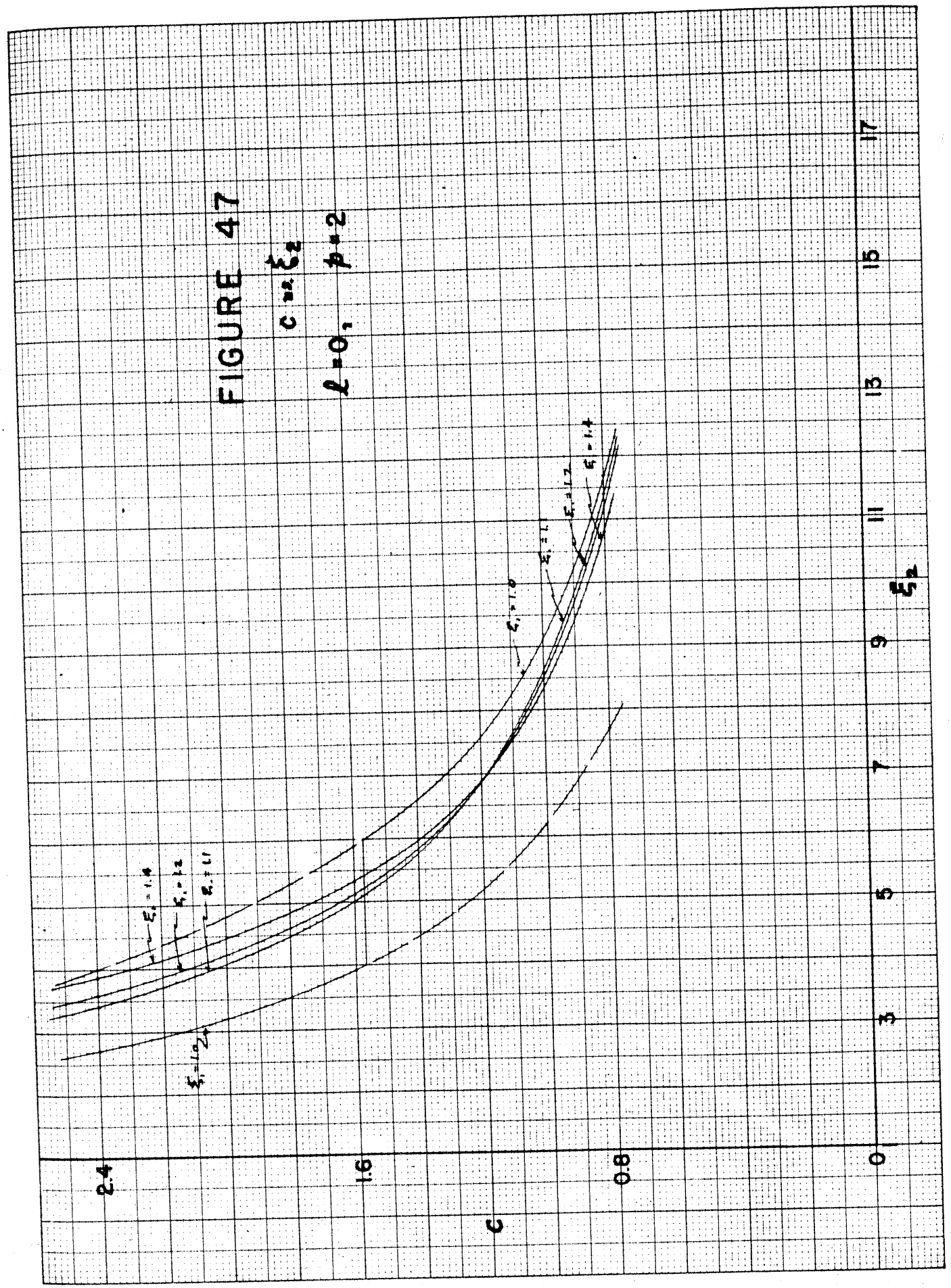
FIGURE 47
c = ξ1, ξ2
l = 0, p = 2
c
ξ2
0
3
5
7
9
11
13
15
17
0.8
1.6
2.4
ξ1 = 1.0
ξ1 = 1.1
ξ1 = 1.2
ξ1 = 1.3
ξ1 = 1.4
ξ1 = 1.2
ξ1 = 1.1

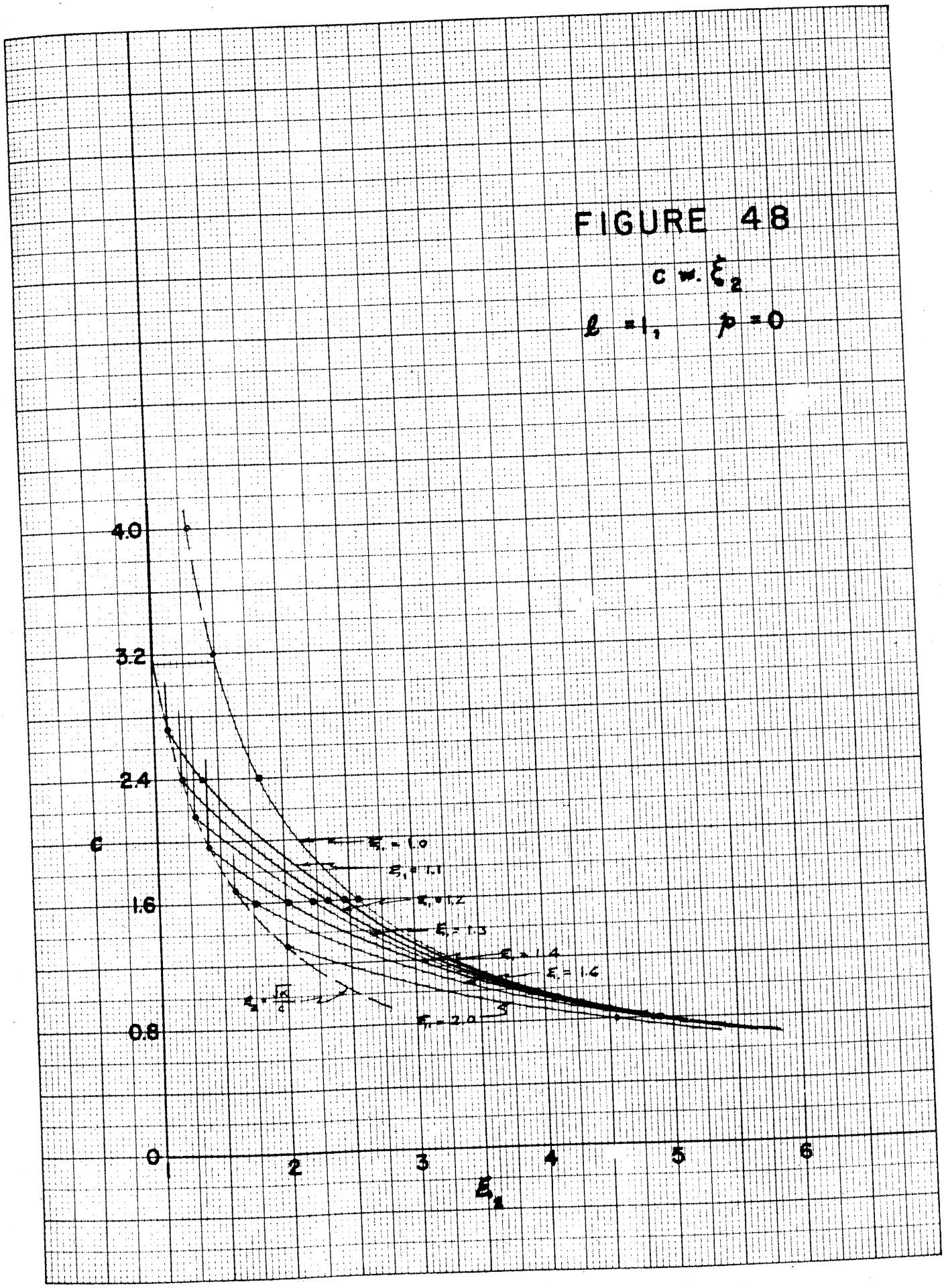
FIGURE 48
c w. ξ2
ℓ = 1, p = 0
4.0
3.2
2.4
1.6
0.8
0
c
2
3
4
5
6
ξ1
ξ1 = 1.0
ξ1 = 1.1
ξ1 = 1.2
ξ1 = 1.3
ξ1 = 1.4
ξ1 = 1.6
ξ1 = 2.0
ξ2 = √K / d

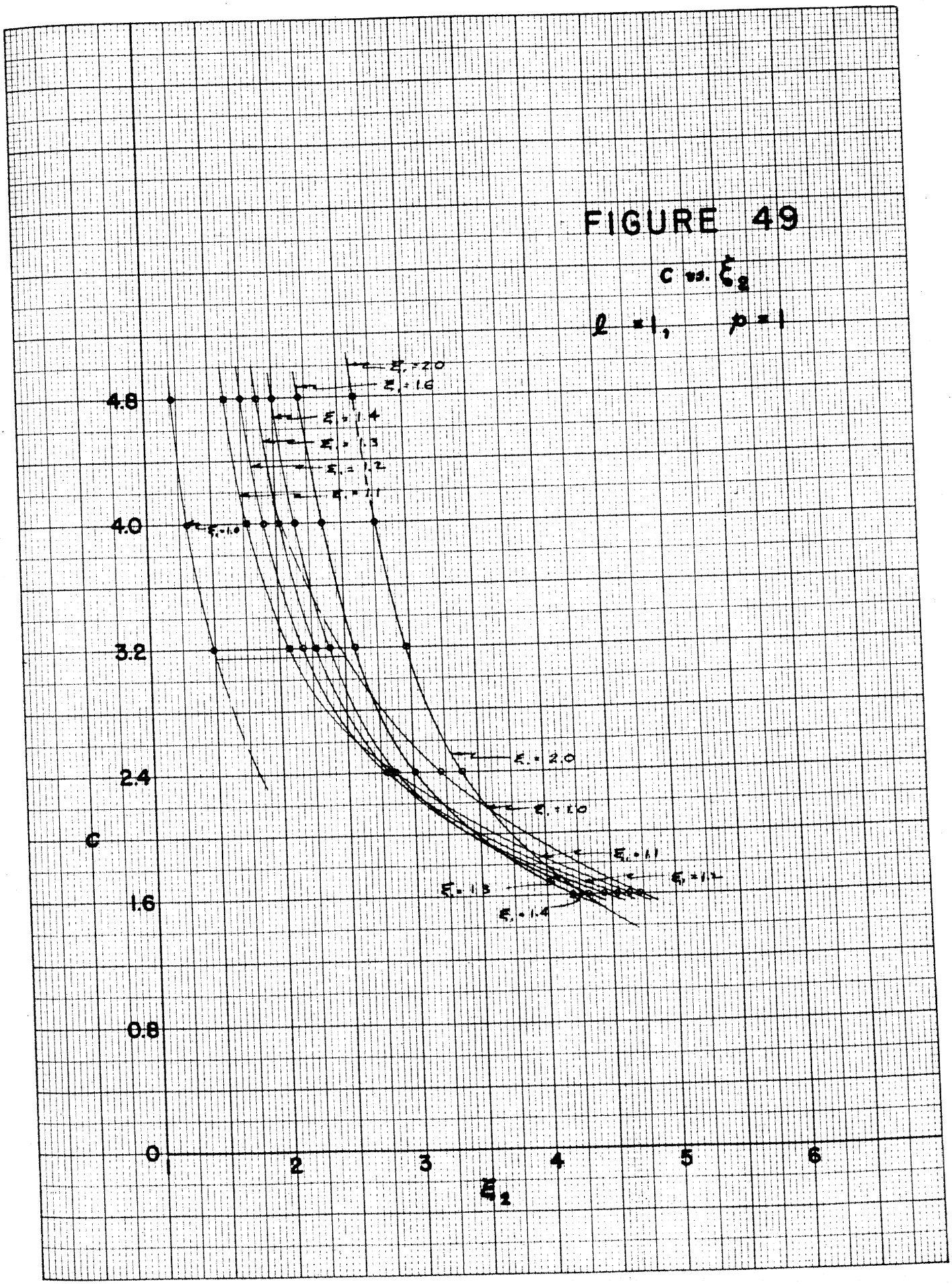
FIGURE 49
C vs. ξ_2
$\ell = 1, \quad p = 1$
$\xi_1 = 2.0$
$\xi_1 = 1.6$
$\xi_1 = 1.4$
$\xi_1 = 1.3$
$\xi_1 = 1.2$
$\xi_1 = 1.1$
$\xi_1 = 1.0$
$\xi_1 = 2.0$
$\xi_1 = 1.0$
$\xi_1 = 1.1$
$\xi_1 = 1.2$
$\xi_1 = 1.3$
$\xi_1 = 1.4$
C
4.8
4.0
3.2
2.4
1.6
0.8
0
1
2
3
4
5
6
ξ_2

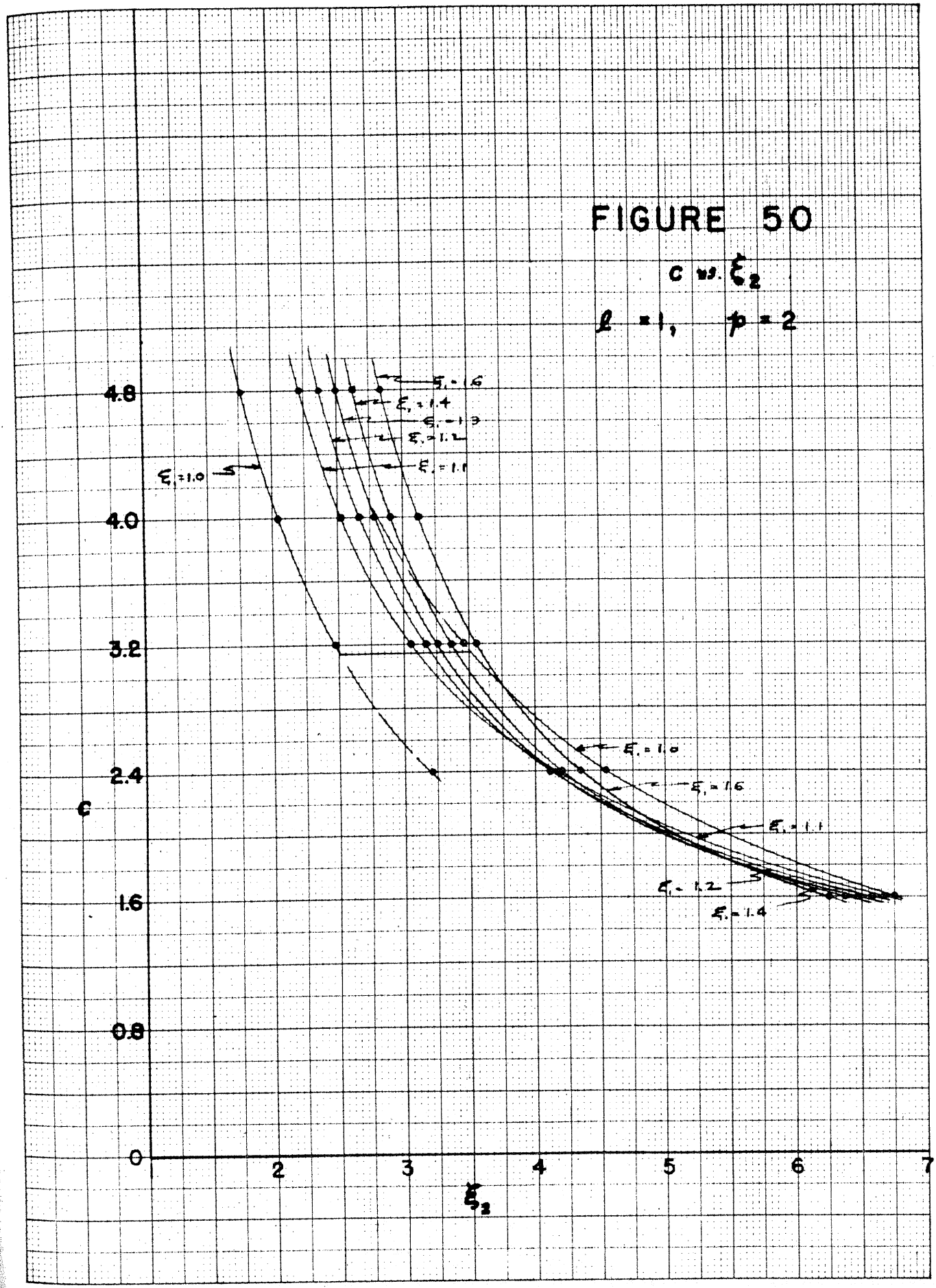
FIGURE 50
c vs. ξ_2
$\ell = 1, \quad p = 2$
4.8
4.0
3.2
2.4
1.6
0.8
0
c
2
3
4
5
6
7
ξ_2
$\xi_1 = 1.6$
$\xi_1 = 1.4$
$\xi_1 = 1.3$
$\xi_1 = 1.2$
$\xi_1 = 1.1$
$\xi_1 = 1.0$
$\xi_1 = 1.0$
$\xi_1 = 1.6$
$\xi_1 = 1.1$
$\xi_1 = 1.2$
$\xi_1 = 1.4$

APPENDIX D

EXPANSION COEFFICIENTS FOR SMCH FUNCTIONS

1. Recursion Formula

The fundamental three-term recursion formula for the SMCH representations has the form

$$A_{n+2}\, a_{n+2} + B_n\, a_n + C_{n-2}\, a_{n-2} = 0 \qquad \text{(D.1)}$$

where

$$A_{n+2} = \frac{(n+1)(n+2)}{(2n+5)(2n+7)}$$

$$B_n = \frac{\alpha - (n+1)(n+2)}{c^2} - \frac{2(n+1)(n+2) - 3}{(2n+1)(2n+5)}$$

$$C_{n-2} = \frac{(n+1)(n+2)}{(2n-1)(2n+1)} \qquad \text{(D.2)}$$

It is apparent that (D.1) can be developed as a continued fraction, in the form

$$\frac{a_\ell}{a_{\ell-2}} = -\frac{C_{\ell-2}}{B_\ell + A_{\ell+2}\frac{a_{\ell+2}}{a_\ell}}$$

$$= -\frac{C_{\ell-2}}{B_\ell - \dfrac{A_{\ell+2}\, C_\ell}{B_{\ell+2} - \cdots - \dfrac{A_n\, C_{n-2}}{B_n + A_{n+2}\frac{a_{n+2}}{a_n}}}} \qquad \text{(D.3)}$$

If the series is to converge, the value of $a_\ell / a_{\ell-2}$ will be unaffected by the last term a_{n+2}/a_n, provided n is chosen sufficiently larger than ℓ. In practice, examination of the numerical values of terms of the series will reveal whether n has been chosen large enough.

The ratio may be approached in the opposite direction by developing (D.1) in the alternate form,

$$\frac{a_{\ell-2}}{a_\ell} = -\frac{A_\ell}{B_{\ell-2} + C_{\ell-4}\frac{a_{\ell-4}}{a_{\ell-2}}}$$

$$= -\frac{A_\ell}{B_{\ell-2} - \dfrac{A_{\ell-2}C_{\ell-4}}{B_{\ell-4} - \cdots \cdots - \dfrac{A_{-n+2}C_{-n}}{B_{-n} + C_{-n-2}\dfrac{a_{-n-2}}{a_{-n}}}}} \qquad \text{(D.4)}$$

2. Additional Coefficients

It was found that in order to take advantage of the five-figure accuracy of the tabulated coefficients, it was necessary to extend the tables in both directions. Values of the ratios $a_\ell / a_{\ell-2}$ were computed using (D.3) and then from the last tabulated coefficient a_n the higher orders computed. Additional coefficients computed in this fashion are given in Table 12.

Similarly the ratio

$$\frac{\left(\dfrac{d_{-n}}{\rho}\right)}{\left(\dfrac{d_{-(n-2)}}{\rho}\right)}$$

was computed by means

of (D.4), and using (6.21). Additional higher orders of the coefficients $d_{-n}(c)/\rho$ computed thus are listed in Table 13.

TABLE 12

	C	0.8	1.6	2.4	3.2	4.0	4.8	
$\ell=0$ $m=1$		.(7)12734						a_8
		(0)20909	.(7)18666					a_{10}
		.(13)23282	.(10)83661	(8)87990				a_{12}
		(16)191740	(12)27491	.(10)64756				a_{14}
		.(9)12067	(5)69068	(2)36479				a_{16}
			.(7)13697	.(4)16232				a_{18}
			(20)21986	.(7)58490				a_{20}
$\ell=1$ $m=1$		.188658						a_9
		(0)11928						a_{11}
		.(13)11640	.(0)44259	.(8)50693				a_{13}
		.(17)84918	.(2)12878	.(10)33147	.(8)15582	(7)28227	.(6)27577	a_{15}
			.(15)29035	(12)16800	(10)14016	(9)39566	.(8)55443	a_{17}
			(8)52231	.(15)67944	.(2)10063	(1)44292	.(10)89088	a_{19}
			(21)74997	.(17)22441	(5)59023	.(13)40516	.(11)11704	a_{21}
					(7)28811	.(15)30855	.(13)12806	a_{23}
						.(17)1987	.(15)1185	a_{25}

TABLE 13

	c	0.8	1.6	2.4	3.2	4.0	4.8	
$\ell=0$ $m=1$		.(12)73328						d_{-12}/ρ
		-(15)69316						d_{-14}/ρ
		.(18)49246	.(12)51528	-(11)68564				d_{-16}/ρ
			.(14)11379	.(13)33936				d_{-18}/ρ
			-(17)20130	-(15)13466				d_{-20}/ρ
$\ell=1$ $m=1$		.(8)13254						d_{-9}/ρ
		-(11)22164						d_{-11}/ρ
		.(14)25385	.(10)43056					d_{-13}/ρ
		-.(17)21185	-(12)14361	-(9)12148	.(7)87396*			d_{-15}/ρ
			.(15)36486	.(13)69353	-(9)88488	-(8)17615	-(7)12151	d_{-17}/ρ
				-(14)31185	.(11)70603	.(10)21896	.(9)21654	d_{-19}/ρ
				.(16)11333	-(13)45545	-(12)22016	-(11)31243	d_{-21}/ρ

* Correction to erroneous value of .(7)87383 tabulated in SMCH, p. 98.

APPENDIX E

"RADIAL" SOLUTIONS IN THE VICINITY OF THE POLE

1. Langer's Solutions

The treatment of Langer's method, outlined in Chapter VII, introduces the functions

$$F(x,c) = \left[\frac{v(x)}{w(x)}\right]^{\frac{1}{2}} J_1[v(x)] \tag{E.1}$$

$$G(x,c) = \left[\frac{v(x)}{w(x)}\right]^{\frac{1}{2}} N_1[v(x)] \tag{E.2}$$

where $J_1(v)$ and $N_1(v)$ are the usual Bessel functions of argument v, and

$$w(x) \triangleq \sqrt{\frac{A}{x} + B}$$
$$v(x) \triangleq \int_0^x w(z)\,dz \tag{E.3}$$

Here

$$A = \frac{c^2 - \alpha(c)}{2}$$
$$B = \frac{3c^2 + \alpha(c)}{4} = c^2 - \frac{A}{2} \tag{E.4}$$

The derivatives with respect to x are

$$F'(x,c) = \sqrt{v\,w}\left\{J_0(v) - \frac{J_1(v)}{2}\left[\frac{1}{v} + \frac{w'}{w^2}\right]\right\}$$
$$G'(x,c) = \sqrt{v\,w}\left\{N_0(v) - \frac{N_1(v)}{2}\left[\frac{1}{v} + \frac{w'}{w^2}\right]\right\} \tag{E.5}$$

Some of these functions may be indeterminate at $x = 0$. In any case at $x = 0$ the expressions reduce to:

$$F(0,c) = 0$$
$$G(0,c) = -\frac{1}{\pi}\sqrt{\frac{2}{A}} \tag{E.6}$$
$$F'(0,c) = \sqrt{2A}$$
$$G'(0,c) = -\infty$$

For small values of x, these functions have been computed for $\ell = 0$, $c = 2.4$ and $\ell = 1$, $c = 4.0$, 4.8; the results are given in Tables 14 to 16. The power series solution of the reduced equation (7.5) using the expansion (7.6) is also given under the headings $\hat{F}$ and $\hat{F}'$.

2. Connection to SMCH Solutions

These solutions have been joined to the SMCH series representations at $x = 0.1$. The function J in the tables is the solution computed from the power series $\hat{F}$. From F the function J has also been computed and is given as $[J]$. Since the power series representation is more accurate it has been the one used in further calculations. Similarly, from $\hat{F}$ and G, the function K has been computed. Following this, γ, β, and χ have also been computed. The function $[J]$ is of interest mainly for comparison with J; the difference between these two functions should be an indication of the accuracy with which $G(x,c)$ approximates the exact solution of (7.5). A typical set of solutions is shown by Figure 51.

3. An Alternate Representation

In this appendix we are seeking irregular solutions of the equation

$$X''(x) + \left(\frac{A}{x} + B\right) X(x) = 0 \qquad (E.7)$$

obtained from (7.5) by neglecting all terms beyond the second in (7.6), and substituting from (E.4). Because of the approximation we must confine our interest in the argument to values in the range $0 \leq x \ll 1$.

This equation is a special case of the confluent hypergeometric equation and so is formally satisfied by Whittaker's[1] functions; however, the expressions are not in a convenient form for calculation owing to the occurrence of imaginaries in real expressions. When $c < (\ell+1)\pi/2$, there is a turning point of (E.7) for a value of $\chi > 0$, which implies a zero of $w^2(\chi)$ there, in close proximity to the pole at the origin; it will be remembered that

$$w^2(\chi) = \frac{A}{\chi} + B \qquad (E.8)$$

For smaller values of χ, $w^2(\chi)$ is negative, $w(\chi)$ is imaginary, and Langer's solutions as given by (E.1) and (E.2) become complex. To circumvent this difficulty Langer has proposed alternate forms which employ the modified Bessel functions of the first and second kinds, eliminating the occurrence of imaginaries and yielding real functions. This method has been tried for the case where $\ell = 1$, $c = 2.4$; it was found that the results deviated greatly from what one must expect on general considerations, and so they were rejected. Trial seems to be the only way of determining the region of validity of Langer's approximations. Their failure here is apparently due to the proximity of the zero and pole of $w^2(\chi)$.

A third attack on the problem is possible. Equation (E.7) is equivalent in form to the radial equation arising in the quantum mechanical problem of a particle in a positive energy state being scattered

---

(1) E. T. Whittaker and G. N. Watson, "Modern Analysis," Chap. XVI, 4th Ed., MacMillan, 1948.

by a repulsive Coulomb field.[1] Yost, Wheeler, and Breit have developed exact formulas[2] and computed the functions necessary to the study of this problem. Their results have been used to compute solutions of (E.7) for the case $\ell = 1$, $c = 2.4$; the data may be found in Table 17. The work of Yost, Wheeler and Breit is useful for any smaller values of c, but values greater than 2.4 correspond to energies higher than they have considered, and extrapolation in this region is not too reliable.

4. WKBJ Solutions

When $0 < (c^2 - \alpha) \ll 1$, the Langer solutions are found by trial to be concave away from the x axis, and so are not valid. This is probably due to the zero of $w^2(x)$ which, although occurring at a value of $x < 0$, is still extremely close to the pole at the origin. In this event the WKBJ approximation is fairly satisfactory to project the SMCH solutions in toward the pole from known values. We use

$$\psi_1(x, c) = \frac{1}{\sqrt{w(x)}} \cos[v(x) - v(x_0)]$$

$$\psi_2(x, c) = \frac{1}{\sqrt{w(x)}} \sin[v(x) - v(x_0)] \qquad \text{(E.9)}$$

and form linear combinations of the two to join at $x = 0.1$ to the SMCH solutions already established. The results for $\ell = 0$, $c = 1.6$ and

---

(1) N. F. Mott and H. S. W. Massey, "Theory of Atomic Collisions," p. 52, 2nd Ed., Oxford, 1949. The substitution $X = \rho L$ transforms their Eq. (25) to a form identical with our (E.7), after placing n (the quantum number relating to angular momentum) equal to zero.

(2) F. L. Yost, J. A. Wheeler, and G. Breit, "Coulomb Wave Functions in Repulsive Fields," Phys. Rev. 49, 174 (1936); J. Terres. Mag. and Atmos. Elec. 40, 443 (1935).

and $\ell = 1$, $c = 3.2$ are given in Tables 18 and 19. Figure 52 is typical and shows the deviation from the power series solution as $\chi \rightarrow 0$. From other results it is estimated that the solutions for $\ell = 1$, $c = 3.2$ are not sufficiently accurate below $\chi = 0.4$ to indicate the behavior of the system satisfactorily.

In addition to those mentioned in Appendix C, use has been made of the following tables:

"Tables of the Bessel Functions of the First Kind of Orders Zero and One," Computation Laboratory, Harvard, 1947.

"Tables of the Bessel Functions $Y_0(x)$, $Y_1(x)$, $K_0(x)$, $K_1(x)$," National Bureau of Standards, U. S. Govt. Printing Office, 1948.

"Bessel Functions, Part I, Functions of Orders Zero and Unity," Vol. VI, British Assoc. for the Advancement of Science, Cambridge, 1937.

TABLE 14

x	F	G	F′	G′	$\hat{F}$	$\hat{F}'$	[J]	[J]′	E
0	0	−.10832	1.6549	$-\infty$	0	1.0	0	3.3270	1.0
.001	.0016538	−.38761	1.6526	−2.384	.0009992	.99863	.0033248	3.3224	1.001
.01	.016437	−.40156	1.6323	−1.1481	.0099308	.98610	.033045	3.2815	1.01
.02	.032648	−.41088	1.6099	−.7618	.019721	.97180	.065635	3.2365	1.02
.04	.064395	−.42170	1.5649	−.36203	.038861	.94201	.12946	3.1460	1.04
.10	.15415	−.42405	1.4253	.20897	.092502	.84391	.30990	2.8654	1.10

x	J	K	J′	K′	$\hat{F}$	β	$\mathcal{I}(\xi_1)$	E
0	0	−.19086	3.3502	$-\infty$	0+	$0^{-\pi+}$	0	1.0
.001	.0033499	−.68280	3.3456	−4.035	.8291	.69225	.43323	1.001
.01	.033270	−.70588	3.3036	−1.8591	1.7770	1.05822	.59884	1.01
.02	.066069	−.72069	3.2557	−1.1808	2.7572	1.28286	.65498	1.02
.04	.13019	−.73658	3.1559	−.4813	6.557	1.41945	.70853	1.04
.10	.30990	−.73181	2.8270	.50847	−5.5598	-1.39^{0+}284	.77511	1.10

$$J = 3.3502\,\hat{F}$$

$$K = .1662\,\hat{F} + 1.7620\,G$$

$A = 1.3694$ $\qquad$ $\ell = 0$

$B = 5.0753$ $\qquad$ $c = 2.4$

TABLE 15

λ	G	G′	$\hat{F}$	$\hat{F}'$	[J]	[J]′	E
.00	−.31630	$-\infty$	0	1.00000			1.0
.001	−.31939	−2.447	.000999	.99799			1.001
.005	−.32655	−1.405	.004974	.98971			1.005
.01	−.33233	−.9513	.009897	.97910			1.01
.02	−.33833	−.44895	.019578	.95695			1.02
.04	−.34210	.02305	.038246	.90906			1.04
.06	−.33852	.31944	.055910	.85668			1.06
.10	−.31690	.73609	.087893	.73995			1.10

λ	J	K	J′	K′	γ	β	$\Sigma(\ell_1)$	E
.00	0	−.74697	5.5681	$-\infty$	0+	$\overset{-\pi+}{0+}$	0	1.0
.001	.005563	−.75381	5.5568	−5.319	1.045	.80740	.54077	1.001
.005	.02770	−.76889	5.5108	−2.862	1.926	1.0919	.66963	1.005
.01	.05511	−.78027	5.4517	−1.795	3.0367	1.2527	.72389	1.01
.02	.10901	−.78998	5.3284	−.6192	8.6030	1.45510	.77211	1.02
.04	.21296	−.79028	5.0617	.4734	−10.692	$\overset{0+:}{-1.47754}$	.80667	1.04
.06	.31131	−.77368	4.7701	1.1492	−4.1508	−1.33438	.82507	1.06
.10	.48947	−.7079	4.1201	2.0793	−1.9816	−1.10342	.85291	1.10

$J = 5.5681\,\hat{F}$

$K = .4609\,\hat{F} + 2.3616\,G$

A = 2.0256

B = 14.987

$\ell = 1$

c = 4.0

TABLE 16

x	F	G	F′	G′	$\hat{F}$	$\hat{F}'$	[J]	[J]′	E
0	0	-.21277	2.9920	$-\infty$	0	1.0	0	4.3572	1.0
.001	.002985	-.21742	2.9788	-3.6942	.000998	.99552	.004347	433.80	1.001
.005	.014793	-.22820	2.9249	-2.0850	.004944	.97749	.02154	4.2595	1.005
.01	.029251	-.23659	2.8577	-1.3496	.009774	.95472	.04260	4.1617	1.01
.02	.057151	-.24578	2.7226	-0.56922	.019091	.90847	.08323	3.9649	1.02
.10	.23077	-.19165	1.6097	1.4219	.076282	.51690	.33609	2.3442	1.10

x	J	K	J′	K′	r	β	$\Sigma(\varepsilon_i)$	E
						$-\pi+:$		
0	0	-.30681	4.4058	$-\infty$	0+	0+	0	1.00
.001	.004397	-.31325	4.3860	-5.0625	.86637	.71392	.20179	1.001
.005	.021782	-.32775	4.3066	-2.7469	1.5678	1.00302	.26461	1.005
.01	.043062	-.33857	4.2063	-1.6925	2.4853	1.18825	.29802	1.01
.02	.084110	-.34934	4.0025	-.57943	6.9077	1.42703	.33368	1.02
.10	.33608	-.25609	2.2763	2.1877	-1.0405	$0+:$ -.80924	0.44750	1.10

$J = 4.4058\ \hat{F}$

$K = .2657\ \hat{F} + 1.4420\ G$

$A = 4.4761$

$B = 20.802$

$\ell = 1$

$c = 48$

TABLE 17

χ	$\hat{G}$	$\hat{G}'$	$\hat{F}$	$\hat{F}'$	ξ
.00	∞	$-\infty$	0	1.0	1.00
.01	.96	-4.6	0.010064	1.01263	1.01
.02	.925	-2.5	.020251	1.02470	1.02
.04	.888	-1.64	.040973	1.04709	1.04
.06	.860	-1.30	.062119	1.06709	1.06
.10	.815	-.98	.10549	1.09965	1.10

χ	J	K	J'	K'	μ	β	$\mathbb{X}(\varepsilon_1)$	ξ
.00	0	$-\infty$	5.1868	$+\infty$	0-	0-	0	1.00
.01	.052200	-4.912	5.2523	93.48	-.2237	-.2201	1.123	1.01
.02	.10504	-4.733	5.3149	12.74	-.4172	-.3953	1.920	1.02
.04	.21252	-4.545	5.4310	8.339	-.6513	-.5773	2.658	1.04
.06	.32220	-4.403	5.5348	6.599	-.8389	-.6979	3.076	1.06
.10	.54716	-4.1761	5.7042	4.9619	-1.1496	-.85489	3.5100	1.10

$$J = 5.1868\ \hat{F}$$

$$K = -0.049\ \hat{F} - 5.116\ \hat{G}$$

$A = -1.2915$

$B = 6.4058$

$\ell = 1$

$c = 2.4$

TABLE 18

χ	ψ_1	ψ_2	ψ_1'	ψ_2'	$\hat{F}$	$\hat{F}'$	[J]	[J]′	ξ
0					0	1.0			1.0
.02	.68157	-.099686	3.8554	.90335	.019989	.99873	.05073	3.6676	1.02
.04	.72750	-.077381	1.3819	1.2276	.039943	.99645	.12102	3.3971	1.04
.06	.74735	-.05208	.71408	1.2883	.059840	.99316	.18748	3.2622	1.06
.08	.75815	-.02612	.41874	1.3046	.079662	.98885	.25174	3.1782	1.08
.10	.76494	0	.24877	1.3073	.099388	.98355	.31472	3.1145	1.10

χ	J	K	J′	K′	$\gamma^{(1)}$	β	$\mathbf{X}(\xi_1)$	ξ
						$-\pi^+$		
0	0		3.1666	$-\infty$	0+	0+	0	1.0
.02	.063297	-1.8505	3.1626	-5.793	.5459	.4997	.83113	1.02
.04	.12648	-1.9036	3.1554	-.974	3.240	1.2714	1.7816	1.04
.06	.18949	-1.9114	3.1449	-.017	185.	1.5654	1.9103	1.06
.08	.25226	-1.9081	3.1313	.306	-10.23	0^+ -1.4733	1.9236	1.08
.10	.31472	-1.9006	3.1145	.44690	-6.9692	-1.42828	1.9260	1.10

$$J = 3.1666\,\hat{F}$$

$$K = -19.123\,\hat{F} + 14.729\,\psi_2$$

$$[J] = .41143\,\psi_1 + 2.3041\,\psi_2$$

$A = .03800$

$B = 2.5410$

$\ell = 0$

$c = 1.6$

TABLE 19

χ	ψ_1	ψ_2	ψ_1'	ψ_2'	$\hat{F}$	$\hat{F}'$	$[J]$	$[J]'$	ξ
0					0	1.0			1.00
.001	.27567	-.11042	64.744	-22.306	.00100	.99987	-.0333	3.0288	1.001
.005	.38938	-.14262	14.472	-2.7325	.004999	.99927	-.0072	7.4488	1.005
.01	.43768	-.14767	6.5927	.06055	.009992	.99829	.02982	7.2848	1.01
.02	.47330	-.13592	2.6217	1.3600	.019963	.99558	.10335	6.8936	1.02
.04	.51456	-.10817	1.1193	1.7081	.039797	.98712	.23083	6.3162	1.04
.10	.54535	.00000	.14286	1.8337	.097724	.93792	.58762	5.6397	1.10

χ	J	K	J'	K'	Γ	β	$\mathbb{X}(\xi_1)$	ξ
0	0		6.01306	$-\infty$	0+	$0^{-\pi+\varepsilon}$	0	1.0
.001	.006013	-.99908	6.01231	-230.16	.02612	.02611	.02008	1.001
.005	.03006	-1.3947	6.00871	-48.657	.12349	.12287	.14110	1.005
.01	.06008	-1.5520	6.0028	-20.550	.29211	.28420	.37750	1.01
.02	.12004	-1.6489	5.9865	-6.5190	.91832	.74284	1.0269	1.02
.04	.23930	-1.7437	5.9356	-1.3880	4.2764	1.34108	1.6434	1.04
.10	.58762	-1.7061	5.6397	1.8222	-3.0950	$-1.2583^{0+\varepsilon}$	1.8041	1.10

$J = 6.0131\,\hat{F}$

$K = -3.1285\,\psi_1 + 1.2375\,\psi_2$

$[J] = 1.0775\,\psi_1 + 2.9917\,\psi_2$

$A = .11916$

$B = 10.180$

$\ell = 1$

$c = 3.2$

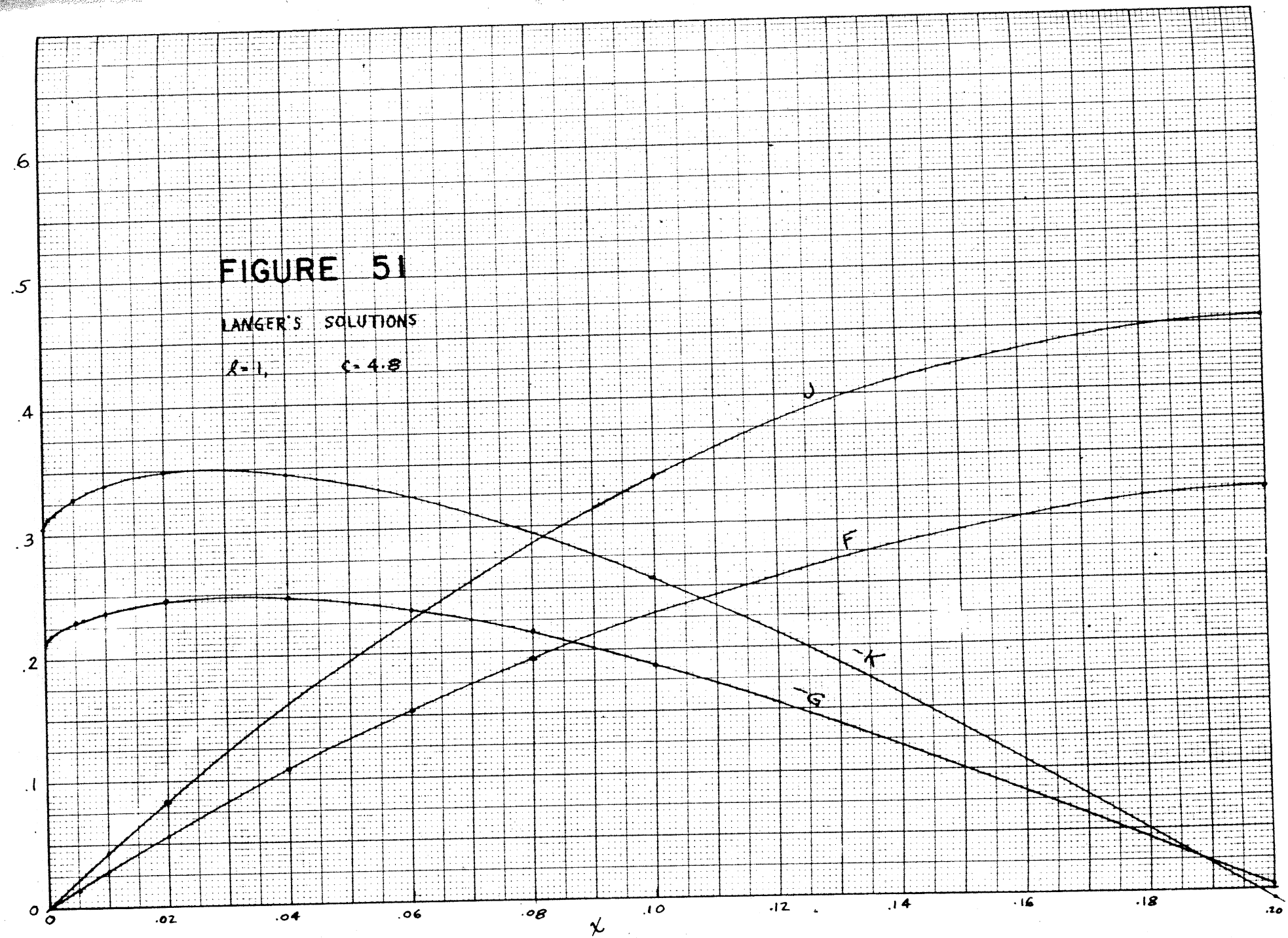
FIGURE 51
LANGER'S SOLUTIONS
$\ell = 1$, $c = 4.8$
J
F
-K
-G
0
.1
.2
.3
.4
.5
.6
0
.02
.04
.06
.08
.10
.12
.14
.16
.18
.20
χ

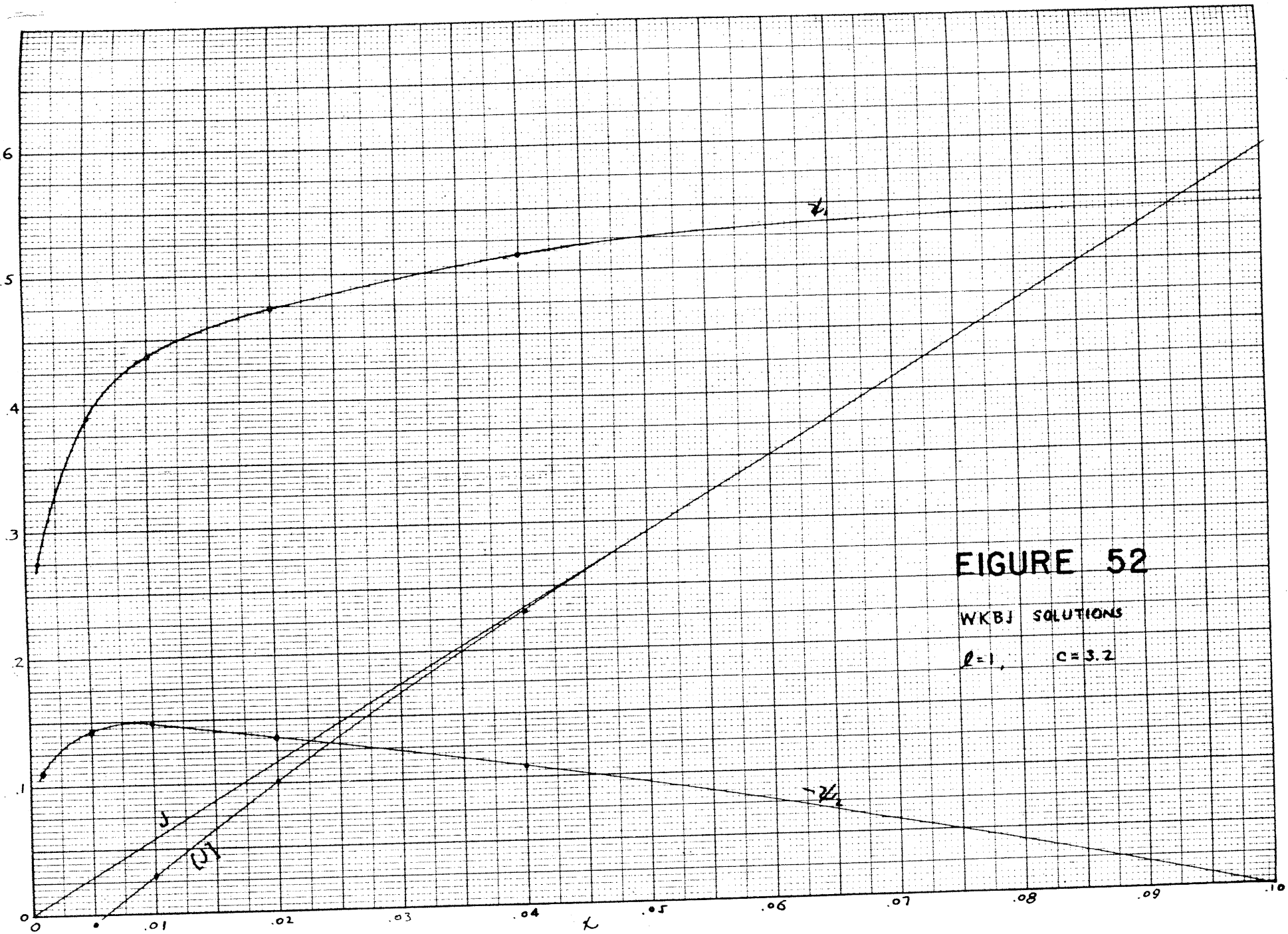

FIGURE 52

WKBJ SOLUTIONS

$\ell = 1$, $c = 3.2$

APPENDIX F

FUNCTIONS RELATED TO LOSSES IN THE WALLS

1. The Functions Ψ_ℓ and g_ℓ^p

In Chapter VIII it was shown that the loss in a single cavity wall could be described by

$$W_1(\xi_1, c) \sim \delta_1 \mu_1 A_0^2 f(c) \Psi_\ell(\xi_1, c) \tag{F.1}$$

where δ_1 is the skin depth, A_0 the field amplitude at a given reference point, and $f(c)$ a function only of the reduced frequency c. The function Ψ_ℓ is defined by (8.24),

$$\Psi_\ell(\xi_1, c) = \frac{c^2}{N_\Theta(c)} X_{\ell p}^2(\xi_1, c) \, \mathcal{Q}_\ell(\xi_1, c) \tag{F.2}$$

The ratio of the losses in the two walls is then

$$\frac{W_1}{W_2} = \frac{\delta_1 \mu_1}{\delta_2 \mu_2} \frac{\Psi_\ell(\xi_1, c)}{\Psi_\ell(\xi_2, c)} \tag{F.3}$$

The electrical characteristics of the conducting wall materials enter this expression only through the skin depth factors. Consequently, it is simpler to discuss the effect of cavity geometry in terms of the function defined by

$$g_\ell^p(\xi_1, \xi_2, c) \triangleq \frac{\Psi_\ell(\xi_1, c)}{\Psi_\ell(\xi_2, c)} \tag{F.4}$$

which is independent of material properties. Upon specification of the wall materials, the actual loss ratio is given directly by

$$\frac{W_1}{W_2} = \frac{\delta_1 \mu_1}{\delta_2 \mu_2} \, g_\ell^p(\xi_1, \xi_2, c) \tag{F.5}$$

Throughout this work the term loss ratio will refer to g_ℓ^p , but it is obvious that it differs from W_1/W_2 only by the constant factor $\delta_1\mu_1/\delta_2\mu_2$.

Tables 20 to 28 give the results of computations of Ψ_ℓ and g_ℓ^p together with corresponding pairs of values of ξ . The results have been shown graphically in Figures 53 to 68. The function $X_\ell(\xi_1,c)$, an intermediate in the calculation of Ψ_ℓ , is also given in the tables; its computation, together with the method of finding values of ξ_2 , has been discussed in Appendix C.

2. The Function

Also necessary to the calculation of Ψ_ℓ is the function $\Omega_\ell(\xi_1,c)$, which amounts to a surface integral over a spheroidal surface for which ξ_1 is constant. We have to calculate

$$\Omega_\ell(\xi_1,c) = \frac{1}{\sqrt{\xi_1^2-1}}\int_{-1}^{1}\sqrt{\xi_1^2-\eta^2}\,[S_\ell(\eta,c)]^2\,d\eta \qquad (F.6)$$

Now from (6.27) we have

$$S_\ell(\eta,c) = \sum_{n=0,1}^{\infty\,\prime} d_n^\ell(c)\, P_{n+1}^1(\eta) \qquad (F.7)$$

If $\ell=1$, for example, then

$$[S_1(\eta,c)]^2 = [d_1^1 P_2^1]^2 + 2\, d_1^1 d_3^1 P_2^1 P_4^1$$

$$+ [d_3^1 P_4^1]^2 + 2\, d_1^1 d_5^1 P_2^1 P_6^1 + \ldots \qquad (F.8)$$

The coefficients d_n^ℓ drop off so rapidly with increasing n that only a few terms need be taken. The function (F.6) is then expressible as a sum of integrals, each of the form

$$A_{mn}(\xi_1) = \frac{1}{\sqrt{\xi_1^2-1}} \int_{-1}^{1} \sqrt{\xi_1^2-\eta^2}\, M_{mn}(\eta^2)\, d\eta \qquad (F.9)$$

where $M_{mn}(\eta^2)$ is a polynomial in η^2 ; this is apparent from the nature of the associated Legendre polynomials[1] involved in (F.7). By the elementary transformation $t^2 = \xi_1^2 - \eta^2$ the integrals (F.9) are readily evaluated although for the higher orders the expressions are unwieldy. We can then write (F.6) as

$$\textcircled{\sim}_\ell(\xi_1, c) = \sum_{m=0,1}^{\infty\,\prime} \sum_{n=0,1}^{\infty\,\prime} a_{mn}(c)\, A_{mn}(\xi_1) \qquad (F.10)$$

where

$$a_{mn}(c) \triangleq d_m^\ell(c)\; d_n^\ell(c) \qquad (F.11)$$

The coefficients $a_{mn}(c)$ are given in Table 29. The functions $A_{mn}(\xi_1)$ have been computed and are tabulated in Tables 30 and 31. The values of $\textcircled{\sim}_\ell(\xi_1, c)$ given by (F.10) will be found in Tables 20 to 28; the final digit is probably uncertain by two units. As $\xi_1 \to 1$, the function $\textcircled{\sim}_\ell(\xi_1, c)$ grows infinite. The function $\Omega_\ell(\xi_1, c)$, related to $\textcircled{\sim}_\ell(\xi_1, c)$ by (8.26), remains regular and is readily interpolated, so it was used in this region in preference to $\textcircled{\sim}_\ell(\xi_1, c)$.

---

(1) G. Prévost, "Tables de Fonctions Sphériques et de leurs Intégrales" Paris, 1933.

3. Normalization Integrals

Related in character to the functions just discussed are the surface integrals involved in expression (10.9), necessary to the computation of the normalization factor, and useful in analyzing frequency behavior. These can be expanded in double series, following the technique of the preceding section, and require evaluation of integrals of the forms

$$\int_{-1}^{1} P_{m+1}^{1} P_{n+1}^{1} \, d\eta$$

$$\int_{-1}^{1} P_{m+1}^{1} P_{n+1}^{1} \, \eta^2 \, d\eta$$

$$\int_{-1}^{1} \left[(1-\eta^2)(P_{m+1}^{1})' - \eta P_{m+1}^{1}\right]\left[(1-\eta^2)(P_{n+1}^{1})' - \eta P_{n+1}^{1}\right] \frac{d\eta}{1-\eta^2} \qquad \text{(F.12)}$$

The last of these can be simplified, if we define a new function $L_n(\eta)$ by the relation

$$L_n(\eta) \triangleq \sqrt{1-\eta^2}\, P_{n+1}^{1}(\eta) \qquad \text{(F.13)}$$

for then

$$\frac{d}{d\eta}\left[L_n(\eta)\right] = \left[\sqrt{1-\eta^2}\,(P_{n+1}^{1})' - \frac{\eta}{\sqrt{1-\eta^2}}\, P_{n+1}^{1}\right] \qquad \text{(F.14)}$$

and the last integral of (F.12) becomes

$$\int_{-1}^{1} L_m'(\eta)\, L_n'(\eta)\, d\eta \qquad \text{(F.15)}$$

The differential equation satisfied by $L_n(\eta)$ is

$$(1-\eta^2)L_n''(\eta) + (n+1)(n+2)L_n(\eta) = 0 \qquad \text{(F.16)}$$

from which it may be shown by the usual methods that the functions $L_n(\eta)$ form an orthogonal set, and that (F.15) vanishes unless $n = m$.

The orthogonality properties and recurrence relations can be made use of to obtain the following useful relations:

$$\int_{-1}^{1} P_{m+1}^1 P_{n+1}^1 \, d\eta = \begin{cases} \dfrac{2(n+1)(n+2)}{(2n+3)} & , \quad n = m \\ 0 & , \quad n \neq m \end{cases}$$

$$\int_{-1}^{1} P_{m+1}^1 P_{n+1}^1 \eta^2 \, d\eta = \begin{cases} \dfrac{2(n+1)(n+2)}{(2n+3)^2}\left[(2n+3) - \dfrac{(n+4)(n+3)}{(2n+5)} - \dfrac{n(n-1)}{(2n+1)}\right], & n = m \\ \dfrac{2(n+2)(n+1)n(n-1)}{(2n+1)(2n+3)(2n-1)} & , \quad n = m+2 \\ 0 & , \quad n > m+2 \end{cases}$$

$$\int_{-1}^{1} \left[(1-\eta^2)(P_{m+1}^1)' - \eta P_{m+1}^1\right]\left[(1-\eta^2)(P_{n+1}^1)' - \eta P_{n+1}^1\right] \frac{d\eta}{1-\eta^2}$$

$$= \int_{-1}^{1} L_m'(\eta) L_n'(\eta) \, d\eta$$

$$= \begin{cases} \dfrac{2(n+1)^2(n+2)^2}{2n+3} & , \quad n = m \\ 0 & , \quad n \neq m \end{cases} \qquad \text{(F.17)}$$

To aid in the evaluation of the normalization factor and frequency characteristic, the value of these integrals for various indices is tabulated in Table 32. From these and the coefficients of Table 29 may be computed the integrals occuring in Eq. (10.9) and Table 33 gives these for $\ell = 1$.

4. Discussion of the Graphs

Figures 53 to 55 give the behavior of $\Psi_\ell(\xi_1, c)$ versus ξ_1, for different values of c and ℓ. These curves all approach unity for large values of ξ_1. When c is less than $(\ell+1)\pi/2$ then Ψ_ℓ is zero at $\xi_1 = 1$, and has a maximum at a value of ξ_1 slightly less than $\sqrt{\alpha}/c$. This displacement of the maximum grows more and more pronounced (on a logarithmic scale) as c approaches $(\ell+1)\pi/2$. If c exceeds $(\ell+1)\pi/2$ then Ψ_ℓ becomes infinite as $\xi_1 \to 1$. Letting $y = \log \chi_1 = \log(\xi_1 - 1)$, then for extremely small values of χ_1 $(<.01)$ the relation

$$\log \Psi_\ell = \text{constant} + \frac{y}{2} - 2 \log y \qquad \text{(F.18)}$$

is approximately true.

Figures 56 to 64 show how g_ℓ^p varies with ξ_1 for various modes and representative values of the parameter c. The function is computed from (F.4) using corresponding values of ξ_1 and ξ_2 as found in Appendix C. Since ξ_2 is generally large enough that $\Psi_\ell(\xi_2, c)$ is quite close to one, one finds that curves of $g_\ell^p(\xi_1)$ closely resemble the corresponding curves of $\Psi_\ell(\xi_1, c)$. As before, the value of c with respect to $(\ell+1)\pi/2$ determines whether g_ℓ^p is zero or infinite when $\xi_1 = 1$. The maxima are slightly more displaced from $\sqrt{\alpha}/c$.

The mode for which $p=0$ is somewhat different. For values of $\xi_1 > \sqrt{\alpha}/c$, the function g_ℓ^p is unity since the mode is then degenerate, with $\xi_1 = \xi_2$. The mode cannot exist if $c > (\ell+1)\pi/2$.

In Figure 65 is plotted $g_\ell^p(\xi_1, c)$ for the $\ell=1$, $p=1$ mode, for several values of c. Also shown is the envelope of these curves which enables one to determine the maximum possible value of g_ℓ^p when ξ_1 is specified.

Figures 66 to 68 show g_ℓ^p as a function of reduced frequency c when ξ_1 is held constant. The maximum of each of these curves is obtained from a plot such as Figure 65. As ξ_1 approaches unity, the peak of g_ℓ^p increases in amplitude and moves nearer $(\ell+1)\pi/2$ until at $\xi_1=1$ the function becomes infinite at $c=(\ell+1)\pi/2$. From these curves one can find how g_ℓ^p varies with ξ_1 when ξ_2 is held fixed, as in Figures 13 and 14.

TABLE 20

$\xi(\xi_1)$	$\beta(\xi_1)$	$\chi(\xi_1)$	$\omega(\xi_1)$	$\Omega(\xi)$	$\Psi(\xi_1)$	ξ_2	$\psi(\xi_2)$	ξ_3	$\psi(\xi_3)$	ξ_4	$\psi(\xi_4)$	g_0°	g_0'	g_0''
1.0	0-	0	∞		0	3.565		7.690	1.027	11.675		0	0	0
1.2	-.41922	3.1999	2.1791	1.44455	0.7794	2.94	1.194	7.16	1.031	11.15	1013	.6528	.7759	.7693
1.4	-.69451	4.6407	1.7603	1.7247	1.3243	2.46	1.282	6.80	1.034	10.80	1.0135	1.033	1.280	1.307
1.6	-.85414	5.1822	1.5998	1.9982	1.5008	2.10	1.383	6.60	1.036	10.60	1.014	1.085	1.447	1.479
1.8	-.90204	5.2928	1.5155		1.4830	1.8	1.483	6.54	1.037	10.54	1.014	1.0	1.430	1.462
2.0	-.87976	5.2632	1.4642		1.4168	2.0		6.57	1.0365	10.57	1.014	↓	1.366	1.396
2.4	-.72941	5.1384	1.4060		1.2968			6.76	1.0345	10.76	1.0135		1.253	1.279
3.0	-.38137	4.9898	1.3643		1.1866			7.21	1.030	11.20	1.0125		1.151	1.171
4.0	.31090	4.8618	1.3349		1.1022			8.09	1.024	12.07	1.011		1.076	1.090
6.0	$\pi+$: -1.32260	4.7673	1.3154		1.0443			10.01		13.98				
9.0	1.02171	4.7254	1.3070		1.0195			12.97	1.009	16.92	1.005		1.009	1.013
12	$2\pi+$: .25333	4.7106	1.3041		1.0109			15.96		19.90				
20	$4\pi+$: .33863	4.6985	1.3018		1.0039			23.94	1.002	27.87	1.001		1.001	1.002
∞		4.6917	1.3005		1.0000		1.0		1.0		1.0	1.0	1.0	1.0

$l = 0$

$c = 0.8$

TABLE 21

ξ_1	$\beta(\xi_1)$	$\chi(\xi_1)$	$\omega(\xi_1)$	$\Omega(\xi_1)$	$\psi(\xi_1)$	ξ_2	$\psi(\xi_2)$	ξ_3	$\psi(\xi_3)$	ξ_4	$\psi(\xi_4)$	g^1_0	g^2_0	g^3_0
1.0	$-\pi+;$ $0+$	0	∞	1.0717	∞	1.973		3.930		5.892		∞	∞	∞
1.04	1.2714	1.7816		1.1460	2.7669	2.762	1.058	4.722	1.019	6.684	1.009	2.615	2.715	2.742
1.06	1.5654	1.9103		1.1731	2.6459	2.947	1.050	4.907	1.018	6.869	1.009	2.512	2.600	2.622
1.08	$0+;$ 1.4733	1.9236		1.2000	2.3652	3.012	1.047	4.972	1.017	6.934	1.008	2.259	2.326	2.346
1.1	-1.4282	1.9260	2.6771	1.2268	2.1578	3.040	1.046	5.000	1.017	6.962	1.008	2.063	2.122	2.141
1.2	-1.2537	1.9314	2.0497	1.3596	1.6614	3.147	1.043	5.108	1.016	7.070	1.008	1.593	1.635	1.648
1.4	-.9256	1.9367	1.6522	1.6188	1.3466	3.352	1.037	5.313	1.015	7.276	1.008	1.299	1.327	1.336
1.6	-.6006	1.9394	1.4998	1.8733	1.2258	3.554	1.033	5.515	1.014	7.478	1.007	1.187	1.209	1.217
2.0	.04465	1.9421	1.3709		1.1235	3.959	1.027	5.919	1.012	7.882	1.006	1.101	1.101	1.117
2.4	.68748	1.9435	1.3155		1.0797	4.359		6.321		8.284				
3.0	$\pi+;$ -1.49161	1.9443	1.2759		1.0483	4.961	1.017	6.923	1.008	8.886	1.005	1.026	1.040	1.043
4.0	.11067	1.9452	1.2479		1.0260	5.962	1.012	7.925	1.006	9.888		1.014	1.026	
6.0	$2\pi+;$ .17120	1.9457	1.2293		1.0112	7.963		9.926		11.889				
8.0	$3\pi+;$ .23063	1.9459	1.2230		1.0062	9.963	1.004	11.926		13.889		1.002		
10	$4\pi+;$ .28963	1.9460	1.2201		1.0040	11.963		13.926		15.889				
∞		1.94615	1.2151		1.0000		1.0		1.0		1.0	1.0	1.0	1.0

$l = 0$

$c = 1.6$

TABLE 22

ξ_1	$\beta(\xi_1)$	$\mathrm{X}(\xi_1)$	$\Theta(\xi_1)$	$\Omega(\xi_1)$	$\Psi(\xi_1)$	ξ_2	$\Psi(\xi_2)$	ξ_3	$\Psi(\xi_3)$	ξ_4	$\Psi(\xi_4)$	s^1	s^2	s^3
1.0	0+	0	∞	1.0083	∞	1.504	1.120	2.712		3.988		∞	∞	∞
1.001	.69223	.49323		1.0095	4.1267	1.756	1.080	2.990	1.022	4.293	1.011	3.821	4.038	4.082
1.01	1.05822	.59884		1.0205	2.5149	1.892	1.065	3.135	1.020	4.420	1.010	2.361	2.466	2.490
1.02	1.22286	.65498		1.0327	2.1474	1.953	1.060	3.200	1.019	4.487	1.010	2.026	2.107	2.126
1.04	1.41945	.70853		1.0570	1.8098	2.032	1.054	3.283	1.018	4.571	1.009	1.717	1.778	1.794
1.1	0+ −1.39284	.77511	2.4649	1.1295	1.4427	2.155	1.047	3.412	1.017	4.702	1.009	1.378	1.429	1.430
1.2	−.96588	.83394	1.8828	1.2489	1.2757	2.325	1.039	3.589	1.015	4.881	1.008	1.228	1.257	1.266
1.3	−.61842	.86464	1.6452	1.3666	1.1984	2.466	1.035	3.735	1.014	5.029	1.007	1.158	1.182	1.190
1.4	−.30503	.88416	1.5136	1.4830	1.1528	2.590	1.031	3863	1.013	5.158	1.006	1.118	1.138	1.145
1.6	.27230	.90791	1.3717	1.7133	1.1016	2.820	1.025	4099	1.012	5.396	1.006	1.075	1.089	1.095
2.0	1.34123	.93076	1.2516		1.0564	3.250	1.019	4.537	1.009	5.836	1.005	1.037	1.047	1.051
2.4	2+ −.77843	.94159	1.2000		1.0365	3.667	1.015	4.960		6.261		1.021		
3.0	.71803	.94979	1.1630		1.0221	4.283	1.011	5.581	1.006	6.884	1.003	1.011	1.016	1.019
4.0	2+ .02906	.95582	1.1369		1.0120	5.296	1.007	6.598		7.903		1.005		
6.0	4+ −1.40408	.95997	1.1195		1.0052	7.304	1.003	8.610	1.001	9.917	1.000	1.002	1.004	1.005
∞		.96319	1.1063		1.0000		1.0		1.0		1.0	1.0	1.0	1.0

$l = 0$

$c = 2.4$

TABLE 23

ξ_1	$\beta(\xi_1)$	$X(\xi_1)$	$\omega(\xi_1)$	$\Omega(\xi_1)$	$\Psi(\xi_1)$	ξ_2	$\Psi(\xi_2)$	ξ_3	$\Psi(\xi_3)$	ξ_4	$\Psi(\xi_4)$	g_1^0	g_1'	g_1''
1.0	0-	0	∞	1.7029	0	4.900	1.235	9.340	1.057	13.430	1.028	0	0	0
1.3	-.01554	1.38689	3.1137	2.5864	.01263	4.875	1.235	9.320	1.057	13.410	1.028			
1.6	-.06125	3.5724	2.6975	3.3692	.07262	4.840	1.240	9.260	1.058	13.350	1.028	.059	.0686	.071
2.0	-.21080	8.5572	2.5192	4.3634	.37114	4.550	1.275	9.050	1.061	13.150	1.029	.299	.350	.361
2.4	-.46005	13.9485	2.4485		1.0041	4.070	1.355	8.710	1.069	12.830	1.031	.741	.941	.974
3.0	-.70456	17.357	2.3913		1.5196	3.270	1.505	8.380	1.072	12.570	1.034	1.010	1.481	1.490
4.5	-.23326	16.1175	2.3729		1.2838	4.5	1.2838	9.020	1.061	13.120	1.029	1.000	1.210	1.248
6.0	.71024	15.2954	2.3275		1.1486			10.310	1.047	14.360	1.027	↓	1.097	1.122
9.0	-.25317 (**)	14.738	2.3168		1.0615			13.100	1.029	17.130	1.017		1.032	1.044
12	-1.0983 (**)	14.557	2.3132		1.0340					20.050	1.012			
20	-1.1065 (**)	14.410	2.3102		1.0119									
∞		14.330	2.3086		1.0000		1.0		1.0		1.0	1.0	1.0	1.0

$\ell = 1$

$c = 0.8$

TABLE 24

ε_1	$\beta(\varepsilon_1)$	$\chi(\varepsilon_1)$	$\omega(\varepsilon_1)$	$\Omega(\varepsilon_1)$	$\psi(\varepsilon_1)$	ε_2	$\psi(\varepsilon_2)$	ε_3	$\psi(\varepsilon_3)$	ε_4	$\psi(\varepsilon_4)$	ε_5	$\psi(\varepsilon_5)$	g^0	g^1	g^2	g^3
1.0	0	0	∞	1.5482	0	2.555	1.235	4.710	1.058	6.740	1.027	8.730	1.016	0	0	0	0
1.1	-.12253	1.9827	3.9825	1.4250	.19424	2.460	1.260	4.635	1.060	6.665	1.027	8.655	1.016	.154			
1.2	-.26519	3.6543	3.1369	2.0808	.37973	2.335	1.295	4.540	1.062	6.570	1.028	8.560	1.016	.401	.489	.506	.512
1.4	-.60677	6.5196	2.6149	2.5621	1.3790	2.010	1.425	4.315	1.069	6.355	1.031	8.355	1.019	.968	1.290	1.338	1.356
1.6	-.77986	7.3843	2.4190	3.0213	1.6365	1.760	1.580	4.200	1.074	6.245	1.033	8.245	1.018	1.036	1.524	1.584	1.601
2.0	-.61611	7.1498	2.2560		1.4309	2.0		4.310	1.070	6.350	1.031	8.350	1.017	1.0	1.337	1.388	1.407
2.4	-.18991	6.8479	2.1912		1.2748			4.585	1.061	6.615	1.028	8.610	1.016	↓	1.202	1.240	1.255
3.0	.60072	6.6077	2.1389		1.1587			5.110	1.049	7.130	1.024	9.120	1.014		1.105	1.132	1.143
4.0	π: -1.08496	6.4389	2.1035		1.0820			6.045	1.034	8.050	1.019	10.030	1.011		1.046	1.062	1.070
5.0	4.3619	6.3693	2.0884		1.0505			7.020	1.024	9.010	1.015	10.980	1.010		1.026	1.035	1.040
6.0	2π: -1.1559	6.3303	2.0805		1.0344			8.005	1.019	9.985	1.011	11.955	1.009		1.000	1.0000	1.0000
9.0	3π: .42083	6.2851	2.0707		1.0149			10.975	1.010	12.935	1.008	14.900	1.006				
∞		6.2504	2.0631		1.0000		1.0		1.0		1.0		1.0	1.0	1.0	1.0	1.0

$l = 1$

$c = 1.6$

TABLE 25

ξ_1	$\beta(\xi_1)$	$\chi(\xi_1)$	$\omega(\xi_1)$	$\Omega(\xi_1)$	$\Psi(\xi_1)$	ξ_2	$\Psi(\xi_2)$	ξ_3	$\Psi(\xi_3)$	ξ_4	$\Psi(\xi_4)$	ξ_5	$\Psi(\xi_5)$	g^0	g^1	g^2	g^3
1.0	0-	0	∞	1.3360	0	1.815	1.232	3.200	1.058	4.535	1.027	5.850	1.016	0	0	0	0
1.01	-.2201	1.123		1.3586	.6304	1.705	1.275	3.110	1.065	4.445	1.025	5.760	1.015	.495	.592	.615	.621
1.02	-.3953	1.920		1.3810	1.321	1.620	1.325	3.035	1.070	4.370	1.025	5.690	1.015	.997	1.235	1.290	1.302
1.04	-.5773	2.608		1.4257	1.839	1.530	1.380	2.955	1.074	4.290	1.027	5.605	1.017	1.332	1.710	1.790	1.810
1.06	-.6979	3.076		1.4700	2.063	1.460	1.450	2.905	1.075	4.240	1.028	5.555	1.018	1.424	1.920	2.008	2.030
1.1	-.85489	3.5100	3.3986	1.5574	2.1840	1.360	1.593	2.835	1.077	4.170	1.032	5.495	1.018	1.371	2.028	2.116	2.145
1.2	-.98417	3.7512	2.6672	1.7692	1.9576	1.225	1.880	2.785	1.081	4.115	1.033	5.435	1.019	1.041	1.811	1.895	1.921
1.3	-.92678	3.7068	2.3744	1.9723	1.7017	1.3	1.902	2.805	1.079	4.140	1.033	5.465	1.018	1.000	1.577	1.647	1.672
1.4	-.79502	3.6408	2.2144	2.1697	1.5310			2.860	1.075	4.195	1.032	5.515	1.018		1.424	1.484	1.504
1.6	-.44051	3.5430	2.0442		1.3385			3.010	1.067	4.345	1.030	5.665	1.017		1.254	1.300	1.316
1.8	-.03362	3.4836	1.9557		1.2379			3.185	1.059	4.520	1.027	5.840	1.016		1.169	1.205	1.218
2.4	1.2931	3.4039	1.8455		1.1153			3.750	1.041	5.080	1.021	6.400	1.013		1.071	1.092	1.101
3.0	$\pi+i$ .46440	3.3716	1.8000		1.0673			4.335	1.030	5.655	1.017	6.970	1.012		1.036	1.049	1.055
4.0	$2\pi+i$ 1.25695	3.3500	1.7692		1.0356			5.325	1.019	6.640	1.013	7.955	1.009		1.016	1.022	1.026
6.0	$2\pi+i$ .35368	3.3358	1.7491		1.0152			7.315	1.010	8.625	1.009	9.935	1.007				
∞		3.3252	1.7339		1.0000		1.0		1.0		1.0		1.0	1.0	1.0	1.0	1.0

$l = 1$

$c = 2.4$

TABLE 26

ξ_1	$\beta(\xi_1)$	$\chi(\xi_1)$	$\theta(\xi_1)$	$\Omega(\xi_1)$	$\psi(\xi_1)$	ξ_2	$\psi(\xi_2)$	ξ_3	$\psi(\xi_3)$	ξ_4	$\psi(\xi_4)$	g^1	g^2	g^3
1.0	$-\pi+$	0	∞	1.1001	∞	1.485		2.463		3.450		∞	∞	∞
1.1	-1.2583	1.8041	2.9896	1.2784	1.9461	2.070	1.090	3.050	1.038	4.030	1.020	1.785	1.875	1.908
1.2	-.92132	1.8118	2.1796	1.4458	1.5336	2.175	1.081	3.155	1.034	4.135	1.019	1.419	1.484	1.505
1.3	-.59293	1.8163	1.9346	1.6070	1.3679	2.275	1.073	3.255	1.032	4.235	1.018	1.275	1.326	1.344
1.4	-.26744	1.8190	1.8006	1.7642	1.2770	2.375	1.066	3.355	1.030	4.335	1.017	1.198	1.240	1.256
1.6	.37943	1.8219	1.6576		1.1793	2.575	1.055	3.555	1.027	4.535	1.016			
2.0	$-\pi+1$ -1.4748	1.8246	1.5382		1.0976	2.977	1.040	3.957	1.021	4.937	1.013	1.056	1.076	1.084
2.4	-.19067	1.8258	1.4903		1.0648	3.378	1.030	4.358	1.017	5.338	1.011			
3.0	$-2\pi+$ -1.4086	1.8266	1.4521		1.0385	3.980	1.021	4.960	1.013	5.940	1.009	1.017	1.025	1.029
4.0	$-3\pi+$ -1.3467	1.8272	1.4261		1.0205	4.980	1.013	5.960	1.009	6.940	1.007			
5.0	$-4\pi+$ -1.2863	1.8274	1.4150		1.0128	5.980	1.009	6.960	1.007	7.940	1.005			
6.0	$-5\pi+$ -1.2266	1.8276	1.4091		1.0088	6.980	1.007	7.960	1.005	8.940	1.004			
∞		1.8279	1.3963		1.0000		1.0		1.0		1.0	1.0	1.0	1.0

$l = 1$

$c = 3.2$

TABLE 27

ξ_1	$\beta(\xi_1)$	$\chi(\xi_1)$	$\Theta(\xi_1)$	$\Omega(\xi_1)$	$\Psi(\xi_1)$	ξ_2	$\Psi(\xi_2)$	ξ_3	$\Psi(\xi_3)$	ξ_4	$\Psi(\xi_4)$	g^1	g^2	g^3
1.0	$0^{-\pi+1}$	0	∞	.8959	∞	1.307		2.030		2.794		∞	∞	∞
1.001	.80740	.54077		.8973	5.4134	1.480	1.144	2.230	1.051	3.000	1.026	4.732	5.151	5.276
1.005	1.0919	.66963		.9027	3.7308	1.550	1.126	2.300	1.047	3.072	1.025	3.313	3.563	3.640
1.01	1.2527	.72389		.9095	3.1022	1.586	1.117	2.336	1.046	3.108	1.024	2.777	2.966	3.029
1.02	1.45510	.77211		.9230	2.5263	1.630	1.108	2.380	1.044	3.152	1.023	2.280	2.420	2.470
1.04	-1.47754^{0+}	.80667		.9499	1.9968	1.674	1.101	2.424	1.042	3.200	1.022	1.814	1.917	1.954
1.06	-1.33438	.82507		.9765	1.7450	1.710	1.095	2.460	1.041	3.235	1.021	1.594	1.676	1.709
1.1	-1.10342	.85251	2.2458	1.0292	1.5062	1.768	1.087	2.518	1.038	3.294	1.021	1.386	1.451	1.475
1.2	-.59123	.9015	1.7467	1.1586	1.3100	1.902	1.073	2.660	1.034	3.440	1.019	1.221	1.267	1.286
1.3	-.03565	.92586	1.5456	1.2839	1.2227	2.024	1.063	2.785	1.031	3.565	1.018	1.151	1.186	1.201
1.4	.42879	.9405	1.4364	1.4064	1.1717	2.134	1.056	2.900	1.028	3.680	1.017	1.110	1.140	1.152
1.6	1.3136	.95739	1.3176		1.1145	2.350	1.045	3.120	1.024	3.905	1.015	1.067	1.089	1.099
1.8	$-.97277^{3\pi+1}$	.96668	1.2562		1.0833	2.550	1.037	3.327	1.021	4.110	1.013	1.045	1.061	1.069
2.0	-.13318	.97252	1.2190		1.0640	2.760	1.031	3.540	1.018	4.325	1.012	1.032	1.045	1.051
2.4	$-1.5208^{2\pi+1}$	.97927	1.1792		1.0436	3.170	1.023	3.955	1.014				1.029	
3.0	.82870	.98417	1.1477		1.0259	3.780	1.016					1.010		
4.0	$-1.4050^{4\pi+1}$	.98768	1.1262		1.0138	4.785	1.010							
5.0														
∞		.99179	1.1016		1.0000		1.0		1.0		1.0	1.0	1.0	1.0
												$l=1$		
												$c=4.0$		

TABLE 28

ξ_1	$\beta(\xi_1)$	$X(\xi_1)$	$\Theta(\xi_1)$	$\Omega(\xi_1)$	$\Psi(\xi_1)$	ξ_2	$\Psi(\xi_2)$	ξ_3	$\Psi(\xi_3)$	ξ_4	$\Psi(\xi_4)$	δ^1	δ^2	δ^3
1.0	$-\pi+$: $0+$	0	∞	.72313	∞	1.206		1.760		2.375		∞	∞	∞
1.001	.71392	.20179		.72419	2.7641	1.320	1.147	1.898	1.053	2.520	1.028	2.410	2.625	2.689
1.005	1.00302	.26461		.72841	2.1359	1.370	1.130	1.955	1.049	2.580	1.027	1.890	2.036	2.080
1.010	1.18825	.29802		.73368	1.9272	1.403	1.121	1.993	1.047	2.620	1.026	1.719	1.841	1.878
1.020	1.42703	.33368		.74419	1.7286	1.445	1.110	2.036	1.045	2.662	1.025	1.557	1.654	1.686
1.1	$0+$: $-.80524$	.41750	1.8043	.82683	1.3187	1.608	1.082	2.212	1.037	2.842	1.022	1.219	1.272	1.290
1.2	$-.05116$	.45411	1.3974	.92693	1.2083	1.750	1.065	2.365	1.033	2.999	1.019	1.135	1.170	1.186
1.3	.38882	.47248	1.2331	1.0243	1.1542	1.875	1.055	2.495	1.028	3.133	1.018	1.094	1.123	1.134
1.4	1.1793	.48371	1.1428	1.1197	1.1212	1990	1.047	2.616	1.026	3.255	1.016	1.071	1.093	1.104
1.6	$\pi+$: $-.85380$	.49678	1.0462		1.0826	2.203	1.038	2.835	1.022	3.481	1.014	1043	1.059	1.068
1.8	.20393	.50578	.99577		10656	2.420	1.031	3.056	1.019	3.706	1.012	1.029	1041	1.048
2.0	1.2354	.50866	.96516		1.0471	2.626	1026	3.265	1016	3917	1.011	1.021		
2.5	$2\pi+$: 6 1013	.51489				3.138	1.018	3.790	1.012	4.442	1.009			
3.0	$3\pi+$: $-.05992$	.51793	.90634		1.0195	3.652	1.013					1.0065		
4.0	$4\pi+$: 1.4583	.52073	.88867		1.0104	4.654	1.008					1.0024		
∞		.52407	.86834		1.0000		1.0		1.0		1.0	1.0	1.0	1.0

$l = 1$

$c = 4.8$

TABLE 29

	c: 0.8	1.6	2.4	3.2	4.0	4.8	a_{mn}
l = even	.97518	.90895	.82049				a_{00}
	-.0081810	-.029003	-.054311				a_{02}
	.(4)68633	.(3)92544	.0035957				a_{22}
	.(4)35383	.(3)49180	.0020030				a_{04}
	.(5)12839	.(6)26609	.(5)48898				a_{44}
	-(6)30	-.(4)157	-.(3)1326				a_{24}
l = odd	0.96179	.85811	.71619	.56687	.43306	.32513	a_{11}
	-.0075190	-.026618	-.049209	-.067464	-.077448	-.079412	a_{13}
	.(4)38781	.(3)82570	.0033812	.0080289	.013851	.019396	a_{33}
	.(4)26973	.(3)38051	.0015708	.0037791	.0066445	.0095377	a_{15}
		.(6)17	.(5)345	.(4)2519	.(3)10193	.(3)27979	a_{55}
				.(7)27298	.(6)26325	.(5)14467	a_{77}
		-.(4)1180	-.(3)1079	-.(3)4497	-.0011883	-.0023296	a_{35}
				-(6)829	-.(5)518	-.(4)2012	a_{57}
					.(4)60	.(3)168	a_{37}
					-.(3)3376	-.(3)6858	a_{17}

TABLE 30

A_{00}	A_{02}	A_{22}	A_{04}	A_{44}	A_{24}	ξ_1
2.90407	-1.09178	6.29560	-.11232	9.101	-1.3673	1.1
2.22868	-.66453	5.02979	-.05119	7.29	-.8152	1.2
1.95367	-.47683	4.52615	-.02905	6.80	-.5771	1.3
1.80168	-.36810	4.2518	-.0183	6.51	-.444	1.4
1.63816	-.24607	3.9601	-.0088	6.174	-.2892	1.6
1.55228	-.1795	3.8085	-.005	5.994	-.2092	1.8
1.5	-.1380	3.717	-.003	5.876	-.1599	2.0
1.44076	-.08996	3.6148		5.732	-.1036	2.4
1.39831	-.0555	3.539		5.624	-.0629	3.0
1.37053	-.0400	3.507		5.577	-.0451	3.5
1.36839	-.0300	3.4870		5.547	-.0340	4.0
1.36074	-.0237	3.4740		5.527		4.5
1.35536	-.01877	3.4651		5.512		5.0
1.34848	-.0128	3.4539		5.493		6.0
1.34171	-.0071	3.4429		5.476		8
1.33998	-.00565	3.4400		5.472		9
1.33871	-.004609	3.4377		5.469	-.005233	10
1.33706	-.00323	3.43497		5.464		12
1.33467	-.00119	3.43087		5.458		20
1.33367	-.00030	3.42914		5.4554		40
1.33333	0	3.42857	0	5.454545	0	∞

l = even.

TABLE 31

A_{11}	A_{13}	A_{33}	A_{15}	A_{55}	A_{77}	A_{35}	A_{57}	ξ_1
4.57225	-1.96938	8.04248	-.21430	11.5641	15.140	-1.737	-2.446	1.1
3.61290	-1.17581	6.45725	-.0936	9.3210	12.190	-1.033	-1.451	1.2
3.23050	-.83344	5.82564	-.0517	8.4254	11.027	-.729	-977	1.3
3.02220	-.63795	5.48104	-.0319	7.9356	10.407	-.564	-.791	1.4
2.80103	-.42179	5.11440	-.0155	7.4131	9.73	-.374	-.525	1.6
2.6864	-.30559	4.92372	-.0082	7.1423	9.364	-.269	-.375	1.8
2.61720	-.23389	4.80836	-.00470	6.9786	9.143	-.202	-.280	2.0
2.54431	-.15169	4.67830	-.00190	6.7947	8.898	-.129	-.174	2.4
2.48526	-.09216	4.58557	-.00069	6.6626	8.726	-.075	-.104	3.0
2.44543	-.04989	4.52048	-.00035	6.5699	8.608	-.0413	-.0565	4.0
2.43542	-.03903	4.50385	-.00014	6.5462	8.579	-.0326	-.0447	4.5
2.42843	-.03139	4.49212	-.00009	6.5295	8.558	-.0265	-.0362	5.0
2.41952	-.02160	4.47723	-.00004	6.5083	85311	-.0185	-.0253	6.0
2.40855	-.00949	4.45884		6.4820	8.4973	-.0083	-.0113	9.0
2.40691	-.007645	4.45608		6.4781	8.4922	-.00657	-.00919	10
2.40479	-.00532	4.45250		6.4730	8.4856	-.00455	-.0064	12
2.40172	-.00191	4.44733		6.4657	8.4760	-.00164	-.0023	20
2.4	0	4.44444	0	6.46154	8.47069	0	0	∞

A_{37}	A_{17}	ξ_1
-.1766	-.01782	1.1
-.0808	-.00710	1.2
-.0431		1.3
-.0202		1.4
0	0	∞

l = odd

	$\int_{-1}^{1} P_{m+1}^{1} P_{n+1}^{1} dy$	$\int_{-1}^{1} P_{m+1}^{1} P_{n+1}^{1} y^2 dy$	$\int_{-1}^{1} L_m^1 L_n^1 dy$	m	n
	1.33333	.266667	2.666667	0	0
	0	.457143	0	0	2
	0	0	0	0	4
	3.42857	1.6	41.1428	2	2
	0	1.038961	0	2	4
l even	0	0	0	2	6
	5.45455	2.65734	163.636	4	4
	0	1.56643	0	4	6
	0	0	0	4	8
	7.46666	3.68265	418.133	6	6
	2.4	1.02857	14.4	1	1
	0	.76190	0	1	3
	0	0	0	1	5
	4.4444	2.13564	88.888	3	3
	0	1.30536	0	3	5
	0	0	0	3	7
l odd	6.46154	3.17203	271.385	5	5
	0	1.82444	0	5	7
	0	0	0	5	9
	8.47059	4.19071	609.882	7	7
	0	2.33525	0	7	9
	0	0	0	7	11
	10.4762		1152.381	9	9

TABLE 33

① $\int_1^\infty S^2 dy$	② $\int_1^\infty f^3 S^2 dy$	③ $\int_1^\infty \frac{1}{c^2}(y')^2 dy$	②+③ $\int_1^\infty [f^3 S^2 + \frac{1}{c^2}(y')^2] dy$	c
1.30856	.97794	21.648	22.626	0.8
2.06313	.84380	4.8556	5.6994	1.6
1.73390	.66862	1.8428	2.5114	2.4
1.39633	.49631	.86752	1.36383	3.2
1.10156	.35420	.46844	.82264	4.0
.86834	.24957	.28137	.53094	4.8

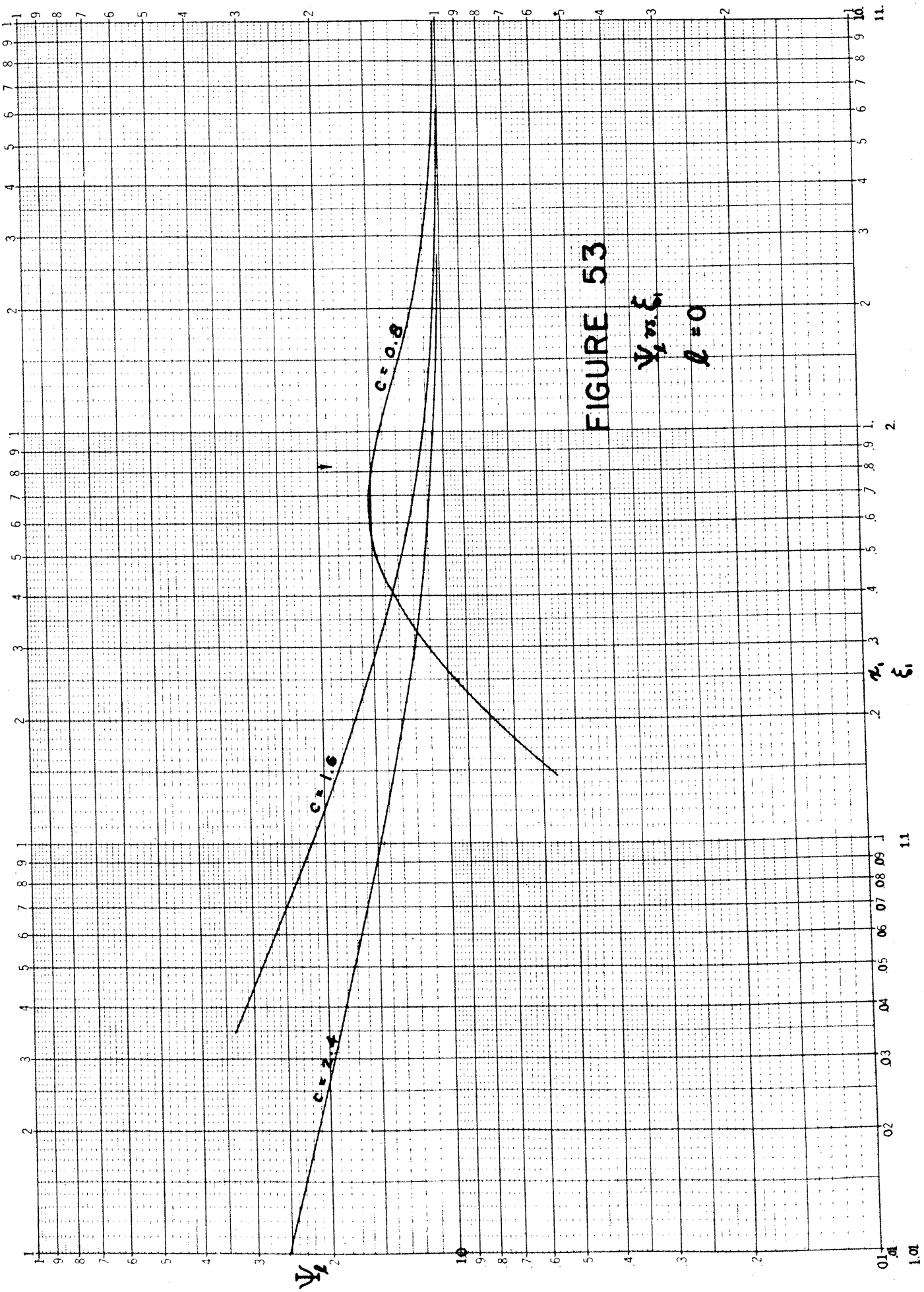

FIGURE 53
Ψ_2 vs ξ_1
$\ell = 0$

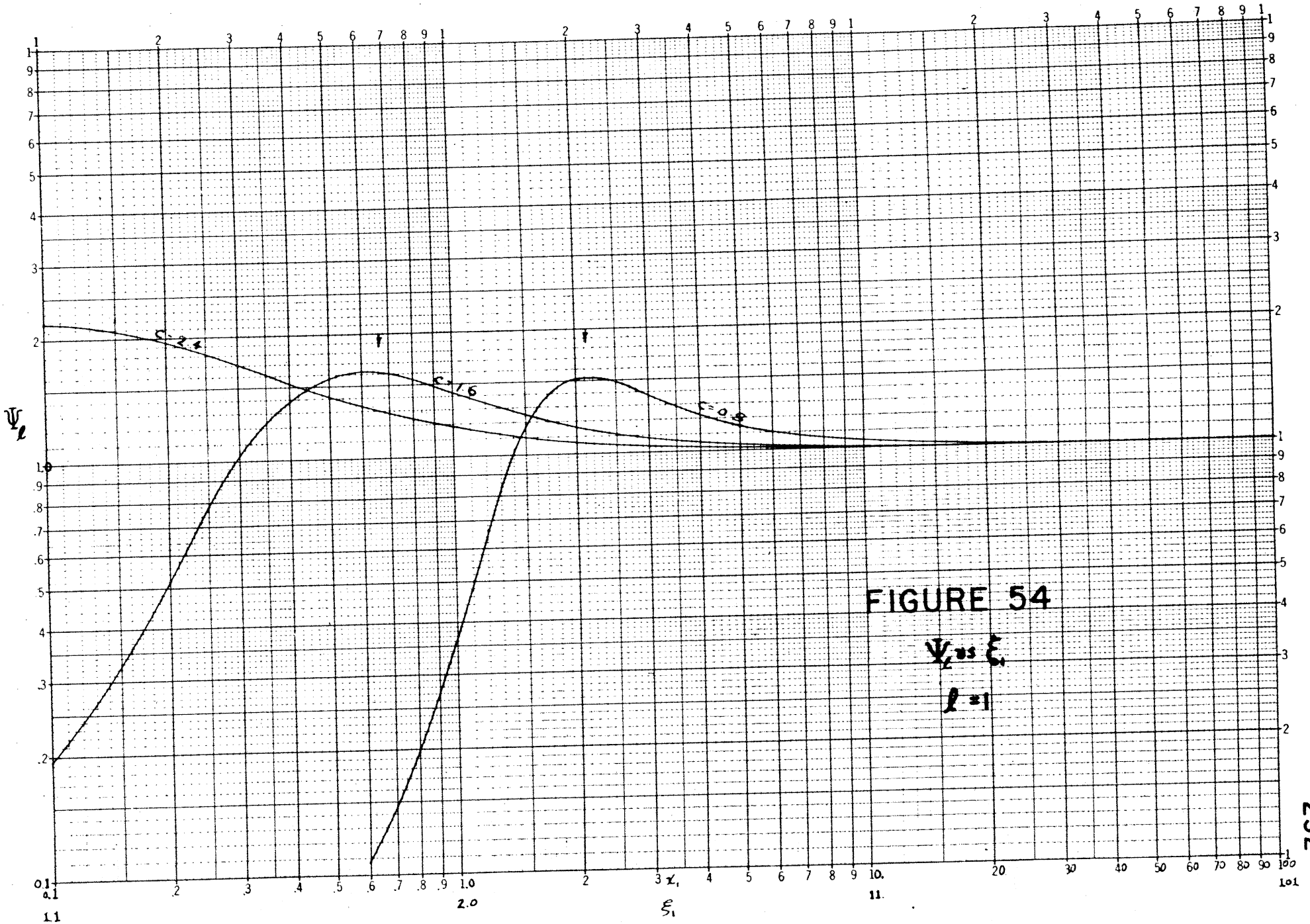

FIGURE 54

Ψ_ℓ vs ξ_1

$\ell = 1$

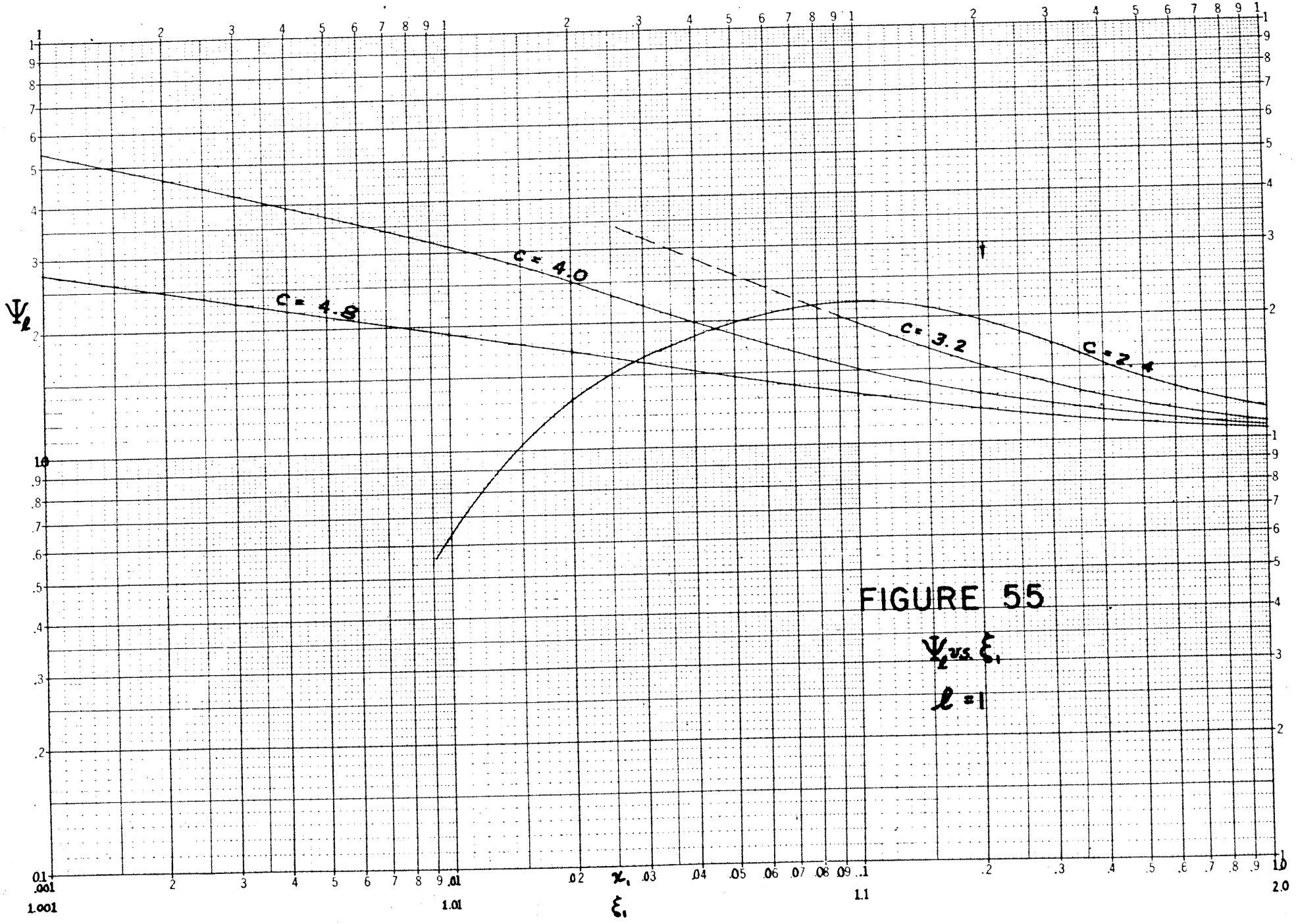

FIGURE 55

Ψ_ℓ vs. ξ_1

$\ell = 1$

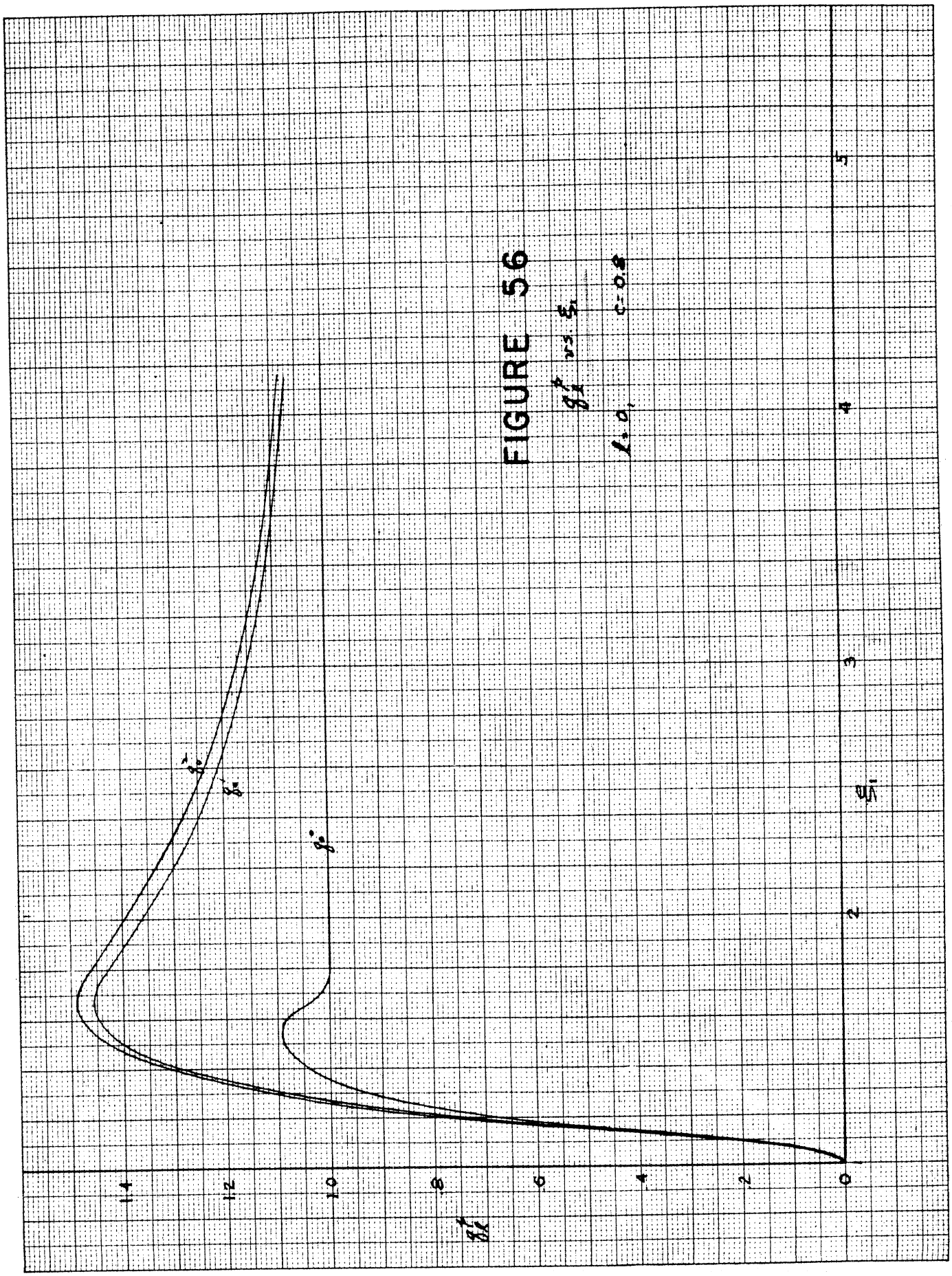

FIGURE 56

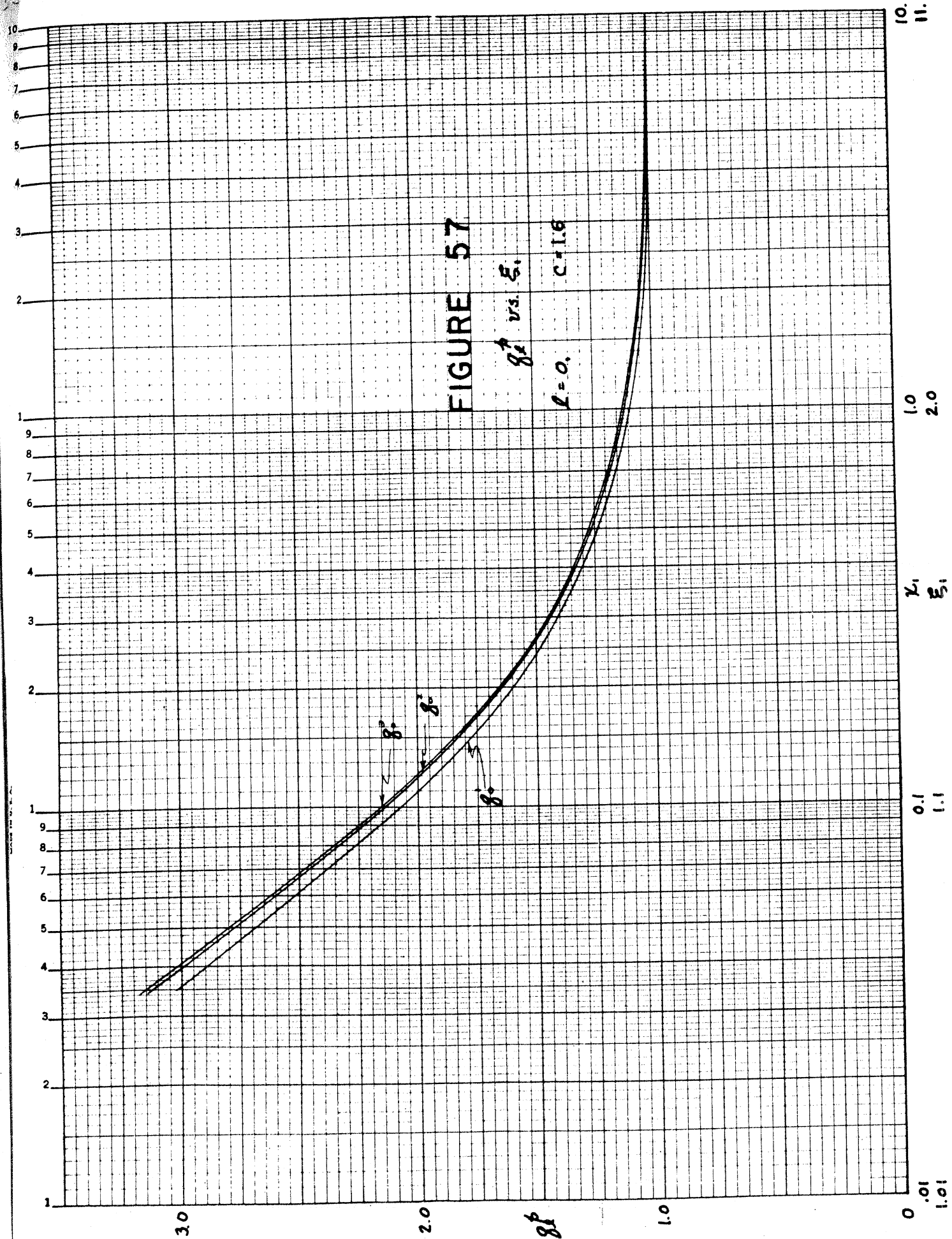
FIGURE 57
g_i^* vrs. ξ_i
$L = 0.$
$C = 1.6$
g^b
χ_i
ξ_i
3.0
2.0
1.0
0
.01
1.01
0.1
1.1
1.0
2.0
10.
11.

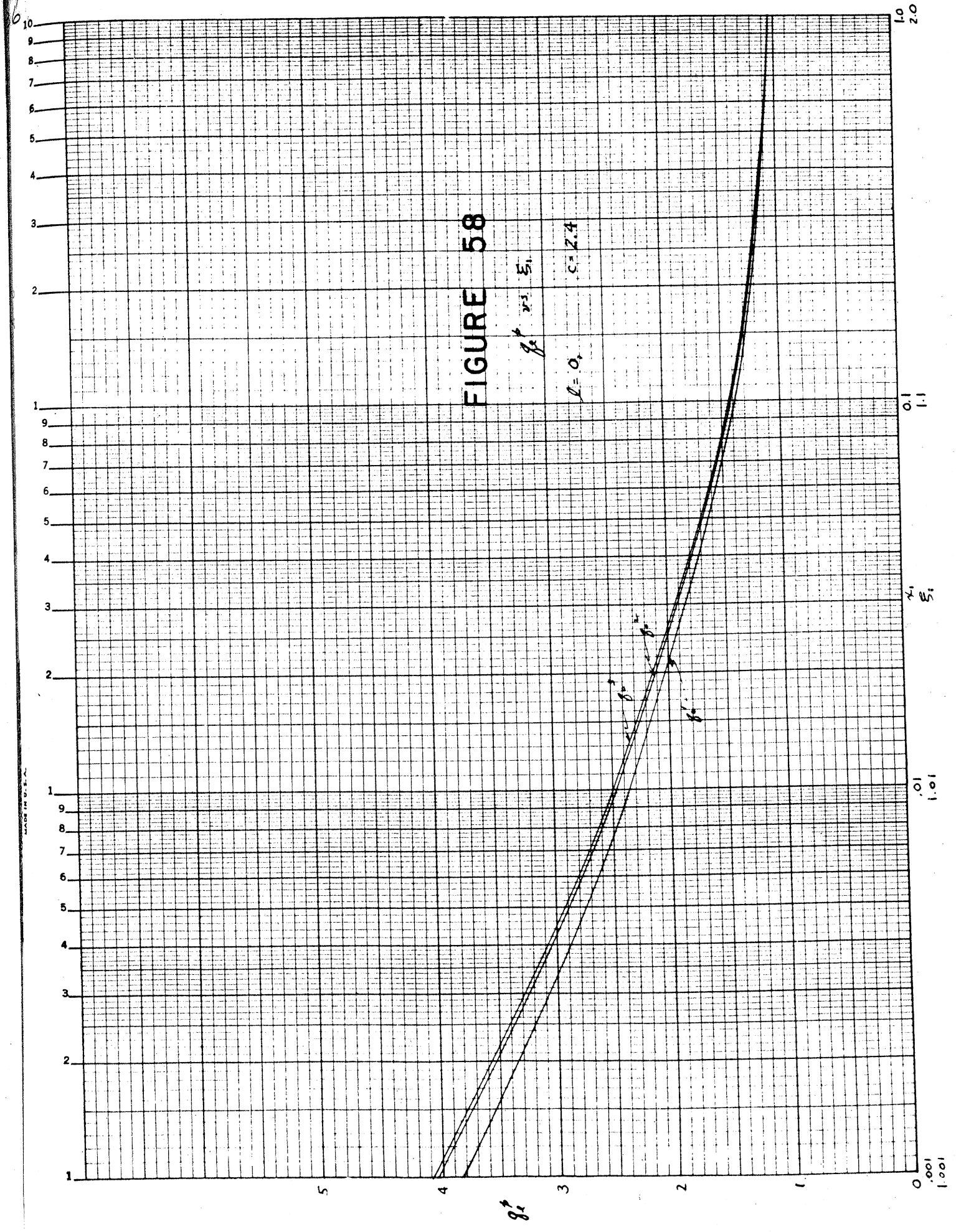
FIGURE 58
c = 2.4
ξ_i
x_i
g_i'
10
9
8
7
6
5
4
3
2
1
0
1.0
2.0
0.1
1.1
.01
1.01
.001
1.001

38
37

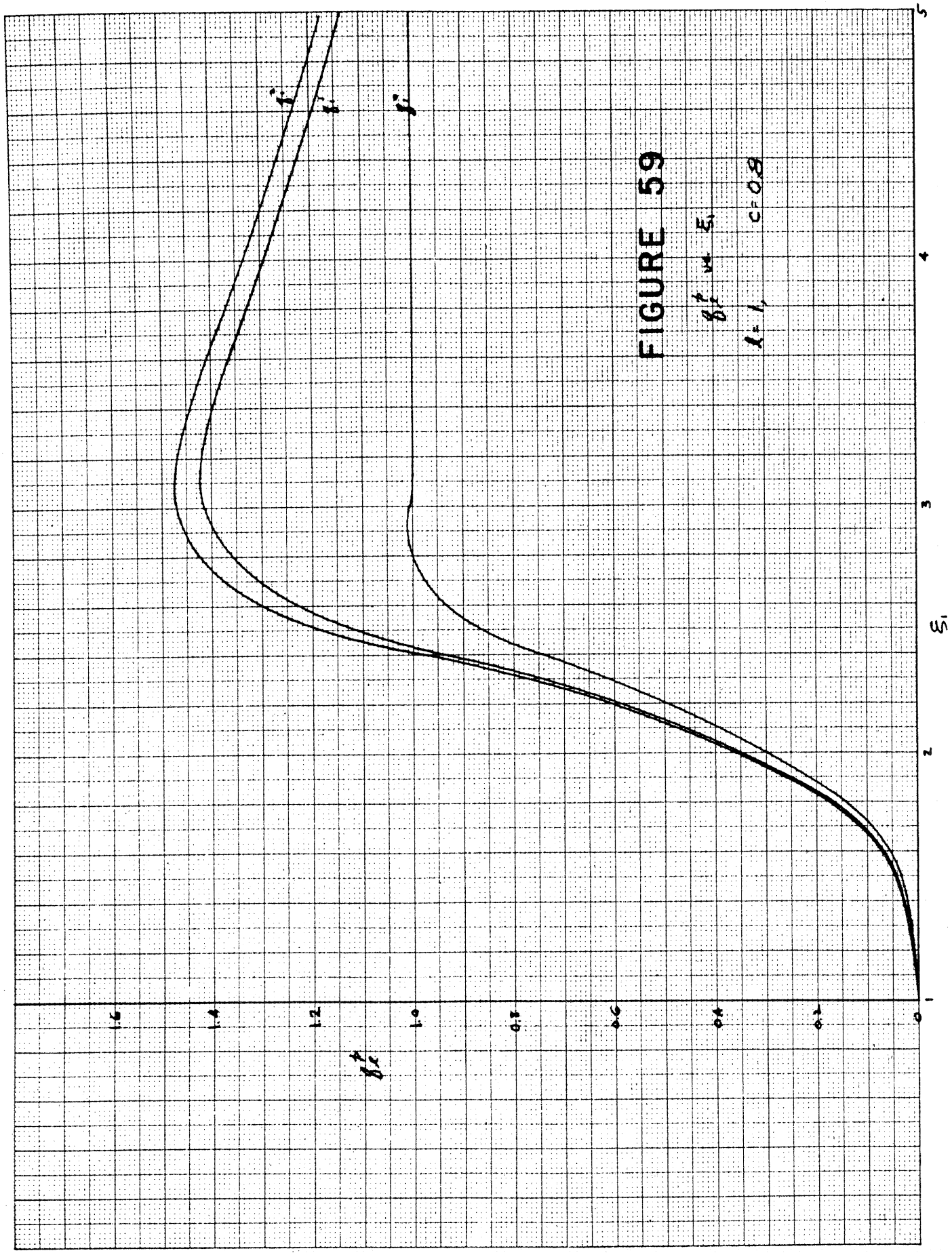

FIGURE 59

g_{1x}^{+} vs. ξ_1

$\lambda = 1$, $c = 0.8$

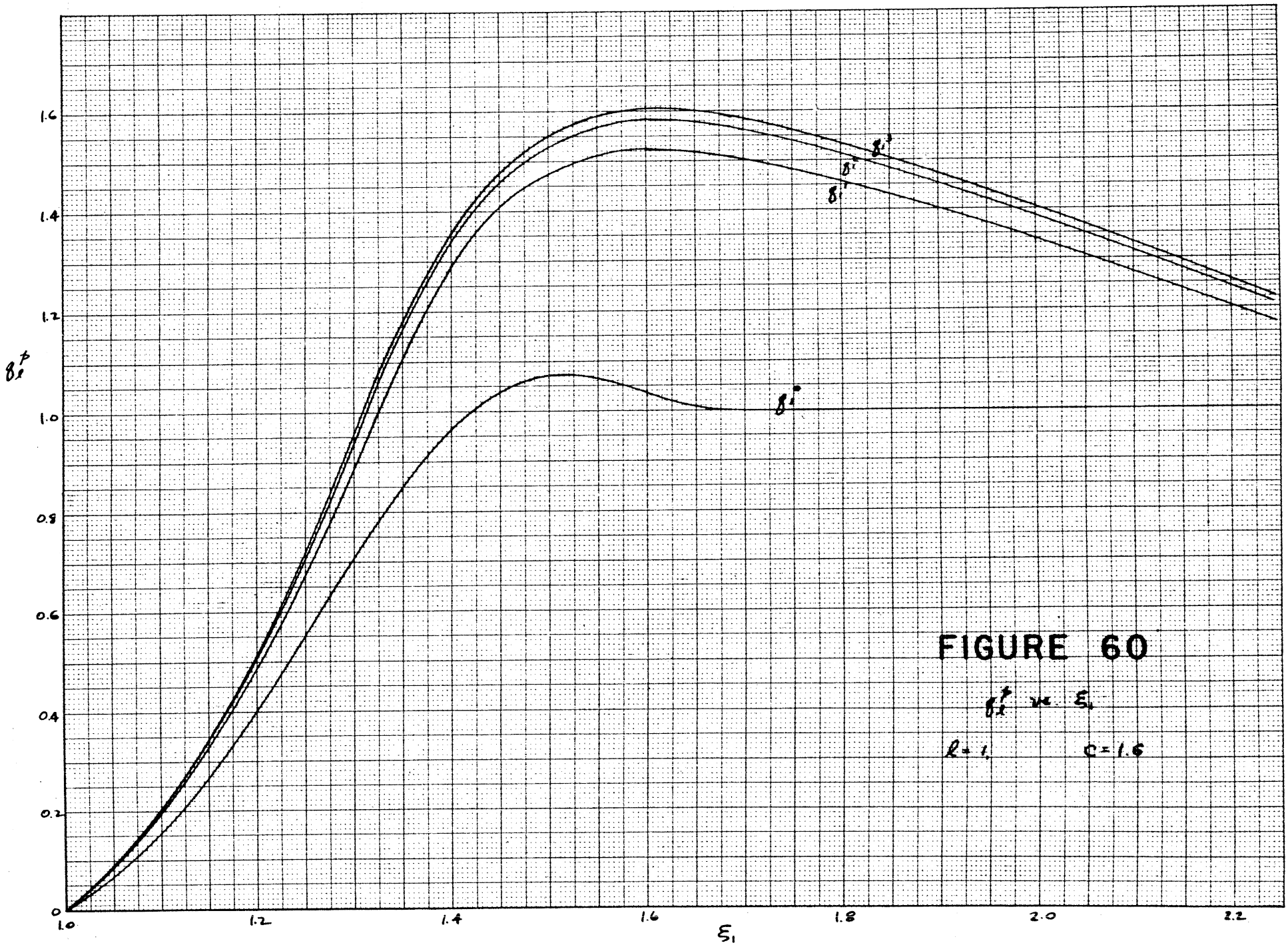

FIGURE 60

g_l^p vs ξ_1

$l = 1$, $c = 1.6$

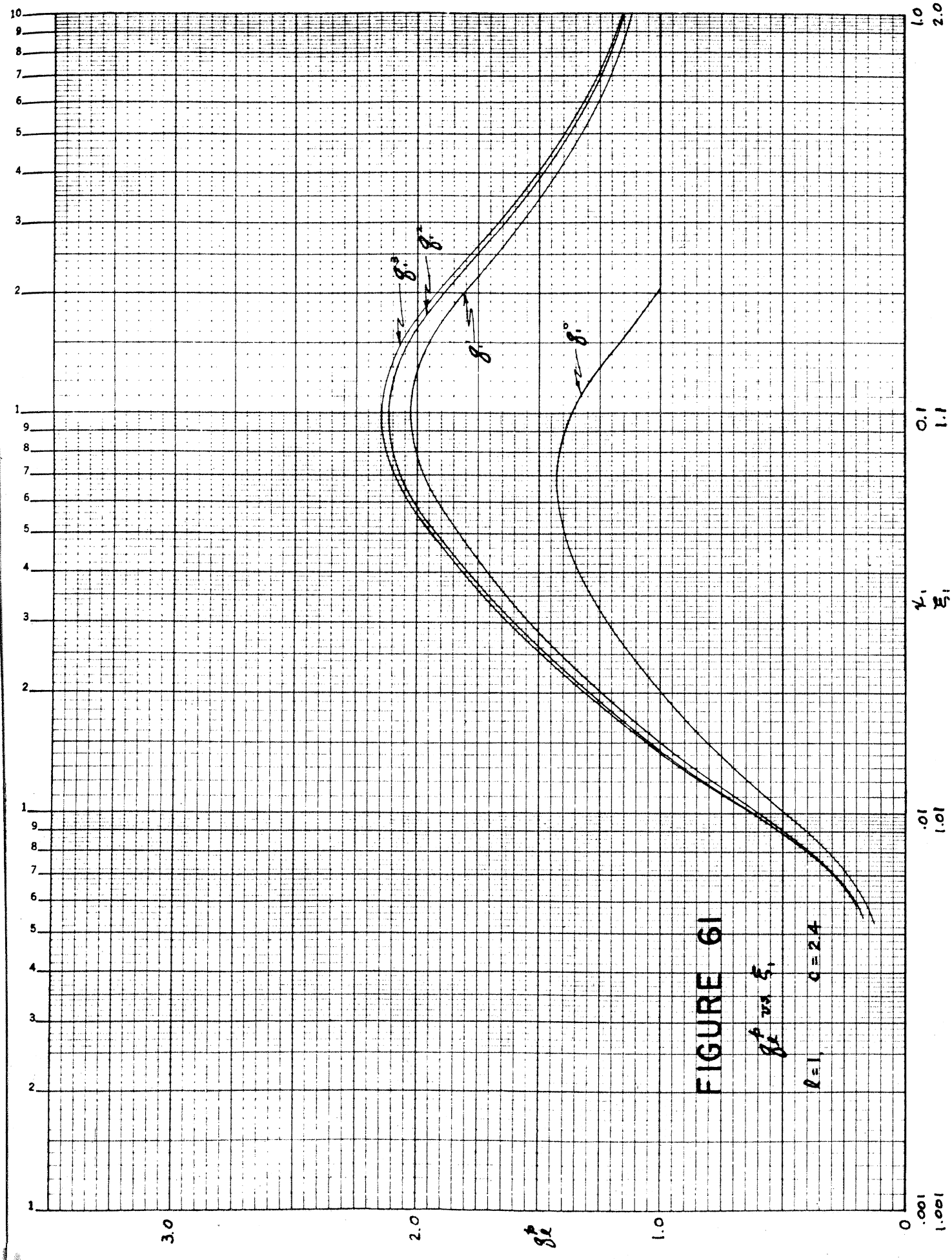
10
9
8
7
6
5
4
3
2
1
1.0
2.0
0.1
1.1
.01
1.01
.001
1.001
3.0
2.0
1.0
0
β_ℓ^ϕ
γ_1, ξ_1
β_ℓ^{ϕ} vs ξ_1
$\ell = 1$, $q = 2.4$
β_1^0
β_1^1
β_1^2
β_1^3

FIGURE 61

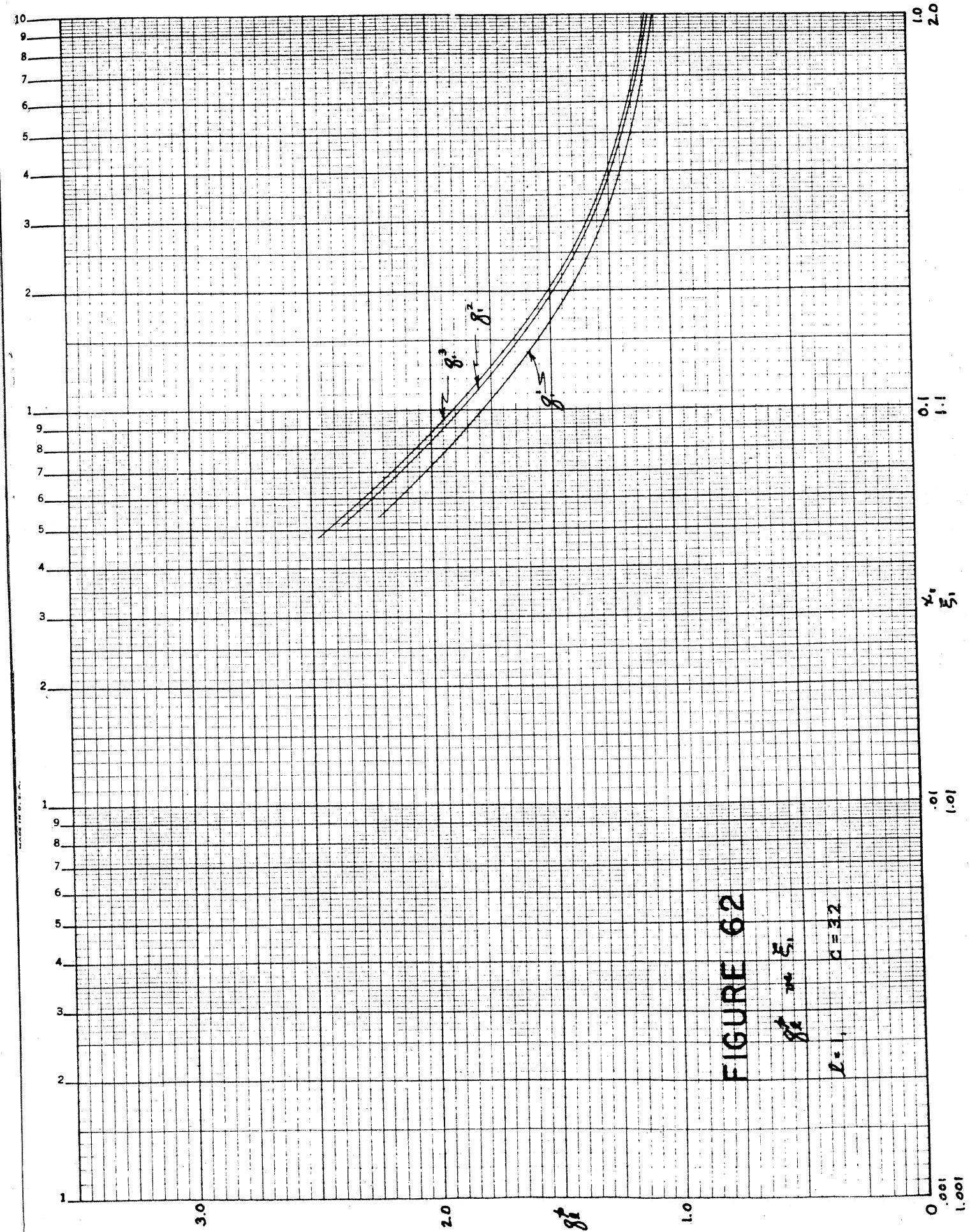
10
9
8
7
6
5
4
3
2
1
9
8
7
6
5
4
3
2
1
9
8
7
6
5
4
3
2
1
3.0
2.0
1.0
0
1.0
2.0
0.1
1.1
.01
1.01
.001
1.001
β^3
β^2
β^1
β^4
ξ_1
η_1
g^+
g^+
ξ_1
η_1
$\zeta = 1,$
$c = 3.2$

FIGURE 62

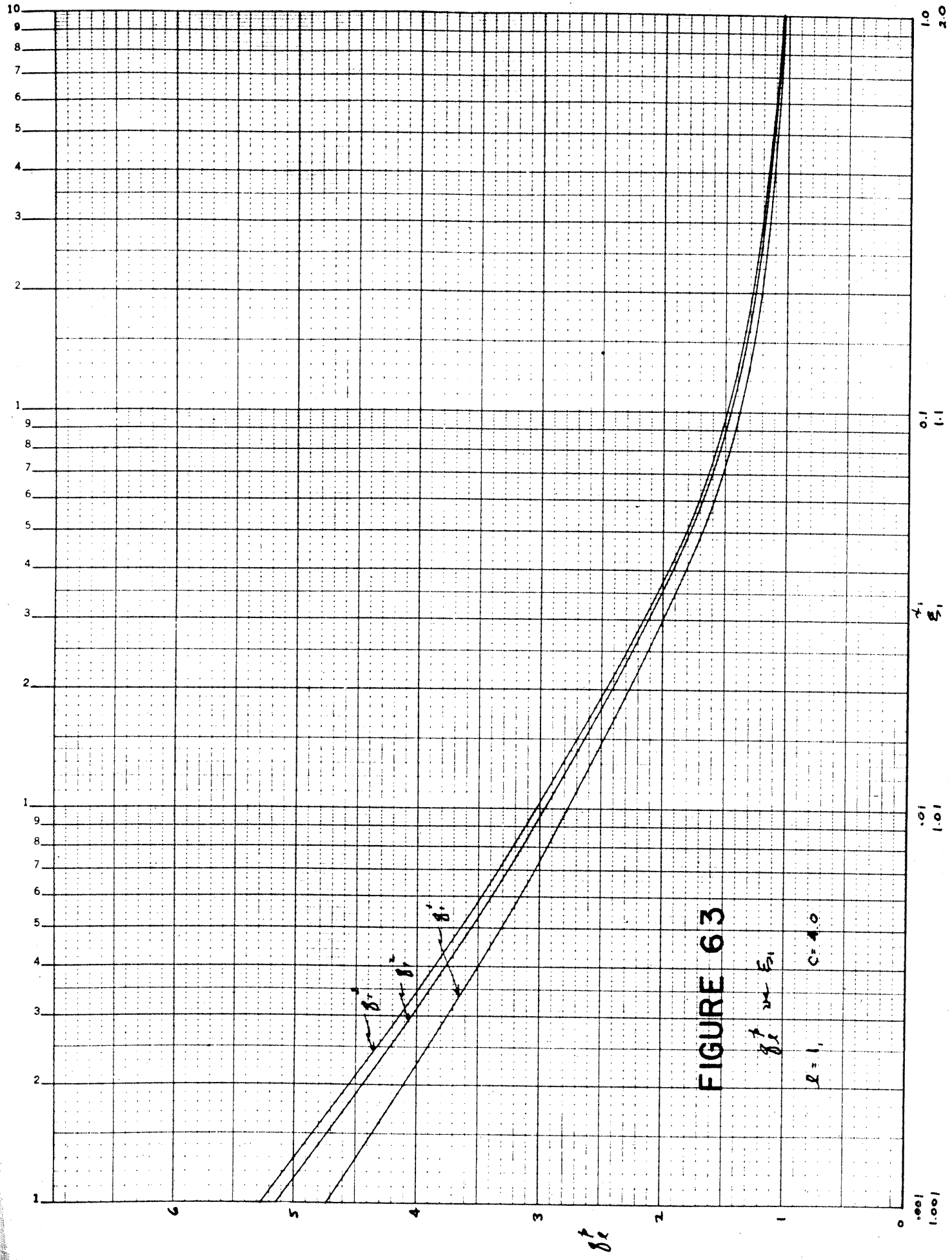
10
9
8
7
6
5
4
3
2
1
9
8
7
6
5
4
3
2
1
9
8
7
6
5
4
3
2
1
6
5
4
3
2
1
0
1.0
2.0
0.1
1.1
.01
1.01
.001
1.001
β_1^1
β_1^2
β_1^3
β_2^t
β_2^t vs E_{2i}
$C = 4.0$
$L = 1,$

FIGURE 63

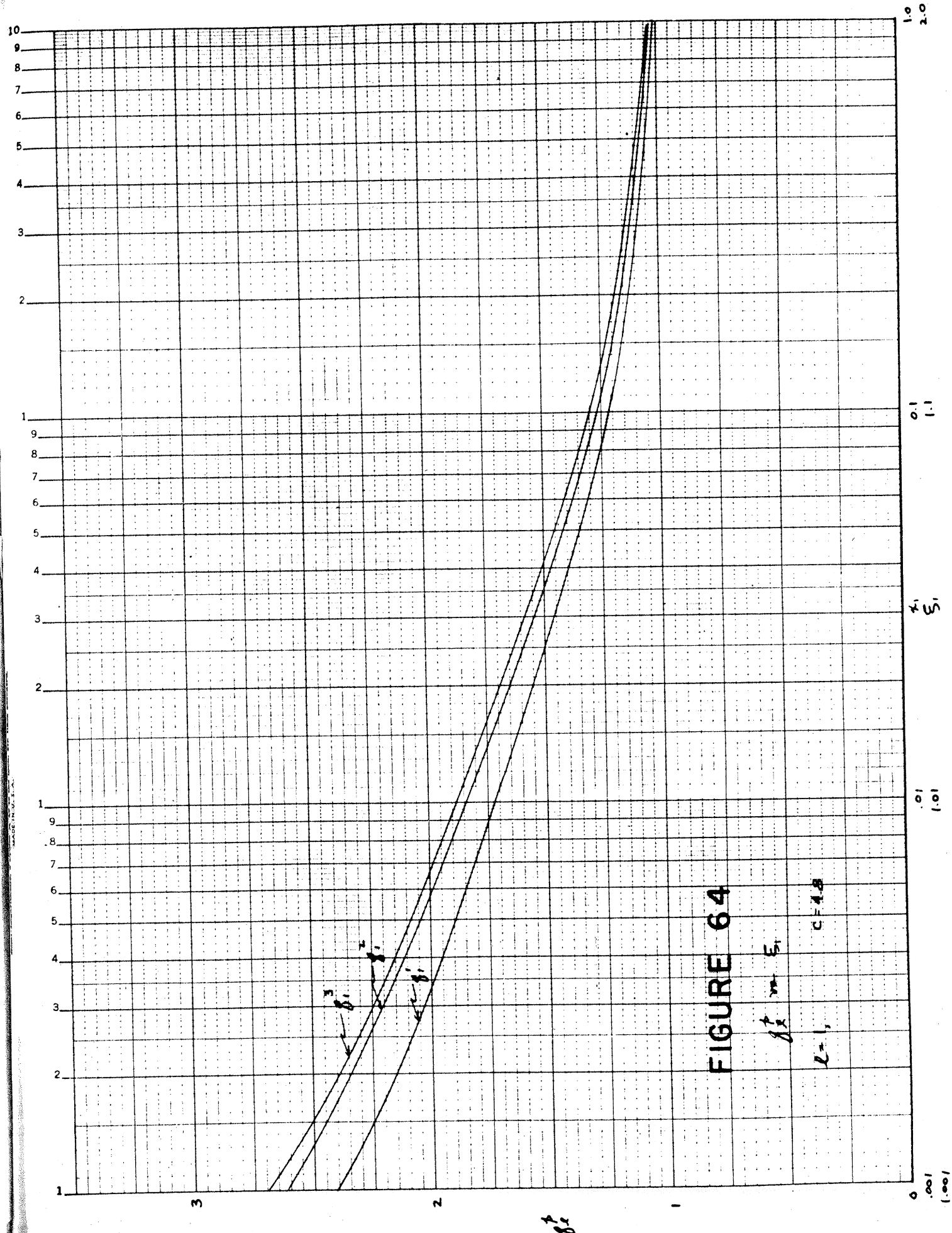
10
9
8
7
6
5
4
3
2
1
1.0
2.0
0.1
1.1
.01
1.01
.001
1.001
3
2
1
β_x^+
ξ_i
β_x^+ vs ξ_i
C = 1.8
L = 1,
β_1'
β_2'
β_3'

FIGURE 64

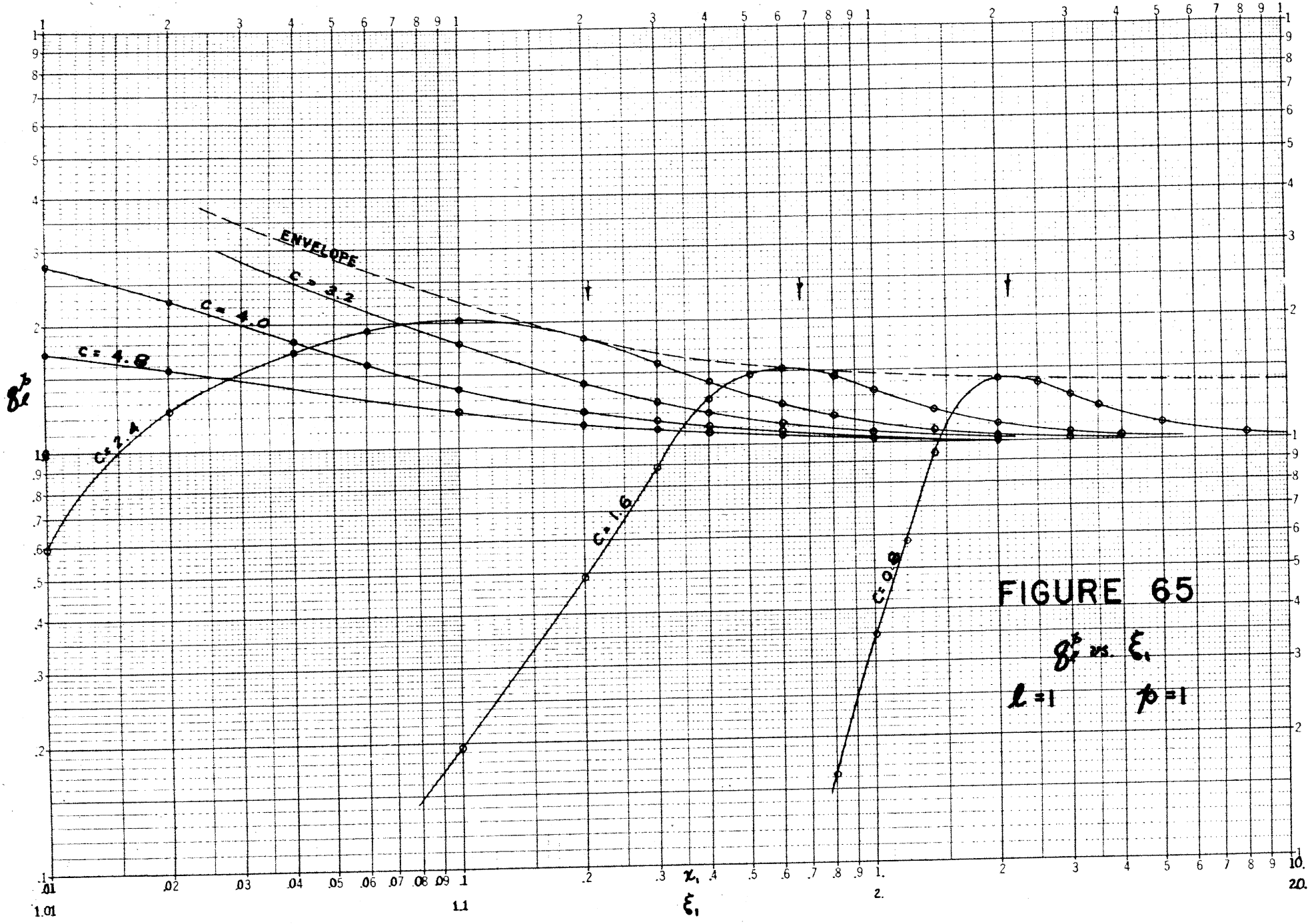

FIGURE 65

g_ℓ^p vs. ξ_1

$\ell = 1$ $p = 1$

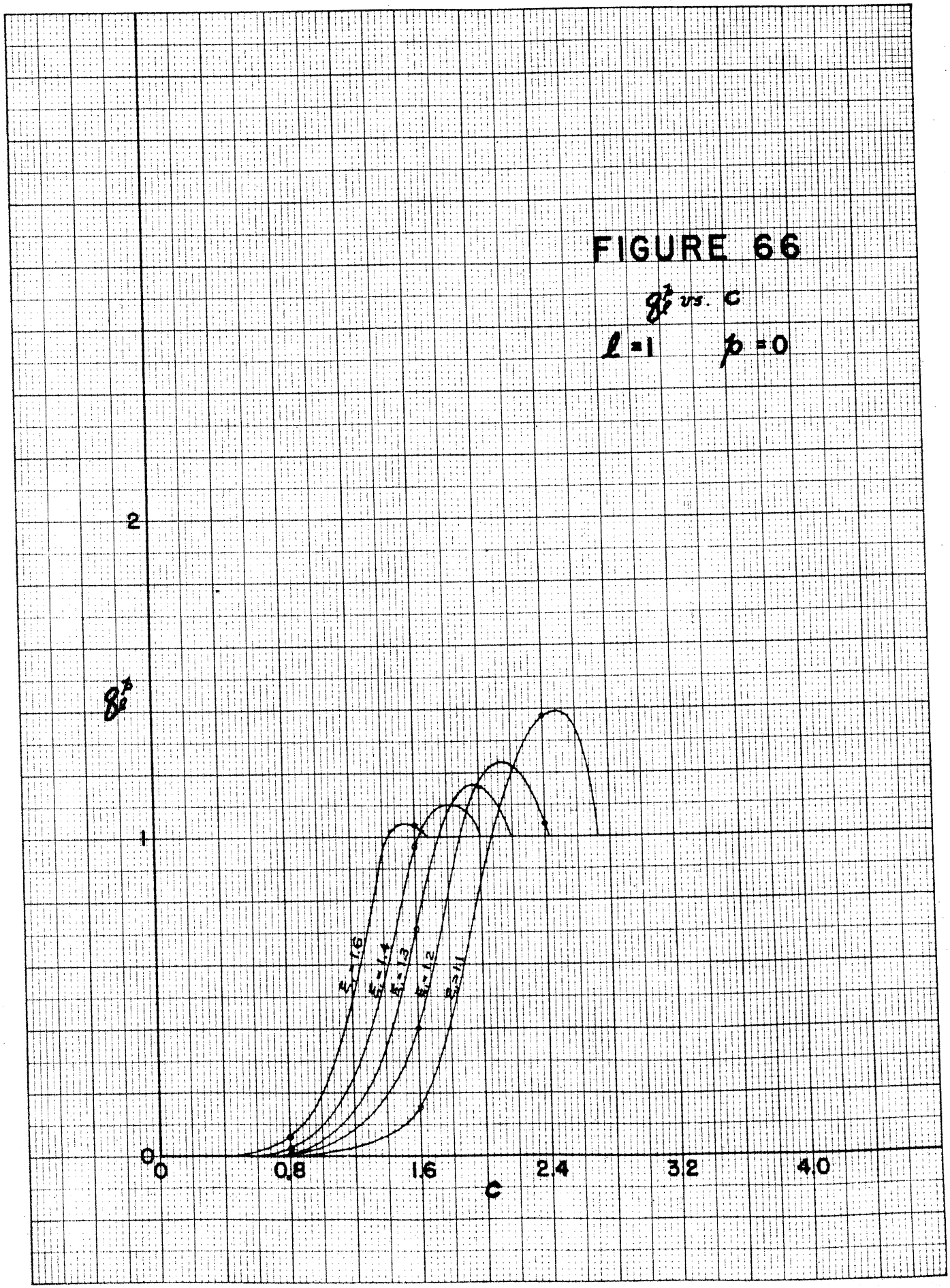
FIGURE 66
g_2^1 vs. c
$\ell = 1$ $p = 0$
g_2^p
2
1
0
0
0.8
1.6
2.4
3.2
4.0
c
$a_2 = 1.6$
$a_2 = 1.4$
$a_2 = 1.3$
$a_2 = 1.2$
$a_2 = 1.1$

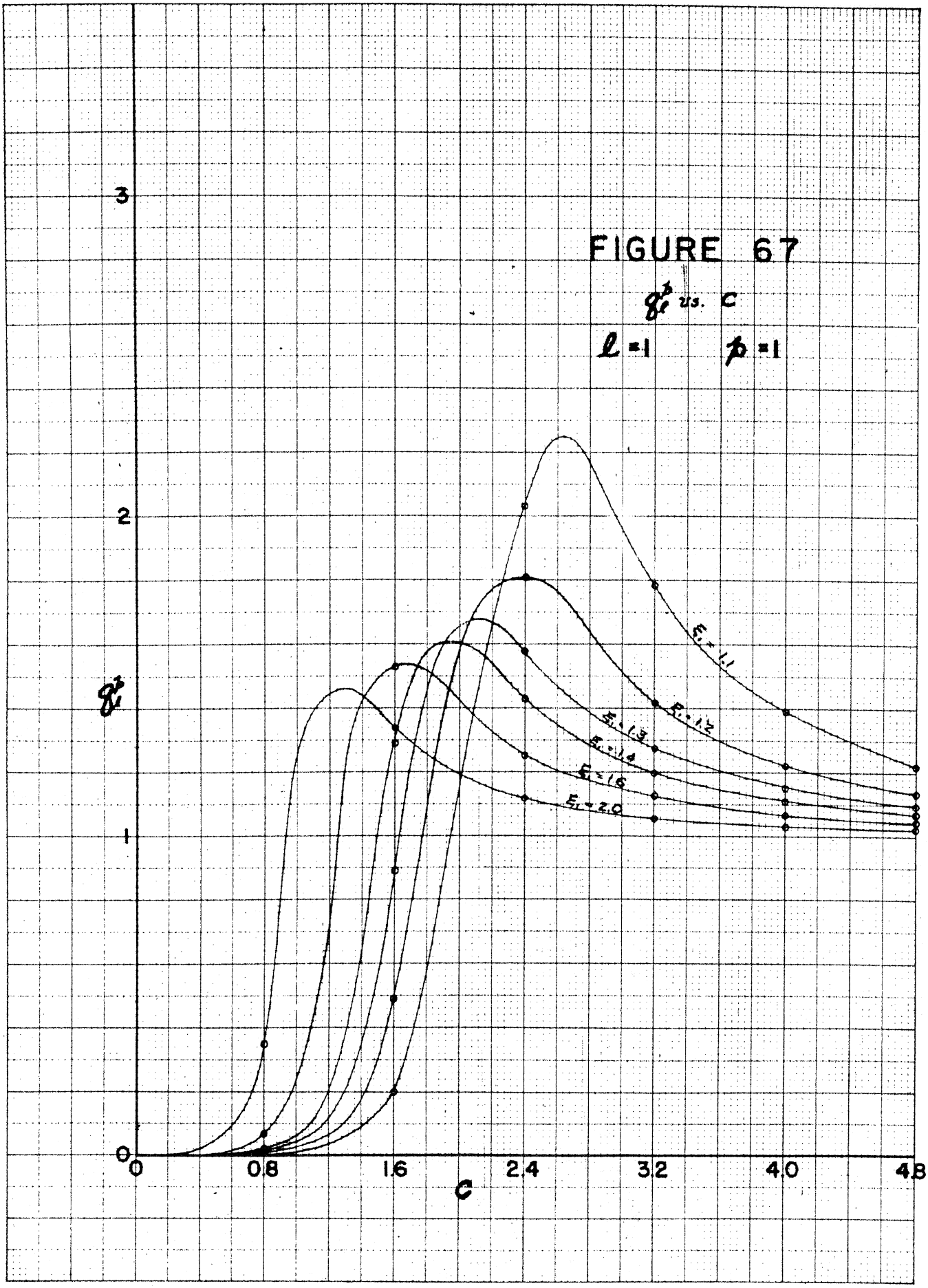
FIGURE 67
$q_\ell^{\frac{1}{2}}$ vs. C
$\ell = 1$ $p = 1$
$q_\ell^{\frac{1}{2}}$
C
0
0.8
1.6
2.4
3.2
4.0
4.8
1
2
3
$E_1 = 1.1$
$E_1 = 1.2$
$E_1 = 1.3$
$E_1 = 1.4$
$E_1 = 1.6$
$E_1 = 2.0$

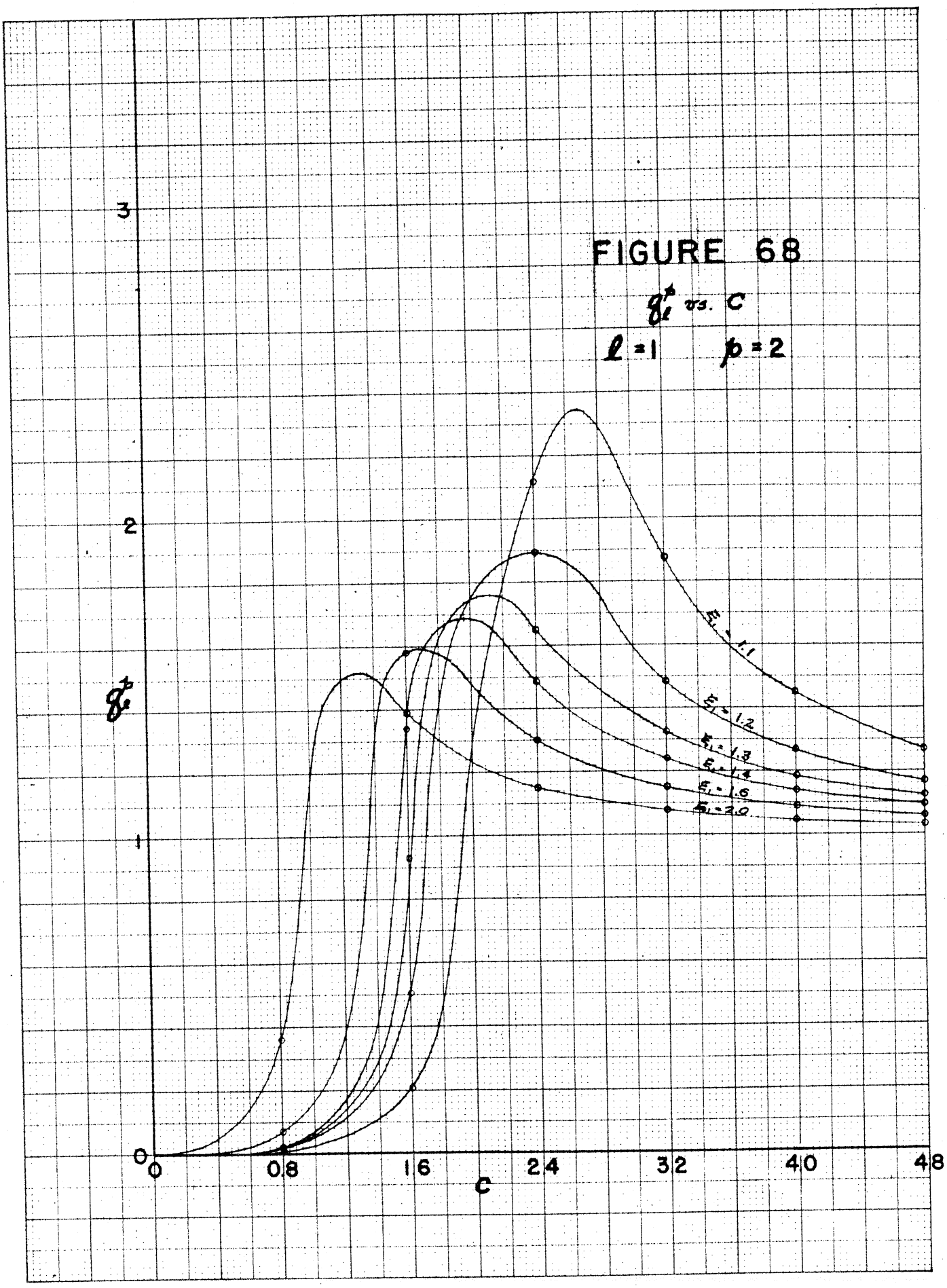
FIGURE 68
g_ℓ^* vs. C
$\ell = 1$ $p = 2$
g_ℓ^*
3
2
1
0
0
0.8
1.6
2.4
3.2
4.0
4.8
C
$E_1 = 1.1$
$E_1 = 1.2$
$E_1 = 1.3$
$E_1 = 1.4$
$E_1 = 1.6$
$E_1 = 2.0$

APPENDIX G

BIOGRAPHICAL NOTE

The author was born November 4, 1920, to John C. and Geraldine N. Simons, an engineer and a school teacher of Philadelphia, Pennsylvania. He acquired his secondary education in the public schools of that city and matriculated at Drexel Institute of Technology in 1937. While there, he was awarded the J. Peterson Ryder scholarship and was elected to Tau Beta Pi, Phi Kappa Phi, and Blue Key. He received the Drexel Technical Journal Prize in successive years for articles entitled "Controlled Atmospheres" and "Tempered Glass." In the course of his cooperative curriculum at Drexel, the author was employed by Industrial By-Products and Research Corporation, Kimble Glass Company, Proctor Electric Company, and Drever Company. He received his B.S. degree in Chemical Engineering from that institution in 1942, graduating with first honors.

Upon graduation, he entered the supervisory training program of Atlas Powder Company, but left after six months to enlist in the U. S. Naval Reserve. During three and one-half years war service, nearly all in submarine duty, he participated in six submarine war patrols in Pacific waters; when he left sea duty, he was qualified as Executive Officer. He was released to inactive duty in August, 1946, with the rank of Lieutenant, U.S.N.R.

In the fall of 1946, the author entered the Graduate School of Massachusetts Institute of Technology in pursuit of a Doctorate in Physics. He was chosen a Tau Beta Pi Fellow for the year 1947-48, but within a week was also notified of the award of a Research Fellowship

in Industrial Electronics; his tenure of this grant was eventually three years. He chose to decline the stipend of the former award and was subsequently named the first Honorary Tau Beta Pi Fellow. The M.I.T. chapter of Sigma Xi elected him to full membership in 1949. His doctoral thesis investigation (to which this note is appended) was performed under the supervision of Professor John C. Slater. Upon completion of the research, but before the formality of setting down the results was accomplished, the author left Cambridge in November 1949 to accept a position as supervisory engineer with the Atomic Power Division of the Westinghouse Electric Corporation, Pittsburgh, Pennsylvania. His work with Westinghouse includes the direction of a group developing control systems for nuclear power plants for submarine propulsion.

Reviewing here his several academic awards and prizes, the author feels they are all overshadowed by one, the former Hildred E. Dodge, to whom he was married July 31, 1949, in Cambridge.

ACKNOWLEDGMENT

For patient guidance and enlightening discussions, the author is indebted to Professor J. C. Slater, who supervised this thesis. Acknowledgment is also made to Professors L. J. Chu and G. Harvey, who served as readers. A considerable part of the computing was done by the excellent Joint Computing Group of the Research Laboratory of Electronics, under the direction of Pauline Leighton. The tedious task of typing was competently handled by Helen Borcik. For numerous technical suggestions the author is indebted to Samuel Sensiper of M.I.T., and to Dr. Sidney Krasik and Dr. Sylvan Wallach of Westinghouse Atomic Power Division. The research was materially aided by the services furnished by the Research Laboratory of Electronics, and by the grant of a Research Fellowship in Industrial Electronics from that laboratory; for this assistance the author takes pleasure in making acknowledgment to Professors J. A. Stratton and A. G. Hill, Directors of the Laboratory. Recognition is gratefully given of the cooperative attitude of Mr. M. A. Schultz, Westinghouse Atomic Power Division. Finally, this work would not have been completed without the constant inspiration and encouragement of my wife.